**Imperial College
London**

STRUCTURAL STAINLESS STEEL DESIGN: RESISTANCE BASED ON DEFORMATION CAPACITY

A thesis submitted to the University of London for the degree of

Doctor of Philosophy

By

Mahmud Ashraf

*Department of Civil and Environmental Engineering
Imperial College London
London SW7 2AZ
United Kingdom*

August 2006.

ABSTRACT

Since stainless steel is an expensive material, it is important that, when used in structural applications, its particular properties are appropriately taken into account in the design process. At present, design rules tend to treat stainless steel in much the same fashion as carbon steel despite the fundamental differences in the basic material stress-strain behaviour. The cross-section classification approach is well suited for ordinary carbon steel for its idealised elastic, perfectly plastic material behaviour. In the case of stainless steel, material nonlinearity initiates at very low stresses leading to significant strain hardening without showing any yield point. Adoption of the traditional cross-section classification for stainless steel is misleading in terms of material behaviour and also is responsible for the observed conservatism provided by the existing design codes. The primary objective of the present research is therefore to devise a rational continuous design method for structural stainless steel exploiting its special features without doing any cross-section classification.

All available test results on material coupons have been analysed to obtain appropriate material models for different grades. Effects of cold-working on the corner regions of stainless steel sections have been investigated and hence proposals have been made for the prediction of the corner strength using the basic material properties. A consistent approach has been adopted to develop numerical models for different cross-sections and members subjected to various types of loading. Measured material and geometric properties, predicted enhanced strength at the cold-worked corners and predicted initial imperfections have been used in highly nonlinear FE models. Once verified against the test results, the FE models have been used to generate useful results where test results are scarce.

A continuous relationship between the cross-section slenderness and the deformation capacity has been developed using the available stub column load-deformation results. Corner strength enhancements and post-buckling effects have been appropriately incorporated into the design method to obtain accurate predictions for the compression resistance of cross-sections using the proposed material model. A concept of generalised shape factor, which considers the nonlinear distribution of bending stresses, has been successfully utilised to predict the bending resistance of cross-sections. Once verified for the cross-sections, the basic concept of deformation capacity has been extended to stainless steel members. New sets of column curves have been proposed to predict the flexural buckling resistance. Beam-column interactions have also been investigated and hence recommendations have been made to obtain values for interaction factors to obtain appropriate ultimate load predictions. Comparison between test results and predicted results obtained using the current Eurocode (prEN 1993-1-4, 2004) and the proposed design method has been made. The comparison revealed that the proposed method offers much more accurate and consistent predictions for similar levels of calculation for all the considered cases.

ACKNOWLEDGEMENTS

CONTENTS

CHAPTER 7 – DESIGN OF STAINLESS STEEL MEMBERS

CHAPTER 8 – DESIGN METHOD

NOTATION

α Imperfection factor for relevant buckling mode

        Constant in the expression for imperfection amplitude (Chapter 2)

β Cross-section slenderness based on the most slender element

β' Cross-section slenderness parameter without considering plate edge restraints

χ Buckling reduction factor for relevant mode

        Aspect ratio for an RHS (= shorter side/longer side, Chapter 6)

δ_u Axial deformation of a stub column at ultimate load

ε Strain

ε_0 Material proof strain (= $\sigma_{0.2}/E_0$)

ε_{cr} Elastic critical buckling stress for a plate

ε_{LB} Deformation capacity of a cross-section defined by the axial strain of a stub column at ultimate load (= δ_u/L)

ε_{nom} Nominal or Engineering strain

ε_{pu} Plastic strain at ultimate stress

$\varepsilon_{t0.2}$ Total strain at 0.2% proof stress

$\varepsilon_{t1.0}$ Total strain at 1% proof stress

ε_{true} True strain

ε_{true}^{pl} True plastic strain

ϕ Coefficient to determine buckling reduction factor χ

ϕ_c Corner enhancement factor

γ Constant in the expression for imperfection amplitude

κ Beam-column interaction coefficient

$\bar{\lambda}$ Non-dimensional column slenderness

$\bar{\lambda}_0$ Limiting slenderness ratio for a specific buckling curve

σ Stress

$\sigma_{0.01}$ 0.01% proof stress

$\sigma_{0.2}$ 0.2% proof stress

$\sigma_{1.0}$ 1% proof stress

$\sigma_{0.2,c}$ 0.2% proof strength of the corner material

$\sigma_{0.2,v}$ 0.2% proof strength of virgin material

σ_{cr} Elastic critical buckling stress of a plate element

σ_{LB} Local buckling stress of a cross-section

σ_u Ultimate stress

$\sigma_{u,c}$ Ultimate strength of corner material

$\sigma_{u,f}$ Ultimate strength of roll-formed flat material

$\sigma_{u,v}$ Ultimate strength of virgin material

σ_y Yield stress

ν Poisson's ratio

e_N Shift in neutral axis when a cross-section is subjected to uniform compression

f_{ya} Average yield strength of a cross-section

f_{yb} Nominal yield strength of the basic material

k Numerical coefficient that depends on the type of forming as follows:

        $k = 7$ for cold rolling

        $k = 5$ for other methods of forming

k_{cor} Proportion of the corner area within a cross-section ($= A_c/A_g$)

m Strain hardening exponent based on $\sigma_{0.2}$ and σ_u

        Numerical exponent (in Equations 4.2 and 4.3)

n Ramberg-Osgood strain hardening exponent,

        Number of 90^0 bends in a cross-section with an internal radius $r \leq 5t$ (fractions of 90^0

        bends should be counted as fractions of n; only in Equation 4.1)

$n'_{0.2,1.0}$ Strain hardening exponent based on $\sigma_{0.2}$ and $\sigma_{1.0}$

r_i Internal radius of a corner.

t Nominal thickness of a plate element

A_c Total area of corners within a cross-section

A_{eff} Effective area for Class 4 (slender) cross-sections

A_f Total area of flat region within a cross-section

A_g Gross cross-sectional area

B_c Numerical constant

C_1 Numerical constant

C_2 Numerical constant

E_0 Young's modulus (initial tangent modulus)

$E_{0.2}$ Tangent modulus (stiffness) at 0.2% proof stress

F_u Peak (ultimate) load of stub column

I Moment of inertia of a cross-section (second moment of area)

K Effective length factor which depends on the column end conditions

L Geometric length or span of a structural element

L_e Effective length of a column

$M_{c,Rd}$ Bending resistance of a cross-section

$M_{y,c,Rd}$ Bending resistance of a cross-section about y axis

$M_{y,Ed}$ Design value of bending moment applied about the y-axis of a cross-section

$M_{z,Ed}$ Design value of bending moment applied about the z axis of a cross-section

$M_{z,c,Rd}$ Bending resistance of a cross-section about z axis

$N_{b,Rd}$ Flexural buckling resistance of a member

N_{cr} Elastic critical buckling load

$N_{c,Rd}$ Compression resistance of a cross-section

N_{Ed} Design value of axial compression applied to a cross-section

LIST OF FIGURES

LIST OF TABLES

CHAPTER - ONE

INTRODUCTION

1.1 BACKGROUND

Stainless steel is gaining wider usage in construction due to its durability, corrosion resistance, ease of maintenance, aesthetics and fire resistance. Although it cannot replace carbon steel and other widely used construction materials, it has an important role where durability, safety or aesthetic requirements cannot be cost effectively met by other materials.

English metallurgist Harry Brearley invented stainless steel in 1912 in his search for an alloy to protect cannon bores from erosion, which led to the first commercial production of stainless steel in August, 1913. During World War I, stainless steel had been used to manufacture valves for aircraft engines. Later, during the period of 1919-1923, Sheffield cutlers started regular production of stainless steel cutlery, surgical scalpels and tools. The first structural appearance of a stainless steel roof occurred in America in 1924. The other significant early use of stainless steel in building construction occurred in 1930, when the top seven arches of The Chrysler Building in New York were designed using stainless steel cladding. Examples of the use of stainless steel in construction are presented in Section 1.3.

In spite of the benefits which stainless steel offers, its application in structures has been inhibited by a lack of appropriate design guidance which makes the optimum use of its properties. Design is primarily based on published rules for carbon steel, even though stainless steel exhibits fundamentally different material behaviour, which includes nonlinear stress-strain characteristics without any well defined yield point, varying elastic modulus and significant strain hardening. Design recommendations for appropriate exploitation of these special features should explore the full potential of the structural use of stainless steel. The recyclabilty, durability and corrosion resistance, which avoids the use of toxic coatings, offered by stainless steel, make it a viable option as an environmentally friendly construction material for building sustainable structures in future.

1.2 MATERIAL PROPERTIES AND CLASSIFICATION

Stainless steel is not a single alloy but rather the name applies to a group of iron based alloys containing a minimum of 10.5% chromium. Chromium is the most important alloying element in stainless steels because it provides their basic corrosion resistance by creating a very thin, invisible surface film in oxidising environments. This film is an oxide that protects the steel from attack in an aggressive environment. As chromium is added to steel, a rapid reduction in corrosion rate is observed to around 10% because of the formation of this protective layer or passive film. In order to obtain a compact and continuous passive film, a chromium content of at least 10.5% is required. Passivity increases fairly rapidly with increasing chromium content up to about 17%.

The other commonly added elements are nickel and molybdenum. Nickel promotes an austenitic structure and increases ductility and toughness. It also reduces the corrosion rate and is thus advantageous in acid environments. Molybdenum substantially increases the resistance to both general and localised corrosion. It increases the mechanical strength and hardness and promotes a ferritic structure.

Over the years since the start of the development of stainless steels the number of grades has increased rapidly. Appendix C shows the stainless steels that are standardised in different parts of the world. Since the structure has a decisive effect on properties, stainless steels have traditionally been divided into categories depending on their microstructure at room temperature. This gives a rough division in terms of both composition and properties. Stainless steels can thus be divided into six groups: austenitic, ferritic, duplex (ferritic-austenitic), martensitic, martensitic-austenitic and precipitation hardening steels. The names of the first five refer to the dominant components of the microstructure, whilst the last group refers to the fact that these steels are hardened by a special mechanism involving the formation of precipitates within the microstructure. Table 1.1 gives a summary of the compositions within these different categories and Figure 1.1 shows a relative comparison of the stress-strain behaviour for the main four categories of stainless steel (Leffler, 2000).

The most widely used stainless grades are the austenitic 1.4301 and 1.4306, which form more than 50% of the global production of stainless steel. The next most widely used grades are the ferritic steels such as 1.4006, followed by the molybdenum-alloyed austenitic steels 1.4401 and 1.4404. These grades together make up over 80% of the total tonnage of stainless steels (Leffler, 2000). The dominant product form for stainless steel is the cold rolled sheet. The

other products such as bars, hot rolled plates, tubes etc. individually form only a third or less of the total amount of cold rolled sheet.

Table 1.1: Composition and properties of different stainless steel categories.

Category	Composition					Ferro-Magnetism
	C	Cr	Ni	Mo	Others	
Austenitic	< 0.08	16-30	8-35	0-7	N, Cu, Ti, Nb	Non-magnetic
Ferritic	< 0.08	12-19	0-5	< 5	Ti	Magnetic
	< 0.25	24-28	-	-	-	
Duplex	< 0.05	18-27	4-7	1-4	N, W	Magnetic
Martesitic	> 0.10	11-14	0-1	-	V	Magnetic
	> 0.17	16-18	0-2	0-2	-	
Martensitic-austenitic	< 0.10	12-18	4-6	1-2	-	Magnetic
Precipitation hardening	-	15-17	7-8	0-2	Al	Magnetic
	-	12-17	4-8	0-2	Al, Cu, Ti, Nb	
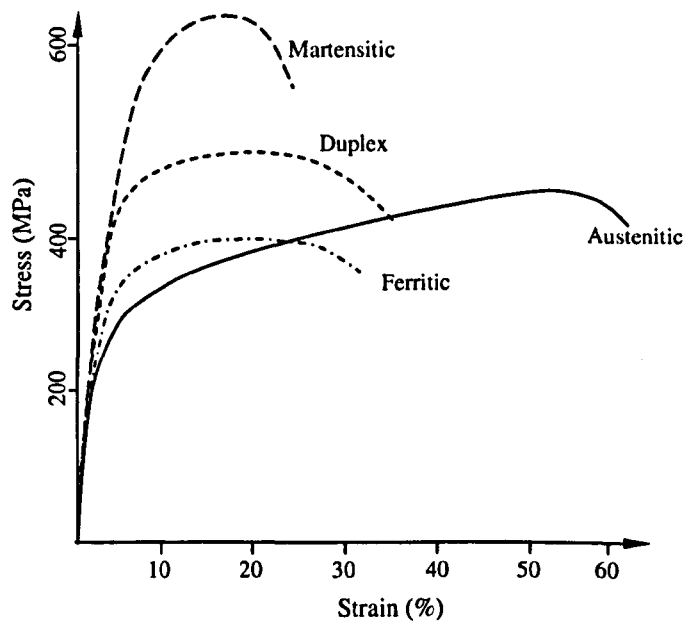
Figure 1.1: Typical stress-strain curves for the primary categories of stainless steel.

1.3 STRUCTURAL IMPORTANCE AND USES IN CONSTRUCTION

The aesthetics of stainless steel has been an important factor in its specification for structural applications. Its appeal results principally from the surface finish and its ability to retain its appearance without deterioration over time. Upper façade of the Chrysler building (1928-30) and the Gateway Arch (1965) are examples of early use of stainless steel in structures as

shown in Figure 1.2(a) and (b). Availability and low initial cost of ordinary steel restricted stainless steel's use primarily to architectural applications, except for use as reinforcing bars in highly corrosive environments such as the Progresso Pier in Mexico (Figure 1.2c). This pier was constructed in 1941 and is still in perfect working condition despite no major maintenance. Another pier, in parallel to the existing, was constructed in 1961 using ordinary steel reinforcement, which has eventually been washed away because of corrosion. These examples clearly verify the durability, corrosion resistance and, of course, low maintenance requirement for stainless steel when compared to ordinary carbon steel.

| (a) Chrysler building, New York (1930) | (b) Gateway Arch, St. Louis (1965) |

(c) Progresso pier, Mexico (1941)
Existing pier built using stainless steel rebar, remains of the other pier using carbon steel.

Figure 1.2: Early uses of stainless steel in structures.

With the advancements in research, stainless steel members are now used structurally in addition to its architectural use. The low maintenance cost, if not zero, is most likely to offer lower life cycle cost than carbon steel. Stainless steel is not only durable but also completely

recyclable and hence it could offer more sustainable solutions to structural design. Moreover, at elevated temperatures, stainless steel offers better retention of strength and stiffness than carbon steel, owing to the beneficial effects of the alloying elements (Gardner, 2005). Thus the cost associated with fire design could be significantly reduced by using stainless steel. Stainless steels, particularly the austenitic grades, offer very high ductility and impact resistance and are, therefore, particularly suited to applications such as offshore structures, crash barriers and structures susceptible to blast loading.

Figure 1.3 shows some modern examples of structural stainless steel in different parts of the world. All the structural components of the recently built (in 1995) greenhouse at Bergianska trädgården, Stockholm, Sweden are made of austenitic Grade 1.4401. The choice of stainless steel was justified by the fact the maintenance would be very complicated without causing harm to the plants. In Singapore, Expo Station is the first Mass Rapid Transport station on the new Changi Airport Line that visitors encounter after leaving the airport. The station has elevated platforms surmounted by two roof structures – one of which is a 38 metre diameter stainless steel disc over the ticket hall constructed in 2001. A very recent monument, the Dublin Spire, has been constructed in 2003 in Dublin, Ireland. It is a 120 m high free standing tapered column made of cold-formed stainless steel plate. In 2004, Paddington Basin, London gained a notch of urbane style with the opening of three pioneering bridges – one of which is the Helix Bridge, which is a glass tube in a stainless steel coil using a previously untested composite fabrication technique. The steel coil rotates at a speed synchronised with the linear motion of the extending and retracting bridge as it moves forward and back across West End Quay, London. These are a few of the diverse uses of stainless steel, in addition to its general application in building frames, in recent times.
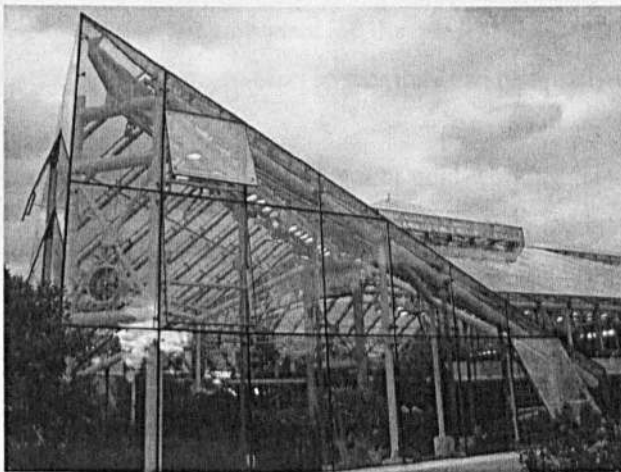
Green house at Bergianska trädgården, Sweden (1995)   Expo Station, Singapore (2001)

Figure 1.3: Recent examples of structural use of stainless steel.

Dublin Spire, Ireland (2003)   The Helix Bridge, London (2004)
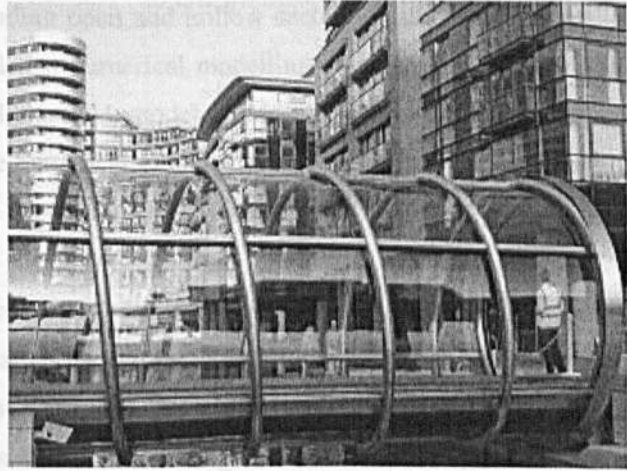
Figure 1.3 (contd.): Recent examples of structural use of stainless steel.

1.4 OUTLINE OF THE THESIS

This chapter provides a broad introduction to the basics of stainless steel as a construction material, its advantages and prospects when compared to ordinary carbon steel and finally some examples showing its evolution in structural applications.

Chapter 2 contains a review of the literature relevant to the present research. The whole subject area has been divided into specific categories to discuss different aspects in the necessary detail. Chapter 3 provides all necessary material and geometrical details for the tests considered in the present research in tabular form to facilitate the development of the design method. Since the proposed method is primarily based on available test data, the whole process of reviewing and retrieving the required test results from the available literature formed a major component of the present research. Test results have been organised and presented in such a fashion so that they can be readily used in further research.

Chapter 4 investigates the effect of cold-working on stainless steel with specific reference to the corner regions within a cross-section. Detailed investigations have been carried out using measurements from the available literature and models have been proposed to predict the corner material strength utilising the basic material properties.

Chapter 5 presents the development and verification of the numerical models used in this research project. Numerical modelling techniques for material behaviour, stub columns, long columns, beams and beam-columns have been considered with special reference to initial imperfections. The whole numerical modelling scheme included different material grades, six

different types of cross-sections including open and hollow sections, and also different end conditions for long columns. A consistent numerical modelling approach has been adopted using a compound Ramberg-Osgood material model, measured geometric properties and predicted initial imperfections. All the numerical models have been verified against available test results and additional results were generated where necessary.

Development of the proposed design method for structural stainless steel is explained in Chapters 6 and 7. Cross-section resistances against compression and bending have been investigated and a more rational design method has been developed in Chapter 6, based on the deformation capacity of cross-sections. Once validated against the test results, this concept is then extended to members in Chapter 7, which investigates the flexural buckling behaviour and beam-column interactions in stainless steel. New sets of column curves and improved interaction formulas have been proposed in Chapter 7.

The developed design method is summarised and demonstrated using worked examples in Chapter 8. The performance of the proposed method has been compared with the existing Eurocode for all available test results.

Finally Chapter 9 provides a review of the important findings from the present research and also identifies the limitations and the scope for further research in this field is required to establish the proposed method into a complete and useful design tool for structural stainless steel.

CHAPTER - TWO

LITERATURE REVIEW

2.1 INTRODUCTION

This chapter reviews several aspects of the use of stainless steel in structural engineering. Widespread study has been made of previous laboratory testing programmes involving the determination of basic material properties leading to its response to cold-working, the evaluation of initial imperfections and finally cross-section and member resistance to different types of loading. This chapter gives a brief description of the key features of each considered testing schemes, whilst Chapter 3 presents all relevant details required to develop the design guidance based on the deformation capacity of cross-sections. Now-a-days numerical modelling techniques are employed in most research projects to produce reliable sets of data based on models that have been validated using available test results. Numerical modelling approaches for stainless steel structures have been discussed herein, identifying the important aspects for use in the present research. Design philosophies of the available guidance on structural stainless steel have also been reviewed with a view to investigating their limitations and exploiting their useful features.

2.2 LABORATORY TESTING PROGRAMMES

All major testing programmes relevant to the present research have been reviewed to obtain the basic data required to develop design guidance for structural stainless steel. Since no laboratory testing was undertaken as a part of the present research, this investigation formed the very basis of the whole project. This section briefly describes the important aspects of the testing programmes; all necessary details are given in Chapter 3.

Johnson and Winter (1966) carried out the early laboratory tests on stainless steel beams with top hat cross-sections and columns with I and box cross-sections. The columns were formed by channel sections joined by means of structural adhesive to avoid material changes due to

welding or punching. All sections were austenitic Grade 1.4301. The research was intended to obtain basic information to be used in developing design guidance. An effective width formulation was proposed to predict the beam response, whereas the tangent modulus approach was found to produce satisfactory predictions for the column strength.

Publication of the first ASCE standard ANSI/ASCE-8-90 in 1990 specifying the design rules for stainless steel structures was the eve for extensive research programmes on stainless steel designed to investigate its performance and hence to modify the proposed formulations. Rasmussen and Hancock (1993a and 1993b) studied the behaviour of stainless steel columns and beams with square and circular hollow sections, SHS and CHS. Tension and compression tests on material coupons cut from the finished specimens were carried out to identify the differences in material response when subjected to different types of loading. The results were compared to the ASCE standard ANSI/ASCE-8-90 (1990) and hence an 'extended version' of this design guidance was proposed to provide more accurate predictions for tubular cross-sections.

Hyttinen (1994) performed tests on SHS beams and beam-columns produced from austenitic and ferritic grades. Material coupons were also tested as a part of the research programme. The results were compared with the guidelines specified for beam-columns in prENV 1993-1-4 (1994) and ANSI/ASCE-8-90 (1990). Hyttinen (1994) proposed to use material properties obtained from the finished tubes instead of using the properties of annealed flat strip as were adopted in both the Eurocode and ASCE design guidance.

Talja and Salmi (1995) carried out a similar test programme on stainless steel SHS and RHS beams, columns and beam-columns produced from austenitic Grade 1.4301. The performance of the beam-column interaction formulas given in prENV 1993-1-4 (1994) was investigated, although no proposals were made in this regard. Later Talja (1997) performed further beam-column tests on welded I sections and circular hollow sections CHS.

Mirambell and Real (2000) investigated the deflections of stainless steel beams by performing tests on SHS and I sections produced from austenitic grades. The obtained deflections both for simply supported and continuous beams were compared to those obtained from ENV 1993-1-4 (1996). Using the secant modulus to determine deflections was found to produce overestimations and hence proposals were made to consider the variation in elastic modulus along the length to obtain more accurate deflection predictions.

Macdonald et al (2000) and Rhodes et al (2000) carried out material coupon and column tests on small lipped channel cross-sections produced from austenitic Grade 1.4301. Material coupons were cut from the finished cross-sections and were tested only in tension. Full cross-sections were also subjected to tensile loading to investigate the effect of cold-working. Concentric and eccentric compression testes were carried out on columns to investigate flexural buckling behaviour and beam-column interactions. Resistances were compared to both ANSI/ASCE-8-90 (1990) and ENV 1993-1-4 (1996) predictions obtained using virgin and full section material properties. Rhodes et al (2000) concluded that the available design approaches greatly under-estimated the bending resistance of cross-sections and produced scattered predictions.

Gardner (2002) performed an extensive laboratory testing programme to investigate the behaviour of austenitic Grade 1.4301 and also the response of stainless steel cross-sections and members when subjected to compression, bending and flexural buckling. The reported test results (Gardner and Nethercot, 2004a and 2004b) performed on hollow sections - SHS, RHS and CHS – make a significant contribution to the understanding of structural stainless steel. A new design approach based on the cross-section deformation capacity was developed for structural hollow sections. The proposed method was found to provide much more accurate predictions than the available Eurocode ENV 1993-1-4 (1996).

Several testing programmes on stainless steel hollow sections have been undertaken in the Hong Kong University of Science and Technology as reported by Young and Hartono (2002), Liu and Young (2003), Young and Liu (2003) and Young and Lui (2005). All these tests involve hollow sections produced mainly from austenitic Grade 1.4301 apart from a few RHS sections of duplex grade. Test programmes were intended to obtain material properties as well as cross-section behaviour through testing of stub columns. Flexural buckling tests on fixed ended columns were also carried out. Test results were compared to predictions obtained from the available design guidance, although no specific design proposals were made in spite of the observed deviations.

Kuwamura et al (2003) provided a significant amount of test data on the behaviour of stainless steel cross-sections by performing 73 stub column tests on 6 different types of section. Most of the aforementioned investigations were limited to hollow sections, whereas Kuwamura (2003) tested angle, channel, lipped channel and I section stub columns along with SHS and CHS. The main purpose of the research was to obtain limiting width-to-thickness ratios for different cross-sections. However the reported load-deformation behaviour of stub columns has been used in the present research to determine the deformation capacities of

cross-sections and thus played a significant role in developing the design method proposed in Chapter 6.

Lecce and Rasmussen (2004a and 2004b) investigated the distortional buckling behaviour of stiffened and unstiffened lipped channel cross-sections produced from austenitic and ferritic grades. Stub column and distortional buckling tests were accompanied by material coupon tests performed both in tension and compression. The obtained results have been used to investigate the performance of North American and Australian/New Zealand standards. The Direct Strength Method (Schafer, 2002) was found to produce better predictions than the considered standards in the case of distortional buckling.

It should be noted that Bredenkamp and van den Berg (1995) performed tests on stainless steel columns produced from ferritic Grade 1.4003. Material coupons were also tested under both tension and compression. The column strengths were predicted using different techniques and the tangent stiffness method was found to produce the best predictions, although some of the reported strengths were even higher than the Euler predictions as discussed in Section 3.5.2. Hence this set of experimental results has not been considered in the present research.

2.3 NUMERICAL MODELLING

Finite Element Analysis (FEA) was first developed in 1943 although its use was restricted to expensive mainframe computers generally owned by the aeronautics, automotive, defense, and nuclear industries until 1980. With the rapid reduction in the cost of computers and the phenomenal increase in computing power, numerical modelling technique using FEA has evolved to an incredible precision. Now-a-days supercomputers are able to produce accurate results for almost all kinds of parameters. Structural engineering has been utilising the full potential of this method to achieve significant savings in both time and cost. Numerical modelling techniques have made it possible to design highly indeterminate and innovative structures that we now see all around the world. In the case of stainless steel, its relatively high cost makes FE modelling almost an inseparable part of research programmes.

Talja and Salmi (1995) employed the general purpose FE package ABQUS V5.2 (1992) to simulate column tests performed on SHS and RHS including both material and geometrical nonlinearities. The cross-sections were modelled using shell elements with the corners being idealised by straight lines.

Stangenberg (2000a and 2000b) reported parametric studies using numerical models for I sections under compression, bending and flexural buckling. The stainless steel members were modelled using the MARC 7.3 program utilising 8-noded thick shell elements. Measured material and geometric properties were incorporated with assumed initial imperfections. The developed models were verified against the test results and later used in parametric studies.

Mirambell and Real (2000) developed numerical models for their tested beams using ABAQUS V5.6 (1996). The performance of the numerical models was in close agreement with the test results for the simply supported beams. However the local buckling effects, which were not considered in the adopted FE modelling technique, resulted in some discrepancies.

Gardner and Nethercot (2004c) reported a 'consistent' approach for modelling stainless steel stub columns and long columns using ABAQUS V5.8 (1999). 9-noded thin shell elements were used to develop the FE models which included material and geometric nonlinearity as well as measured initial imperfections. The results obtained from the developed models were found to be in good agreement with the test results.

Lecce and Rasmussen (2005) developed FE models for stainless steel channel sections based on their performed tests to investigate distortional buckling. Shell elements of FE package ABAQUS V6.4 (2001) have been used in the numerical modelling. More than 500 models with varying geometrical properties were analysed to propose design guidance for simple and lipped channel sections. Measured geometric imperfections and different types of material models based on the measured properties were used to investigate their individual effects on load-end shortening behaviour of stub columns.

Other studies concerning FE modelling of stainless steel structures, although not quite in accordance with the scope of the present research, have been reported by Rasmussen et al (2002) and Boh et al (2004). Rasmussen et al (2002) described the development of numerical models for analysing stainless steel plates in compression using ABAQUS V5.7 (1997). Excellent agreement was reported between the experimental and numerical ultimate loads, load-displacement curves and load-strain curves when the compressive material stress-strain curve was used in the FE models. Boh et al (2004), on the other hand, considered the modelling of stainless steel corrugated panels subjected to blast loading. First order shell elements in ABAQUS V6.3 (2002) were used in the models.

2.4 EFFECTS OF COLD-WORKING ON STAINLESS STEEL

Stainless steel exhibits pronounced strain hardening when subjected to cold-work. Johnson and Winter (1966) observed that the 0.2% proof strength of the cold-formed corner material was approximately 1.5 – 2 times higher than the flat material and hence identified the 'strong effect of cold-working' on both the hardness of cold-rolled sheet and the properties of cold-formed corners. This investigation obliged almost all of the later research programmes to investigate the effect of cold-working on stainless steel.

Mechanical properties of the cold-formed corners have been reported by Coetzee et al (1990), van den Berg and van der Merwe (1992), Rasmussen and Hancock (1993a and 1993b), Hyttinen (1994), Gardner (2002), Gardner and Talja (2003) and Lecce and Rasmussen (2004a). All the reported results have been analysed in Chapter 4 to devise models for the prediction of corner strength using the knowledge of the basic material and geometric properties of a cross-section. In addition to the corner regions, the flat material strength could also be highly affected in the case of roll-formed cross-sections. Using the virgin material strength, which is generally recommended by the existing design codes, significantly under estimates member resistances. All the aforementioned references investigated the material coupons cut from the finished cross-sections and observed significant effects of cold-working. The 0.2% proof strength of the flat material is significantly increased as compared to the virgin sheet and hence recommendations were made to use the appropriate material properties obtained through testing.

2.5 INITIAL IMPERFECTIONS

2.5.1 Geometric imperfections

The importance of initial imperfections has been recognised by researchers for more than three decades. At early stages the research was limited to ordinary carbon steel sections. More recently, the development of design codes for stainless steel requires identification of geometric imperfection characteristics for stainless steel members. This section reviews the investigations, which are in accordance with the scope of the present research, made on local imperfections for both carbon steel and stainless steel. A review on global imperfections for different types of columns is, however, presented in Section 5.4.

Initial plate imperfection amplitude ω_0 is often considered as a fixed multiple of plate thickness, i.e. $\omega_0 = Kt$, where K is a constant. Dawson and Walker (1972) showed that an

adequately conservative fit to test data on cold-formed steel cross-sections could be achieved with an imperfection amplitude of 0.2t. Though this approach is the simplest way of predicting imperfections, its general applicability is questionable since it does not consider the other important parameters such as material strength, fabrication process and boundary conditions. They also proposed the following expressions for the collapse and elastic post-buckling of simply supported, geometrically imperfect plates with stress-free edges, which behave in the same way as the stiffened compression elements of thin-walled structural sections.

$$\frac{\omega_0}{t} = \alpha \left(\frac{\sigma_y}{\sigma_{cr}} \right)^{0.5} \tag{2.1}$$

$$\frac{\omega_0}{t} = \gamma \left(\frac{\sigma_y}{\sigma_{cr}} \right) \tag{2.2}$$

in which ω_0 is the initial imperfection amplitude, t is the plate thickness, σ_y is the material yield stress, σ_{cr} is the plate critical buckling stress and γ and α are constants. These two equations are much more rational in the sense that they include both material property and boundary conditions in addition to the thickness of the plate. The shape of imperfection was taken as the lowest Eigenmode as obtained from buckling analysis.

Hopperstad et al. (1997) studied the reliability of nonlinear finite element analysis in predictions of the ultimate strength of aluminium plates subjected to in-plane compression. Outstand and internal elements, both welded and non-welded, produced from different aluminium alloys were analysed for a wide range of b/t ratios. Cruciform sections were tested to determine the behaviour of outstand elements of varying widths. In the case of outstand elements a geometric imperfection field was introduced with respect to the global co-ordinate system in the finite element model according to Equation 2.3.

$$\omega = \omega_0 \frac{y}{b} \cos \frac{\pi x}{L} \tag{2.3}$$

in which b and L are the plate width and length respectively, whereas, x and y are the global co-ordinate variables. From the numerical study it was observed that the effect of imperfection amplitude diminishes with increasing plate slenderness.

Schafer and Peköz (1998) carried out investigations on the distribution and magnitude of geometric imperfections as well as residual stresses for modelling cold-formed steel members. Experimental results and previous research data were used to propose some rules of thumb for

the prediction of maximum local imperfection in a stiffened element. A simple linear regression analysis based on plate width w yielded Equation 2.4, and an alternative rule based on an exponential fit to the thickness t is given Equation 2.5. These rules of thumb apply only for a width-to-thickness ratio less than 200, and a material thickness of less than 3mm.

$$\omega_0 \approx 0.006w \qquad\qquad (2.4)$$

$$\omega_0 \approx 6te^{-2t} \qquad\qquad (2.5)$$

An experimental program was undertaken to examine the actual imperfection distributions and to check the existence of periodicity in actual members. Imperfection measurements taken on eleven lipped channel sections showed evidence of periodicity in the considered sections. Hence Schafer and Peköz (1998), for a limited study, proposed to use at least two fundamentally different Eigenmode shapes summed together for the imperfection distribution with imperfection magnitudes taken from the reported rules of thumb. But for general study, if modal imperfections are used, a range of imperfection magnitudes should be investigated.

Sun and Butterworth (1998) developed a non-linear finite element model for steel angle compression members eccentrically loaded through one leg. The models incorporated initial geometric imperfections in the form of half sine waves along the length and four different values, 0.167t, 0.333t, 0.5t and 0.667t, as multiples of plate thickness t were used as amplitudes for imperfection distribution. Numerical predictions using an initial imperfection of 0.333t produced the best agreement with the test results.

Chou et al. (2000) conducted FE modelling of cold-formed lipped channel and hat section carbon steel stub-columns with varying imperfection amplitudes. Eigenmodes with different amplitudes obtained from Dawson and Walker's (1972) proposal and also expressed as multiples of the plate thickness were adopted for modelling initial imperfections. Ultimate load predictions obtained using Dawson and Walker's (1972) proposal were consistent, giving the lowest standard deviation.

Gardner (2002) investigated the imperfection profile of stainless steel closed sections experimentally, although, no clear local imperfection mode emerged from the measured data. Hence the lowest buckling mode, obtained from an elastic Eigenmode analysis, was used as the initial local imperfection mode in the FE models. The suitability of Dawson and Walker's (1972) proposed formulations, Equations 2.1 and 2.2, was investigated, and hence Equation 2.6 was proposed, based on the measured imperfections, to be used for roll-formed stainless steel SHS and RHS.

$$\frac{\omega_0}{t} = 0.023\left(\frac{\sigma_{0.2}}{\sigma_{cr}}\right) \tag{2.6}$$

Kaitila (2002) studied the imperfection sensitivity of cold-formed lipped channel columns numerically. A large number of closely spaced Eigenvalues with almost similar Eigenmodes were obtained using elastic buckling analysis. The Eigenmodes, for which Eigenvalues were very close to the local buckling load, were used to represent the distribution of initial imperfection. Amplitude of h/200, where h is the depth of the section, was reported to produce the closest agreement with test results.

Dubina and Ungureanu (2002) investigated the influence of imperfections on cold-formed steel channel and lipped channel sections. Local imperfections were introduced using the following three techniques: (a) symmetrical sine shape, affine with the first local Eigenmode, (b) asymmetrical sine shape, affine with the fifth Eigenmode and (c) real shape obtained from the measured imperfections. Results obtained using the measured imperfections produced the best predictions. However Schafer and Peköz's (1998) proposed amplitudes were recognised to be 'helpful' when used in distributions defined by Eigenmodes.

In a recent study, Lecce and Rasmussen (2005a) reported detailed measurements of imperfections performed using calibrated lasers on stainless steel lipped channel sections. However, no specific pattern for imperfection distribution or magnitude emerged from the obtained results.

A summary of the discussed literature on local imperfections is presented in Table 5.4.

2.5.2 Residual stresses

Residual stresses are the stresses which exist within a member even when no external loading is applied. These stresses are introduced during the manufacturing process due to differential cooling or inelastic material deformations because of bending. However, if the material properties are obtained from the coupons cut from the finished cross-sections, the bending residual stresses are automatically re-introduced within the coupons and explicit recognition of such stresses is not necessary (Rasmussen and Hancock, 1993 and Gardner, 2002). It is the thermal residual stresses that require appropriate recognition.

Stainless steel has a higher coefficient of thermal expansion, and a lower value of thermal conductivity than carbon steel. It is therefore likely that thermal residual stresses would be

greater in stainless steel cross-sections. Bredenkamp et al (1992) observed that the magnitude of residual stresses in built-up stainless steel I-sections were of the same order as in the equivalent carbon steel section, although Lagerqvist and Olsson (2001) carried out a similar study and found considerably higher residual stresses in the stainless steel sections. However these are too few investigations to make any general guidelines on the distribution and magnitude of thermal residual stresses. Hence, in FE modelling, higher magnitudes for initial imperfection amplitude are often adopted to make allowance for residual stresses (Stangenberg 2000a and 2000b).

Gardner (2002), after reviewing the available relevant literature, used an idealised rectangular distribution around the weld for thermal residual stresses in cold-formed stainless steel SHS and RHS. However, when incorporated into the FE models, residual stresses did not seem to have any significant effect on the load deformation behaviour of stub columns.

Section 5.3.7 explains the techniques adopted in the present study and shows the effects of thermally induced residual stresses on stainless steel cross-sections.

2.6 DESIGN GUIDANCE ON STRUCTURAL STAINLESS STEEL

The early tests on stainless steel recognised the requirement of special design considerations for such a nonlinear material with low proportionality and extensive strain hardening capabilities. The first design guidance on stainless steel was published by the American Iron and Steel Institute in 1968, and was entitled 'Specification for the design of light gage cold-formed stainless steel structural members'. The proposed design rules were based primarily on the work carried out by Johnson and Winter (1966). Availability of more test results provided better understanding of the material and member behaviour and consequently a revised version of the Code was published in 1974 (AISI, 1974).

In 1990, the first ASCE standard ANSI/ASCE-8-90 entitled 'Specification for the design of cold-formed stainless steel structural members' was published by the American Society of Civil Engineers to provide the LRFD and ASD criteria for the design of structural stainless steel. This ASCE standard has been revised in 2002 as SEI/ASCE 8-02 based on a larger amount of available test data. Proposed modifications have recently been outlined by Lin et al (2005).

The publication of 'Design Manual for Structural Stainless Steel' was sponsored by the Nickel Development Institute, NiDI in 1994, on behalf of the members of the European

Stainless Steel Development and Information group, Euro Inox. The contents of this Manual relate to an in-depth study carried out by the Steel Construction Institute on the structural application of stainless steel for onshore and offshore structures. This Manual was prepared for the guidance of suitably qualified engineers experienced in the design of carbon steel structural steelwork though not necessarily in stainless steel structures. It comprised (a) Part I – The Recommendations, which were formulated in terms of limit state philosophy and, where appropriate, comply with those in the ENV 1993-1-1 (1992) (b) Part II – The Commentary to allow designers to assess the basis of the Recommendations and to facilitate the development of revisions as and when new data become available and (c) Part III – The Design Examples to demonstrate the use of the Recommendations. The second edition of this Design Manual has been published by Euro Inox in 2002 entitled 'Design Manual for Structural Stainless Steel'. It was prepared by The Steel Construction Institute exploiting the test results of the ECSC funded project 'Development of the use of stainless steel in construction'. This project also led to the scope of the Manual being extended to cover circular hollow sections and fire resistant design.

Eurocode 3 deals with the design of steel structures. Part 1.1, containing general rules and rules for buildings, was issued by CEN as ENV 1993-1-1 in 1992. At the same time, work started to prepare a Eurocode covering the design of structural stainless steel, and later, it was published as ENV 1993-1-4 in 1996. It gives supplementary provisions for the design of buildings and civil engineering works using austenitic and duplex stainless steel. The basic approach followed in ENV 1993-1-4 (1996) was to adopt the rules for carbon steel and make modifications as necessary where stainless steel test data indicated different behaviour. In the cases where no data were available, the rules for carbon steel were generally suggested. The revised and updated version prEN 1993-1-4 has recently been published in 2004. It includes modified material definition, cross-section classification and column buckling curves based on available test results.

Baddoo and Burgan developed a design guide entitled 'Structural design of stainless steel' based on recommendations provided in BS 5950: Part 1 (2000). The Steel Construction Institute published this design guidance in 2000. It includes recommendations, design examples, section properties and member capacities for commonly used stainless steel sections produced from the widely used grades including the austenitic Grade 1.4301, 1.4401 and 1.4404 and duplex Grade 1.4362 and 1.4462. This guide provides recommendations on the selection of an appropriate grade depending on usage, information on the mechanical and physical properties of stainless steel, different aspects related to material behaviour, cross-section and member design as well as connections, fabrication and fire resistant design. A

comprehensive set of design tables is presented, giving gross and effective section properties, section classification and member capacities for a wide range of cold formed stainless steel sections.

All the aforementioned design codes are based on analogies with carbon steel and hence adopt the traditional cross-section classification system based on an elastic, perfectly-plastic material model. Experimental evidence has now established that stainless steel exhibits completely nonlinear stress-strain behaviour, for which a continuous approach would be more appropriate. A 'new approach' for the structural design of stainless steel hollow sections was developed by Gardner and Nethercot (2004d), which utilises the material nonlinearity, determines the deformation capacity of cross-sections using a continuous slenderness parameter without making any section classification and hence provides accurate predictions for cross-section resistances. The performance of the proposed method was validated for SHS, RHS and CHS and, on average, 21% increase in member resistances was achieved when compared to ENV 1993-1-4 (1996).

2.7 DISCUSSION

A brief overview of the subject areas covered within this thesis has been presented in this chapter. Detailed review of the relevant literature is presented in the later chapters where appropriate. Research in stainless steel structures has flourished during the last decade although the focus has been limited to experimental investigations and validation of the available design codes. Design recommendations have not really overcome the barrier of retaining the analogies with ordinary carbon steel and hence appropriate exploitation of the material behaviour has been nonexistent. The new approach proposed by Gardner and Nethercot (2004d) has explored a new technique for designing nonlinear metallic materials without using the traditional section classification system. The present research is aimed at providing a generalised design method for structural stainless steel utilising its special features yet producing designer friendly guidance by optimising the required volume of calculations.

CHAPTER - THREE

TEST RESULTS

3.1 INTRODUCTION

In structural engineering, laboratory testing of structural components plays a very significant role in understanding the behaviour of a material and a structure as a whole. All the proposed design rules are either based on or verified against test results. As a part of the present study, a substantial number of test results from different sources have been analysed to identify the special characteristics of stainless steel which were, later, used to investigate the behaviour of stainless steel members, resulting in more rational design proposals by providing appropriate recognition of these features.

Mechanical properties of metallic materials are obtained through tension tests on standard coupons collected either from a virgin sheet or from within a cross-section. Like all metallic structures stainless steel members are also formed of thin plates which are often susceptible to buckling. But unlike other steels, stainless steel exhibits significantly different stress-strain behaviour in tension and compression, which was first reported by Johnson and Winter (1966). Hence design of stainless steel structures should not rely only on the conventional tension coupon tests, rather, accurate knowledge of compression behaviour is required. Coupon tests performed on different grades of stainless steel have been analysed to establish relationships between the tensile and compressive properties. Moreover, coupons cut from the corner regions of finished cross-sections have also been tested to investigate the effect of strain hardening on stainless steel as explained in detail in Chapter 4.

Stub columns are tested to investigate the behaviour of cross-sections as well as to understand the interaction between individual plate elements within a cross-section. Structural members such as long columns and beams are tested to obtain a real picture of the interaction between the local and global phenomena. All these test results have been used not only to devise new

design methods but also to validate the FE models used to conduct parametric studies as explained in Chapter 5.

3.2 MATERIAL COUPON TESTS

All available coupon test results have been analysed to obtain a comprehensive view of the special characteristics such as rounded, nonlinear stress-strain behaviour, relatively low proportional limit and very high ductility as offered by stainless steel. In the absence of any well-defined yield point the design strength for stainless steel is normally taken as 0.2% material proof stress which is denoted as $\sigma_{0.2}$. Stainless steel is very sensitive to cold-working which results in a significant increase in $\sigma_{0.2}$ with a corresponding decrease in ductility. This phenomenon is explained in Chapter 4 by comparing the strength of a virgin sheet to that of the finished cross-section and also by studying the properties of cold-worked corners. Compressive coupons are now tested in many research schemes involving stainless steel to understand the behaviour of structural components more accurately. Most of the tests involve austenitic Grade 1.4301 since this the most commonly used form of structural stainless steel.

3.2.1 Uniaxial tests on stainless steel coupons

Rasmussen and Hancock (1993a and 1993b) conducted tensile and compressive coupon tests on material cut from cold-formed stainless steel SHS made of austenitic Grade 1.4306. Longitudinal tension and compression coupons were cut from two flat faces and one corner region. The tension and compression coupons were reported to be curved longitudinally after being cut from the section because of the through thickness residual stresses. However, it was believed, these stresses were re-introduced within the coupons when they were straightened (elastically) prior to testing. Tensile coupons were tested in accordance with AS 1391 using a low strain rate (<15 $\mu\varepsilon$/s) at strains less than 20000μs, whereas, at higher strains, the strain rate was increased up to 500 $\mu\varepsilon$/s. In the case of compression coupons a bracing jig was used to prevent lateral buckling. Young and Liu (2003), Liu and Young (2003) and Lecce and Rasmussen (2004a) followed the same standard with similar loading rates for their tested coupons.

Talja and Salmi (1995) carried out tests on tension and compression coupons cut from the flat faces of SHS and RHS of austenitic Grade 1.4301. The main purpose of the study was to provide test data for the development of Eurocode 3. EN 10002-1 (1990) has been followed in the testing scheme. A lower rate of 0.311 mm/min was used for strains below 0.2% (equivalent to 43.2 $\mu\varepsilon$/s for a specimen length of 120 mm). The strain rate was increased to

10.4 mm/min (equivalent to 1445 $\mu\varepsilon$/s) beyond 0.2% strain. Macdonald et al (2000) followed the same standard for testing tensile coupons cut from the cold-formed lipped channels.

Gardner (2002) carried out a comprehensive investigation into the behaviour of austenitic Grade 1.4301. Tension and compression coupons were cut from the cold-formed and annealed hollow cross-sections. Coupons were tested following ASTM 370-87a (1987) keeping the strain rates within the specified limits. A specially designed bracing jig was used to test the compression coupons. Mirambell and Real (2000) reported tension tests conducted by the stainless steel producers following the same standard on coupons extracted from cold-formed stainless steel SHS and RHS, and welded I sections.

Other available stainless steel coupon tests have been reported by Korvink et al (1995), Stangenberg (2000a) and Laubscher and van der Merwe (2003). All the reported mechanical properties are summarised in Tables 3.1 – 3.4. The most commonly reported parameters are initial elastic modulus E_0, 0.2% proof stress $\sigma_{0.2}$ and Ramberg-Osgood parameter n. Two other important parameters – ratio of 1% proof stress to 0.2% proof stress $\sigma_{1.0}/\sigma_{0.2}$ and strain hardening exponent $n'_{0.2,1.0}$ to define the curve between these two proof stresses are also reported in these Tables. These values are the best-fit to the experimental results. Nonlinear material modelling techniques are, however, explained in Chapter 5.

Table 3.1: Mechanical properties for austenitic Grade 1.4301 in tension.

Reference	Section and its forming process		Testing standard	E_0 (N/mm^2)	$\sigma_{0.2}$ (N/mm^2)	σ_u (N/mm^2)	ε_u	$\sigma_{1.0}/\sigma_{0.2}$	Ramberg-Osgood coefficients	
									n	$n'_{0.2.1.0}$
Talja and Salmi (1995)	SHS 60×60×5	Roll-formed	SFS-EN 10002 – 1 (1990)	185000	566	753	42	1.12	4.8	3.6
	SHS 60×60×5	Roll-formed		181000	530	669	45	1.11	4.1	3.7
	SHS 60×60×5	Roll-formed		184000	544	761	48	1.13	4.7	3.5
Macdonald et al (2000)	CL 28×15×8×2.5	Roll-formed	BS EN 10002 – 1 (1991)	n/a	480	553	n/a	1.08	6.2	3.9
	CL 38×17×10×3	Roll-formed		n/a	460	541	n/a	1.08	7.5	4.0
Mirambell and Real (2000)	SHS 80×80×3	Roll-formed	ASTM	165600	422	658	n/a	1.16	4.8	3.3
	RHS 120×80×4	Roll-formed		161200	442	661	n/a	1.15	6.2	3.4
Gardner (2002)	SHS 80×80×4	Roll-formed	ASTM A370 – 87a (1987)	186600	457	706	43	1.15	5.0	3.5
	SHS 100×100×2	Roll-formed		201300	382	675	56	1.11	6.6	2.8
	SHS 100×100×3	Roll-formed		195800	388	691	57	1.12	5.6	3.2
	SHS 100×100×4	Roll-formed		191300	465	713	45	1.12	5.7	3.7
	SHS 100×100×6	Roll-formed		198400	501	715	39	1.14	5.2	3.9
	SHS 100×100×8	Roll-formed		202400	328	653	52	1.15	6.4	2.6
	SHS 150×150×4	Roll-formed		206000	314	659	54	1.14	6.8	2.2
	RHS 60×40×4	Roll-formed		192800	489	705	40	1.21	3.9	4.6
	RHS 120×80×3	Roll-formed		209300	419	739	54	1.16	4.1	3.6
	RHS 120×80×6	Roll-formed		194500	509	714	40	1.12	5.3	3.6
	RHS 150×100×4	Roll-formed		205800	297	663	62	1.16	8.0	2.4
	RHS 100×50×2	Roll-formed		208000	403	707	57	1.10	6.9	2.6
	RHS 100×50×3	Roll-formed		203600	479	716	48	1.18	4.2	4.2
	RHS 100×50×4	Roll-formed		208000	471	702	45	1.13	5.2	3.5
	RHS 100×50×6	Roll-formed		187200	605	754	36	1.13	5.7	4.5

Table 3.1(contd.): Mechanical properties for austenitic Grade 1.4301 in tension.

Reference	Section and its forming process		Testing standard	E_0 (N/mm²)	$\sigma_{0.2}$ (N/mm²)	σ_u (N/mm²)	ε_u	$\sigma_{1.0}/\sigma_{0.2}$	Ramberg-Osgood coefficients	
									n	$n'_{0.2,1.0}$
Young and Liu (2003)	RHS 120×40×2	Roll-formed	AS 1391 (1991)	198000	350	649	72	1.19	5.0	2.9
	RHS 120×40×5	Roll-formed		194000	424	676	61	1.16	5.0	3.2
	RHS 120×80×3	Roll-formed		193000	366	648	68	1.18	5.0	3.0
	RHS 120×80×6	Roll-formed		194000	443	678	61	1.16	5.0	3.3
Liu and Young (2003)	SHS 70×70×2	Roll-formed	AS 1391 (1991)	195000	337	636	60	1.19	4.0	2.8
	SHS 70×70×5	Roll-formed		194000	444	688	61	1.16	5.0	3.3
Talja and Salmi (1995)	RHS 150×100×3	Press-braked	SFS-EN 10002 – 1 (1990)	197200	294	626	66	1.20	5.9	2.6
	RHS 150×100×6	Press-braked		193600	339	651	59	1.19	7.1	2.9
	RHS 150×100×6	Press-braked		198200	320	668	66	1.20	5.1	2.7
Korvink et al (1995)	Flat plate	-	n/a	184960	280	713	60	1.20	5.9	2.7
	Flat Plate (T)	-		194400	278	688	61	1.19	5.9	2.7
Stangenberg (2000)	I 160×80	Welded	n/a	198000	300	624	n/a	1.20	6.4	2.7
	I 160×80	Welded		202000	299	610	n/a	1.20	5.3	2.8
	I 160×160	Welded		198000	300	624	n/a	1.20	6.4	2.7
	I 160×160	Welded		198000	300	610	n/a	1.20	5.3	2.7
	I 320×160	Welded		198000	300	624	n/a	1.20	6.4	2.7
	I 320×160	Welded		201000	304	615	n/a	1.19	5.8	2.7
Kuwamura (2003)	L, C, Lip C, I	Press-braked	n/a	203000	279	641	n/a	1.21	5.0	2.6
Lecce and Rasmussen (2004a)	Lip C	Press-braked	AS 1391 (1991)	193000	251	703	76	1.22	5.0	2.3

Table 3.2: Mechanical properties for austenitic Grade 1.4301 in compression.

Reference	Section and its forming process		Testing standard	E_0 (N/mm^2)	$\sigma_{0.2}$ (N/mm^2)	$\sigma_{1.0}/\sigma_{0.2}$	Ramberg-Osgood coefficients	
							n	$n'_{0.2,1.0}$
Talja and Salmi (1995)	SHS 60×60×5	Roll-formed	SFS- EN 10002 – 1	186500	463	1.17	3.2	3.2
Gardner (2002)	SHS 80×80×4	Roll-formed	ASTM A370 – 87a (1987)	203200	416	1.31	3.5	3.1
	SHS 100×100×2	Roll-formed		207100	370	1.21	4.7	2.4
	SHS 100×100×3	Roll-formed		208800	379	1.23	3.8	2.6
	SHS 100×100×4	Roll-formed		203400	437	1.29	3.9	2.9
	SHS 100×100×6	Roll-formed		197900	473	1.25	4.4	2.6
	SHS 100×100×8	Roll-formed		205200	330	1.19	6.4	2.1
	SHS 150×150×4	Roll-formed		195400	294	1.24	4.5	2.3
	RHS 60×40×4	Roll-formed		193100	469	1.32	3.6	3.0
	RHS 120×80×3	Roll-formed		197300	429	1.25	4.2	2.9
	RHS 120×80×6	Roll-formed		192300	466	1.27	4.4	2.8
	RHS 150×100×4	Roll-formed		200300	319	1.21	4.7	2.0
	RHS 100×50×2	Roll-formed		205900	370	1.19	5.2	2.4
	RHS 100×50×3	Roll-formed		200900	455	1.26	4.1	3.0
	RHS 100×50×4	Roll-formed		203900	439	1.28	3.8	3.3
	RHS 100×50×6	Roll-formed		206300	494	1.31	4.0	3.2
Talja and Salmi (1995)	RHS 150×100×3	Press-braked	SFS- EN 10002 – 1	206600	305	1.20	4.8	2.6
	RHS 150×100×6	Press-braked		204800	345	1.20	3.2	2.9
Korvink et al (1995)	Flat Plate	-	n/a	175320	264	1.20	5.2	2.4
	Flat Plate (T)	-		192150	280	1.20	5.3	2.5
Lecce and Rasmussen (2004a)	Lipped C	Press-braked	AS 1391 (1991)	187000	242	1.20	8.0	2.2

Table 3.3: Mechanical properties for austenitic Grade 1.4306.

Reference	Section and its forming process		Test type	Testing standard	E_0 (N/mm^2)	$\sigma_{0.2}$ (N/mm^2)	σ_u (N/mm^2)	ε_u	$\sigma_{1.0}/\sigma_{0.2}$	Ramberg-Osgood coefficients	
										n	n'$_{0.2,1.0}$
Rasmussen and Hancock (1993a and 1993b)	SHS 80×80×3	Roll-formed	Tension	AS 1391 (1991)	194000	420	695	49.6	1.17	4.9	3.1
	SHS 80×80×3	Roll-formed	Tension		194000	395	695	49.5	1.18	4.5	3.1
	SHS 80×80×3	Roll-formed	Tension		195000	420	695	48	1.20	3.7	3.2
	SHS 80×80×3	Roll-formed	Tension (T)		187000	415	640	49	1.18	4.0	3.1
	SHS 80×80×3	Roll-formed	Compression		195000	420	-	-	1.16	4.2	3.0
	SHS 80×80×3	Roll-formed	Compression		197000	410	-	-	1.17	4.1	3.1
	SHS 80×80×3	Roll-formed	Compression		196000	440	-	-	1.18	3.6	3.1
	SHS 80×80×3	Roll-formed	Compression (T)		199000	505	-	-	1.17	4.6	3.2
Mirambell and Real (2000)	I 100×100	Welded	Tension	ASTM	160110	414	605	n/a	1.15	6.4	3.1

Note: (T) refers to coupons collected from the transverse direction of roll-forming.

Table 3.4: Mechanical properties for ferritic Grades 1.4016 and 1.4003 and duplex Grade 1.4462.

Grade	Reference	Section and its forming process		Test type	Testing standard	E_0 (N/mm²)	$\sigma_{0.2}$ (N/mm²)	ε_u	$\sigma_{1.0}/\sigma_{0.2}$	Ramberg-Osgood coefficients n	$n'_{0.2,1.0}$
Ferritic 1.4016	Korvink et al (1995)	Flat plate	-	Tension	n/a	190930	308	32	1.16	6.5	3.2
		Flat plate	-	Tension (T)		212510	334	30	1.16	6.2	3.2
		Flat plate	-	Compression		186040	312	-	1.17	6.3	3.1
		Flat plate	-	Compression (T)		214720	344	-	1.15	6.6	3.2
	Lecce and Rasmussen (2004a)	Lip C	Press-braked	Tension	AS 1391 (1991)	185000	291	34	1.15	7.0	3.3
		Lip C	Press-braked	Compression		193000	271	-	1.17	6.0	3.1
Ferritic 1.4003	Korvink et al (1995)	Flat plate	-	Tension	n/a	188300	277	n/a	1.14	7.0	3.3
		Flat plate	-	Tension (T)		219700	302	n/a	1.15	7.2	3.4
		Flat plate	-	Compression		204080	269	-	1.15	7.3	3.3
		Flat plate	-	Compression (T)		224450	300	-	1.14	7.5	3.2
	Laubscher and van der Merwe (2003)	Angle	Hot-rolled	Tension	n/a	204800	307	37	1.15	7.0	3.2
		Angle	Hot-rolled	Compression		205000	325	-	1.14	7.5	3.4
	Lecce and Rasmussen (2004a)	Lip C	Press-braked	Tension	AS 1391 (1991)	195000	338	37	1.14	7.0	3.4
		Lip C	Press-braked	Compression		208000	339	-	1.14	8.0	3.4
Duplex 1.4462	Stangenberg (2000)	I 160x160	Welded	Tension	n/a	202000	524	n/a	1.15	4.6	3.3
		I 160x160	Welded	Tension		201000	522	n/a	1.14	5.4	3.4

Note: (T) refers to coupons collected from the transverse direction of roll-forming.

3.2.2   Analysis of coupon test results

The coupon test results presented in Tables 3.1 to 3.4 have been grouped according to the Grade and process of manufacturing. Stainless steel members used in structures are generally cold-formed. These sections are formed following two different processes – roll-forming and press-braking. These processes play an important role in the material behaviour since stainless steel is very sensitive to cold-working. In the case of the press-braking process the stress-strain behaviour of the flat region within a section remains almost the same as the virgin plate, but there is a localised increase in $\sigma_{0.2}$ near the corner regions. On the other hand, the roll-forming process causes significant changes to the flat material properties since the whole section is subjected to strain hardening to some extent. Hence the coupons extracted from the roll-formed sections and those from the press-braked sections show significantly different values for $\sigma_{0.2}$ as given in Table 3.1. Welded sections are also grouped with the press-braked ones since the plates used to form the sections do not undergo any cold-working during the forming process.

A considerable amount of coupon tests is available only for austenitic Grade 1.4301 since this is the most commonly used grade in structural applications. A total of 41 tension and 21 compression coupon test results, many of which are actually reported average values from a larger number of individual coupons, are presented in Table 3.1 and 3.2 respectively. Johnson and Winter (1966) first reported the difference in tension and compression behaviour of stainless steel. Later Talja and Salmi (1995), Korvink et al (1995), Gardner and Nethercot (2004a), Lecce and Rasmussen (2004a) conducted series of tests to investigate this phenomenon. Gardner (2002) concluded that, on average, the $\sigma_{0.2}$ is 5% lower in compression than in tension and also investigated the changes in the shape of material stress-strain behaviour in terms of Ramberg-Osgood parameters n and $n'_{0.2,1.0}$. Lecce and Rasmussen (2004a) also observed similar reduction in strength for compression coupons when compared to the tension coupons extracted from the same source.

From the present study it is observed that for austenitic Grade 1.4301, $\sigma_{0.2}$ in compression is approximately 7% lower than the corresponding $\sigma_{0.2}$ in tension. Thus, if a compression member is to be designed based on the tensile material properties, it is proposed herein to reduce the material strength by 7%. However, for all other grades, no specific pattern emerged by analysing the available test results, and hence it is proposed to use tensile material properties in absence of any compression data. The limited number of material coupons do not provide any evidence to suggest compression properties to be different from tensile.

3.2.3   Compound Ramberg-Osgood parameters for material modelling

The material model adopted in the present research involves a two stage Ramberg-Osgood curve which is explained in detail in Chapter 5. This type of formulation requires two exponential parameters n and $n'_{0.2,1.0}$ to define the degree of roundness of the stress-strain behaviour before and after $\sigma_{0.2}$. The adopted model (Gardner and Ashraf, 2006) uses another important parameter 1% proof stress $\sigma_{1.0}$ which could easily be expressed as a fixed multiple of $\sigma_{0.2}$ for different grades. Availability of considerable amount of test data made it possible to investigate difference in tension and compression as well as the forming process for austenitic Grade 1.4301. The compound Ramberg-Osgood parameters for different grades are given in Table 3.5. These values can readily be used to obtain stress-strain behaviour up to 10% plastic strain which could well be regarded as the maximum deformation limit for a structure.

Table 3.5: Compound Ramberg-Osgood parameters obtained from coupon test results.

Type	Grade	Forming process	Tension / Compression	n	$n'_{0.2,1.0}$	$\sigma_{1.0}/\sigma_{0.2}$
Austenitic	1.4301	Press-braked	Tension	5.8	2.7	1.20
			Compression	5.3	2.5	1.20
		Roll-formed	Tension	5.4	3.4	1.14
			Compression	4.3	2.7	1.25
	1.4306	-	-	4.4	3.1	1.17
Ferritic	1.4016	-	-	6.4	3.2	1.16
	1.4003	-	-	7.3	3.3	1.14
Duplex	1.4462	-	-	5.0	3.4	1.15

Figures 1 and 2 show typical stress-strain curves for different grades of stainless steel using the average values of compound Ramberg-Osgood parameters from Table 3.4 and the average values for $\sigma_{0.2}$ as obtained from the Tables 3.1 to 3.4.
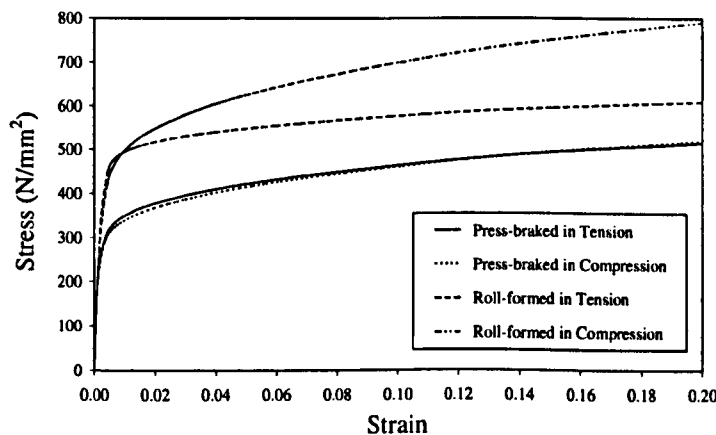
Figure 3.1: Average stress-strain curves up to 20% strain for austenitic Grade 1.4301.
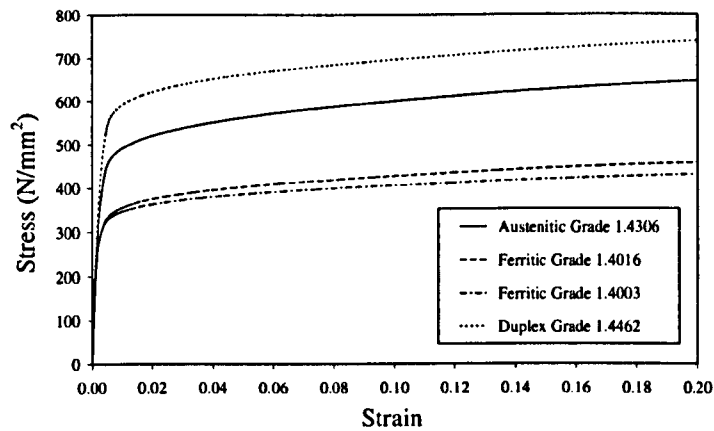
Figure 3.2: Average stress-strain curves up to 20% strain for austenitic Grade 1.4306, ferritic Grades 1.4016, 1.4003 and duplex Grade 1.4462.

3.3 COMPRESSION TESTS ON STAINLESS STEEL STUB COLUMNS

Stub columns are tested to investigate the interaction among different elements within a cross-section as well as to understand the effect of cold-working and initial imperfections on the structural response of a cross-section as a whole. Guidelines provided by the Structural Stability Research Council (Galambos, 1998) state that for cold-formed shapes the optimum length of a stub column should neither be less than 3 times the maximum dimension of the cross-section nor more than 20 times the least radius of gyration of the cross-section so that it is sufficiently short not to fail by overall buckling, yet still long enough to contain representative initial member imperfections. The present research is based on the deformation capacity of cross-sections which is obtained from load-deformation behaviour of stub columns. Hence all available stub column tests on stainless steel stub columns have been analysed to obtain a generalised relationship between the deformation capacity and the resistance of a cross-section under compression. The development of the design process is discussed in detail in Chapter 6 although the definitions of the basic parameters are explained in the following sections.

3.3.1 Cross-section slenderness β

All current design codes classify the cross-sections depending on the width-to-thickness b/t ratios of constituent plate elements within a cross-section. Recognising the continuous stress-strain behaviour of stainless steel, Gardner (2002) proposed a continuous slenderness parameter β to replace the traditional classification approach. This cross-section parameter β includes not only the geometric dimensions but also the material properties and plate boundary conditions.

The elastic critical buckling strain ε_{cr} of a perfect, uniformly compressed flat plate, where buckling occurs in the elastic range, is given by Equation 3.1.

$$\varepsilon_{cr} = \frac{k\pi^2}{12(1-v^2)(b/t)^2}$$ (3.1)

in which v is Poisson's ratio, b is the plate width, t is the plate thickness and k is the buckling coefficient dependent upon edge restraint and loading conditions. The elastic critical buckling strain can be normalised by the elastic strain at the material compressive 0.2% proof stress, defined as $\varepsilon_0 = \sigma_{0.2}/E_0$, to give Equation 3.2.

$$\frac{\varepsilon_{cr}}{\varepsilon_0} = \frac{E_0 k\pi^2}{12\sigma_{0.2}(1-v^2)(b/t)^2} = \frac{k\pi^2}{12(1-v^2)}\frac{1}{\beta'^2}$$ (3.2)

in which the geometrical and material property variables of the plate have been grouped into the single slenderness parameter, β' given by Equation 3.3. The effective flat plate width b for different cross-sections will be measured according to Table 3.6. The parameters $\sigma_{0.2}$ and E_0 will be based on material stress-strain behaviour in compression.

$$\beta' = \frac{b}{t}\sqrt{\frac{\sigma_{0.2}}{E_0}}$$ (3.3)
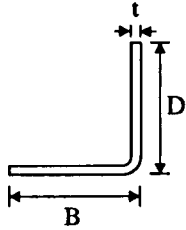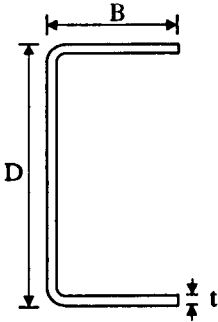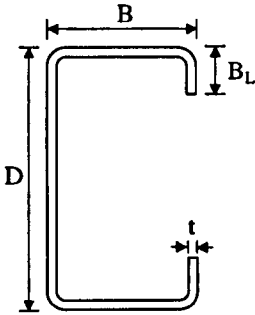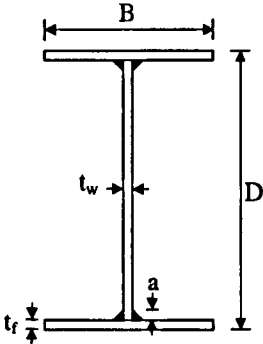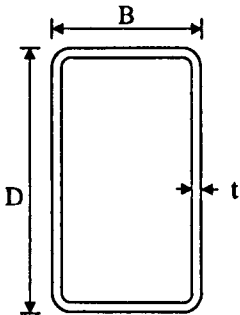
Gardner (2002) modified this definition of β' to account for elements subjected to non-uniform compression by multiplying the right hand side of Equation 3.3 by $\sqrt{4/k}$, where k is the classical buckling coefficient. This coefficient also takes into account of the boundary conditions of plate elements (e.g. $k = 23.9$ and 0.43 for a simply supported plate in pure bending and for an outstand element in pure compression respectively). Thus the generalised form of cross-section slenderness β is given by Equation 3.4

$$\beta = \frac{b}{t}\sqrt{\frac{\sigma_{0.2}}{E_0}}\sqrt{\frac{4}{k}}$$ (3.4)

where k is equivalent to the buckling factor defined as k_σ for internal and outstand compression elements in Tables 4.1 and 4.2 of prEN 1993-1-5 (2003).

Plate buckling, however, only occurs wholly in the elastic range for slender plates, and Equation 3.1 has to be modified to allow for effects including inelastic plate buckling, although the definition of β will remain unchanged.

Table 3.6: Nominal and effective dimensions of compression elements used in the present study.

Section type	Nominal section designations	Effective widths for compressed elements
Angle	$L\,D \times B \times t$	$b_{flange} = B - t/2$ $b_{web} = D - t/2$
Channel	$C\,D \times B \times t$	$b_{flange} = B - t/2$ $b_{web} = D - t$
Lipped channel	$CL\,D \times B \times B_L \times t$	$b_{flange} = B - t$ $b_{web} = D - t$ $b_{lip} = B_L - t/2$
I section	$I\,D \times B \times t_f \times t_w$	$b_{flange} = B/2 - t/2 - a$ $b_{web} = D - 2t_f - 2a$
Rectangular hollow section (RHS)	$D \times B \times t$	$b_{flange} = B - t$ $b_{web} = D - t$

3.3.2 Cross-section deformation capacity ε_{LB}

The basic measure of cross-section deformation capacity adopted in the proposed method has been derived from the load-end shortening responses of stub columns. The deformation capacity of a cross-section ε_{LB} is defined by the end shortening δ_u (corresponding deformation at the ultimate load F_u), as shown in Figure 3.4, divided by the initial length of the stub column L as given by Equation 3.5. This, however, is the axial strain of a stub column at the point of initiation of local buckling and hence it could be named as the local buckling strain of a cross-section.

$$\varepsilon_{LB} = \frac{\delta_u}{L} \tag{3.5}$$
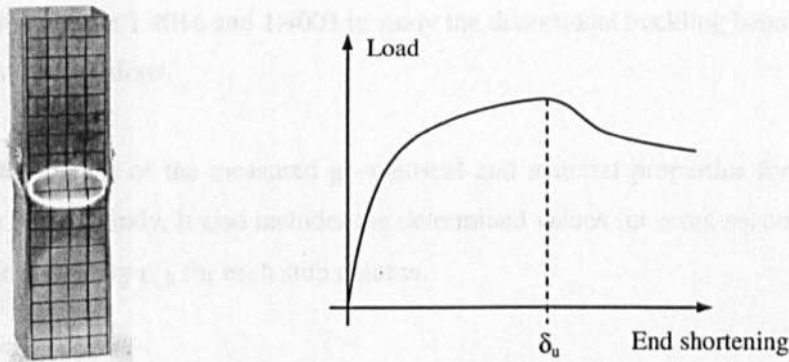
Figure 3.3: Deformed stub column specimens (tested by Gardner, 2002) and typical load-end shortening response of a stub column.

To allow for differences in material properties, the local buckling strain ε_{LB} has been normalised by the elastic strain at the material 0.2% proof stress ε_0, where $\varepsilon_0 = \sigma_{0.2}/E_0$.

3.3.3 Cross-section slenderness β and normalised deformation capacity $\varepsilon_{LB}/\varepsilon_0$ for the tested stub columns

Tests on stainless steel stub columns with hollow cross-sections (SHS and RHS) have been reported by Rasmussen and Hancock (1990), Talja and Salmi (1995), Talja (1997), Gardner (2002), Young and Liu (2003) and Liu and Young (2003). Among these testing schemes Gardner's (2002) was the most extensive involving testing a total of 17 SHS and 18 RHS stub columns having a wide range of variation in plate slenderness. Gardner (2002) used available test results to develop his proposed method for the prediction of compression strength of stainless steel hollow sections. The success of the proposed method for hollow sections opened the way for its extension to cover all types of sections. With a view to obtaining a generalised method to include all types of cross-sections, stub column tests performed on open sections as reported by

Stangenberg (2000a), Kuwamura (2003) and Lecce and Rasmussen (2004a) have been used in the present research.

Kuwamura (2003) investigated the local buckling behaviour of thin-walled stainless steel sections through an extensive testing scheme. A total of 63 stub columns from austenitic Grades 1.4301 and 1.4318 with angle, channel, lipped channel, I and square hollow cross-sections were tested. All the sections were cold-formed by press-braking at the corners apart from the welded I sections. Stangenberg (2000a) reported stub column tests on welded I sections, conducted as a part of the ECSC funded project 'Development of use of stainless steel in construction'. Three specimens were made from austenitic Grade 1.4301 while the other one was from duplex Grade 1.4462. Lecce and Rasmussen (2004a) tested lipped channel stub columns produced from austenitic Grade 1.4301 and ferritic Grades 1.4016 and 1.4003 to study the distortional buckling behaviour of cold-formed stainless steel sections.

Table 3.7 lists the details of the measured geometrical and material properties for stub column tests used in the present study. It also includes the determined values for cross-section slenderness β and deformation capacity ε_{LB} for each stub column.

Table 3.7: Details of stub column test results used in the present research.

Section type	Reference	Grade	Nominal size	L (mm)	$\sigma_{0.2}$ (N/mm^2)	E_0 (N/mm^2)	ε_0 ($\sigma_{0.2}/E_0$)	β	δ_u (mm)	ε_{LB} (δ_u/L)	$\varepsilon_{LB}/\varepsilon_0$
Angle	Kuwamura (2003)	1.4301	25 × 25 × 3	75	279	200000	0.0014	0.91	1.28	0.0171	12.23
			30 × 30 × 3	90	279	200000	0.0014	1.11	0.70	0.0078	5.58
			40 × 40 × 3	120	279	200000	0.0014	1.50	0.50	0.0042	2.99
			40 × 40 × 3	120	279	200000	0.0014	1.49	0.45	0.0038	2.69
			50 × 50 × 3	150	279	200000	0.0014	1.89	0.31	0.0021	1.48
			60 × 60 × 3	180	279	200000	0.0014	2.24	0.25	0.0014	1.00
		1.4318	25 × 25 × 3	75	508	187000	0.0027	1.27	1.12	0.0149	5.50
			30 × 30 × 3	90	508	187000	0.0027	1.53	0.95	0.0106	3.89
			40 × 40 × 3	120	508	187000	0.0027	2.03	0.57	0.0048	1.75
			40 × 40 × 3	120	508	187000	0.0027	2.03	0.60	0.0050	1.84
			50 × 50 × 3	150	508	187000	0.0027	2.56	0.48	0.0032	1.18
			60 × 60 × 3	180	508	187000	0.0027	3.07	0.45	0.0025	0.92
Channel	Kuwamura (2003)	1.4301	50 × 25 × 3	150	279	190000	0.0015	0.93	2.10	0.0140	9.53
			80 × 40 × 3	240	279	190000	0.0015	1.53	1.10	0.0046	3.12
			100 × 50 × 3	300	279	190000	0.0015	1.94	0.90	0.0030	2.04
			100 × 50 × 3	300	279	190000	0.0015	1.92	0.84	0.0028	1.91
			150 × 50 × 3	450	279	190000	0.0015	1.94	0.85	0.0019	1.29
			50 × 50 × 3	150	279	190000	0.0015	1.92	0.70	0.0047	3.18
		1.4318	50 × 25 × 3	150	508	180000	0.0028	1.26	2.00	0.0133	4.72
			80 × 40 × 3	240.5	508	180000	0.0028	1.82	1.40	0.0058	2.06
			100 × 50 × 3	300	508	180000	0.0028	2.34	1.00	0.0033	1.18
			100 × 50 × 3	300	508	180000	0.0028	2.37	1.00	0.0033	1.18
			150 × 50 × 3	450.5	508	180000	0.0028	2.59	1.45	0.0032	1.14

Table 3.7 (contd.): Details of stub column test results used in the present research.

Section type	Reference	Grade	Nominal size	L (mm)	$\sigma_{0.2}$ (N/mm²)	E_0 (N/mm²)	ε_0 ($\sigma_{0.2}/E_0$)	β	δ_u (mm)	ε_{LB} (δ_u/L)	$\varepsilon_{LB}/\varepsilon_0$
Lipped Channel	Kuwamura (2003)	1.4301	100 × 50 × 20 × 3	300	279	186000	0.0015	1.29	1.50	0.0050	3.33
			150 × 50 × 20 × 3	450	279	186000	0.0015	1.95	1.60	0.0036	2.37
			150 × 65 × 20 × 3	450	279	186000	0.0015	1.96	1.20	0.0027	1.78
			200 × 75 × 25 × 3	600	279	186000	0.0015	2.63	1.40	0.0023	1.56
			35 × 17 × 7 × 1	100	279	187500	0.0015	1.31	0.62	0.0062	4.17
			50 × 17 × 7 × 1	150	279	187500	0.0015	2.00	0.50	0.0033	2.24
			50 × 25 × 7 × 1	150	279	187500	0.0015	2.00	0.60	0.0040	2.69
			70 × 25 × 8 × 1	200	279	187500	0.0015	2.74	0.45	0.0023	1.51
		1.4318	100 × 50 × 20 × 3	300	508	180000	0.0028	1.71	2.15	0.0072	2.54
			150 × 50 × 20 × 3	450	508	180000	0.0028	2.60	1.75	0.0039	1.38
			150 × 65 × 20 × 3	450	508	180000	0.0028	2.60	1.80	0.0040	1.42
			200 × 75 × 25 × 3	600	508	180000	0.0028	3.48	2.00	0.0033	1.18
	Lecce and Rasmussen (2004a)	1.4301	105 × 90 × 13 × 2	800	242	187000	0.0013	1.92	n/a	n/a	n/a
			105 × 90 × 13 × 2	800	242	187000	0.0013	1.91	n/a	n/a	n/a
			105 × 90 × 13 × 2	600	242	187000	0.0013	1.90	n/a	n/a	n/a
			105 × 90 × 13 × 2	600	242	187000	0.0013	1.90	n/a	n/a	n/a
		1.4016	67 × 57 × 8 × 1.13	800	271	193000	0.0014	2.21	n/a	n/a	n/a
			67 × 57 × 8 × 1.13	800	271	193000	0.0014	2.21	n/a	n/a	n/a
			55 × 55 × 8 × 1.13	780	271	193000	0.0014	1.82	n/a	n/a	n/a
			55 × 55 × 8 × 1.13	782	271	193000	0.0014	1.81	n/a	n/a	n/a
		1.4003	105 × 85 × 15 × 2	1175	339	208000	0.0016	2.10	n/a	n/a	n/a
			105 × 85 × 15 × 2	1178	339	208000	0.0016	2.10	n/a	n/a	n/a

Table 3.7 (contd.): Details of stub column test results used in the present research.

Section type	Reference	Grade	Nominal size	L (mm)	$\sigma_{0.2}$ (N/mm²)	E_0 (N/mm²)	ε_0 ($\sigma_{0.2}/E_0$)	β	δ_u (mm)	ε_{LB} (δ_u/L)	$\varepsilon_{LB}/\varepsilon_0$
I	Stangenberg (2000)	1.4301	160 × 80 × 10 × 6	451	279	200000	0.0015	0.79	10.00	0.0222	14.78
			160 × 160 × 10 × 6	447	279	198000	0.0015	0.82	7.60	0.0170	11.22
			320 × 160 × 10 × 6	894	279	200000	0.0015	1.79	5.70	0.0064	4.25
		1.4462	160 × 160 × 10 × 7	449	524	202000	0.0026	1.08	6.80	0.0151	5.84
	Kuwamura (2003)	1.4301	50 × 50 × 3 × 3	150	279	200000	0.0014	0.79	2.40	0.0160	11.47
			50 × 100 × 3 × 3	300	279	200000	0.0014	1.75	0.82	0.0027	1.96
			100 × 50 × 3 × 3	300	279	200000	0.0014	1.14	1.40	0.0047	3.35
			100 × 75 × 3 × 3	300	279	200000	0.0014	1.29	1.07	0.0036	2.56
			100 × 100 × 3 × 3	300	279	200000	0.0014	1.77	0.50	0.0017	1.19
			150 × 100 × 3 × 3	450	279	200000	0.0014	1.76	0.60	0.0013	0.96
			200 × 100 × 3 × 3	600	279	200000	0.0014	2.41	0.80	0.0013	0.96
			200 × 150 × 3 × 3	600	279	200000	0.0014	2.74	0.8	0.0013	0.96
		1.4318	50 × 50 × 3 × 3	150	508	194000	0.0026	1.03	1.55	0.0103	3.95
			50 × 100 × 3 × 3	300	508	194000	0.0026	2.35	1.00	0.0033	1.27
			100 × 50 × 3 × 3	300	508	194000	0.0026	1.52	1.40	0.0047	1.78
			100 × 75 × 3 × 3	300	508	194000	0.0026	1.70	1.10	0.0037	1.40
			100 × 100 × 3 × 3	300	508	194000	0.0026	2.33	0.80	0.0027	1.02
			150 × 100 × 3 × 3	450	508	194000	0.0026	2.36	1.25	0.0028	1.06
			200 × 100 × 3 × 3	600	508	194000	0.0026	3.22	1.05	0.0018	0.67
			200 × 150 × 3 × 3	600	508	194000	0.0026	3.64	1.45	0.0024	0.92

Table 3.7 (contd.): Details of stub column test results used in the present research.

Section type	Reference	Grade	Nominal size	L (mm)	$\sigma_{0.2}$ (N/mm^2)	E_0 (N/mm^2)	ε_0 ($\sigma_{0.2}/E_0$)	β	δ_u (mm)	ε_{LB} (δ_u/L)	$\varepsilon_{LB}/\varepsilon_0$
SHS	Rasmussen and Hancock (1990)	1.4306	80 × 80 × 3	300	415	196000	0.0021	1.19	2.0	0.0067	3.17
			80 × 80 × 3	298	415	196000	0.0021	1.18	2.2	0.0074	3.52
	Talja & Salmi (1995)	1.4301	60 × 60 × 5	399	463	186500	0.0025	0.57	9.40	0.0236	9.49
	Gardner (2002)	1.4301	80 × 80 × 4	400	457	186600	0.0024	1.02	7.40	0.0185	7.55
			80 × 80 × 4	400	457	186600	0.0024	0.99	7.20	0.0180	7.35
			80 × 80 × 4	399	457	186600	0.0024	0.99	7.70	0.0193	7.87
			80 × 80 × 4	400	261	206300	0.0013	0.71	8.60	0.0215	16.98
			80 × 80 × 4	400	261	206300	0.0013	0.73	7.10	0.0178	14.04
			100 × 100 × 2	401	370	207100	0.0018	2.18	1.10	0.0017	0.95
			100 × 100 × 2	400	370	207100	0.0018	2.17	0.90	0.0016	0.90
			100 × 100 × 3	400	379	208800	0.0018	1.44	2.20	0.0055	3.03
			100 × 100 × 3	400	379	208800	0.0018	1.46	2.30	0.0058	3.17
			100 × 100 × 4	400	437	203400	0.0021	1.16	4.00	0.0100	4.66
			100 × 100 × 4	400	437	203400	0.0021	1.16	4.00	0.0100	4.65
			100 × 100 × 6	400	473	197900	0.0024	0.77	13.40	0.0335	14.02
			100 × 100 × 6	400	473	197900	0.0024	0.78	13.50	0.0338	14.13
			100 × 100 × 8	399	330	205200	0.0016	0.46	29.00	0.0727	45.18
			100 × 100 × 8	400	330	205200	0.0016	0.46	38.20	0.0955	59.38
			150 × 150 × 4	450	294	195400	0.0015	1.52	1.70	0.0038	2.51
			150 × 150 × 4	451	294	195400	0.0015	1.52	1.60	0.0036	2.36

Table 3.7 (contd.): Details of stub column test results used in the present research.

Section type	Reference	Grade	Nominal size	L (mm)	$\sigma_{0.2}$ (N/mm^2)	E_0 (N/mm^2)	ε_0 ($\sigma_{0.2}/E_0$)	β	δ_u (mm)	ε_{LB} (δ_u/L)	$\varepsilon_{LB}/\varepsilon_0$
SHS	Kuwamura (2003)	1.4301	$50 \times 50 \times 3$	150	279	190500	0.0015	0.62	3.68	0.0245	16.75
			$75 \times 75 \times 3$	225	279	190500	0.0015	0.94	2.17	0.0096	6.59
			$100 \times 100 \times 3$	300	279	190500	0.0015	1.27	1.32	0.0044	3.00
			$125 \times 125 \times 3$	375	279	190500	0.0015	1.61	0.93	0.0025	1.69
			$150 \times 150 \times 3$	450	279	190500	0.0015	1.94	0.66	0.0015	1.00
			$200 \times 200 \times 3$	600	279	190500	0.0015	2.59	0.6	0.0010	0.68
		1.4318	$50 \times 50 \times 3$	150	508	184000	0.0028	0.83	3.54	0.0236	8.55
			$75 \times 75 \times 3$	225	508	184000	0.0028	1.25	2.06	0.0092	3.32
			$100 \times 100 \times 3$	300	508	184000	0.0028	1.70	1.34	0.0045	1.62
			$125 \times 125 \times 3$	375	508	184000	0.0028	2.14	1.07	0.0029	1.03
			$150 \times 150 \times 3$	451	508	184000	0.0028	2.58	1.26	0.0028	1.01
			$200 \times 200 \times 3$	600	508	184000	0.0028	3.44	1.41	0.0024	0.85
RHS	Talja and Salmi (1995)	1.4301	$150 \times 100 \times 3$	1048	305	206600	0.0015	1.97	3.70	0.0035	2.39
			$150 \times 100 \times 6$	1049	345	240800	0.0014	0.95	12.00	0.0114	7.98
	Gardner (2002)	1.4301	$60 \times 40 \times 4$	180	469	193100	0.0024	0.72	6.70	0.0372	15.30
			$60 \times 40 \times 4$	180	469	193100	0.0024	0.72	6.70	0.0373	15.36
			$120 \times 80 \times 3$	360	429	197300	0.0022	1.86	1.60	0.0044	2.04
			$120 \times 80 \times 3$	360	429	197300	0.0022	1.88	1.60	0.0044	2.04
			$120 \times 80 \times 6$	360	466	192300	0.0024	0.96	7.80	0.0217	8.94
			$120 \times 80 \times 6$	360	466	192300	0.0024	0.96	7.90	0.0219	9.05
			$150 \times 100 \times 4$	450	319	200300	0.0016	1.53	2.50	0.0056	3.49
			$150 \times 100 \times 4$	450	319	200300	0.0016	1.52	2.30	0.0051	3.21

Table 3.7 (contd.): Details of stub column test results used in the present research.

Section type	Reference	Grade	Nominal size	L (mm)	$\sigma_{0.2}$ (N/mm^2)	E_0 (N/mm^2)	ε_0 ($\sigma_{0.2}/E_0$)	β	δ_u (mm)	ε_{LB} (δ_u/L)	$\varepsilon_{LB}/\varepsilon_0$
RHS	Gardner (2002)	1.4301	$100 \times 50 \times 2$	301	370	205900	0.0018	2.24	1.20	0.0040	2.22
			$100 \times 50 \times 2$	300	370	205900	0.0018	2.26	1.30	0.0043	2.41
			$100 \times 50 \times 3$	300	455	200900	0.0023	1.60	1.80	0.0060	2.65
			$100 \times 50 \times 3$	300	455	200900	0.0023	1.60	1.80	0.0060	2.65
			$100 \times 50 \times 4$	300	439	203900	0.0022	1.19	3.50	0.0117	5.41
			$100 \times 50 \times 4$	301	439	203900	0.0022	1.21	3.70	0.0123	5.72
			$100 \times 50 \times 6$	300	494	206300	0.0024	0.77	9.30	0.0310	12.95
			$100 \times 50 \times 6$	300	494	206300	0.0024	0.77	9.80	0.0327	13.64

3.4 BENDING TESTS ON STAINLESS STEEL BEAMS

Stainless steel beams were first tested by Johnson and Winter back in 1966. They performed four-point bending tests on hat sections produced from austenitic Grade 1.4301. The flexural specimens were designed to fail either in local buckling or by material yielding. Rasmussen and Hancock (1993b) reported bending tests performed on roll-formed SHS. Talja and Salmi (1995) carried out 4 point bending tests on press-braked hollow sections, 3 SHS and 6 RHS, produced from austenitic Grade 1.4301. Talja (1997) as a part of the ECSC funded project 'Development of the use of stainless steel in construction' performed tests on welded I beams produced from austenitic Grade 1.4301 and duplex Grade 1.4462. Mirambell and Real (2000) investigated the bending behaviour of stainless steel beams by performing 4 point bending tests on roll-formed SHS and welded I sections. All specimens were manufactured from austenitic Grades 1.4301 and 1.4306. Gardner (2002) in his comprehensive testing scheme tested a total of 9 hollow beams, 5 of which were SHS while the remaining 4 were RHS, made of austenitic Grade 1.4301.

In the case of bending, in most practical cases, the strength of a cross-section is determined by its compression flange whose behaviour is analogous to that of a stub column under compression. The bending test results were, therefore, used to verify the method developed for pure compression since in all of the reported bending tests, failure was initiated by the local buckling of the compression flange. However the cross-section slenderness β is capable of taking into account of local buckling of the web in bending by using an appropriate value for k, if this occurs. The complete details of the sections and material properties are given in Chapter 6 where the results have been used to verify the proposed method for bending. Table 3.8 gives a summary of the test results used in the present study.

Table 3.8: Summary of bending test results used in the present research.

Reference	Grade	Section type	No. of tests	Loading configuration
Rasmussen and Hancock (1993b)	1.4306	SHS	1	Simply supported beam loaded at quarter points.
Talja and Salmi (1995)	1.4301	SHS	3	Simply supported beam loaded at quarter points.
	1.4301	RHS	6	
Stangenberg (2000a)	1.4301	I	3	Simply supported beam loaded at quarter points.
	1.4462	I	1	
Mirambell and Real (2000)	1.4306	I	2	Simply supported beam loaded at mid-span.
	1.4301	SHS	2	
	1.4301	RHS	2	
Gardner (2002)	1.4301	SHS	5	Simply supported beam loaded at mid-span.
	1.4301	RHS	4	

3.5 FLEXURAL BUCKLING TESTS ON STAINLESS STEEL COLUMNS

Stainless steel columns have been tested in different parts of the world during the last decade to investigate the suitability of the preliminary design codes which are based on the analogies with carbon steel. These tests produced invaluable sets of data to investigate the differences between carbon steel and stainless steel. The flexural buckling curves in Eurocode 3 Part 1.4, prEN 1993-1-4 (2004), have been revised following the patterns obtained from the test results to take appropriate account of the special features of stainless steel, yet keeping the basic form of the equations to be the same as the Perry-Robertson type formulation. The main research has primarily been limited to comparing test results to the existing design codes. The present research exploits all available test results to propose modified buckling curves which do not require use of the traditional section classification, but, at the same time follow the same type of formulation as Perry-Robertson.

3.5.1 Details of test results

Johnson and Winter (1966) tested a series of pin-ended columns fabricated from austenitic Grade 1.4301. Two types of column, one comprising channels placed back to back to form an I section while the other was fabricated from identical channels placed together to form a box section, were tested to validate the tangent modulus formula for column strength prediction. Rasmussen and Hancock (1993a) reported tests performed on cold-formed SHS columns, having the same cross-section but three different lengths, produced from austenitic Grade 1.4301. Bredenkamp and van den Berg (1995) investigated the performance of built-up I sections manufactured from ferritic Grade 1.4003. Each of the two different cross-sections was tested for various lengths with pinned end conditions. Talja and Salmi (1995) tested SHS and RHS columns produced from austenitic Grade 1.4301. The testing scheme was designed to provide test results for the development of the Eurcode for stainless steel members. A total of 9 columns, 6 of which were arranged to buckle about the major axis, were tested. Ala-Outinen and Oskanen (1997) reported tests on 2 SHS columns produced from austenitic Grade 1.4301. Stangenberg (2000b) reported tests performed on welded I section columns buckled against both the major and the minor axes. The columns were produced from austenitic Grade 1.4301 and duplex Grade 1.4462. Rhodes et al (2000) investigated the performance of stainless steel lipped channel columns produced from austenitic Grade 1.4301. Two different sections were used to obtain a total of 22 columns by changing the overall length. Gardner (2002) tested a total of 20 long columns, 8 SHS and 12 RHS, having a wide variation in cross-sectional dimensions. All the columns were produced from austenitic Grade 1.4301. Liu and Young (2003) and Young and Liu (2003) reported buckling tests performed on fixed-ended SHS and RHS columns respectively. Six different cross-sections, roll-

formed from austenitic Grade 1.4301, were used to produce a total of 24 long columns. All necessary geometrical and material properties are given in Tables 3.9 and 3.10. These tables include determined values for the conventional buckling parameters such as effective length L_e, elastic critical buckling load for the relevant axis of buckling N_{cr} and non-dimensional overall column slenderness $\bar{\lambda}$ which are expressed in Equations 3.6 to 3.9. It is worth mentioning that Table 3.9 and 3.10 do not show the traditional cross-section 'Class' i.e. Class 1, 2, 3 or 4, although the overall column slenderness $\bar{\lambda}$ has been determined based on A_{eff} where appropriate. The cross-section classifications are reported in Chapter 8 where the performance of the proposed method has been compared against the existing Eurocode prEN 1993-1-4 (2004).

$$L_e = KL \tag{3.6}$$

$$N_{cr} = \frac{\pi^2 E_0 I}{L_e^2} \tag{3.7}$$

$$\bar{\lambda} = \sqrt{\frac{A_g \sigma_{0.2}}{N_{cr}}} \quad \text{for Class 1, 2 and 3 cross-sections} \tag{3.8}$$

$$\bar{\lambda} = \sqrt{\frac{A_{eff} \sigma_{0.2}}{N_{cr}}} \quad \text{for Class 4 cross-sections} \tag{3.9}$$

where

K   is the effective length factor which depends on the column end conditions

E_0 is the Young's modulus (initial tangent modulus) under compression

I   is the moment of inertia about the axis of buckling

A_g is the gross cross-sectional area

A_{eff} is the effective cross-sectional area

$\sigma_{0.2}$ is the material 0.2% proof stress in compression

N_{cr} is the elastic critical buckling load

Table 3.9: Minor axis flexural buckling tests performed on stainless steel columns.

Section type	Reference	Grade	Nominal size	A_g (mm^2)	L (mm)	End condition	L_e (mm)	$\sigma_{0.2}$ (N/mm^2)	E_0 (N/mm^2)	N_{cr} (kN)	$\bar{\lambda}$
I	Bredencamp and van den Berg (1995)	1.4003	140 × 70 × 4.5 × 3.5	1106	878	Pin-ended	878	366	196600	665	0.75
			140 × 70 × 4.5 × 3.5	1106	1100	Pin-ended	1100	366	196600	424	0.94
			140 × 70 × 4.5 × 3.5	1106	1282	Pin-ended	1282	366	196600	312	1.09
			140 × 70 × 4.5 × 3.5	1106	1675	Pin-ended	1675	366	196600	183	1.43
			140 × 70 × 4.5 × 3.5	1106	1883	Pin-ended	1883	366	196600	145	1.60
			140 × 70 × 4.5 × 3.5	1106	2295	Pin-ended	2295	366	196600	97	1.96
			140 × 70 × 4.5 × 3.5	1106	2685	Pin-ended	2685	366	196600	71	2.29
			140 × 70 × 4.5 × 3.5	1106	3580	Pin-ended	3580	366	196600	40	3.05
			180 × 90 × 6 × 4.5	1884	1674	Pin-ended	1674	350	196400	501	1.10
			180 × 90 × 6 × 4.5	1884	2293	Pin-ended	2293	350	196400	267	1.51
			180 × 90 × 6 × 4.5	1884	2573	Pin-ended	2573	350	196400	212	1.69
			180 × 90 × 6 × 4.5	1884	3190	Pin-ended	3190	350	196400	138	2.10
			180 × 90 × 6 × 4.5	1884	3541	Pin-ended	3541	350	196400	112	2.33
	Stangenberg (2000b)	1.4301	160 × 80 × 10 × 6	2397	650	Pin-ended	650	279	200000	3842	0.42
			160 × 80 × 10 × 6	2445	1248	Pin-ended	1248	279	200000	1094	0.79
			160 × 80 × 10 × 6	2424	2046	Pin-ended	2046	279	200000	392	1.31
			160 × 160 × 10 × 6	3965	1248	Pin-ended	1248	281	200000	8347	0.37
			160 × 160 × 10 × 6	3990	2049	Pin-ended	2049	280	199000	3154	0.60
			160 × 160 × 10 × 6	3981	3347	Pin-ended	3347	281	200000	1180	0.97

Table 3.9 (contd.): Minor axis flexural buckling tests performed on stainless steel columns.

Section type	Reference	Grade	Nominal size	A_g (mm^2)	L (mm)	End condition	L_e (mm)	$\sigma_{0.2}$ (N/mm^2)	E_0 (N/mm^2)	N_{cr} (kN)	$\bar{\lambda}$
			28 × 15 × 8 × 2.5	143	1222	Pin-ended	1222	446	200000	5.0	3.58
			28 × 15 × 8 × 2.5	143	1122	Pin-ended	1122	446	200000	5.9	3.29
			28 × 15 × 8 × 2.5	143	1022	Pin-ended	1022	446	200000	7.1	3.00
			28 × 15 × 8 × 2.5	143	922	Pin-ended	922	446	200000	8.7	2.70
			28 × 15 × 8 × 2.5	143	822	Pin-ended	822	446	200000	11.0	2.41
			28 × 15 × 8 × 2.5	143	722	Pin-ended	722	446	200000	14.3	2.12
			28 × 15 × 8 × 2.5	143	622	Pin-ended	622	446	200000	19.2	1.82
			28 × 15 × 8 × 2.5	143	522	Pin-ended	522	446	200000	27.3	1.53
			28 × 15 × 8 × 2.5	143	422	Pin-ended	422	446	200000	41.7	1.24
			28 × 15 × 8 × 2.5	143	322	Pin-ended	322	446	200000	71.7	0.94
Lip C	Rhodes et al (2000)	1.4301	28 × 15 × 8 × 2.5	143	222	Pin-ended	222	446	200000	150.8	0.65
			38 × 17 × 10 × 3	229	1222	Pin-ended	1222	428	200000	10.7	3.02
			38 × 17 × 10 × 3	229	1122	Pin-ended	1122	428	200000	12.7	2.77
			38 × 17 × 10 × 3	229	1022	Pin-ended	1022	428	200000	15.3	2.52
			38 × 17 × 10 × 3	229	922	Pin-ended	922	428	200000	18.9	2.28
			38 × 17 × 10 × 3	229	822	Pin-ended	822	428	200000	23.7	2.03
			38 × 17 × 10 × 3	229	722	Pin-ended	722	428	200000	30.7	1.78
			38 × 17 × 10 × 3	229	622	Pin-ended	622	428	200000	41.4	1.54
			38 × 17 × 10 × 3	229	522	Pin-ended	522	428	200000	58.8	1.29
			38 × 17 × 10 × 3	229	422	Pin-ended	422	428	200000	90.0	1.04
			38 × 17 × 10 × 3	229	322	Pin-ended	322	428	200000	154.6	0.80
			38 × 17 × 10 × 3	229	222	Pin-ended	222	428	200000	325.2	0.55

Table 3.9 (contd.): Minor axis flexural buckling tests performed on stainless steel columns.

Section type	Reference	Grade	Nominal size	A_g (mm^2)	L (mm)	End condition	L_e (mm)	$\sigma_{0.2}$ (N/mm^2)	E_0 (N/mm^2)	N_{cr} (kN)	$\bar{\lambda}$
SHS	Rasmussen and Hancock (1993a)	1.4306	80 × 80 × 3	900	1001	Pin-ended	1001	415	194000	1659	0.46
			80 × 80 × 3	900	2000	Pin-ended	2000	415	194000	425	0.93
			80 × 80 × 3	900	3002	Pin-ended	3002	415	194000	190	1.38
	Talja and Salmi (1995)	1.4301	60 × 60 × 5	999	1050	Pin-ended	1050	463	185500	818	0.75
			60 × 60 × 5	999	1700	Pin-ended	1700	463	181000	305	1.23
			60 × 60 × 5	999	2350	Pin-ended	2350	463	184000	162	1.69
	Ala-Outinen and Oskanen (1997)	1.4301	40 × 40 × 4	519	889	Pin-ended	889	592	197980	265	1.08
			40 × 40 × 4	519	888	Pin-ended	888	592	197980	266	1.08
	Gardner (2002)	1.4301	80 × 80 × 4	1093	1900	Pin-ended	1900	416	203200	570	0.89
			80 × 80 × 4	1106	2001	Pin-ended	2001	416	203200	520	0.94
			100 × 100 × 2	723	2000	Pin-ended	2000	370	207125	586	0.53
			100 × 100 × 3	1089	2000	Pin-ended	2000	379	208800	877	0.63
			100 × 100 × 4	1410	2000	Pin-ended	2000	437	203400	1069	0.76
			100 × 100 × 6	2145	2000	Pin-ended	2000	473	197900	1516	0.82
			100 × 100 × 8	2778	2000	Pin-ended	2000	330	205200	1931	0.69
			150 × 150 × 4	2159	2000	Pin-ended	2000	294	195350	3662	0.38
	Liu and Young (2003)	1.4301	70 × 70 × 2	513	1199	Fixed-ended	600	313	195000	2095	0.26
			70 × 70 × 2	522	2000	Fixed-ended	1000	313	195000	764	0.43
			70 × 70 × 2	515	2801	Fixed-ended	1400	313	195000	385	0.60
			70 × 70 × 2	516	3599	Fixed-ended	1800	313	195000	235	0.77
			70 × 70 × 5	1212	1199	Fixed-ended	600	413	194000	4469	0.33
			70 × 70 × 5	1223	2000	Fixed-ended	1000	413	194000	1612	0.56
			70 × 70 × 5	1222	2799	Fixed-ended	1400	413	194000	820	0.78
			70 × 70 × 5	1212	3600	Fixed-ended	1800	413	194000	496	1.00

Table 3.9 (contd.): Minor axis flexural buckling tests performed on stainless steel columns.

Section type	Reference	Grade	Nominal size	A_g (mm^2)	L (mm)	End condition	L_e (mm)	$\sigma_{0.2}$ (N/mm^2)	E_0 (N/mm^2)	N_{cr} (kN)	$\bar{\lambda}$
RHS	Gardner (2002)	1.4301	100×50×3	807	2000	Pin-ended	2000	455	200900	173	1.36
			100×50×4	1018	2000	Pin-ended	2000	439	203900	212	1.44
			100×50×6	1559	2000	Pin-ended	2000	494	206267	299	1.61
			120×80×3	1101	1999	Pin-ended	1999	429	197300	582	0.82
			120×80×6	2115	2000	Pin-ended	2000	466	192300	1006	0.99
			150×100×4	1787	2000	Pin-ended	2000	319	200260	1482	0.59
			60×40×4	673	1000	Pin-ended	1000	469	193100	303	1.02
			100×50×2	522	1000	Pin-ended	1000	370	205900	477	0.55
			100×50×3	804	1000	Pin-ended	1000	455	200900	686	0.68
			100×50×4	1028	1000	Pin-ended	1000	439	203900	869	0.72
			100×50×6	1555	1000	Pin-ended	1000	494	206267	1197	0.80
			120×80×3	1083	1001	Pin-ended	1001	429	197300	2287	0.41
	Young and Liu (2003)	1.4301	120×40×2	593	1199	Fixed-ended	599	326	198000	978	0.36
			120×40×2	596	2000	Fixed-ended	1000	326	198000	351	0.61
			120×40×2	602	2800	Fixed-ended	1400	326	198000	181	0.85
			120×40×2	599	3600	Fixed-ended	1800	326	198000	109	1.09
			120×40×5.3	1524	1200	Fixed-ended	600	394	194000	2046	0.54
			120×40×5.3	1516	2000	Fixed-ended	1000	394	194000	742	0.90
			120×40×5.3	1521	2801	Fixed-ended	1401	394	194000	377	1.26
			120×40×5.3	1516	3600	Fixed-ended	1800	394	194000	229	1.62
			120×80×3	1071	1200	Fixed-ended	600	340	193000	6156	0.22
			120×80×3	1063	2000	Fixed-ended	1000	340	193000	2196	0.37
			120×80×3	1103	2799	Fixed-ended	1400	340	193000	1155	0.53
			120×80×3	1099	3598	Fixed-ended	1799	340	193000	700	0.68

Table 3.9 (contd.): Minor axis flexural buckling tests performed on stainless steel columns.

Section type	Reference	Grade	Nominal size	A_g (mm^2)	L (mm)	End condition	L_e (mm)	$\sigma_{0.2}$ (N/mm^2)	E_0 (N/mm^2)	N_{cr} (kN)	$\bar{\lambda}$
RHS	Young and Liu (2003)	1.4301	120×80×6	2165	1200	Fixed-ended	600	412	194000	11481	0.28
			120×80×6	2171	2000	Fixed-ended	1000	412	194000	4160	0.46
			120×80×6	2156	2800	Fixed-ended	1400	412	194000	2122	0.65
			120×80×6	2203	3600	Fixed-ended	1800	412	194000	1303	0.83

Table 3.10: Major axis flexural buckling tests performed on stainless steel columns.

Section type	Reference	Grade	Nominal size	A_g (mm^2)	L (mm)	End condition	L_e (mm)	$\sigma_{0.2}$ (N/mm^2)	E_0 (N/mm^2)	N_{cr} (kN)	$\bar{\lambda}$
I	Stangenberg (2000b)	1.4301	160 × 80 × 10 × 6	2381	2048	Pin-ended	2048	279	200000	4579	0.38
			160 × 80 × 10 × 6	2374	3343	Pin-ended	3343	279	200000	1724	0.62
			160 × 80 × 10 × 6	2403	5031	Pin-ended	5031	279	200000	782	0.93
			160 × 160 × 10 × 6	3999	2025	Pin-ended	2025	279	198000	8948	0.35
			160 × 160 × 10 × 6	3996	3348	Pin-ended	3348	279	198000	3274	0.58
			160 × 160 × 10 × 6	3981	5145	Pin-ended	5145	279	199000	1381	0.90
		1.4462	160 × 160 × 10 × 7	4350	2050	Pin-ended	2050	523	201000	10012	0.48
			160 × 160 × 10 × 7	4335	3348	Pin-ended	3348	523	201000	3680	0.78
			160 × 160 × 10 × 7	4360	5046	Pin-ended	5046	523	201000	1612	1.19
RHS	Talja and Salmi (1995)	1.4301	150 × 100 × 3	1394	2700	Pin-ended	2700	305	197200	1197	0.53
			150 × 100 × 3	1394	4350	Pin-ended	4350	305	197200	461	0.85
			150 × 100 × 3	1394	6000	Pin-ended	6000	305	197200	242	1.17
			150 × 100 × 6	2708	2700	Pin-ended	2700	345	193600	2150	0.66
			150 × 100 × 6	2678	4350	Pin-ended	4350	345	193600	826	1.06
			150 × 100 × 6	2678	6000	Pin-ended	6000	345	193600	434	1.46

3.5.2 Test results compared against Euler's elastic buckling curve

All the aforementioned test results were compared to the basic elastic buckling curve proposed by Euler in 1759 as shown in Figure 3.4. The basic buckling curve was proposed assuming elastic material behaviour which is now believed to be true only in the case of very slender columns. As the columns become stockier the actual behaviour deviates from this curve as observed from Figure 3.4. Material nonlinearity, initiation of local buckling and the presence of initial imperfections make the actual capacity of a column less than the value predicted by Euler. On the other hand, the presence of cold-worked corners with enhanced material strength increases the ultimate strength limit beyond the basic material 0.2% proof stress $\sigma_{0.2}$. These effects need to be properly addressed to accurately predict the behaviour of stainless steel columns.

Figure 3.4 shows that all the test results lie below the elastic buckling curve except some points obtained from Bredenkamp and van den Berg (1995). This phenomenon points out the possible inaccuracies associated with the testing procedure, the most probable reason being inappropriate allowance for end restraints. These results were, therefore, not used in the present research to devise modified column buckling curves as explained in Chapter 7.
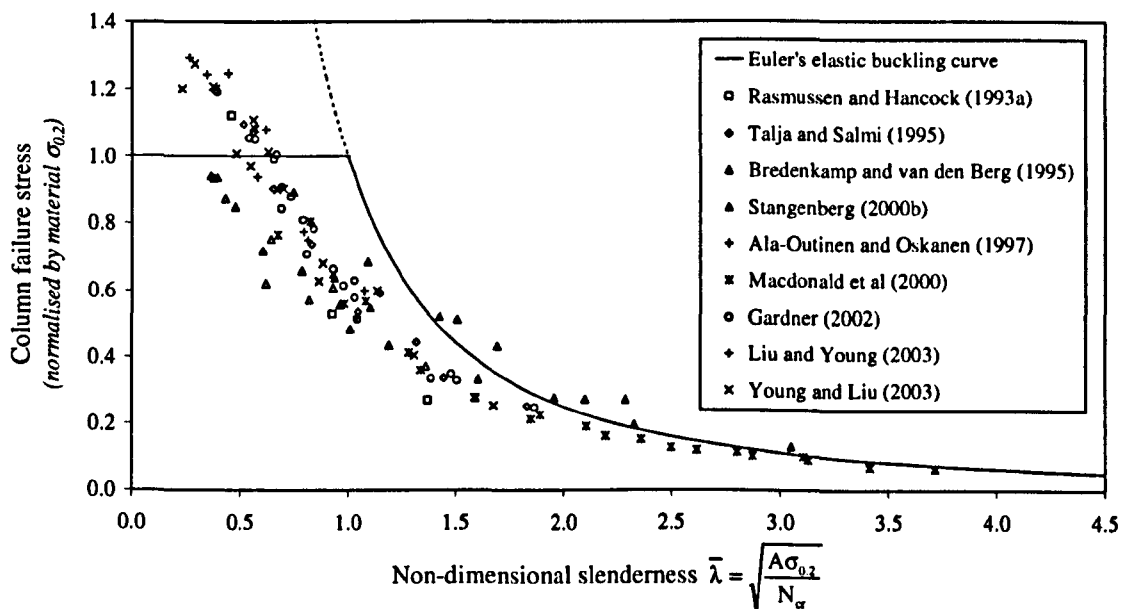
Figure 3.4: Comparing test results against elastic buckling curve proposed by Euler.

3.6 BEAM-COLUMN TESTS

Beam-column tests are performed to investigate the behaviour of a structural element subjected to simultaneous compression and bending. The most common testing technique is to apply an eccentric load to a column which induces both compressive and bending stresses at the same time.

The compressed face of the cross-section is the critical one since it is stressed due to both direct compression and bending.

Hyttinen (1994) carried out an extensive testing scheme on stainless steel hollow sections. A total of 21 beam-column tests were performed on 7 different cross-sections produced from austenitic Grade 1.4301 and ferritic Grades 1.4003 and 1.4512. Bending moments and axial loads were applied using separate loading arrangements. Talja and Salmi (1995) performed 12 eccentric compression tests on SHS and RHS pin-ended columns. All cross-sections were roll-formed from austenitic Grade 1.4301. Rhodes et al (2000) carried out eccentric compression tests on stainless steel lipped channel sections. They tested two lipped channels sections of Grade 1.4301 produced by press-braking. Stangenberg (2000b) reported beam-column tests performed on welded I sections of Grade 1.4301. All of these results have been used to validate the Eurocode interaction formulas by obtaining the cross-sectional resistances using the proposed approach. A summary of the test results are given in Table 3.11 and all necessary details are given in Chapter 7 while verifying the proposed method for beam-column interactions.

Table 3.11: Summary of the beam-column tests used in the present research.

Reference	Grade	Section type	No. of tests	Loading configuration
Hyttinen (1994)	1.4301, 1.4003, 1.4512	SHS	21	Concentrically loaded pin-ended columns were subjected to varying lateral loads
Talja and Salmi (1995)	1.4301	SHS	4	Pin-ended columns were subjected to eccentric load applied through one of the flanges
	1.4301	RHS	8	
Rhodes et al (2000)	1.4301	Lipped Channel	22	Pin-ended columns were subjected to compression with an eccentricity of 8mm.
Stangenberg (2000b)	1.4301	I	6	Pin-ended columns were subjected to compression applied though one of the flanges.

3.7 CONCLUDING REMARKS

All necessary details of test results used in the present research are reported in this chapter. These tests form the basis for the development of the proposed method for obtaining member resistances using deformation capacity of the cross-section. Additional results, wherever available, have been used to validate the proposed methods. Test results on corner coupons are reported and have been analysed in Chapter 4 to develop models for predicting corner strength with the knowledge of the flat material properties. Moreover, test results on initial imperfections have been used in Chapter 5 to develop FE modelling techniques for stainless steel members.

CHAPTER - FOUR

STRENGTH ENHANCEMENT DUE TO COLD-WORK AT THE CORNER REGIONS

4.1 INTRODUCTION

It is well known that the mechanical properties of stainless steel are changed due to cold working of the virgin material. This is due to the material's response to deformation. Stainless steel exhibits pronounced strain hardening, resulting in the corner regions of cold-formed sections having 0.2% proof strengths much higher than that of the virgin material. When seeking improved understanding of the structural response of stainless steel components using numerical analysis, failure to properly allow for the corner regions results in discrepancies between the predictions and the behaviour observed in tests (Gardner and Nethercot, 2001). Models that do not adequately include this effect will, therefore, always be flawed. With the added incentives to use stainless steel members in a structurally highly efficient way – due to their high cost as compared with carbon steel equivalents – it is important that such effects be properly incorporated into the next generation of design rules.

Despite its importance, testing of corner coupons is not a very common practice primarily because of the time and expertise required to cut and test the curved coupons. A simplified method is therefore needed to predict the enhanced corner strength by using the basic material properties and the geometry of a cross-section. This chapter investigates all available test results on corner coupons and hence presents methods for predicting the enhanced strength of the corner regions of cold-formed stainless steel sections.

4.2 MANUFACTURING PROCESSES AND THEIR EFFECTS

Light gauge structural members may be cold-formed by a variety of methods. These fall into two main categories: (1) roll-forming and (2) press-braking. Roll-forming is a mass-

production process requiring rolling machines with a series of two or more roll stands. As the section passes through successive stations in the rolling machine, it is changed in small stages from a flat sheet into the final desired shape. Forming by press-brake is a straight bending, semi manually operated process of more limited production capacity, but requiring only a standard set of punches, dies and tools for most common shapes. A corner can be either 'air' or 'coin' press-braked. In coin press-braking, both the punch and the die should match the final shape required in the corner. In air press-braking the corner is bent initially into a smaller radius than the desired final angle to allow for spring back.

In terms of the material properties of the finished product (as compared to those of virgin sheet), the important difference between the two basic forming methods is as follows: in press-braking strength enhancements are restricted to the corner regions with the properties of the flat parts unaltered, whilst in roll-forming there may be modest strength gains in the flat regions with yet further enhancements in strength in corner regions.

The plastic strains that occur during these cold-forming processes result in an increase in both 0.2% proof strength $\sigma_{0.2}$ and ultimate strength σ_u of the material with a corresponding decrease in ductility. The nature and extent of changes in mechanical properties depend on various factors such as the chemical composition of the material, its prior history of cold work and the type and magnitude of plastic strains caused by the cold work. In general, the factors to be considered in predicting the strength enhancement due to cold-forming at corners are $\sigma_{0.2}$ and σ_u of the virgin material (depends on material composition), the thickness of the steel plate t and the extent of curvature i.e. internal corner radius r_i and included angle (determines the magnitude of plastic strain caused by cold working). In most practical cases the included angle is 90^0 and as such all previous researchers considered only right angles. The present research is also restricted to right angled corners.

4.3 PREVIOUS RESEARCH ON THE EVALUATION OF CORNER STRENGTH

4.3.1 Investigations on carbon steel

Strength enhancement due to cold-forming at the corners of carbon steel sections was first studied by Karren (1967). Based on the examination of a substantial amount of test data, Karren proposed two analytical models to predict the changes caused by cold-forming at the corners. The r_i/t ratio was identified as having a significant effect on the corner strength, a decrease in r_i/t ratio causing an increase in the corner strength. The σ_u/σ_y ratio of the virgin

material was also identified as an important parameter. Karren's test specimens were formed using all three processes i.e. roll-forming, air press-braking and coin press-braking.

ENV 1993-1-3 (1996) accounts for enhanced strength at corners in the design of cold-formed carbon steel sections, by allowing an increase in the average strength of the entire section. The average yield strength f_{ya} is defined by Equation 4.1. It should be noted that ENV 1993-1-3 (1996) only allows strength enhancements for cross-sections that are fully effective.

$$f_{ya} = f_{yb} + (f_u - f_{yb}) k n t^2 / A_g \leq (f_u + f_{yb})/2 \tag{4.1}$$

where, f_{yb} is the nominal yield strength

A_g is the gross cross-sectional area

k is a numerical coefficient that depends on the type of forming as follows:

k = 7 for cold-rolling

k = 5 for other methods of forming

n is the number of 90^0 bends in the cross-section with an internal radius $r \leq 5t$ (fractions of 90^0 bends should be counted as fractions of n)

t is the nominal core thickness of the steel material before cold-forming, exclusive of zinc or organic coatings.

4.3.2 Stainless steel investigations

Johnson and Winter (1966) were the first to investigate the mechanical properties of stainless steel Grade 1.4301 coupons obtained from cold-worked corners which were formed using a hydraulic press-brake to a radius-to-thickness ratio of approximately 2. The significant effect of cold-working in terms of increased 0.2% proof strength was observed. Test results showed an average 80% increase in strength at corners when compared to that of the corresponding flat material.

Coetzee et al (1990) investigated the effect of cold-work on the strength of stainless steel members. Lipped channel sections in three grades of stainless steel were studied: austenitic Grades 1.4301 and 1.4401 and ferritic Grade 1.4003. Four corner specimens from each of the three lipped channel sections were used. All four lipped channel sections were formed by press-braking.

van den Berg and van der Merwe (1992) performed an extensive study on the corner properties for stainless steel austenitic Grade 1.4301 and ferritic Grades 1.4512, 1.4016 and

1.4003. Ten specimens, with a variety of r_i/t ratios, were press-braked for each of the four grades. The measured corner properties were then related to the virgin material properties based on Karren's (1967) methodology. The proposed equations for the prediction of corner 0.2% proof strength $\sigma_{0.2,c}$ are given below (where all symbols have been harmonised with those adopted in the remainder of this research):

$$\sigma_{0.2,c} = \frac{B_c \sigma_{0.2,v}}{\left(\dfrac{r_i}{t}\right)^m} \tag{4.2}$$

where,

$$B_c = 3.289 \left(\frac{\sigma_{u,v}}{\sigma_{0.2,v}}\right) - 0.861 \left(\frac{\sigma_{u,v}}{\sigma_{0.2,v}}\right)^2 - 1.34 \tag{4.3}$$

$$m = 0.06 \left(\frac{\sigma_{u,v}}{\sigma_{0.2,v}}\right) + 0.031 \tag{4.4}$$

$\sigma_{0.2,v}$ is the 0.2% proof strength of virgin material

$\sigma_{u,v}$ is the ultimate strength of virgin material

Hyttinen (1994) carried out tensile tests on coupons collected from the virgin sheets as well as from the cold-formed SHS cross-sections. The sections were produced from austenitic Grade 1.4301 and ferritc Grades 1.4003 and 1.4512. A total of seven corner coupons, 3 from 1.4301 and 2 each from the other ferritic grades, were tested. The corner coupons collected from the ferritic Grades had 4.8 mm flat material on both sides, which is believed to have affected the corner material properties significantly. Moreover the ends of the corner coupons were flattened prior to testing which would have induced some eccentricities. These inconsistencies are the reason that these results have not been used in the development of the proposed method. However the austenitic corner coupon results, which are considered to be more reliable than the ferritic ones, were used to verify the performance of the proposed technique.

Gardner (2002) performed tensile tests on coupons cut from the corners of three square hollow section (SHS) and two rectangular hollow section (RHS) roll-formed stainless steel members produced from austenitic Grade 1.4301. Another test result on a similar coupon cut from a completed roll-formed section was reported by Rasmussen and Hancock (1993). Gardner (2002) observed that the 0.2% proof strengths of the corner material $\sigma_{0.2,c}$ were a consistent multiple of the ultimate strengths of the section's flat material $\sigma_{u,f}$ (cut from within the completed cross-sections). The simple expression given by Equation 4.5 was therefore proposed for the prediction of corner material strength in roll-formed sections.

$$\sigma_{0.2,c} = 0.85\sigma_{u,f} \tag{4.5}$$

It should be noted that the 6 roll-formed hollow sections [5 tested by Gardner (2002) and 1 by Rasmussen and Hancock (1993)] followed a fabrication route whereby flat sheet was first roll-formed into a circular hollow section, then seam-welded and finally shaped into an SHS and RHS. It is believed to be the standard fabrication route for stainless steel SHS and RHS.

Gardner and Talja (2003) reported tests on corner coupons cut from two high strength cold-worked austenitic Grade 1.4318 stainless steel RHS. The corner properties were incorporated into numerical models.

Lecce and Rasmussen (2004) investigated corner material properties for austenitic Grade 1.4301, ferritic Grades 1.4003 and 1.4016. The coupons were cut from the press-braked corners of lipped channel sections. Coupons obtained from Grade 1.4301 and 1.4003 were tested in both tension and compression while Grade 1.4016 coupons were tested in tension only. For longitudinal compression tests ultimate stresses were not available and hence the corresponding strengths obtained from tensile tests were used where necessary. The results reported herein are the average of two identical coupons tested in each case. It should be noted that the ends of the corner coupons were flattened before testing.

All the corner material test results available to the current study are presented in Table 4.1.

Table 4.1: Tests performed on stainless steel corner specimens.

Reference	Grade	Manufacturing Process	Virgin material properties		r_i/t	Corner material properties	
			$\sigma_{0.2,v}$ (N/mm^2)	$\sigma_{u,v}$ (N/mm^2)		$\sigma_{0.2,c}$ (N/mm^2)	$\sigma_{u,c}$ (N/mm^2)
Coetzee et al (1990)	1.4301	Press-braking	296	685	1.28	520	811
					2.24	464	793
					2.23	471	795
					1.15	552	836
	1.4401	Press-braking	277	621	1.42	486	700
					2.05	445	676
					2.13	444	685
					1.37	487	710
	1.4003	Press-braking	299	462	1.35	519	532
					2.20	486	525
					2.25	482	523
					1.38	528	541
van den Berg and van der Merwe (1992)	1.4301	Press-braking	295	671	1.99	452	775
					2.22	425	762
					3.40	407	759
					3.43	397	744
					4.43	398	753
					4.47	374	-
					5.75	362	730
					5.85	358	725
					6.63	366	732
					7.03	-	-

Table 4.1 (contd.): Tests performed on stainless steel corner specimens.

Reference	Grade	Manufacturing Process	Virgin material properties		r_i/t	Corner material properties	
			$\sigma_{0.2,v}$ (N/mm^2)	$\sigma_{u,v}$ (N/mm^2)		$\sigma_{0.2,c}$ (N/mm^2)	$\sigma_{u,c}$ (N/mm^2)
van den Berg and van der Merwe (1992)	1.4512	Press-braking	224	395	1.80	370	431
					1.87	374	431
					3.00	365	424
					3.26	353	418
					4.20	350	420
					4.31	334	412
					5.36	328	409
					5.97	317	403
					6.24	322	405
					7.09	305	399
	1.4016	Press-braking	304	518	1.94	471	574
					2.39	488	583
					3.12	458	564
					3.53	-	-
					4.32	451	560
					4.61	442	553
					5.30	435	551
					6.09	415	547
					6.54	418	548
					7.27	407	548

Table 4.1 (contd.): Tests performed on stainless steel corner specimens.

Reference	Grade	Manufacturing Process	Virgin material properties		r_i/t	Corner material properties	
			$\sigma_{0.2,v}$ (N/mm^2)	$\sigma_{u,v}$ (N/mm^2)		$\sigma_{0.2,c}$ (N/mm^2)	$\sigma_{u,c}$ (N/mm^2)
van den Berg and van der Merwe (1992)	1.4003	Press-braking	277	435	1.61	423	508
					2.25	450	518
					3.08	437	506
					3.16	420	497
					4.09	409	496
					4.33	392	493
					5.10	371	482
					5.64	379	484
					6.25	396	486
					6.70	371	487
Rasmussen and Hancock (1993)	1.4301	Roll-forming	297	614	0.83	580	805
Gardner (2002)	1.4301	Roll-forming	291	628	1.20	594	820
			275	623	0.68	587	820
			304	613	1.60	563	844
			318	612	0.92	631	802
			289	600	1.46	572	809
Gardner and Talja (2003)	1.4318	Roll-forming	361	755	2.09	614	941
			548	986	1.80	807	1162
Lecce and Rasmussen (2004a)	1.4301	Press-braking	251	703	2.02	570	n/a
			242	n/a	1.91	565	n/a
	1.4003	Press-braking	338	483	1.97	544	n/a
			339	n/a	1.97	606	n/a
	1.4016	Press-braking	291	451	2.32	452	n/a

4.4 PERFORMANCE OF VAN DEN BERG AND VAN DER MERWE'S PROPOSED MODEL

To obtain a general solution for the prediction of corner strength using the material properties of the flat material the existing models have been analysed first. All the test results presented in Table 4.1 have been predicted using van den Berg and van der Merwe's proposed model and the results are summarised in Table 4.2.

Table 4.2: Statistical analysis of the predictions of van den Berg and van der Merwe's model.

Reference	Number of tests	Range of r_i/t ratio	Pred. $\sigma_{0.2,c}$ / Test $\sigma_{0.2,c}$	
			Mean	COV
Coetzee et al (1990)	12	1.15 - 2.25	0.92	0.02
van den Berg and van der Merwe (1992)	40	1.61 – 7.27	1.00	0.03
Rasmussen and Hancock (1993)	1	0.83	0.94	-
Gardner (2002)	5	0.68 - 1.60	0.87	0.05
Gardner and Talja (2003)	2	0.99 – 1.31	1.11	0.14
Lecce and Rasmussen (2004a)	10	1.91 – 2.32	0.60	0.46

From the statistical summary of Table 4.2 it is observed that whilst predictions for the data of Coetzee et al (1990) and Gardner (2002) are quite consistent, they are somewhat lower than the test results. In the case of Gardner and Talja's (2003) results, the one poor prediction for Grade 1.4318 (strength level C850) made the standard deviation large. But Lecce and Rasmussen's (2004a) results for tests on austenitic grades were highly underpredicted with an average of 0.39. But for the other grades the average of 6 tests was 0.90. These comparisons suggest that some modification to this model is required.

It is worth mentioning that the method described in this chapter was first proposed by Ashraf et al (2005) and at that time the most recent set of data as reported by Lecce and Rasmussen (2004a) were not available to be included in the analysis. Hence these results along with three results reported by Hyttinen (1994) have been used to validate the proposed models in Section 4.7.

Given the variability in prediction of the data from sources other than that used by van den Berg and van der Merwe, it is of interest to note the factors that might have an influence. One possibility is the production process and Table 4.3 distinguishes between roll-forming and press-braking.

Table 4.3: Predictions of van den Berg and van der Merwe's model for different processes.

Process of corner formation	Number of tests	Predicted $\sigma_{0.2,c}$ / Test $\sigma_{0.2,c}$	
		Mean	COV
Roll-forming	8	0.94	0.14
Press-braking	52	0.98	0.04

It should be noted that the van den Berg and van der Merwe model predictions for the roll-formed sections (which are mostly used in structures) exhibit significantly more scatter, although this is beyond the scope for which their expressions were originally developed and calibrated.

All available test results are plotted in Figure 4.1 showing how $\sigma_{0.2,c}/\sigma_{0.2,v}$ varies with r_i/t. From Figure 4.1 it is clear that except for the van den Berg and van der Merwe (1992) study very few specimens had r_i/t values higher than 2.0. In their study, van den Berg and van der Merwe (1992) formed single corner coupons by cold-working of 2mm thick stainless steel sheets to produce specimens with a wide variation of r_i/t ratios from 1.5 to 7.5. In all other studies the corner coupons were cut from roll-formed RHS, SHS or press-braked lipped channel sections; in these cases, r_i/t ratios were found to be less than 2.5 i.e. in a very different range from the data used to establish van den Berg and van der Merwe's model.
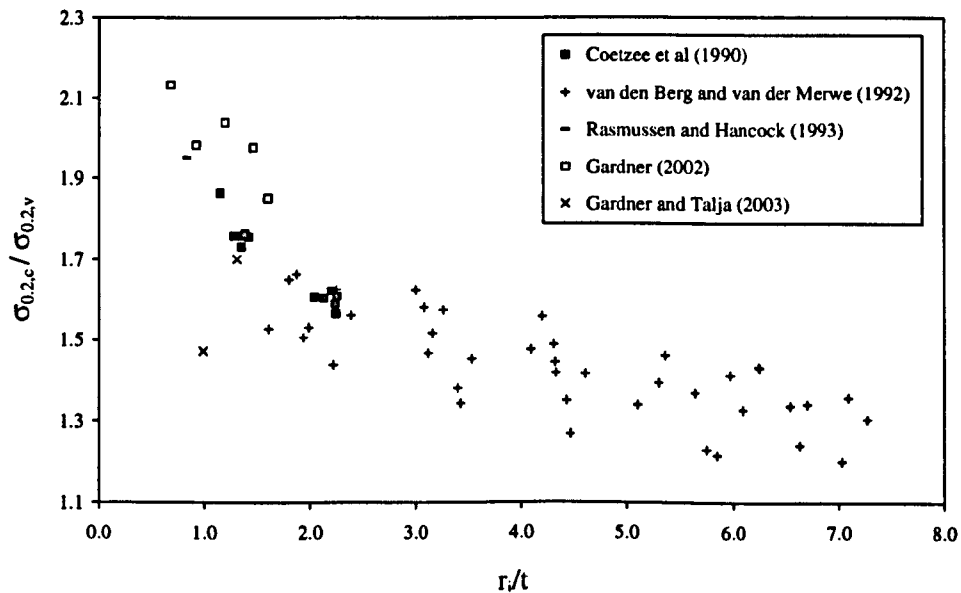
Figure 4.1: Test results on corner coupons from all available studies.

4.5 OBJECTIVE AND METHODOLOGY OF THE PRESENT STUDY

In analysing the full set of results, the first step was to decide on the parameters likely to affect the corner strength. Those considered are: 0.2% proof strength $\sigma_{0.2,v}$ and ultimate strength $\sigma_{u,v}$ of virgin material, internal corner radius r_i and thickness t of the plate to be bent. Similar factors were considered in Karren's (1967) proposed model for the prediction of corner strength for carbon steel.

To establish relationships among these parameters the available test results were plotted with different ordinates such as $\sigma_{0.2,c}/\sigma_{0.2,v}$ and $\sigma_{0.2,c}/\sigma_{u,v}$ and have been analysed using regression techniques. The details of these regression analyses are described in the following sections.

4.6 DEVELOPMENT OF MODELS FOR PREDICTING CORNER STRENGTH

4.6.1 Predicting the 0.2% proof strength of corner material $\sigma_{0.2,c}$ using the 0.2% proof strength of virgin material $\sigma_{0.2,v}$

In Figure 4.2 the data points are classified according to the ratio of $\sigma_{u,v}/\sigma_{0.2,v}$ since this ratio was reported by Karren (1967) to be a significant factor in predicting corner strength. From this figure it is observed that all points lie in a band that rises quite sharply as the value of r_i/t decreases taking the form of an exponential growth.

A single line is fitted to all the test points in this figure. The coefficient of determination, R^2, has been found to be close to unity, which indicates that all the points can be represented by this single line with a good degree of accuracy. According to this analysis the relationship can be expressed as,

$$\sigma_{0.2,c} = \frac{1.881\sigma_{0.2,v}}{\left(\dfrac{r_i}{t}\right)^{0.194}} \tag{4.6}$$

This equation can be used to determine the 0.2% proof strength of the corner; it is simple in the sense that it is independent of the $\sigma_u/\sigma_{0.2}$ ratio of virgin material and, more importantly, it only requires knowledge of 3 easily obtainable parameters. It is of the same form as the basic Equation 4.2, first suggested by van den Berg and van der Merwe (1992), but with constants for the two coefficients B_c and m of Equations 4.3 and 4.4.
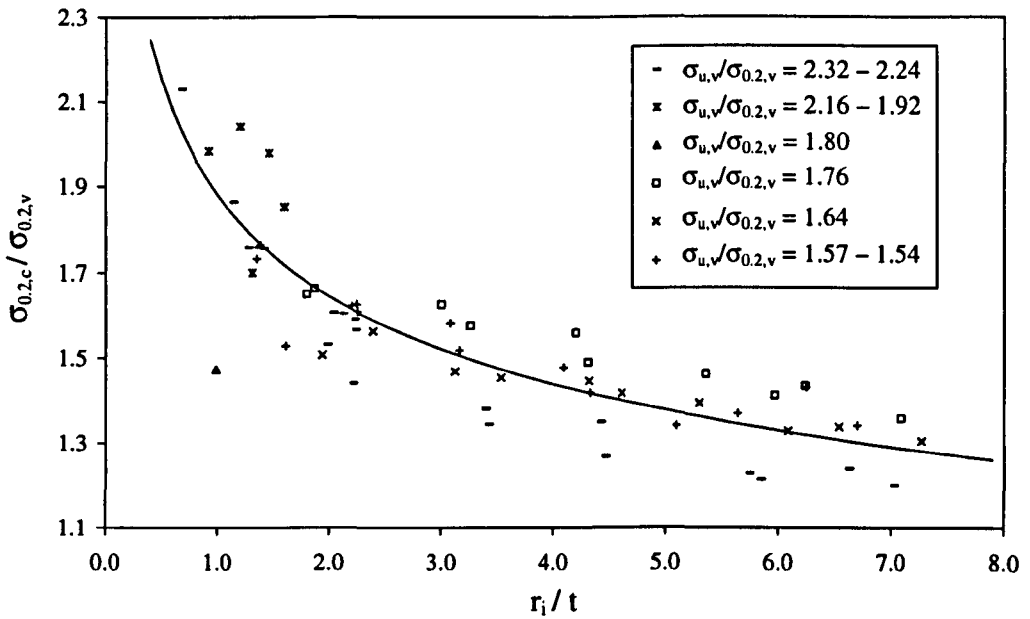
Figure 4.2: Representation of corner coupon tests classified according to $\sigma_u/\sigma_{0.2}$ ratio of virgin material ($\sigma_{u,v}/\sigma_{0.2,v}$) and comparison of Equation 4.6 with all test data.

4.6.2 Predicting the 0.2% proof strength of corner material $\sigma_{0.2,c}$ using the ultimate strength of virgin material $\sigma_{u,v}$

Rather than using the proof strength of the virgin material, Gardner (2002) related the 0.2% corner strength to the ultimate strength of flat material $\sigma_{u,f}$ cut from the completed cross-section (see Equation 4.5). But the value of this parameter $\sigma_{u,f}$ was not available for all the test results considered in the present study. The similar available parameter is the ultimate strength of virgin material, $\sigma_{u,v}$. In this section efforts have been put forward to relate 0.2% corner strength $\sigma_{0.2,c}$ with the ultimate strength of virgin material $\sigma_{u,v}$. All the test data are shown plotted using $\sigma_{0.2,c}/\sigma_{u,v}$ as ordinate and r_i/t as abscissa in Figure 4.3.

From this figure it is observed that the points are rather more scattered than in Figure 4.1. This suggests the need to recognise another parameter. The obvious feature is the $\sigma_u/\sigma_{0.2}$ ratio of the virgin material.

In Figure 4.4 the points have been classified into four groups depending on the $\sigma_{u,v}/\sigma_{0.2,v}$ ratio. A weighted average of the $\sigma_{u,v}/\sigma_{0.2,v}$ ratio was used to produce a single value for each class. This figure clearly indicates the need to include the $\sigma_{u,v}/\sigma_{0.2,v}$ ratio in the relationship between $\sigma_{0.2,c}$ and $\sigma_{u,v}$. To incorporate the effect of $\sigma_{u,v}/\sigma_{0.2,v}$ ratio four different classes were identified and

relationships derived for each. These curves are also shown in this figure. The general expression for the relationship can therefore be taken as:

$$\frac{\sigma_{0.2.c}}{\sigma_{u,v}} = \frac{C_1}{\left(\dfrac{r_i}{t}\right)^{C_2}} \tag{4.7}$$

in which the values of C_1 and C_2 depend on $\sigma_{u,v}/\sigma_{0.2,v}$ ratio and can be obtained from the four curves shown in Figure 4.4.
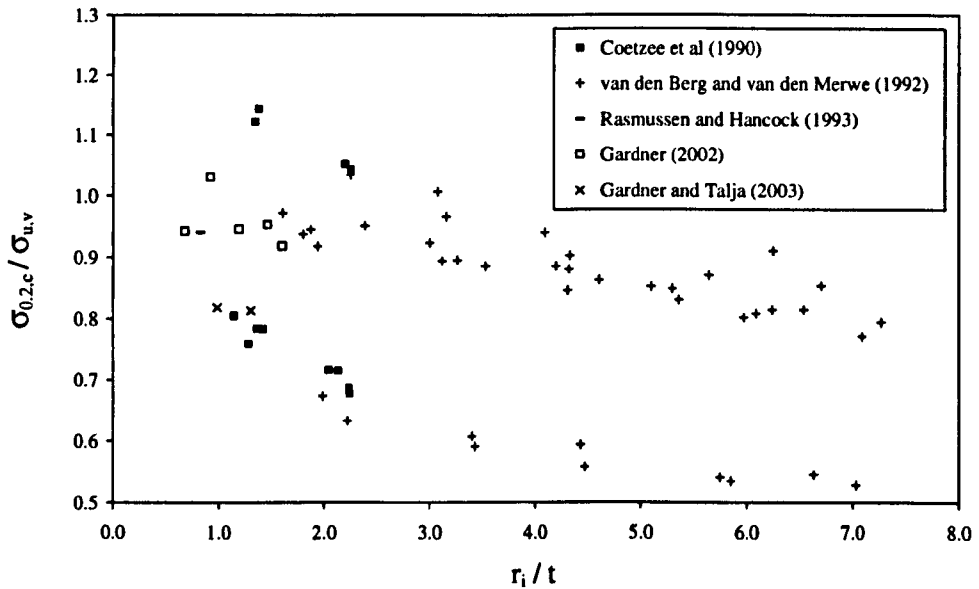
Figure 4.3: Representation of corner coupon tests considering $\sigma_{0.2,c}/\sigma_{u,v}$ as ordinate.
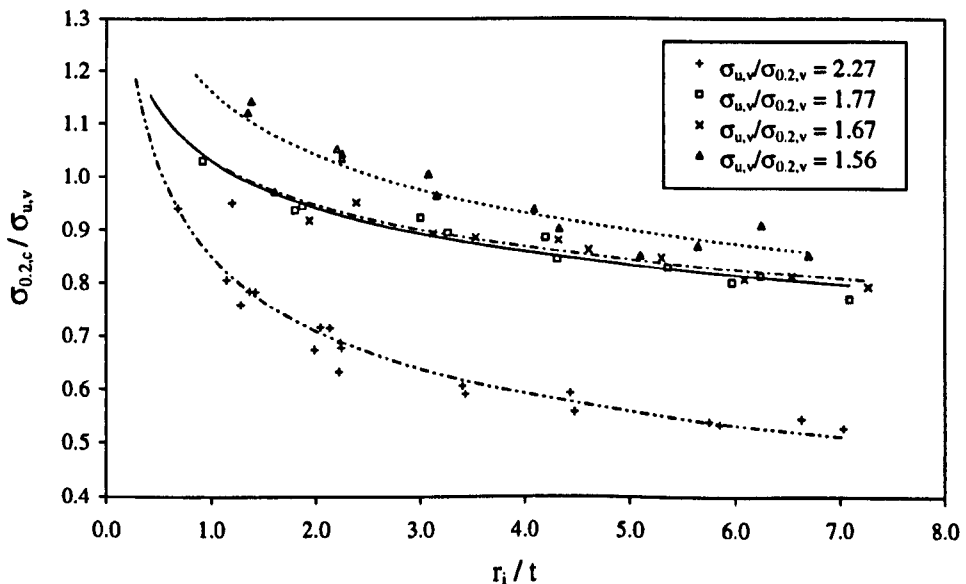
Figure 4.4: Trend lines for corner coupon classes defined according to the $\sigma_{u,v}/\sigma_{0.2,v}$ ratio.

The curves of Figure 4.4 provide discrete values for C_1 and C_2 for different $\sigma_{u,v}/\sigma_{0.2,v}$ ratios. These have been plotted against the $\sigma_{u,v}/\sigma_{0.2,v}$ ratio in Figures 4.5 and 4.6. The equations of fitted straight lines are given in Equations 4.8 and 4.9.
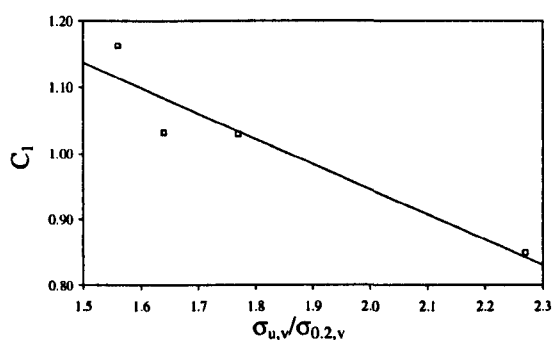
Figure 4.5: Relationship between C_1 and $\sigma_{u,v}/\sigma_{02,v}$
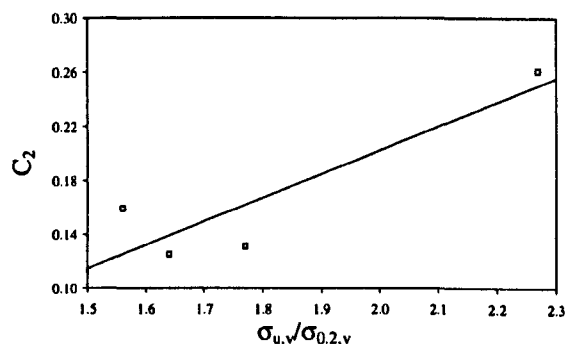
Figure 4.6: Relationship between C_2 and $\sigma_{u,v}/\sigma_{02,v}$

Thus when using Equation 4.7 the coefficients C_1 and C_2 should be determined from:

$$C_1 = -0.382\left(\frac{\sigma_{u,v}}{\sigma_{0.2,v}}\right) + 1.71 \qquad (4.8)$$

$$C_2 = 0.176\left(\frac{\sigma_{u,v}}{\sigma_{0.2,v}}\right) - 0.15 \qquad (4.9)$$

4.6.3 Predicting the 0.2% proof strength of corner material $\sigma_{0.2,c}$ using the ultimate strength of flat material $\sigma_{u,f}$

Gardner (2002) proposed the simplest model for roll-formed sections produced from austenitic Grade 1.4301, as given in Equation 4.5, for prediction of corner 0.2% proof strength $\sigma_{0.2,c}$ from the ultimate strength of flat material $\sigma_{u,f}$. In Figure 4.7 all available roll-formed corner test results are plotted to recalibrate the model.
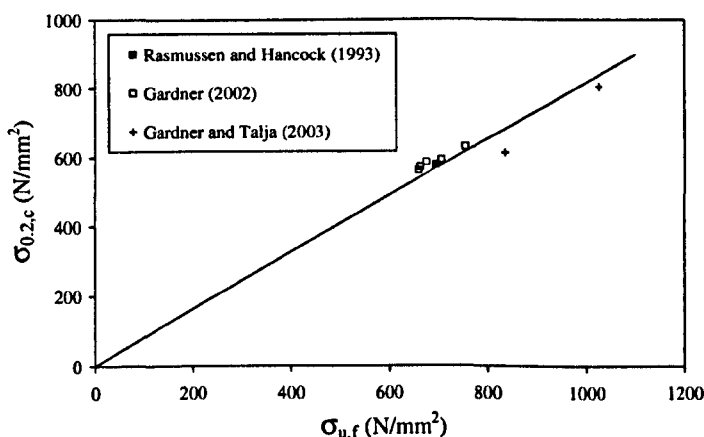
Figure 4.7: All available corner coupon tests for roll-formed sections.

The obtained relationship is given in Equation 4.10.

$$\sigma_{0.2,c} = 0.82\sigma_{u,f} \tag{4.10}$$

However, it should be noted that this equation is based only on test results for roll-formed sections of austenitic Grade 1.4301.

4.6.4 Predicting the ultimate strength of corner material $\sigma_{u,c}$ using the 0.2% proof strength of corner material $\sigma_{0.2,c}$

All the previous models have been concerned with the prediction of the 0.2% proof strength of the corner material $\sigma_{0.2,c}$. In order to obtain a full picture of the changes at the corners due to cold-work, the other important parameter is the ultimate strength $\sigma_{u,c}$.

In Figure 4.8 all available test results are plotted taking $\sigma_{u,v}/\sigma_{0.2,v}$ as abscissa and $\sigma_{u,c}/\sigma_{0.2,c}$ as ordinate. All these points can be approximated by a single straight line passing through the origin with a slope of 0.75. So the expression for predicting $\sigma_{u,c}$ is given by:

$$\sigma_{u,c} = 0.75\sigma_{0.2,c}\left(\frac{\sigma_{u,v}}{\sigma_{0.2,v}}\right) \tag{4.11}$$

This equation can be used to predict the ultimate strength of corner material from a knowledge of three easily obtainable parameters.
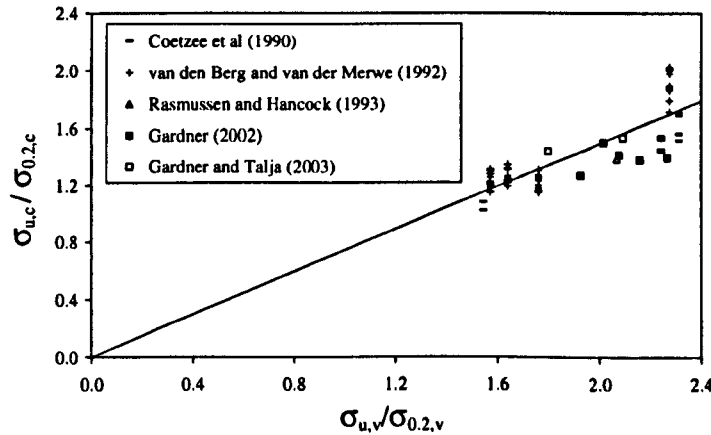
Figure 4.8: All available test results on corner coupon.

4.7 COMPARISONS

All the test results have been predicted using the original van den Berg and van der Merwe (1992) model, the simple power model of Equation 4.6 and the power model using $\sigma_{u,v}$ (Equations 4.7, 4.8 and 4.9) and the results are summarised in Table 4.4. Tests performed by Lecce and Rasmussen (2005a) and Hyttinen (1994) are reported separately in detail in Table 4.5.

Table 4.4: Comparison of corner strength results obtained using the proposed methods and van den Berg and van der Merwe's method.

Reference	Number of tests	van den Berg and van der Merwe model *(Equations 4.2 – 4.4)*		Simple power model *(Equation 4.6)*		Power model using $\sigma_{u,v}$ *(Equations 4.7 – 4.9)*	
		Mean	COV	Mean	COV	Mean	COV
Coetzee et al (1990)	12	0.92	0.02	1.01	0.01	0.99	0.02
van den Berg and van der Merwe (1992)	40	1.00	0.03	1.01	0.06	1.00	0.04
Rasmussen and Hancock (1993)	1	0.94	-	1.00	-	1.01	-
Gardner (2002)	5	0.87	0.06	0.92	0.04	0.93	0.04
Gardner and Talja (2003)	2	1.00	-	1.05	-	1.06	-
Total	60	0.97	0.05	1.00	0.06	1.00	0.04

Table 4.5: Predictions vs test results for the corner coupons reported by Lecce and Rasmussen (2005a) and Hyttinen (1994).

Reference	Grade	Test type	r_i/t	Test $\sigma_{0.2,c}$ (N/mm^2)	van den Berg and van der Merwe model (Equations 4.2 – 4.4)		Simple power model (Equation 4.6)		Power model using $\sigma_{u,v}$ (Equations 4.7 – 4.9)	
					Pred. $\sigma_{0.2,c}$	Pred./Test	Pred. $\sigma_{0.2,c}$	Pred./Test	Pred. $\sigma_{0.2,c}$	Pred./Test
Lecce and Rasmussen (2005a)	1.4301	LT	1.99	570	245	0.43	413	0.72	356	0.62
		LT	2.04	570	243	0.43	411	0.72	353	0.62
		LC	1.89	565	201	0.36	402	0.71	336	0.59
		LC	1.94	565	200	0.35	400	0.71	333	0.59
				Mean		0.39		0.72		0.61
				COV		0.11		0.01		0.03
Lecce and Rasmussen (2005a)	1.4003	LT	1.98	540	499	0.92	555	1.03	524	0.97
		LT	1.98	547	502	0.92	560	1.02	527	0.96
		LC	1.98	610	502	0.82	562	0.92	528	0.87
		LC	1.98	602	499	0.83	556	0.92	525	0.87
	1.4016	LT	2.41	444	441	0.99	461	1.04	453	1.02
		LT	2.23	460	445	0.97	468	1.02	457	0.99
Hyttinen (1994)	1.4301	LT	0.47	669	590	0.88	649	0.97	676	1.01
		LT	0.49	684	585	0.86	641	0.94	665	0.97
		LT	1.11	601	545	0.91	571	0.95	576	0.96
				Mean		0.90		0.98		0.96
				COV		0.06		0.05		0.06

From Table 4.4 it is observed that both the Simple Power Model (Equation 4.6) and the Power Model using σ_u (comprising Equations 4.7, 4.8 and 4.9) give better predictions in the case of Coetzee et al (1990) and Gardner's (2002) test results. Predictions for van den Berg and van der Merwe's (1992) test results are also found to be quite satisfactory using these models. A clearer indication of the relative accuracy of the proposed models is provided by the normal distributions of the predictions given in Figures 4.9, 4.10 and 4.11.
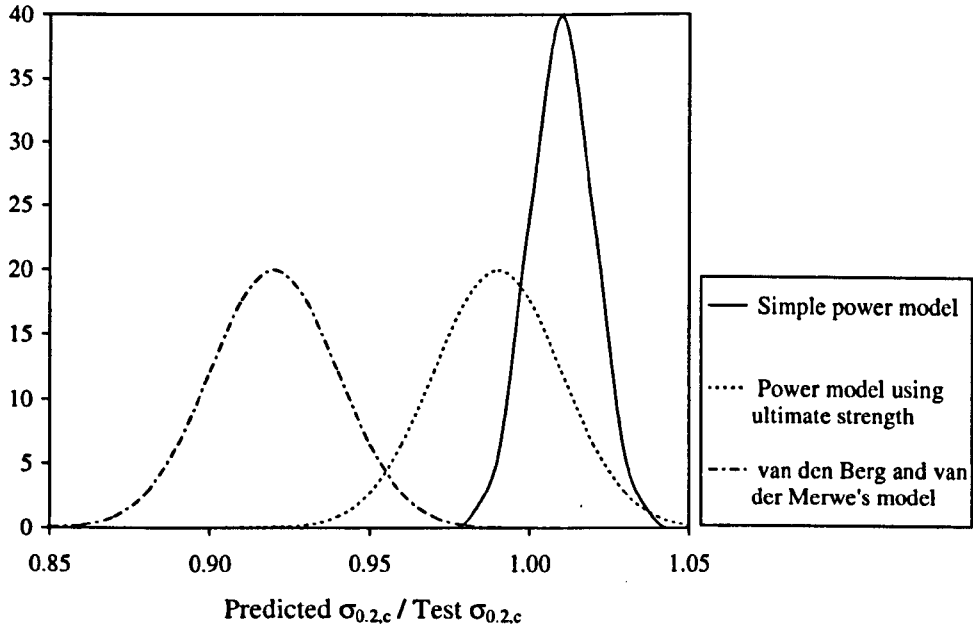
Figure 4.9: Normal distribution of test results of Coetzee et al (number of results = 12).
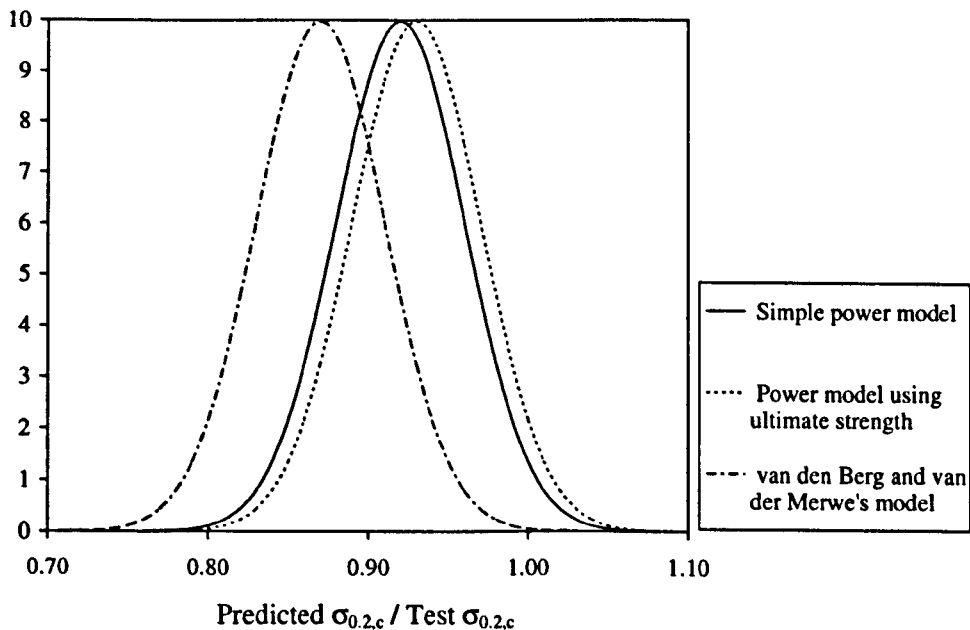
Figure 4.10: Normal distribution of Gardner's test results (number of results = 5).

Predicted $\sigma_{0.2,c}$ / Test $\sigma_{0.2,c}$
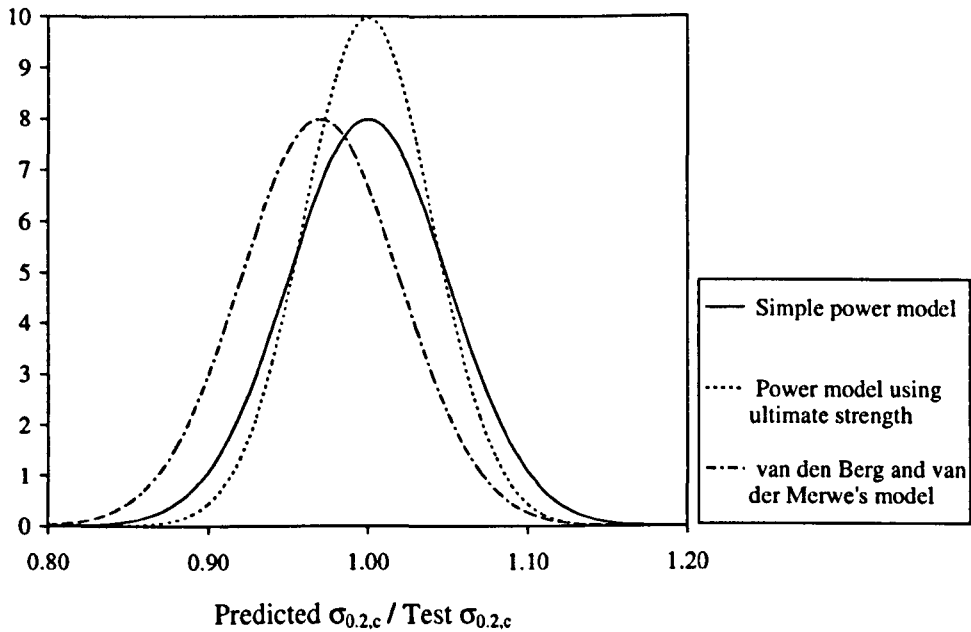
Figure 4.11: Normal distribution of all corner coupon tests (total number of tests = 60).

These figures clearly show that the power model using $\sigma_{u,v}$ gives the most consistent predictions i.e. less scatter, as measured by the standard deviation. Both the proposed models for predicting $\sigma_{0.2,c}$ have an overall average of 1.0, especially giving more accurate predictions for the results of Coetzee et al (1990) and Gardner (2002). It is worth mentioning that the frequency distributions of the obtained predictions were approximately normally distributed.

Table 4.5 compares the predictions for the test results reported by Lecce and Rasmussen (2005a) and Hyttinen (1994). For the austenitic Grade 1.4301 coupons tested by Lecce and Rasmussen (2005a) the predictions are much lower than the actual tested values. This is believed due to the unusually low yield ratio $\sigma_{0.2}/\sigma_u$ shown by the virgin material. The reported material properties give a yield ratio of 0.35, while the normal range for press-braked austenitic Grade 1.4301 varies from 0.45 to 0.52 which can be found from Chapter 3. Moreover development of this method has been dominated by the ferritic alloys since test results on austenitic grade were insufficient to be considered separately. Since austenitic Grade 1.4301 is the most commonly used type of stainless steel showing the maximum amount of strain hardening it might be worth looking at this grade separately once sufficient test data are available. However, in the case of austenitic Grade results of Hyttinen (1994) and ferritic Grade results of Lecce and Rasmussen (2005a), the proposed models give quite accurate predictions.

Results obtained from the proposed model for predicting the ultimate strength of corner material $\sigma_{u,c}$ (Equation 4.11) by using the predicted $\sigma_{0.2,c}$ are given in Table 4.6. This model is not process dependent i.e. it is applicable for both press-braked and roll-formed sections.

From Table 4.6 it is observed that the proposed model for predicting $\sigma_{u,c}$ gives quite satisfactory results, giving an average scatter of less than 10%. So this model can be used along with either Equation 4.6 or Equation 4.7 to predict the ultimate strength of corner material.

Table 4.6: Predictions for $\sigma_{u,c}$ using Equation 4.11 for all available test results.

Reference	Number of tests	Predicted $\sigma_{u,c}$ /Test $\sigma_{u,c}$ ($\sigma_{0.2,c}$ obtained by Eq. 4.6)		Predicted $\sigma_{u,c}$/Test $\sigma_{u,c}$ ($\sigma_{0.2,c}$ obtained by Eq. 4.7)	
		Mean	COV	Mean	COV
Coetzee et al (1990)	12	1.11	0.05	1.09	0.06
van den Berg and van der Merwe (1992)	40	0.98	0.07	0.98	0.08
Rasmussen and Hancock (1993)	1	1.11	-	1.13	-
Gardner (2002)	5	1.04	0.09	1.05	0.10
Gardner and Talja (2003)	2	1.14	0.09	1.13	0.07
All Test results	60	1.02	0.09	1.02	0.09

4.8 CONCLUDING REMARKS

Two power models have been proposed to predict the corner 0.2% proof strength of cold-formed stainless steel structural members based on the properties of the virgin material. These models cover all possible processes of cold working. These models have been verified against all available test data for corner properties and found to give good predictions.

A simplified model to predict the 0.2% proof strength of corner material in roll-formed sections by knowing only the ultimate strength of flat material has been recalibrated.

A further model has been proposed to predict the ultimate strength of corner material and this model has been found to give satisfactory predictions when compared with all available test results.

CHAPTER - FIVE

NUMERICAL MODELLING

5.1 INTRODUCTION

Numerical techniques have now become an invaluable part of most structural research, since they can be employed as an efficient tool for analysing the behaviour of structures provided that suitable care is taken to ensure that the model is appropriate and the input parameters are accurately specified. The sensitivity to changes in these parameters also needs to be properly understood. For an expensive material such as stainless steel it is not practical to verify all the design guidance by testing. A better approach is to first conduct some tests, then to replicate the testing procedures using numerical techniques, and, once the numerical models have been verified, to generate further results through variation of appropriate parameters in the numerical model.

A large number of test results have been used in the present study to develop a consistent finite element (FE) modelling technique using the general purpose FE software package ABAQUS V 6.4 (2003). This chapter describes the development of the FE models, giving special emphasis to the appropriate guidelines for input parameters such as enhanced strength at the corner regions and the extent of this strength enhancement, initial geometric imperfections and the significance of residual stresses. Extensive parametric studies were performed to establish the proposed guidelines. Later these guidelines were incorporated into modelling of structural elements and hence to identify the inconsistencies associated with some test schemes and to generate dependable results where required.

5.2 MATERIAL MODELLING

The development of an appropriate FE model requires a correct representation of the corresponding material characteristics. Inaccurate or inappropriate modelling of the basic material behaviour will overshadow the performance of even the most refined FE models.

Stainless steel exhibits a rounded stress-strain curve and strain hardens to a considerably greater extent than carbon steel, resulting in significant changes in material behaviour during cold-forming processes. This phenomenon leads to enhanced strength properties at the corner regions of stainless steel sections. Special care is required to model the exact response of stainless steel cross-sections with cold-worked corners. This section describes the modelling technique for the basic material behaviour using appropriate measures to account for the highly nonlinear behaviour of stainless steel and then explains how the enhanced strength properties of the cold-worked corner regions could be predicted and incorporated into the FE models.

5.2.1 Modelling of flat material

Stainless steel exhibits a rounded stress-strain curve and the degree of roundness varies from grade to grade, with the austenitic grades demonstrating the greatest nonlinearity and strain hardening. Exact material modelling is paramount to ensure the appropriate exploitation of the special benefits offered by stainless steel. Most of the commonly adopted models for stainless steel are discussed briefly in the following sections.

5.2.1.1 Ramberg-Osgood model

Ramberg and Osgood (1943) proposed the expression given in Equation 5.1 for the description of material stress-strain behaviour, where E_0 is Young's modulus and K and n are constants.

$$\varepsilon = \frac{\sigma}{E_0} + K\left(\frac{\sigma}{E_0}\right)^n \tag{5.1}$$

This basic expression was later modified by Hill (1944) to give Equation 5.2 where R_p is a proof stress and c is the corresponding offset (plastic) strain.

$$\varepsilon = \frac{\sigma}{E_0} + c\left(\frac{\sigma}{R_p}\right)^n \tag{5.2}$$

In both expressions the total strain is expressed as the summation of elastic and plastic strains which are treated separately. The power function is applied only to the plastic strain. The Ramberg-Osgood expression is a popular material model for nonlinear materials since its constants have physical significance and it also provides a smooth curve for all values of strain with no discontinuities. A drawback to this relationship is that it is not explicitly

solvable for stress, although the solution could be obtained using numerical techniques, but this should preferably be avoided in a structural design procedure.

The Ramberg-Osgood expression, as modified by Hill (1944), has been used in an informative Annex of ENV 1999-1-1 (1998) for describing the stress-strain behaviour of aluminium. The proof stress was taken as the value corresponding to the 0.2% offset strain giving the most familiar form of the Ramberg-Osgood expression as given by Equation 5.3.

$$\varepsilon = \frac{\sigma}{E_0} + 0.002\left(\frac{\sigma}{\sigma_{0.2}}\right)^n \tag{5.3}$$

This equation has been found to give excellent prediction of stainless steel material stress-strain behaviour up to the 0.2% proof stress $\sigma_{0.2}$ but highly overpredicts the stresses beyond that level. Figure 5.1 shows a typical comparison between a test result and the corresponding Ramberg-Osgood idealisation (Equation 5.3) for stainless steel.
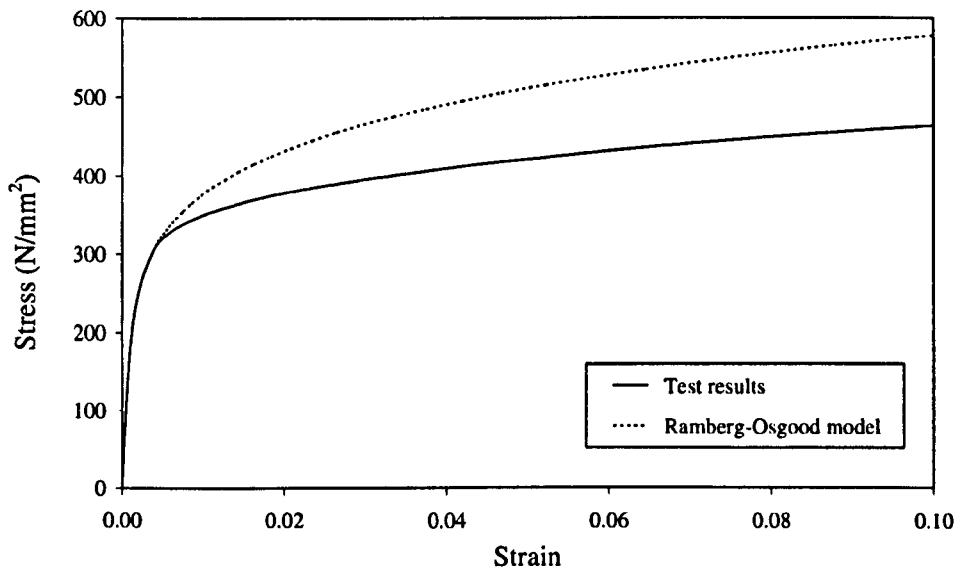
Figure 5.1: Comparison between test results and the Ramberg-Osgood material model for an austenitic Grade 1.4301 material coupon with $\sigma_{0.2} = 296$ N/mm^2 and n = 5.8.

5.2.1.2 Modified Ramberg-Osgood model proposed by Mirambell and Real

Mirambell and Real (2000), as a part of their investigation on the flexural behaviour of stainless steel beams, devised a suitable analytical model for stainless steel stress-strain behaviour. The basic Ramberg-Osgood expression was adopted for stresses up to $\sigma_{0.2}$ where the strain hardening exponent n has been determined using $\sigma_{0.05}$ and $\sigma_{0.2}$ as proposed by

Rasmussen and Hancock (1993b). For stresses beyond $\sigma_{0.2}$ a modified Ramberg-Osgood formula was used by moving the origin from (0, 0) to $(\varepsilon_{t0.2}, \sigma_{0.2})$, where $\varepsilon_{t0.2}$ is the total strain at $\sigma_{0.2}$. This is explained in Figure 5.2 and the proposed relationship is given in Equation 5.4.

$$\varepsilon = \frac{\sigma - \sigma_{0.2}}{E_{0.2}} + \varepsilon_{pu}\left(\frac{\sigma - \sigma_{0.2}}{\sigma_u - \sigma_{0.2}}\right)^n + \varepsilon_{t0.2} \qquad (5.4)$$

where ε_{pu} is the plastic strain at ultimate strength, $\varepsilon_{t0.2}$ is the total strain at $\sigma_{0.2}$ and n is the strain hardening exponent modified using a stress higher than $\sigma_{0.2}$. $E_{0.2}$ is the tangential stiffness at $\sigma_{0.2}$ which can be obtained using Equation 5.5.

$$E_{0.2} = \frac{\sigma_{0.2}E_0}{\sigma_{0.2} + 0.002nE_0} \qquad (5.5)$$
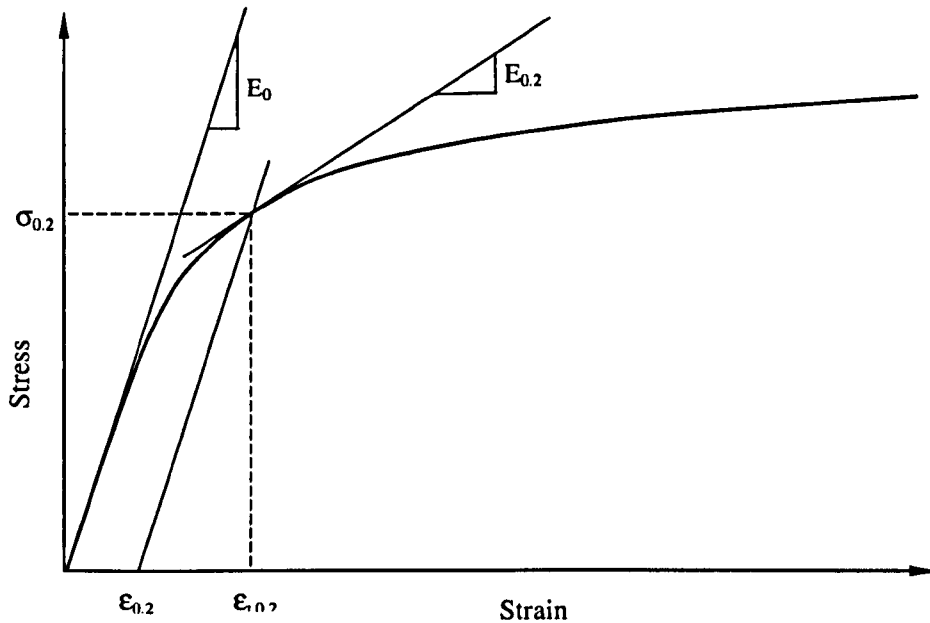
Figure 5.2: Schematic diagram explaining development of modified Ramberg-Osgood Equation.

The proposed relationship was found to be in good agreement with test results. Adoption of two different values for a single parameter n is, however, confusing and no specific guideline was provided, apparently, because of the limited number of test results. Use of ultimate stress σ_u and the corresponding strain ε_u in Equation 5.4 makes its application limited to model tension behaviour only.

5.2.1.3 'Full-range' stress-strain model proposed by Rasmussen

Rasmussen (2001) proposed 'full-range' stress-strain curves for modelling stainless steel alloys following the same approach as proposed by Mirambell and Real (2000). The basic Ramberg-Osgood equation is used up to $\sigma_{0.2}$ with n being determined following Equation 5.6.

$$n = \frac{\ln(20)}{\ln\left(\sigma_{0.2}\big/\sigma_{0.01}\right)} \qquad (5.6)$$

For stresses beyond $\sigma_{0.2}$ the following relationship (Equation 5.7) has been developed by analysing coupon test results obtained from Rasmussen and Hancock (1993), Talja and Salmi (1995), Korvink and van den Berg (1995), Macdonald et al (2000), Olsson (2001) and Burns (2001).

$$\varepsilon = \frac{\sigma - \sigma_{0.2}}{E_{0.2}} + \varepsilon_u\left(\frac{\sigma - \sigma_{0.2}}{\sigma_u - \sigma_{0.2}}\right)^m + \varepsilon_{0.2} \qquad (5.7)$$

This is basically the same expression as proposed by Mirambell and Real (Equation 5.4), the only difference is the notation. However inclusion of a new strain hardening exponent m for stresses beyond $\sigma_{0.2}$ makes it easy to understand; and Equation 5.8 has been developed using test results to obtain m by knowing σ_u.

$$m = 1 + 3.5\frac{\sigma_{0.2}}{\sigma_u} \qquad (5.8)$$

Since inclusion of σ_u and ε_u limits the scope of the formulation to tension only, following guidelines were proposed to obtain equivalent values for these parameters using n, $\sigma_{0.2}$ and E_0 which are given in Equations 5.9 and 5.10.

$$\frac{\sigma_{0.2}}{\sigma_u} = \frac{0.2 + 185(\sigma_{0.2}/E_0)}{1 - 0.0375(n - 5)} \qquad (5.9)$$

$$\varepsilon_u = 1 - \frac{\sigma_{0.2}}{\sigma_u} \qquad (5.10)$$

This model covers the complete stress-strain diagram for stainless steel alloys by using only three basic parameters $\sigma_{0.2}$, E_0 and n. All these relationships are included in the Annex C of prEN 1993-1-4 (2004) to provide guidance for modelling the material behaviour of stainless steel. However each of these empirical formulations possesses considerable scatter which may lead to considerably incorrect material representations. Stainless steel alloys exhibit

significant differences in their stress-strain behaviour not only because of being classified as different grades but also because of the amount of cold-work done during the manufacturing process. Moreover, use of σ_u and ε_u for modelling the compression behaviour of stainless steel could be considered as a practical solution to obtain a generalised material model but, ideally, this should be avoided, if possible.

5.2.1.4 Modified Ramberg-Osgood model proposed by Gardner

Gardner (2002) adopted Mirambell and Real's (2000) approach to obtain a more general and rational material model which could be adopted both in tension and compression without any confusion. The first step was to find a suitable parameter to replace σ_u. Gardner's (2002) proposal was to use the 1% proof stress $\sigma_{1.0}$, instead, to obtain a second strain hardening exponent $n'_{0.2,1.0}$ which could define the exact shape of the curve beyond $\sigma_{0.2}$. Hence Equation 5.11 was proposed by Gardner (2002) for stresses beyond $\sigma_{0.2}$.

$$\varepsilon = \frac{(\sigma - \sigma_{0.2})}{E_{0.2}} + \left(0.008 - \frac{\sigma_{1.0} - \sigma_{0.2}}{E_{0.2}}\right)\left(\frac{\sigma - \sigma_{0.2}}{\sigma_{1.0} - \sigma_{0.2}}\right)^{n'_{0.2,1.0}} + \varepsilon_{t0.2} \qquad (5.11)$$

Gardner (2002) established simple relationships between $\sigma_{1.0}$ and $\sigma_{0.2}$ using test results obtained from his testing programme. Moreover, specific values for $n'_{0.2,1.0}$, in the same way as is done for n, were proposed for different loading conditions i.e. compression and tension. This relationship has been found to give excellent agreement with test results up to 10% strain.

5.2.1.5 Material model adopted in the present research

Gardner's (2002) proposed model has recently been modified by Gardner and Ashraf (2006) to eliminate the observed minor inconsistency caused by considering only the plastic strains at $\sigma_{1.0}$ and $\sigma_{0.2}$. Using the total strains for these points removes this discrepancy, although it does not make any significant physical difference. Hence Equation 5.12 has been adopted for material modelling for stresses beyond $\sigma_{0.2}$ in the present research.

$$\varepsilon = \frac{(\sigma - \sigma_{0.2})}{E_{0.2}} + \left(\varepsilon_{t1.0} - \varepsilon_{t0.2} - \frac{\sigma_{1.0} - \sigma_{0.2}}{E_{0.2}}\right)\left(\frac{\sigma - \sigma_{0.2}}{\sigma_{1.0} - \sigma_{0.2}}\right)^{n'_{0.2,1.0}} + \varepsilon_{t0.2} \qquad (5.12)$$

All available coupon test results have been analysed in Chapter 3 and Table 3.5 lists a summary of the parameters required for this model. All these parameters are the best fit values to the test results, not being obtained using any empirical relationship. Appropriate

recognition of the manufacturing processes has been made to account for the sensitivity to strain hardening.

This model in conjunction with Table 3.5 can provide stress-strain behaviour for stainless steel with the knowledge of the most commonly available parameters $\sigma_{0.2}$ and E_0.

5.2.2 Modelling of corner material

The effect of cold-work on the corners has been explained in Chapter 4 and models have been proposed to predict the enhanced material strength using easily obtainable parameters. These models have been used to obtain the 0.2% proof stress of the corner material $\sigma_{0.2,c}$.

To obtain the complete stress-strain behaviour other required parameters are Young's modulus E_0, strain hardening exponents n and $n'_{0.2,1.0}$, and 1% proof stress $\sigma_{1.0}$. Unavailability of all necessary test details for corner coupons prevented determination of all these parameters in a similar fashion as was done for flat material in Chapter 3. As a result, these parameters were taken to be the same as those for the flat material. This assumption was found to give considerably accurate predictions for the load-deformation responses of structural elements as will be shown later in this chapter.

5.2.3 Incorporating the material behaviour in ABAQUS

Material behaviour is required to be specified in FE models in the form of a multi-linear stress-strain curve, defined in terms of true stress σ_{true} and true plastic strain ε_{true}^{pl}. The relationships between these input parameters and the nominal stress and strain are given in Equations 5.13 and 5.14.

$$\sigma_{true} = \sigma_{nom}\left(1 + \varepsilon_{nom}\right) \tag{5.13}$$

$$\varepsilon_{true}^{pl} = \ln\left(1 + \varepsilon_{nom}\right) - \frac{\sigma_{true}}{E} \tag{5.14}$$

5.3 MODELLING OF STUB COLUMNS

Numerical models have been developed for all the stub columns reported in Table 3.4 to establish a consistent technique which could subsequently be used to conduct parametric studies. However complete load-deformation behaviour was available for 28 stub columns with 4 different cross-section types and hence these results have been used in performing the parametric studies. The developed FE models have been used to investigate the effects of

different key parameters i.e. corner strength enhancement, initial imperfections and residual stresses, on the behaviour of stub columns. Hence specific guidelines have been proposed, which were later employed to obtain additional results, where required, as part of the basis for a design method as explained in Chapter 6.

5.3.1 Boundary conditions and load application

The ends of the stub columns were fixed against all degrees of freedom except for the vertical displacement at the loaded edges. All boundary conditions are shown in Figure 5.3. Constraint equations were used to ensure that all nodes at the loaded end act as a group to move vertically. Nodal loads were applied to the constrained node set.

Top end is free for displacement along vertical axis only

Base is fixed against all degrees of freedom.

L 25 × 25 × 3   I 50 × 50 × 3 × 3
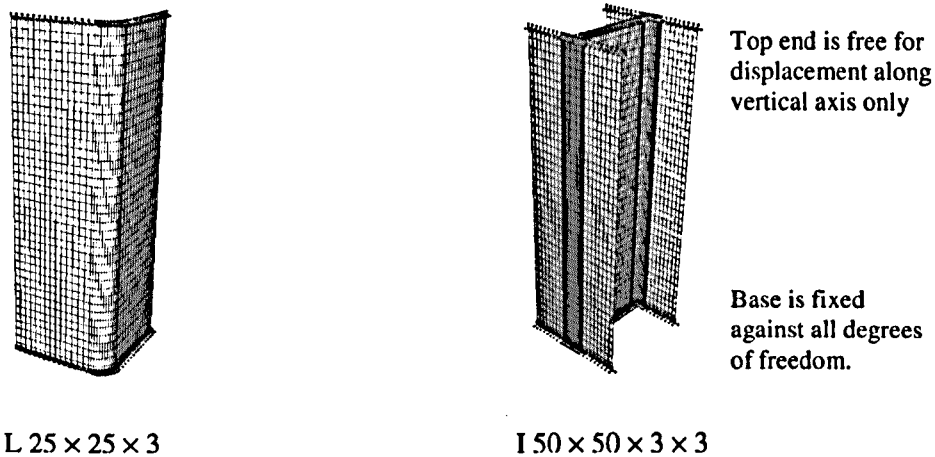
Figure 5.3: Typical boundary conditions applied to the stub columns.

5.3.2 Method of analysis

Availability of sophisticated FE packages such as ABAQUS tempt researchers to go beyond the simple elastic analysis in almost every case. In the present research an elastic linear analysis technique using the *BUCKLING command was used only to obtain the Eigenmodes, which were subsequently used to represent initial geometric imperfections. To understand the actual response of the stub columns, a 'static stress analysis' method was used to analyse the nonlinear behaviour. The nonlinear effects arising from geometric and material nonlinearity were included using the 'NLGEOM' option and the *PLASTIC command respectively as stated in ABAQUS. All the stub columns were treated as geometrically nonlinear static problems involving buckling, where the load-displacement response shows a negative stiffness making the structure 'unstable' after reaching the peak load. ABAQUS offers several techniques to analyse this type of problem and among the available options the 'modified Riks method' was chosen because of its simplicity and widespread use in similar applications.

5.3.3 Selection of an appropriate element

Shell elements are generally used to model thin-walled structures. ABAQUS includes general-purpose shell elements as well as elements that are specifically formulated to analyse 'thick' and 'thin' shell problems. The general-purpose shell elements provide robust and accurate solutions to most applications although, in certain cases, for specific applications, enhanced performance may be obtained using the thin or thick shell elements; for example, if only small strains occur and five degrees of freedom per node are desired.

General-purpose shell elements include transverse shear deformation. They use thick shell theory as the shell thickness increases and become discrete Kirchhoff thin shell elements as the thickness decreases; the transverse shear deformation becomes very small as the shell thickness decreases. Thin shell elements are needed in cases where transverse shear flexibility is negligible. For homogeneous shells this occurs when the thickness is less than about 1/15 of a characteristic length on the surface of the shell, such as the distance between supports. All stainless steel stub columns considered in the present research fall within this category.

Stainless steel structural members are generally modelled using either of the following two shell elements - general-purpose S4R (Lecce and Rasmussen 2005b, Ellobody and Young 2005) or thin-shell S9R5 (Mirambell and Real 2000, Gardner and Nethercot 2004c). The first is a 4-noded general purpose shell element, while the second is a 9-noded thin-shell element. Both of these elements use reduced (lower-order) integration to form the element stiffness, which usually provides more accurate results (provided the elements are not distorted or loaded in in-plane bending) and significantly reduces the running time, especially in three dimensions. S9R5 has five degrees of freedom per node, three displacements and two rotations, which makes it more economical than S4R.

Both of these elements were considered initially to find the more suitable one to be used for the parametric studies. Keeping all other parameters the same, only the element type was changed and the resulting load-deformation results have been compared with the tests results. The results are given in Table 5.1, while Figure 5.4 shows typical comparisons for the load-deformation behaviour obtained using S4R and S9R5 elements with the test results.
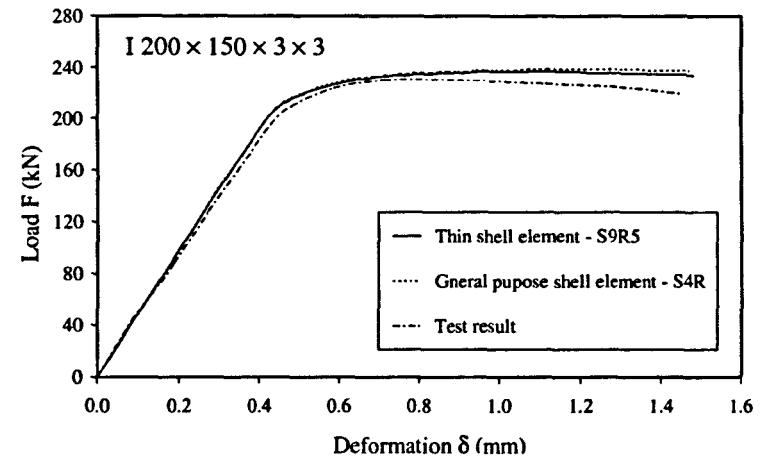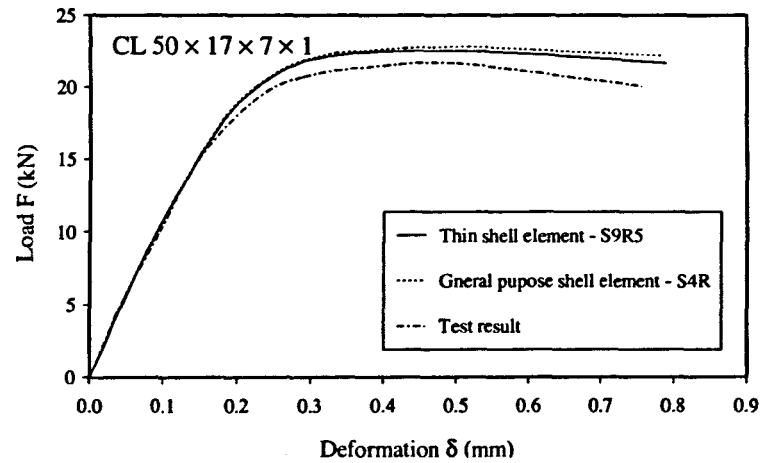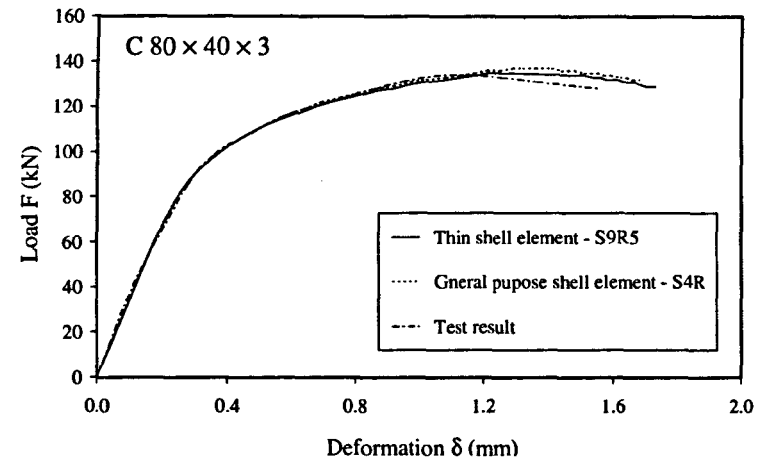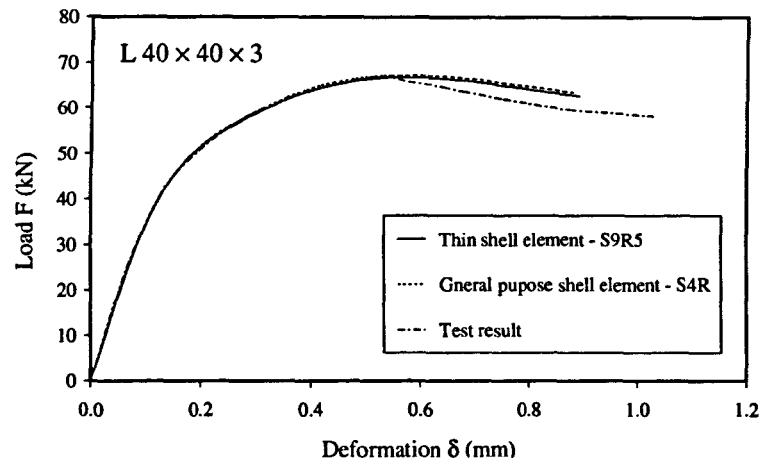
Figure 5.4: Performance of S4R and S9R5 elements in FE modelling of stainless steel stub columns.

Table 5.1: Load-deformation results obtained from FE models of stub columns using general purpose shell element S4R and thin-shell element S9R5.

Section type	Designation	Test Results		General purpose shell element: S4R		Thin-shell element: S9R5	
		F_u (kN)	δ_u (mm)	FE F_u / Test F_u	FE δ_u / Test δ_u	FE F_u / Test F_u	FE δ_u / Test δ_u
Angle	25 × 25 × 3	55.87	1.28	0.94	1.00	0.90	0.98
	30 × 30 × 3	59.38	0.70	0.99	1.27	0.97	1.20
	40 × 40 × 3	66.86	0.50	1.01	1.10	1.00	1.10
	40 × 40 × 3	65.64	0.45	1.04	1.27	1.03	1.31
	50 × 50 × 3	68.69	0.31	1.03	1.29	1.03	1.32
	60 × 60 × 3	69.61	0.25	1.05	1.24	1.06	1.24
Channel	50 × 25 × 3	106.04	2.10	1.04	1.77	0.95	1.29
	80 × 40 × 3	134.18	1.10	1.02	1.17	1.00	1.15
	100 × 50 × 3	146.23	0.90	1.02	0.93	1.01	0.93
	100 × 50 × 3	140.43	0.83	1.07	1.02	1.06	1.04
	150 × 50 × 3	156.00	0.85	0.99	0.87	0.99	0.84
	50 × 50 × 3	125.02	0.72	1.02	1.00	1.02	1.11
Lipped Channel	100 × 50 × 20 × 3	211.39	1.50	1.03	1.24	1.02	1.27
	150 × 50 × 20 × 3	197.04	1.60	1.02	0.96	1.00	0.93
	150 × 65 × 20 × 3	214.77	1.20	1.07	1.42	1.05	1.19
	200 × 75 × 25 × 3	232.78	1.40	1.03	1.21	1.02	1.14
	33 × 17 × 7 × 1	23.66	0.62	0.98	0.84	0.98	0.89
	50 × 17 × 7 × 1	21.68	0.50	1.05	1.04	1.04	0.98
	50 × 22 × 7 × 1	24.27	0.60	1.05	1.02	1.01	0.98
	68 × 25 × 8 × 1	26.10	0.62	1.06	1.29	1.05	1.31
I Sections	50 × 50 × 3 × 3	151.79	2.40	0.94	1.29	0.89	1.21
	50 × 100 × 3 × 3	190.74	0.73	0.95	1.18	0.94	1.12
	100 × 50 × 3 × 3	170.57	1.34	0.93	1.25	0.91	1.10
	100 × 75 × 3 × 3	199.16	1.07	0.97	1.08	0.96	1.08
	100 × 100 × 3 × 3	201.49	0.49	1.05	1.45	1.04	1.45
	150 × 100 × 3 × 3	199.98	0.61	1.12	1.20	1.12	1.20
	200 × 100 × 3 × 3	206.75	0.80	1.02	1.00	1.02	1.00
	200 × 150 × 3 × 3	230.40	0.89	1.04	1.20	1.03	1.12
All Sections		**Average**		**1.02**	**1.16**	**1.00**	**1.12**
		COV		**0.04**	**0.17**	**0.05**	**0.13**

The comparisons show that there is no significant difference between the results obtained using two commonly employed shell elements except for a few stocky sections where the load-deformation curves become completely flat near the peak load F_u making the prediction of δ_u very difficult. In such cases the closest possible value to the test result was taken as δ_u. The stockier sections generally undergo a considerable amount of strain hardening before

failure. Although the deformation capacity of a cross-section is obtained using δ_u, the resulting discrepancies for these sections do not significantly affect the compression resistance of a cross-section since the material stress reaches relatively flat region beyond $\sigma_{0.2}$. However 5-noded thin shell element S9R5 gives better predictions both in terms of average ultimate load and the corresponding deformation. Moreover this element requires less time to converge to a solution. Because of these advantages S9R5 thin shell element has been used for modelling stainless members in the present research.

5.3.4 Convergence study – selecting a suitable mesh

One of the most important aspects of FE modelling is to identify a suitable mesh size. Finer meshes are always preferred to obtain better predictions. But there is no general guideline for this fineness. As a result a convergence study is a pre-requisite to find a suitable mesh for any FE investigation. Although finer meshes generally provide better predictions, they make the whole process more expensive in terms of the time taken to perform an analysis. A compromise is therefore needed between the level of accuracy and the solution cost.

Two different mesh sizes were used to replicate the load-deformation response of stub columns considered in the present research. The number of elements in the finer mesh was 4 times higher than the corresponding coarse mesh. Each of the stub columns was analysed using both of these meshes and the results are given in Table 5.3. Typical load-deformation response of an angle stub column model using different meshes is shown in Figure 5.5.
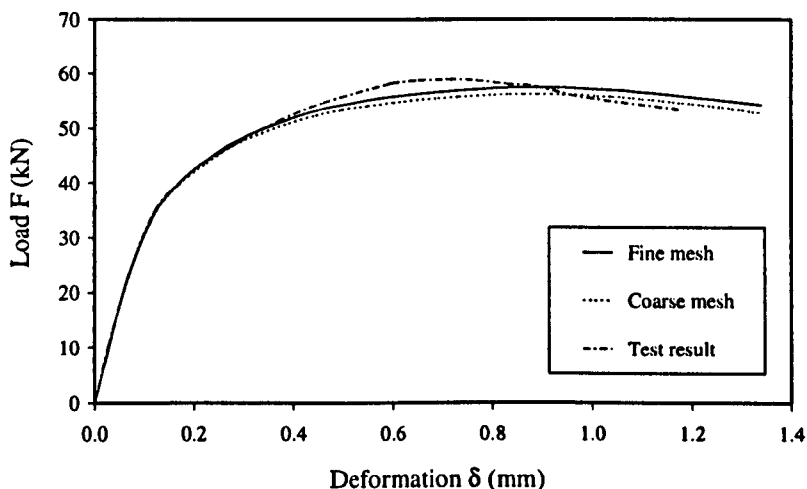
Figure 5.5: Typical load-deformation behaviour of L 30 × 30 × 3 stub column using different mesh.

Table 5.2: Load-deformation results obtained from FE models of stub columns using different meshes.

Section type	Designation	Test Results		Coarse mesh		Fine mesh	
		F_u (kN)	δ_u (mm)	FE F_u / Test F_u	FE δ_u / Test δ_u	FE F_u / Test F_u	FE δ_u / Test δ_u
Angle	$25 \times 25 \times 3$	55.87	1.28	0.90	0.99	0.90	1.00
	$30 \times 30 \times 3$	59.38	0.70	0.95	1.19	0.97	1.20
	$40 \times 40 \times 3$	66.86	0.50	0.96	1.00	1.00	1.10
	$40 \times 40 \times 3$	65.64	0.45	1.01	1.24	1.03	1.29
	$50 \times 50 \times 3$	68.69	0.31	1.02	1.35	1.03	1.29
	$60 \times 60 \times 3$	69.61	0.25	1.06	1.24	1.06	1.24
Channel	$50 \times 25 \times 3$	106.04	2.10	0.96	1.35	0.95	1.29
	$80 \times 40 \times 3$	134.18	1.10	1.01	1.12	1.01	1.15
	$100 \times 50 \times 3$	146.23	0.90	1.01	0.98	1.01	0.97
	$100 \times 50 \times 3$	140.43	0.83	1.06	0.98	1.06	1.00
	$150 \times 50 \times 3$	156.00	0.85	0.99	0.86	0.99	0.86
	$50 \times 50 \times 3$	125.02	0.72	1.02	1.03	1.02	1.03
Lipped Channel	$100 \times 50 \times 20 \times 3$	211.39	1.50	1.03	1.31	1.02	1.27
	$150 \times 50 \times 20 \times 3$	197.04	1.60	1.02	0.93	1.00	0.93
	$150 \times 65 \times 20 \times 3$	214.77	1.20	1.07	1.55	1.05	1.19
	$200 \times 75 \times 25 \times 3$	232.78	1.40	1.04	1.28	1.02	1.14
	$33 \times 17 \times 7 \times 1$	23.66	0.62	0.98	0.90	0.98	0.89
	$50 \times 17 \times 7 \times 1$	21.68	0.50	1.05	1.08	1.04	1.00
	$50 \times 22 \times 7 \times 1$	24.27	0.60	1.04	1.05	1.01	1.00
	$68 \times 25 \times 8 \times 1$	26.10	0.62	1.06	1.29	1.05	1.31
I Sections	$50 \times 50 \times 3 \times 3$	151.79	2.40	0.88	1.16	0.89	1.21
	$50 \times 100 \times 3 \times 3$	190.74	0.73	0.93	1.19	0.94	1.12
	$100 \times 50 \times 3 \times 3$	170.57	1.34	0.91	1.13	0.91	1.10
	$100 \times 75 \times 3 \times 3$	199.16	1.07	0.96	1.06	0.96	1.08
	$100 \times 100 \times 3 \times 3$	201.49	0.49	1.04	1.57	1.04	1.45
	$150 \times 100 \times 3 \times 3$	199.98	0.61	1.11	1.34	1.12	1.20
	$200 \times 100 \times 3 \times 3$	206.75	0.80	1.04	1.08	1.02	1.00
	$200 \times 150 \times 3 \times 3$	230.40	0.89	1.05	1.13	1.03	1.12
All Sections			**Average**	**1.01**	**1.16**	**1.00**	**1.12**
			COV	**0.06**	**0.16**	**0.05**	**0.13**

The results of Table 5.2 showed that there is a little improvement in predictions for both peak load F_u and the corresponding deformation δ_u when using the adopted finer mesh. No further refinement was attempted since the predictions were found to be in good agreement with the test results. The finer mesh was used in the subsequent FE models.

5.3.5 Extent of corner enhancement

Previous research showed that enhanced strength should be included beyond the curved corner of the numerical models to achieve the exact replication of the test results. Karren (1967) found that for carbon steel sections the effect of cold-forming extends beyond the corner to a distance approximately equal to the thickness t. Abdel-Rahman and Sivakumaran (1997) observed increased yield strengths at a distance of $0.5\pi r_i$ from the curved corner portions of cold-formed carbon steel lipped channel cross-sections. But stainless steel exhibits far more pronounced strain hardening than carbon steel and so, it may be assumed that extension to a distance t is a lower bound. Gardner (2002) carried out an extensive parametric study on stainless steel hollow sections to investigate the extent of cold-working. The numerical study revealed that, for stainless steel roll-formed sections, if the corner properties are extended up to 2t beyond the curved portion of cross-sections good agreement with test results is obtained.

Most of the open cross-sections considered in the present research were formed by the press-braking process – unlike Gardner's (2002) roll-formed hollow sections. A parametric study was carried out to investigate the extent to which corner enhancement continues beyond the curved region in this case. Keeping all other parameters to be the same, three different cases were studied – enhanced strength only in the curved corner region, enhanced strength region extended to a distance t beyond the corner and enhanced strength region extended to a distance 2t beyond the corner. Figure 5.6 illustrates these cases and Figure 5.7 shows typical changes in the load-deformation behaviour of stub columns due to a change in the extent of the enhanced corner strength. Ultimate load carrying capacity, F_u and deformation at ultimate load, δ_u for each model are compared to the test results in Table 5.3.
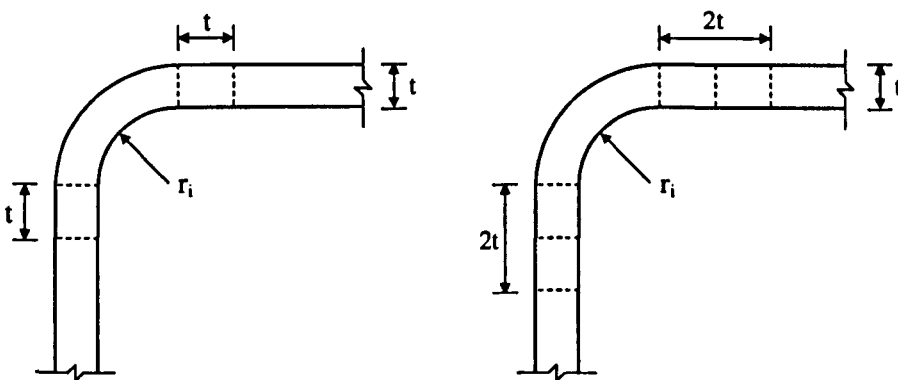
Figure 5.6: Different cases considered to study the extent of corner enhancement.
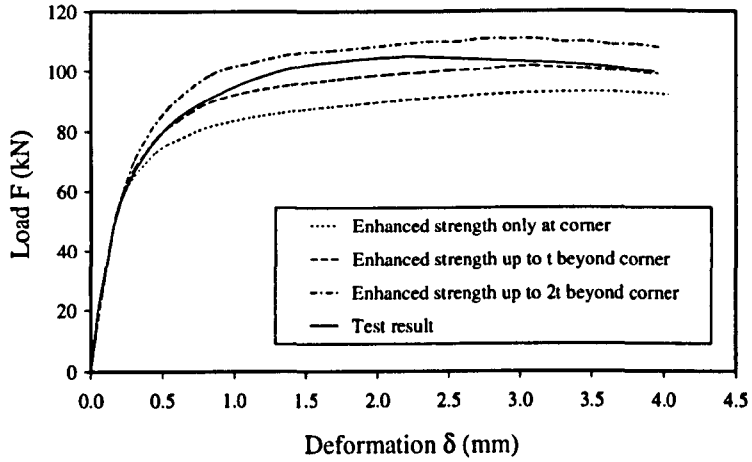
(a) Channel section $50 \times 25 \times 3$ with $\beta = 0.93$
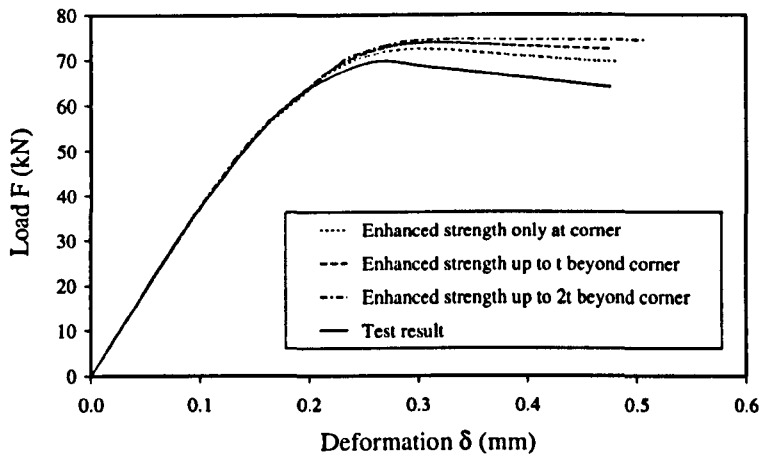
(b) Angle section $60 \times 60 \times 3$ with $\beta = 2.24$

Figure 5.7: Typical load-deformation behaviour for different cases of strength enhancement.

Table 5.3: Load-deformation results obtained from FE models of stub columns using different conditions for corner strength enhancement.

Section type	Designation	Cross-section Slenderness β	Test Results		Extent of enhanced strength used in FE models					
					Corner only		Up to t beyond corner		Up to 2t beyond corner	
			F_u (kN)	δ_u (mm)	FE F_u/ Test F_u	FE δ_u/ Test δ_u	FE F_u/ Test F_u	FE δ_u/ Test δ_u	FE F_u/ Test F_u	FE δ_u/ Test δ_u
Angle	25 × 25 × 3	0.91	55.87	1.28	0.81	0.99	0.90	1.00	0.96	0.77
	30 × 30 × 3	1.11	59.38	0.70	0.88	1.13	0.97	1.20	1.01	1.14
	40 × 40 × 3	1.50	66.86	0.50	0.93	1.02	1.00	1.10	1.01	0.96
	40 × 40 × 3	1.49	65.64	0.45	0.96	1.16	1.03	1.29	1.06	1.31
	50 × 50 × 3	1.89	68.69	0.31	0.99	1.23	1.03	1.29	1.04	1.35
	60 × 60 × 3	2.24	69.61	0.25	1.04	1.20	1.06	1.24	1.07	1.32
Channel	50 × 25 × 3	0.93	106.04	2.10	0.88	1.61	0.95	1.29	1.05	1.40
	80 × 40 × 3	1.53	134.18	1.10	0.95	1.13	1.01	1.15	1.07	1.27
	100 × 50 × 3	1.94	146.23	0.90	0.98	0.89	1.01	0.97	1.07	1.00
	100 × 50 × 3	1.92	140.43	0.83	1.02	1.00	1.06	1.00	1.12	1.13
	150 × 50 × 3	1.94	156.00	0.85	0.98	0.82	0.99	0.86	0.99	0.86
	50 × 50 × 3	1.92	125.02	0.72	0.98	1.00	1.02	1.03	1.09	1.24
Lipped Channel	100 × 50 × 20 × 3	1.29	211.39	1.50	0.93	1.19	1.02	1.27	1.11	1.38
	150 × 50 × 20 × 3	1.95	197.04	1.60	0.96	0.63	1.00	0.93	1.09	1.04
	150 × 65 × 20 × 3	1.96	214.77	1.20	1.00	1.00	1.05	1.19	1.14	1.73
	200 × 75 × 25 × 3	2.63	232.78	1.40	0.97	1.02	1.02	1.14	1.10	1.43
	33 × 17 × 7 × 1	1.31	23.66	0.62	0.90	0.79	0.98	0.89	1.06	0.90
	50 × 17 × 7 × 1	2.00	21.68	0.50	0.97	0.64	1.04	1.00	1.15	1.28
	50 × 22 × 7 × 1	2.00	24.27	0.60	0.98	0.55	1.01	1.00	1.12	1.27
	68 × 25 × 8 × 1	2.74	26.10	0.62	0.98	1.00	1.02	1.31	1.13	1.42
All Sections				**Average**	**0.95**	**1.00**	**1.01**	**1.11**	**1.07**	**1.21**
				COV	**0.06**	**0.24**	**0.04**	**0.13**	**0.05**	**0.19**

Table 5.4 clearly shows that for the press-braked stainless steel sections, the enhanced strength needs to be extended up to t beyond the corner to obtain the best predictions using FE models. This effect varies with the cross-section slenderness β, showing a significant effect for the relatively stocky sections with low β. As the section becomes more slender the local buckling is dominated by the plate slenderness and the effect of enhanced strength corners loses its significance. This effect is obvious in Figure 5.7. All considered stub column models were analysed without any enhanced strength (FE $F_{u,c0}$) and the results were compared to those obtained using corner enhancement up to t (FE $F_{u,ct}$). The results are shown in Figure 5.8. This figure illustrates the importance of using corner properties in the FE models, especially for the relatively stocky cross-sections where this effect is almost directly proportional to β.
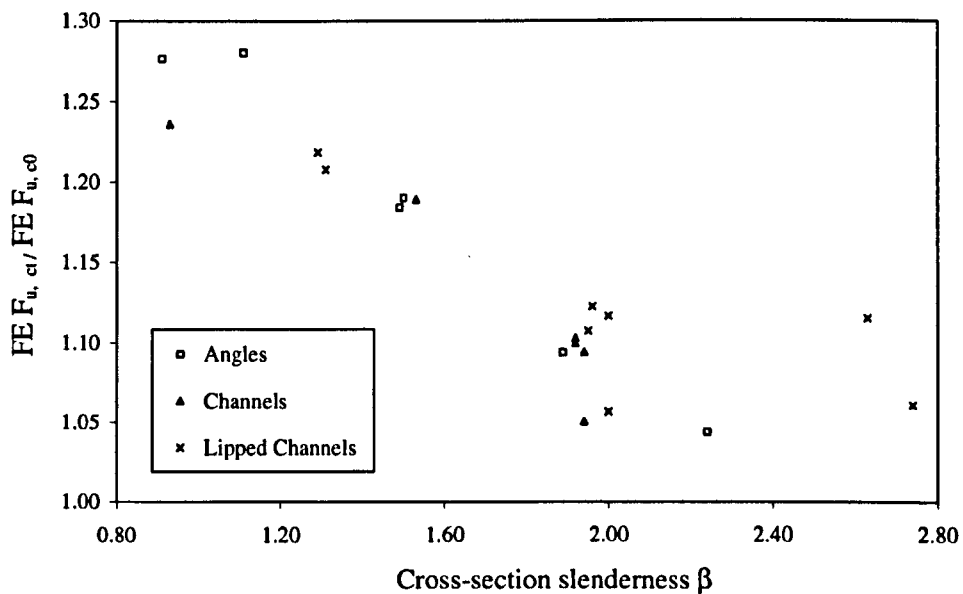
Figure 5.8: Variation of the effect of corner enhancement with cross-section slenderness β.

The present research uses enhanced properties up to t and 2t beyond the corner for the press-braked and roll-formed sections respectively.

5.3.6 Geometric imperfections

Geometric imperfections are an inseparable property of real steel members, with the potential to significantly influence their structural behaviour. When performing an FE analysis to predict the ultimate load, the model should, in general, include both local and global initial imperfections.

Despite the importance of initial geometrical imperfections in the FE analysis of steel members, there are no general guidelines for their specification. Predictions are normally conducted by either modelling the structure with an assumed initial out-of-plane deflection or by using assumed small transverse forces. Accurate knowledge of distribution, shape and magnitude of imperfections is a prerequisite for numerically simulating the response of a structural member. In the absence of a suitable measured data, the magnitude and distribution of imperfections - which is likely to be a complex function of the rolling and fabrication process, material strength and geometrical properties of the cross-section - must be predicted. The present study provides guidelines for predicting the shape and magnitude of initial imperfections for stub columns for use in FE modelling.

5.3.6.1 Summary of the literature review

The importance of initial geometric imperfections in steel components has been recognised by researchers for more than three decades. Early research was limited to ordinary carbon steel sections. As an example, imperfection sensitivity of stiffened steel plates, of the type widely used in offshore floating construction, was studied by Mateus and Witz (2001) and Grondin et al. (1999). Recently, the development of design codes for stainless steel has required identification of geometric imperfection characteristics for stainless steel sections. This section investigates the geometric imperfections of stub columns subjected to axial compression, beginning by providing a summary of the literature review reported in detail in Chapter 2.

Sine waves are one of the most commonly used shapes to define the distribution of initial imperfections. The most commonly adopted technique is to perform an elastic buckling analysis prior to the nonlinear analysis and to use one of the Eigenmodes, chosen depending on specific criteria, as the initial shape. The main challenge is to select the appropriate Eigenmode which can represent the actual state of imperfection so that the model closely represents the actual (experimental) behaviour. The maximum amplitude is often taken as a percentage of plate thickness. This type of relationship is always likely to be case sensitive and no specific approach has, so far, been reported that is generally applicable.

Table 5.4 gives a summary of the previous research performed on geometric imperfections, where t is the plate thickness, ω_0 is the imperfection amplitude, $\sigma_{0.2}$ and σ_{cr} are 0.2% proof stress of material and elastic critical plate buckling stress respectively.

Table 5.4: Summary of the previous research performed on local geometric imperfections.

Researcher	Structural component/configuration	Experimental/ Numerical	Imperfection model proposed/used		Comment
			shape	magnitude	
Dawson and Walker (1972)	Simply supported steel plates under compression and bending.	Experimental	-	$\omega_0/t = \alpha\,(\sigma_y/\sigma_{cr})^{0.5}$ $\omega_0/t = \gamma\,(\sigma_y/\sigma_{cr})$	Proposed imperfections can be used in designing cold-formed steel sections.
Hopperstad et al. (1997)	Aluminium cruciform sections under compression.	Numerical	$\omega = \omega_0\,(y/b)\cos(\pi x/L)$	0.01t to 0.1t	Stocky plates are more sensitive to imperfection amplitude.
Schafer and Peköz (1998)	Cold-formed steel lipped channels	Experimental	Eigenmodes	$\omega_0 = 0.006w$ $\omega_0 = 6te^{-2t}$	Periodicity was observed in imperfection distribution.
Sun and Butterworth (1998)	Roll-formed steel angles subjected to eccentric compression.	Experimental and numerical	Half sine waves	0.167t, 0.333t, 0.5t and 0.667t	Amplitude of 0.333t observed to give best results.
Chou et al. (2000)	Cold-formed steel lipped channels and hat sections under compression.	Numerical	Eigenmodes	0.1t, 0.5t and Dawson and Walker's proposal	Dawson and Walker's proposed method with α = 0.3 gave consistent results.
Gardner (2002)	Roll-formed stainless steel hollow sections under compression	Experimental and numerical	1st Eigenmode	$\omega_0/t =$ $0.023(\sigma_{0.2}/\sigma_{cr})$	For SHS and RHS the proposed magnitude gave good predictions
Kaitila (2002)	Cold-formed steel lipped channels	Numerical	Eigenmodes	0 to h/200 where h is the web height.	No general guidelines emerged from the study.
Dubina and Ungureanu (2002)	Cold-formed steel channels and lipped channels	Numerical	Eigenmodes (1st and 5th) and measured imperfections.	Schafer and Peköz's proposals.	Actual distribution gave the best results when used in numerical modelling. Schafer and Peköz's proposal was found 'helpful'.

5.3.6.2 Modelling of distribution and magnitude

The present study is concerned with the behaviour of stainless steel stub columns with angle, channel, lipped channel and I sections. Test results reported by Kuwamura (2003) and Stangenberg (2000a) have been used to verify the models developed using the FE package ABAQUS V6.4. A total of 33 stub column test results giving full load-deformation behaviour are available from these two sources. No imperfection measurements are available from these two references. Hence the load-deformation data available from these sources were utilised to develop a general rule for the shape and magnitude of geometrical imperfections.

The most commonly used technique, employing Eigenmodes to define the initial geometry of a structure, was adopted in the present work. Elastic analyses of the stub columns were first conducted to produce the Eigenmodes. Once the Eigenmodes have been obtained, the main focus is selection of the most suitable one which leads to a close replication of the actual load-deformation behaviour. Figure 5.9 shows some typical Eigenmodes obtained from numerical analysis. Each of the first three Eigenmodes was used individually to study the effect of imperfection distribution on load-deformation response. Figure 5.10 shows the typical load-deformation behaviour for stub columns as a result of changing the shape of the imperfection distribution.

In ABAQUS the nodal displacements of an Eigenmode are normalised using the maximum displacement that occurs within the structure and thus the maximum displacement is set equal to 1. By specifying an appropriate multiplying factor, commonly known as the amplitude, the nodal co-ordinates of the Eigenmode under consideration can be defined accordingly. The present study is also concerned with devising a representative value for the amplitude to be used in the imperfection distribution defined by the Eigenmodes. Schafer and Peköz's (1998) proposal was used by various researchers and was found 'helpful'. But the proposals are 'too simple an analysis to have general applicability' and should be examined before using it as a general guideline. Gardner's (2002) proposed relationship for imperfection amplitude includes both material and geometrical properties and gave good predictions for roll-formed stainless steel sections. Initial imperfections for all the stub columns considered in the present study were modelled using these two approaches and were compared with the test results. The obtained FE results are compared and discussed in the following section.
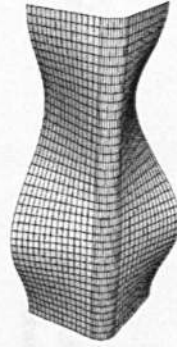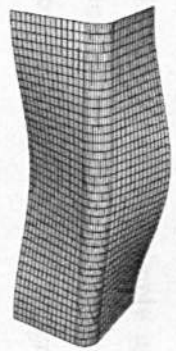
Eigenmodes 1, 2 and 3 for L 25 × 25 × 3
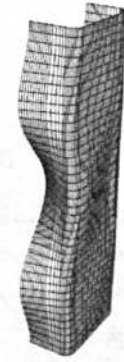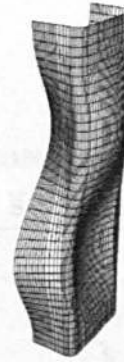
Eigenmodes 1, 2 and 3 for C 50 × 25 × 3
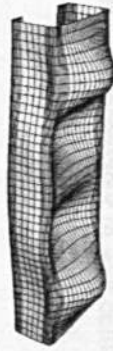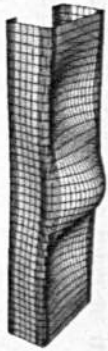
Eigenmodes 1, 2 and 3 for CL 100 × 50 × 20 × 3
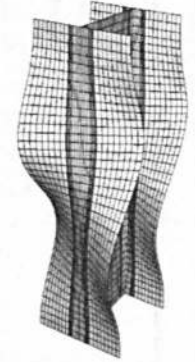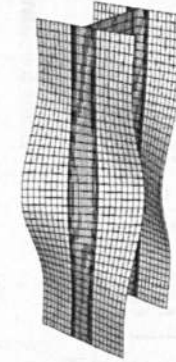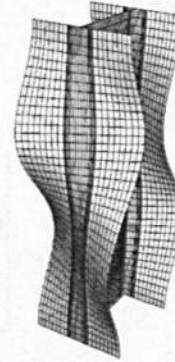
Eigenmodes 1, 2 and 3 for I 50 × 50 × 3 × 3

Figure 5.9: Typical Eigenmodes obtained by performing elastic analysis for stainless steel open sections.
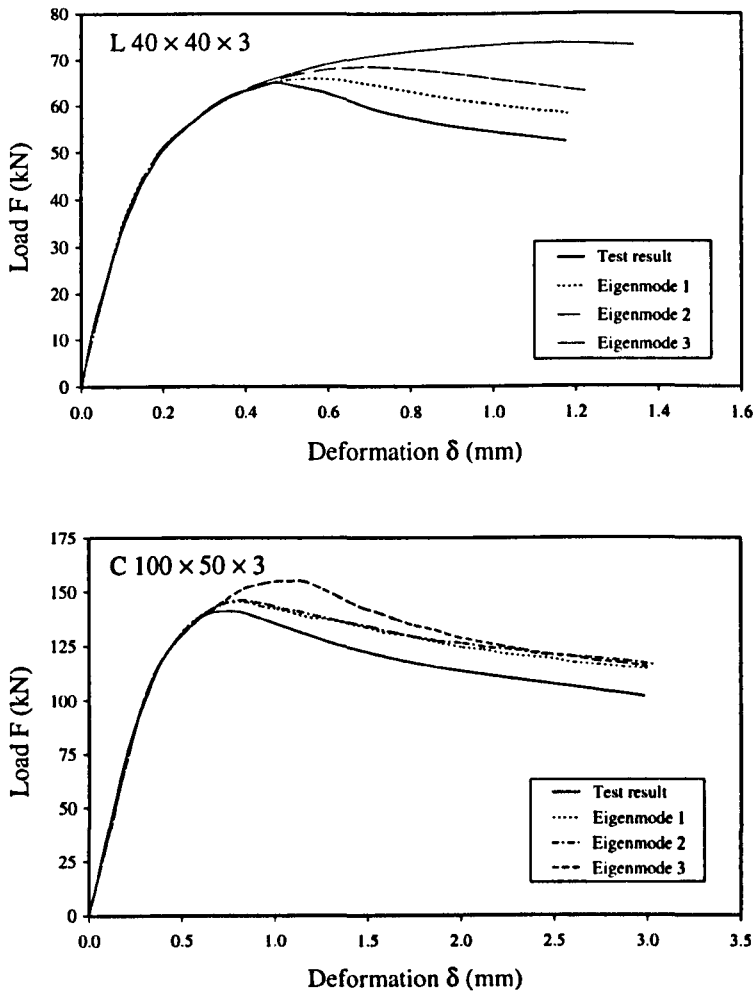
Figure 5.10: Typical variations in load-deformation behaviour of stub columns as a result of using different imperfection distributions (Eigenmodes).

5.3.6.3 Results and analysis

Each stub column was analysed six times, involving 3 Eigenmodes and 2 imperfection amplitudes, and the load-deformation results are compared in Tables 5.5 and 5.6. The mean and the coefficient of variation (COV) of the obtained FE results were also calculated and are reported herein.

Angle sections are observed to be the most sensitive to imperfection mode. Angles are formed by two outstand plates with a free edge, whereas all other sections have at least one relatively stable plate which is simply supported along both edges. The inherent instability resulting from the reduced support for the component plates may be the reason for making the angle sections more sensitive to imperfection shape.

From the average scatter of results it is observed that the peak load F_u is less sensitive to imperfection shape than is the corresponding deformation δ_u. In the case of imperfection amplitude, Gardner's (2002) proposed technique gives relatively consistent results and predictions closer to the test results than does Shafer and Peköz's (1998) proposed method. The best prediction is obtained when Eigenmode 1 is used in conjunction with the amplitude taken from Gardner's (2002) proposal.

Table 5.5: Load-deformation results using imperfection amplitude from Schafer and Peköz's (1998) proposed model.

Designation	Imperfection amplitude ω_0 (mm)	Eigenmode 1		Eigenmode 2		Eigenmode 3	
		FE F_u / Test F_u	FE δ_u / Test δ_u	FE F_u / Test F_u	FE δ_u / Test δ_u	FE F_u / Test F_u	FE δ_u / Test δ_u
L 25 × 25 × 3	0.15	0.85	0.68	0.85	0.82	0.90	1.22
L 30 × 30 × 3	0.18	0.88	0.84	0.90	1.03	0.96	1.69
L 40 × 40 × 3	0.24	0.92	0.79	0.93	0.91	0.99	1.29
L 40 × 40 × 3	0.24	0.94	1.01	0.94	0.96	1.00	1.36
L 50 × 50 × 3	0.30	0.96	1.34	1.01	1.68	1.13	2.33
L 60 × 60 × 3	0.36	1.02	1.83	1.10	1.90	1.24	2.38
C 50 × 25 × 3	0.21	0.91	0.98	0.91	0.88	0.92	1.13
C 80 × 40 × 3	0.40	0.90	1.02	0.92	0.89	0.97	1.33
C 100 × 50 × 3	0.53	0.92	1.04	0.94	0.93	1.02	1.64
C 100 × 50 × 3	0.53	0.95	1.09	0.95	0.96	1.00	1.61
C 150 × 50 × 3	0.83	0.88	1.14	0.86	1.07	0.90	0.95
C 50 × 50 × 3	0.30	0.94	1.17	0.97	1.08	1.02	1.36
CL 100 × 50 × 20 × 3	0.53	0.95	1.20	0.90	0.99	0.91	1.15
CL 150 × 50 × 20 × 3	0.83	0.98	1.32	1.04	1.81	0.99	1.42
CL 150 × 65 × 20 × 3	0.83	1.03	1.62	0.99	1.50	1.01	1.66
CL 200 × 75 × 25 × 3	1.13	1.03	1.42	1.07	1.75	1.04	1.68
CL 33 × 17 × 7 × 1	0.17	0.90	0.83	0.93	1.03	0.90	0.92
CL 50 × 17 × 7 × 1	0.28	1.03	1.27	1.08	1.69	1.04	1.25
CL 50 × 22 × 7 × 1	0.28	1.01	1.04	0.98	0.90	0.99	1.12
CL 68 × 25 × 8 × 1	0.38	1.04	1.71	1.01	1.52	1.02	1.71
I 50 × 50 × 3 × 3	0.27	0.79	0.45	0.80	0.61	0.82	0.81
I 50 × 100 × 3 × 3	0.26	0.89	1.06	0.89	1.10	0.91	1.14
I 100 × 50 × 3 × 3	0.57	0.83	0.65	0.83	0.66	0.85	0.76
I 100 × 75 × 3 × 3	0.57	0.86	0.71	0.87	0.76	0.86	0.83
I 100 × 100 × 3 × 3	0.57	0.94	1.44	0.99	1.42	1.01	1.70
I 150 × 100 × 3 × 3	0.87	0.97	1.69	0.98	1.54	1.05	1.54
I 200 × 100 × 3 × 3	1.17	0.94	1.63	0.96	1.56	0.99	1.44
I 200 × 150 × 3 × 3	1.17	1.02	1.58	1.01	1.67	0.99	1.47
I 160 × 80 × 10 × 6	0.83	0.95	0.52	0.96	0.46	0.95	0.48
I 160 × 160 × 10 × 6	0.84	0.99	0.65	0.95	0.48	0.99	0.61
I 320 × 160 × 10 × 6	1.80	0.97	0.85	0.98	0.73	1.00	0.92
I 160 × 160 × 10 × 6	0.84	0.95	0.65	0.93	0.55	0.95	0.66
All Sections	**Average**	**0.94**	**1.10**	**0.95**	**1.12**	**0.98**	**1.30**
	COV	**0.07**	**0.34**	**0.07**	**0.38**	**0.08**	**0.34**

Table 5.6: Load-deformation results using imperfection amplitude from Gardner's (2002) proposed model.

Designation	Imperfection amplitude ω_0 (mm)	Eigenmode 1		Eigenmode 2		Eigenmode 3	
		FE F_u / Test F_u	FE δ_u / Test δ_u	FE F_u / Test F_u	FE δ_u / Test δ_u	FE F_u / Test F_u	FE δ_u / Test δ_u
L $25 \times 25 \times 3$	0.02	0.90	1.00	0.92	1.58	0.96	1.76
L $30 \times 30 \times 3$	0.02	0.97	1.20	0.96	1.51	1.02	2.56
L $40 \times 40 \times 3$	0.04	1.00	1.10	0.99	1.00	1.05	1.82
L $40 \times 40 \times 3$	0.04	1.03	1.29	1.05	1.45	1.13	2.31
L $50 \times 50 \times 3$	0.07	1.03	1.29	1.08	1.61	1.20	2.55
L $60 \times 60 \times 3$	0.10	1.06	1.24	1.16	1.77	1.31	2.30
C $50 \times 25 \times 3$	0.02	0.95	1.29	0.96	1.34	0.95	1.31
C $80 \times 40 \times 3$	0.04	1.01	1.15	0.99	1.18	1.03	1.27
C $100 \times 50 \times 3$	0.07	1.01	0.97	1.01	1.03	1.07	1.23
C $100 \times 50 \times 3$	0.07	1.06	1.00	1.04	1.07	1.10	1.22
C $150 \times 50 \times 3$	0.07	0.99	0.86	0.95	0.86	0.98	0.88
C $50 \times 50 \times 3$	0.07	1.02	1.03	1.02	1.04	1.03	1.06
CL $100 \times 50 \times 20 \times 3$	0.02	1.02	1.27	1.00	1.19	1.00	1.23
CL $150 \times 50 \times 20 \times 3$	0.06	1.00	0.93	1.06	1.72	0.99	1.18
CL $150 \times 65 \times 20 \times 3$	0.06	1.05	1.19	1.02	1.26	1.05	1.58
CL $200 \times 75 \times 25 \times 3$	0.11	1.02	1.14	1.08	1.92	1.07	1.73
CL $33 \times 17 \times 7 \times 1$	0.01	0.98	0.89	0.99	1.03	0.98	0.96
CL $50 \times 17 \times 7 \times 1$	0.02	1.04	1.00	1.07	0.74	1.05	0.98
CL $50 \times 22 \times 7 \times 1$	0.02	1.01	1.00	1.01	0.87	1.03	1.14
CL $68 \times 25 \times 8 \times 1$	0.04	1.05	1.31	1.02	1.44	1.04	1.70
I $50 \times 50 \times 3 \times 3$	0.01	0.89	1.21	0.89	1.18	0.91	1.21
I $50 \times 100 \times 3 \times 3$	0.06	0.94	1.12	0.93	1.21	0.95	1.28
I $100 \times 50 \times 3 \times 3$	0.03	0.91	1.10	0.91	1.10	0.92	1.27
I $100 \times 75 \times 3 \times 3$	0.03	0.96	1.08	0.96	1.07	0.96	1.08
I $100 \times 100 \times 3 \times 3$	0.06	1.04	1.45	1.06	1.67	1.09	1.83
I $150 \times 100 \times 3 \times 3$	0.06	1.06	1.20	1.13	1.38	1.18	1.55
I $200 \times 100 \times 3 \times 3$	0.11	1.02	1.00	1.05	1.09	1.07	1.07
I $200 \times 150 \times 3 \times 3$	0.14	1.03	1.12	1.04	1.03	1.08	0.99
I $160 \times 80 \times 10 \times 6$	0.03	1.03	0.80	1.02	0.76	1.02	0.75
I $160 \times 160 \times 10 \times 6$	0.03	1.05	1.03	1.06	1.03	1.08	1.15
I $320 \times 160 \times 10 \times 6$	0.14	1.01	0.81	1.01	0.75	1.02	0.85
I $160 \times 160 \times 10 \times 6$	0.05	0.99	1.00	0.99	0.93	0.99	1.02
All Sections	**Average**	**1.00**	**1.10**	**1.01**	**1.21**	**1.04**	**1.40**
	COV	**0.05**	**0.14**	**0.06**	**0.26**	**0.08**	**0.35**

5.3.6.4 Conclusions

Numerical modelling of stainless steel stub columns must make appropriate provision for the shape and magnitude of initial geometrical imperfections. Proposals made by previous researchers were analysed and two different models have been used in the FE analysis of several different stub columns. Based on careful comparisons against test results it was observed that Gardner's (2002) proposed model produced the best results. This model was originally proposed by using the measured imperfections in roll-formed stainless steel hollow sections. The present study shows that this relationship can be used to predict initial imperfection magnitudes for all types of stainless steel stub columns when the shape is modelled using the first Eigenmode obtained from an elastic analysis.

5.3.7 Residual Stresses

Residual stresses are induced into cold-formed stainless steel members as a result of the deformations during the cold-forming process and due to the thermal gradients that are produced during welding. Due to the inherent uncertainty associated with the magnitude and distribution of residual stresses, their effect is often taken into account in numerical models with an appropriate increase in the magnitude of assumed initial geometric imperfections (Stangenberg 2000a).

Both Rasmussen and Hancock (1993) and Gardner (2002) observed that the tension and compression coupons cut from finished sections were curved longitudinally because of the through-thickness bending residual stresses. As a part of the testing procedure, the coupons are straightened, which re-introduces the bending residual stress within the coupons. So, if the material properties are established using coupons cut from within the cross-section, the effects of bending residual stresses are inherently present, and do not need to be defined explicitly in the numerical models. It is only the membrane stresses induced through welding that need to be explicitly defined in numerical models.

Lagerqvist and Olsson (2001) measured residual stresses in two welded I girders of austenitic and austenitic-ferritic stainless steel. The obtained pattern resembles the established models for carbon steel but no specific guidelines were proposed. In the case of angle, channel and lipped channel sections the bending residual stresses were ignored in numerical models. However, in the case of I sections, the thermally induced residual stresses were modelled following the established guidelines for carbon steel (ECSC, 1984), as shown in Figure 5.11, since no specific guidance is currently available for stainless steel.

Flange:
$a_1 = 0.075b_f$
$a_2 = 0.125b_f$

Web:
$a_1 = 0.075d_1$
$a_2 = 0.125\ d_1$

Note: σ_y has been replaced by $\sigma_{0.2}$ in the case of stainless steel
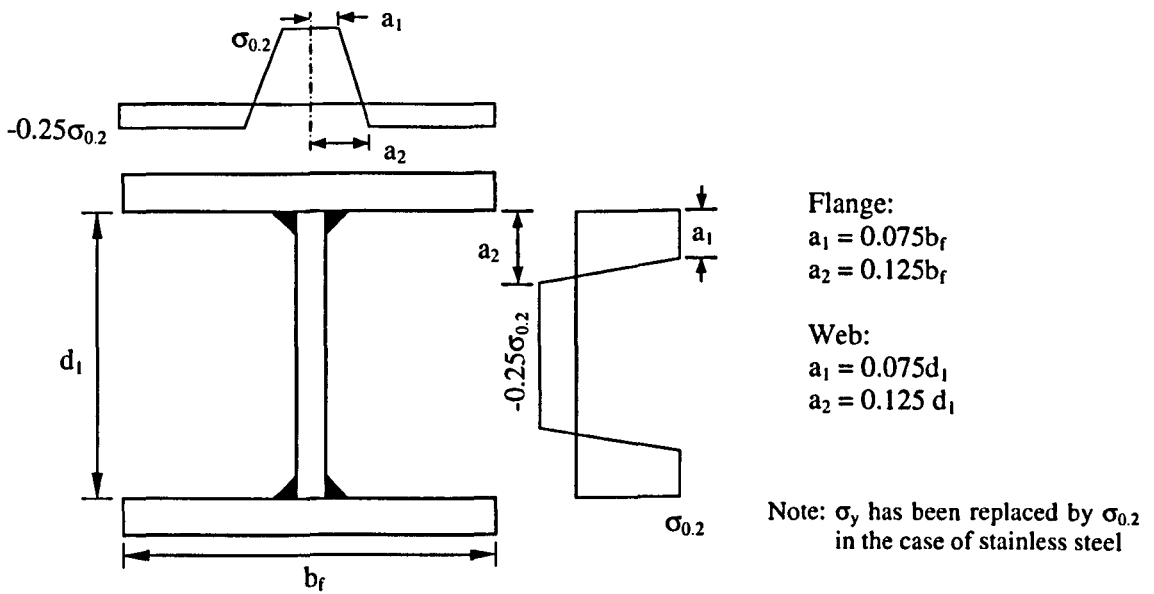
Figure 5.11: Assumed residual stress distribution for welded I sections.

Each of the I section stub columns was modelled twice – with and without residual stresses. The results are compared to the test results in Table 5.7. From the obtained results it is observed that the effect of residual stresses on the peak load F_u and the corresponding deformation δ_u is not very significant. However inclusion of residual stress reduced the initial stiffness of I stub columns which resulted in higher values for δ_u. This suggests that the actual residual stress (thermal) pattern for stainless steel might be different from that of carbon steel. Figure 5.12 shows typical variation in load-deformation behaviour due to the inclusion of residual stresses.

Table 5.7: Load-deformation results obtained from FE models of I stub columns with and without residual stresses.

Designation	Test Results		Without Residual Stress		With Residual Stress	
	F_u (kN)	δ_u (mm)	FE F_u / Test F_u	FE δ_u / Test δ_u	FE F_u / Test F_u	FE δ_u / Test δ_u
50 × 50 × 3 × 3	151.79	2.40	0.89	1.21	0.89	1.19
50 × 100 × 3 × 3	190.74	0.73	0.94	1.12	0.94	1.18
100 × 50 × 3 × 3	170.57	1.34	0.91	1.10	0.92	1.22
100 × 75 × 3 × 3	199.16	1.07	0.96	1.08	0.97	1.17
100 × 100 × 3 × 3	201.49	0.49	1.04	1.45	1.05	1.55
150 × 100 × 3 × 3	199.98	0.61	1.12	1.20	1.15	1.38
200 × 100 × 3 × 3	206.75	0.80	1.02	1.00	1.06	1.05
200 × 150 × 3 × 3	230.40	0.89	1.03	1.12	1.05	1.22
All Sections	Average		0.99	1.16	1.00	1.24
	COV		0.08	0.11	0.09	0.12
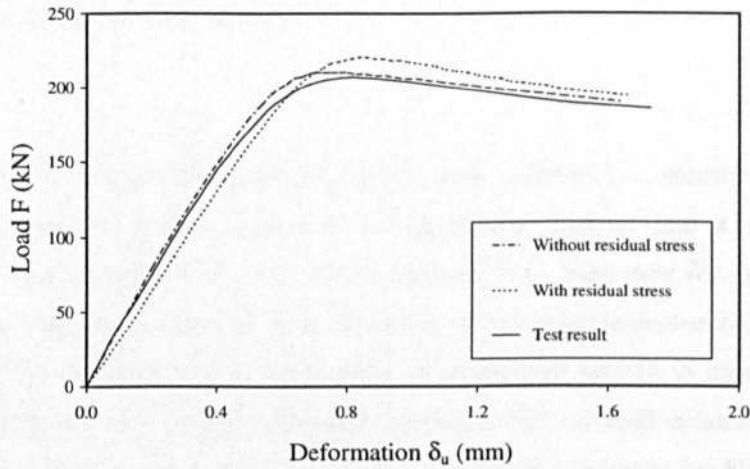
Figure 5.12: Typical load-deformation behaviour of I 200 × 150 × 3 × 3 stub column modelled with and without thermal residual stresses.

5.3.8 Concluding remarks

Numerical modelling techniques for stainless steel open sections have been explained in detail, giving specific guidelines for the modelling of corner regions, initial imperfections and residual stresses. The numerical models for press-braked stainless steel sections give the closest predictions to the tests when the enhanced corner properties are used up to a distance equal to the plate thickness beyond the corner region. The initial imperfection distribution can be modelled using the first Eigenmode with the corresponding amplitude obtained using Gardner's (2002) proposal. Thermal residual stresses were explicitly defined in the case of I sections but did not seem to have any significant effect. The performances of all numerical models were compared to the experimentally obtained load-deformation response and failure modes, where available. Some typical failure modes obtained using ABAQUS are shown in Figure 5.13. The FE results have been found to be in good agreement with the test results.

L 25×25×3   C 50×25×3   CL 150×65×20×3   I 50×50×3×3
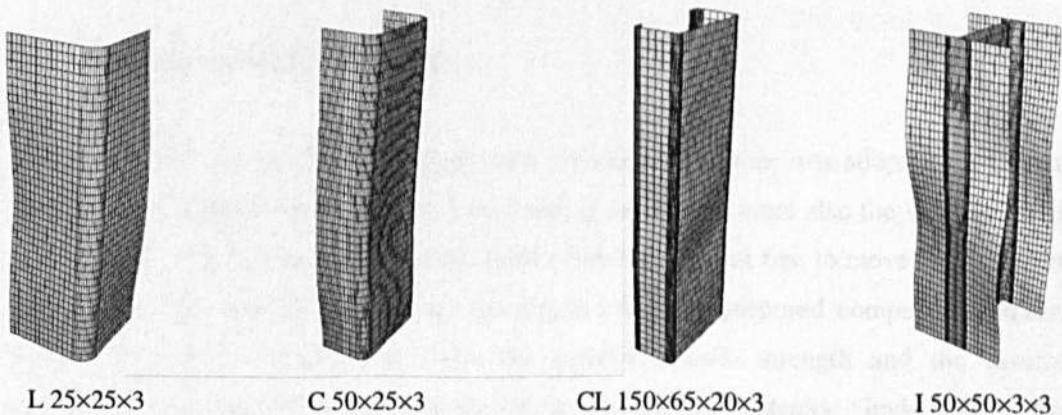
Figure 5.13: Typical failure modes obtained using ABAQUS for stainless steel stub columns.

5.4 MODELLING OF LONG COLUMNS

5.4.1 General

The successful modelling techniques adopted for stub columns i.e. material modelling for both flat and corner regions, selecting an appropriate element and a suitable mesh, incorporating local imperfections and residual stresses, have been used for long columns as well. The other important concerns were the inclusion of global imperfections, definition of correct boundary conditions and the application of appropriate loading. A comprehensive FE modelling scheme was developed involving fixed-ended SHS and RHS columns tested by Lui and Young (2003) and Young and Lui (2003) , pin-ended I columns buckling about both major and minor axes as reported by Stangenberg (2000b) and pin-ended lipped channel columns tested by Rhodes et al (2000). A detailed investigation has been made to select the appropriate distribution and magnitude of global imperfections and to assess its importance.

5.4.2 Fixed-ended SHS and RHS columns

This section describes the modelling techniques adopted for 8 SHS and 16 RHS fixed ended columns tested by Liu and Young (2003) and Young and Liu (2003) respectively. The models were developed using the measured cross-sectional and material properties. Only tensile tests were performed on the coupons collected from the roll-formed cross-sections. As mentioned in Chapter 3, for austenitic Grade 1.4301 compressive strength is, on average, 7% lower than the corresponding tensile strength. The columns were modelled using both the reported tensile strength and the reduced compressive strength. Effect of imperfection amplitude on column resistance has been investigated by giving special recognition to the type of distribution used. The distributions were obtained from elastic analysis and an appropriate shape was selected by investigating the first 20 Eigenmodes.

5.4.2.1 Development of FE models

Thin-shell S9R5 element has been used with a similar mesh that was adopted for the stub columns. The boundary conditions and the loading techniques were also the same as for the stub columns – the base was completely fixed while the top was free to move only along the vertical axis. The material model was developed using the proposed compound Ramberg-Osgood parameters (Table 3.5). Both the reported tensile strength and the assumed compressive strength (7% lower than the tensile strength for austenitic Grade 1.4301) have been used separately to study the effect of material strength.

Initial geometric imperfections were introduced using the Eigenmodes obtained from linear elastic analysis. Gardner (2002) modelled 16 SHS and 20 RHS pin-ended columns and from his study it was observed that an initial out of straightness of L/2000, where L is the column length, produced the best FE predictions. In the case of pin-ended columns, Eigenmode 1 always represents a global buckling mode. But in the case of fixed-ended columns it could not be taken for granted – the buckling modes obtained from the elastic analyses were a complex function of column length and cross-sectional properties. In the case of some FE models no global buckling mode was observed among the first 20 Eigenmodes considered. Rather, the failure modes for these columns were dominated by local failure, which makes using an amplitude of L/2000 inappropriate since this magnitude was proposed by Gardner (2002) for global buckling. Since the column behaviour resembled stub columns, the proposed guideline for the local imperfection as stated in Section 5.3.6.2 has been used and the obtained results have been compared to the test results.

Initial imperfection distributions in actual columns are believed to be a combination of global and local out-of-straightness. Although Eigenmodes are generally used to define these unpredictable imperfections in numerical models, the key issue is how to choose a representative distribution. In the case of the present research, it was even more difficult since all the considered test results were obtained from previous literature and, in most of the cases, imperfection patterns were not available. However, the main objective was to obtain a simplified solution for incorporating initial imperfections so that numerically predicted load-deformation behaviour resembles those obtained from test results.

When elastic analysis produced both global and local buckling modes, these were combined with amplitudes of L/2000 and $0.023(\sigma_{cr}/\sigma_{0.2})t$ for the global and the local mode respectively. However, this type of combination has been found to have no significant effect on the column behaviour. The buckling behaviour is dominated by the global imperfection, and the addition of local imperfections to the numerical model has been observed not to affect the column resistance. Hence the combination of global and local imperfections has not been considered in the present study.

5.4.2.2 Results and analysis

Table 5.8 compares the results obtained using the reported tensile material properties and the assumed compressive properties. In both the cases the imperfection magnitude was taken as

L/2000. The average results show that an assumed 7% reduction in the reported tensile $\sigma_{0.2}$ reduces the overall prediction for F_u by 4%, although the scatter remains almost the same.

Table 5.8: FE results for the SHS and RHS fixed-ended columns using reported tensile and predicted compressive material properties.

Designation	Cross-section slenderness β	Member slenderness $\bar{\lambda}$	Test F_u (kN)	FE F_u / Test F_u (Tensile)	FE F_u / Test F_u (Compressive)
70 × 70 × 2	1.42	0.26	190	0.82	0.73
	1.40	0.43	188	0.79	0.74
	1.43	0.60	159	0.93	0.82
	1.42	0.77	115	1.01	0.99
70 × 70 × 5	0.62	0.33	669	0.97	0.90
	0.61	0.56	510	1.04	0.99
	0.61	0.78	407	1.01	1.00
	0.62	1.00	281	1.14	1.15
120 × 40 × 2	2.47	0.36	167	1.01	0.94
	2.46	0.61	141	1.18	1.11
	2.43	0.85	96	1.26	1.04
	2.45	1.09	84	0.98	0.99
120 × 40 × 5.3	0.97	0.54	717	0.86	0.83
	0.98	0.90	417	0.99	0.99
	0.98	1.26	261	1.08	1.10
	0.98	1.62	164	1.20	1.21
120 × 80 × 3	1.74	0.22	398	0.87	0.83
	1.76	0.37	394	0.86	0.81
	1.68	0.53	337	1.01	0.97
	1.69	0.68	311	1.14	1.07
120 × 80 × 6	0.87	0.28	1222	1.06	0.98
	0.87	0.46	970	1.04	0.98
	0.88	0.65	860	0.96	0.92
	0.86	0.83	612	1.12	1.11
All Sections			Average	1.01	0.97
			COV	0.12	0.13

Further investigations have been carried to find the reasons for this observed scatter. The adopted imperfection amplitude L/2000 has been reported to perform well (Gardner and Nethercot, 2004c) for pin-ended hollow stainless steel columns, for which the first Eigenmode always represents a global buckling modes when analysed elastically. The first 20 Eigenmodes for each of these columns have been carefully studied, which revealed that 8 of the considered 24 columns exhibited only local buckling modes. These columns are the

relatively stocky ones with slender cross-sections. Their buckling behaviour resembles that for the stub columns, and hence the developed FE models for these columns were analysed again with an imperfection amplitude of $0.023(\sigma_{cr}/\sigma_{0.2})t$, which performed well for stub columns. The obtained results using revised imperfections are compared to the test ultimate load in Table 5.9.

Table 5.9: FE results for SHS and RHS long columns using local buckling amplitude instead of L/2000 where appropriate.

Designation	Cross-section slenderness β	Member slenderness $\bar{\lambda}$	Test F_u (kN)	FE F_u / Test F_u [L/2000]	FE F_u / Test F_u [$0.023(\sigma_{0.2}/\sigma_{cr})t$]
70 × 70 × 2	1.42	0.26	190	0.73	0.89
	1.40	0.43	188	0.74	0.93
	1.43	0.60	159	0.82	1.02
120 × 40 × 2	2.47	0.36	167	0.94	0.95
	2.46	0.61	141	1.11	1.13
	2.43	0.85	96	1.04	1.06
120 × 80 × 3	1.74	0.22	398	0.83	0.92
	1.76	0.37	394	0.81	0.92
All Sections			Average	0.88	0.98
			COV	0.16	0.09

The obtained results show significant improvement in the ultimate load predictions. Initially the average prediction for these 8 columns was 0.88 with a COV of 0.16, whilst changing the imperfection amplitude made the average 0.98 with a COV of 0.09. The significance of using an appropriate mode and amplitude for modelling imperfections is obvious from this comparison. FE models can predict the actual behaviour only if a suitable Eigenmode and its corresponding amplitude is selected. If a global buckling mode is obtained from the elastic analysis, using an amplitude of L/2000 gives quite accurate prediction. Whilst, on the other hand, if the Eigenmodes are dominated by local buckling then the amplitude should be taken as $0.023(\sigma_{0.2}/\sigma_{cr})t$, where σ_{cr} is the elastic critical plate buckling stress and t is the plate thickness.

The overall mean prediction of the ultimate load for these 24 fixed-ended columns, using the most appropriate imperfection mode and its corresponding amplitude, is 1.00 with a COV of 0.09. Only a few failure modes were reported from the testing scheme. These modes were found to be in good agreement with those obtained from the developed FE models. Some

typical Eigenmodes and the corresponding failure modes for these hollow section columns are given in Figure 5.14.

Eigenmode 1: Local imperfections were used since no global mode obtained among the first 20 Eigenmodes.
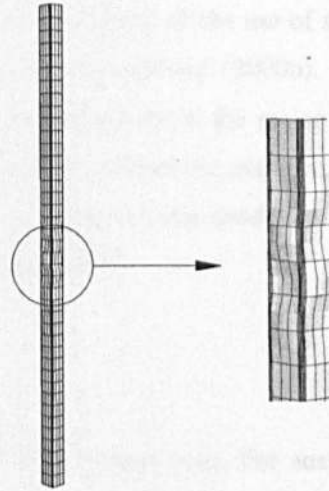
Obtained failure mode showing local failure.

(a) 2.0 m long 70 × 70 × 2 SHS tested by Liu and Young (2003)

Eigenmode 1: Global amplitude of L/2000 was used in the analysis. Subsequent local modes were not combined due to their insignificance in affecting failure load.
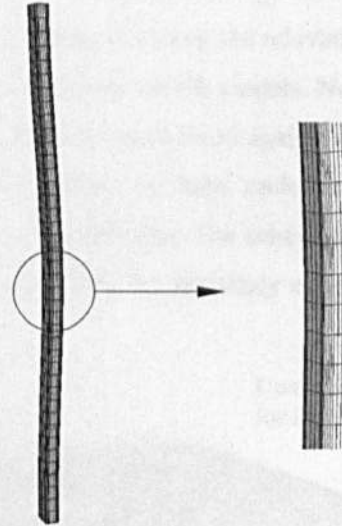
Obtained failure mode showing global failure.

(b) 2.8 m long 120 × 80 × 6 RHS tested by Young and Lui (2003)

Figure 5.14: Typical imperfection modes and failure modes obtained for fixed-ended SHS and RHS columns.

5.4.3 Pin-ended I section columns

A total of 15 welded I columns were modelled as a part of the present research. All these columns were tested as a part of the ECSC project 'Development of the use of stainless steel in construction' and the results have been reported by Stangenberg (2000b). Six columns were tested for minor axis buckling while the rest were tested about the major axis. Special support conditions were used to force the columns to buckle about the major axis; these will be discussed in the following section. Three of these columns were produced from Duplex Grade 1.4462 while the rest were from austenitic Grade 1.4301.

5.4.3.1 Development of FE models

Material properties were taken from the reported tensile coupon tests. For austenitic Grade 1.4301 the reported $\sigma_{0.2}$ was reduced by 7% to obtain a representative value for behaviour in compression.

In the testing procedure pinned boundary conditions were provided by welding a triangular bar with an apex angle of 60^0 to the loading platen. Load was applied through the 90^0 groove made at the end plates of the columns. The groove was positioned along the relevant buckling axis. End plates have been modelled using C3D20 solid elements in FE models. Nodes along the relevant centreline of the outer surfaces of both end plates were fixed against all degrees of freedom, except for the corresponding axis of rotation at both ends and vertical displacement at the loaded end to obtain pinned boundary conditions. The schematic diagram of the testing procedure and the corresponding FE idealisation for boundary conditions and load application is shown in Figure 5.15.

Loading platen with a 60^0 triangular
rod attached for load application

Constrained nodes
for load application

Base plate with a
90^0 groove
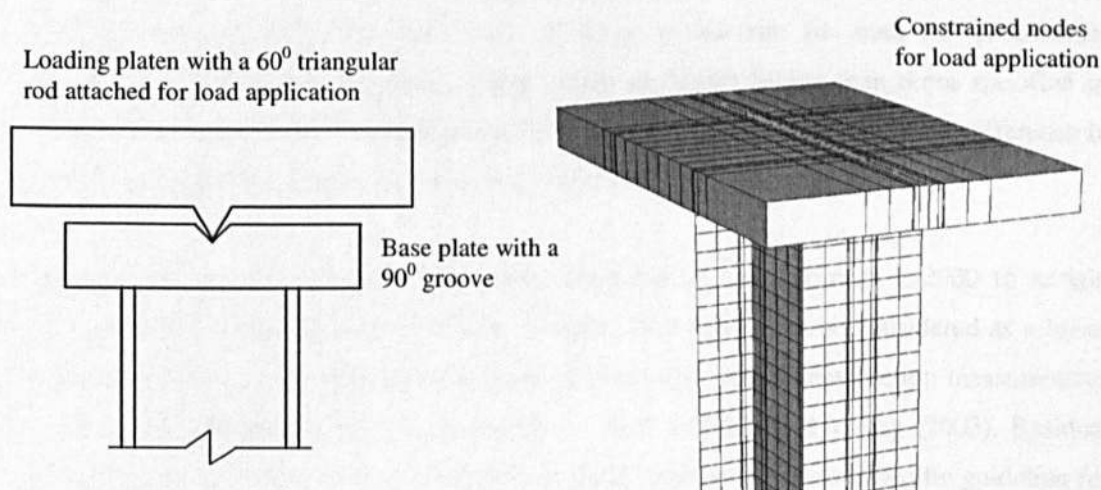
Figure 5.15: FE simulation of knife-edge pin-ended boundary condition.

For major axis buckling, lateral supports were provided by support beams at quarter points along the length to prevent any possible rotation about the minor axis. In the FE models similar arrangements were introduced by restraining the appropriate translational degrees of freedom at the flange tips. This idealisation is shown in Figure 5.16.
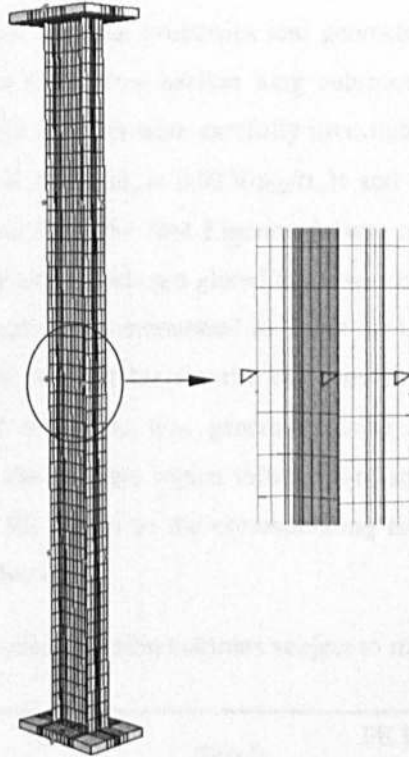
Figure 5.16: FE simulation of the lateral supports used in major axis buckling test.

No measurements for the initial imperfections were available from the report of Stangenberg (2000b). He developed FE models using a global imperfection of L/300 for the minor axis buckling and L/400 for the major axis buckling to account for both the geometrical imperfections and residual stresses. These values are much higher than those specified in design codes and tolerance standards. No specific explanation was given for the difference in global imperfections adopted for minor and major axis buckling.

In the present study, generally, the global imperfection was taken as L/2000 to remain consistent with other FE models of long columns. This value may be considered as a lower bound apart from a few exceptions as observed from the overall imperfection measurements reported by Gardner (2002), Young and Liu (2003) and Liu and Young (2003). Residual stresses were not included, firstly, because of the unavailability of any specific guideline for stainless steel and, secondly, the adoption of the carbon steel residual stress pattern produced

no significant changes in the ultimate load carrying capacity for stainless steel stub columns (Section 5.3.7).

5.4.3.2 Results and analysis

The importance of using appropriate material properties and geometric imperfections were emphasized in the previous section for hollow section long columns. Hence, in this case, Eigenmodes obtained from the elastic analysis were carefully investigated and an appropriate imperfection amplitude i.e. for local mode $\omega_o = 0.023(\sigma_{0.2}/\sigma_{cr})t$ and for global mode $\omega_0 = L/2000$ used. For the minor axis buckling the first Eigenmode was always showing global buckling, whilst in the case of major axis buckling a global mode was obtained within the first few Eigenmodes apart from 2 exceptions as mentioned in Table 5.11. Stangenberg (2000b) adopted higher global imperfection magnitudes for the columns subjected to minor axis buckling. Hence an additional set of results was generated using a global imperfection amplitude of L/1000 to account for the possible higher initial out-of-straightness in this case. Table 5.10 compares the obtained FE results to the corresponding test results for I section long columns subject to minor axis buckling.

Table 5.10: FE results for pin-ended I section columns subject to minor axis buckling.

Cross-section Designation [Grade]	Cross-section slenderness β	Member slenderness $\bar{\lambda}$	Test F_u (kN)	FE F_u / Test F_u [L/1000]	FE F_u / Test F_u [L/2000]
160×80×10×6 [1.4301]	0.82	0.42	627	1.01	1.03
	0.85	0.79	420	1.06	1.10
	0.84	1.31	270	0.97	1.03
160×160×10×6 [1.4301]	0.85	0.37	1120	1.11	1.14
	0.86	0.60	745	1.18	1.21
	0.86	0.97	582	1.04	1.09
All Sections			**Average**	**1.07**	**1.09**
			COV	**0.06**	**0.06**

Results obtained using FE models are, on average, in good agreement with test results. It is believed that some of the columns might have had a higher initial out-of-straightness which led Stangenberg (2000b) to adopt a much higher value of L/300 while conducting the FE modelling. Moreover, he used the tensile coupon tests to replicate the compressive behaviour which might lead him to increase the initial imperfection amplitude to obtain results close to the test values. Making appropriate adjustments to the material behaviour leads to reliable results using reasonable imperfections. Figure 5.17 shows a typical Eigenmode and

corresponding failure mode for pin-ended I long columns subjected to minor axis buckling obtained from the FE analysis.

Eigenmode 1 showing global buckling   Column failure mode
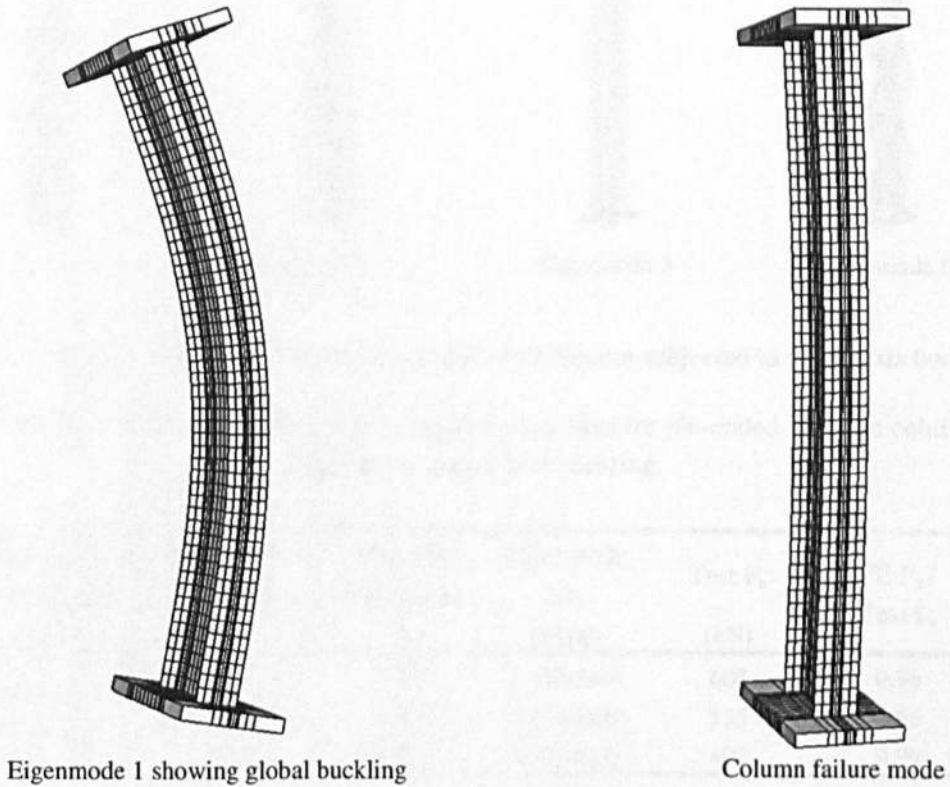
Figure 5.17: Imperfection mode and the corresponding failure mode obtained for1.248m long pin-ended I 160×80 column subjected to minor axis buckling.

I sections subjected to major axis buckling showed significant variations in their Eigenmodes as obtained from the elastic analysis. For the shorter columns the first few Eigenmodes were local which were followed by a global mode, if any. As the columns become longer the global buckling modes appear at a lower Eigenmode. In some cases obtained local buckling modes showed very localised deformations and hence subsequent modes were investigated to select a shape to reflect the periodic nature of local imperfections. The first few Eigenmodes for 2.05 m long duplex I 160×160 column are given in Figure 5.18, which shows very localised buckles in the first few Eigenmodes which led to the use of Eigenmode 6 for local imperfections to be distributed along the member. Table 5.11 compares the FE predictions for the column capacities against test results. The overall comparison gives only 6% variation with an average of 1.01 which demonstrates the accuracy of the adopted modelling technique. Figure 5.19 shows some typical failure modes along with the corresponding imperfection distribution.

Eigenmode 1   Eigenmode 3   Eigenmode 5   Eigenmode 6
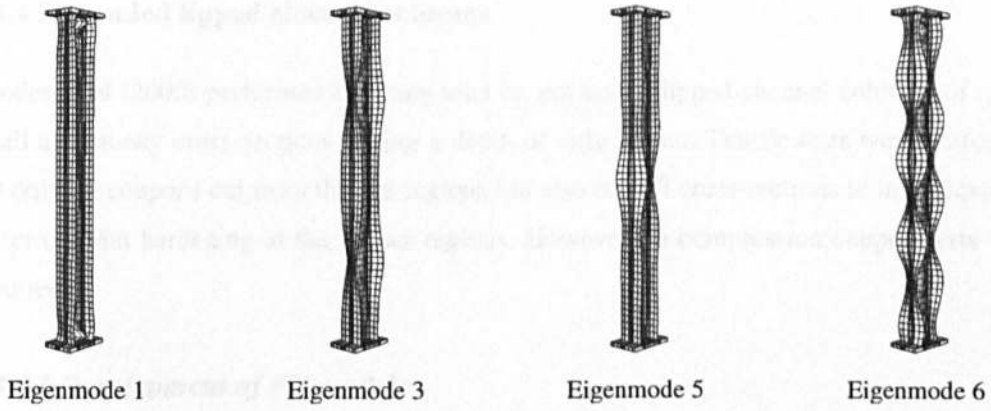
Figure 5.18: Eigenmodes for 2.05 m long I 160×160 column subjected to major axis buckling.

Table 5.11: FE results with the type of imperfection used for pin-ended I section columns subjected to major axis buckling.

Cross-section Designation [Grade]	Cross-section slenderness β	Member slenderness $\bar{\lambda}$	Eigenmode No. (Type)	Test F_u (kN)	FE F_u / Test F_u
160×80×10×6 [1.4301]	0.82	0.38	5 (Global)	664	0.96
	0.82	0.62	1 (Global)	535	0.95
	0.83	0.93	1 (Global)	402	0.99
160×160×10×6 [1.4301]	0.86	0.35	10 (Local)	1108	1.02
	0.85	0.58	3 (Global)	860	1.03
	0.85	0.90	1 (Global)	725	0.94
160×160×10×6 [1.4462]	1.08	0.48	6 (Local)	1930	1.05
	1.08	0.78	1 (Global)	1490	1.07
	1.09	1.19	1 (Global)	990	1.12
All Sections				**Average**	**1.01**
				COV	**0.06**

Eigenmode 10   Failure mode (local)   Eigenmode 5   Failure mode (Global)

(a) I 160×160 – 2.05m   (b) I 160×80 – 2.048m
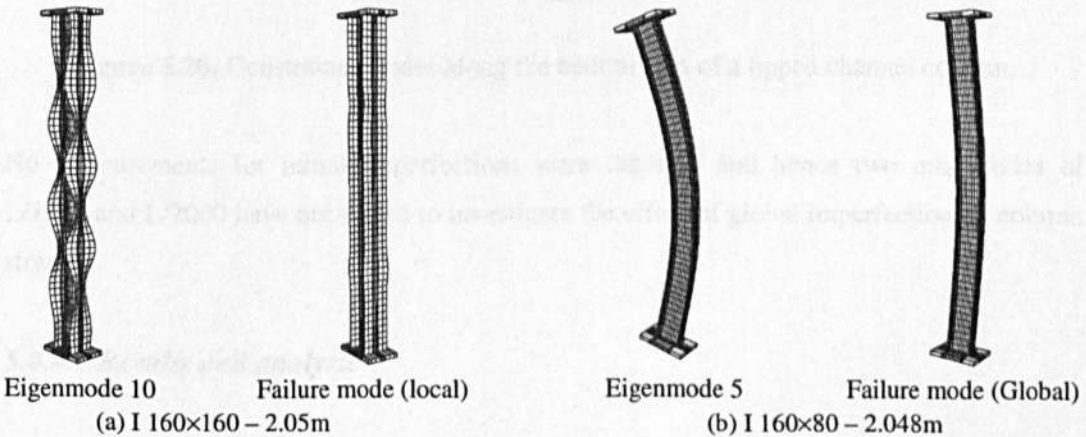
Figure 5.19: Eigenmodes and the corresponding failure modes for I 160 × 160 and I 160 × 80 pin-ended columns (Grade 1.4301) subjected to major axis buckling.

5.4.4 Pin-ended lipped channel columns

Rhodes et al (2000) performed buckling tests on pin-ended lipped channel columns of rather small and stocky cross-sections having a depth of only 28mm. Tensile tests were performed not only on coupons cut from the flat regions but also on full cross-sections to investigate the effect of stain hardening at the corner regions. However no compression coupon tests were reported.

5.4.4.1 Development of FE models

Material properties were taken from the reported tensile coupon tests by making a 7% reduction of the 0.2% proof stress. Corner strength was predicted using the simple power model proposed in Chapter 4 (Equation 4.6). Boundary conditions were modelled using the similar procedure followed for I sections and a line load was applied along the neutral axis using constraint equations. Figure 5.20 shows typical constrained nodes used for defining boundary conditions as well as for the load application.
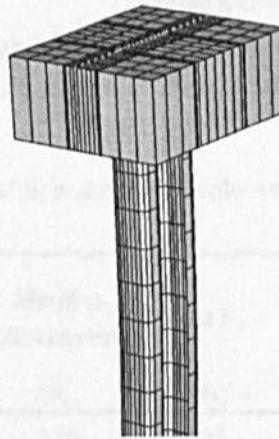
Figure 5.20: Constrained nodes along the neutral axis of a lipped channel column.

No measurements for initial imperfections were reported and hence two magnitudes of L/1000 and L/2000 have been used to investigate the effect of global imperfection on column strength.

5.4.4.2 Results and analysis

In all cases Eigenmode 1 was used to model geometric imperfections since it showed a global buckling mode similar to all other pin-ended columns subjected to minor axis buckling.

Rhodes et al (2000) selected the cross-section dimensions in such a way that no local buckling occurs. All the FE models also showed the same trend by buckling globally. Figure 5.21 shows a typical imperfection mode and the corresponding failure mode for one of the lipped channel columns, whilst Table 5.12 compares the FE results for the ultimate load against the test values.

Eigenmode 1   Failure mode   Global failure
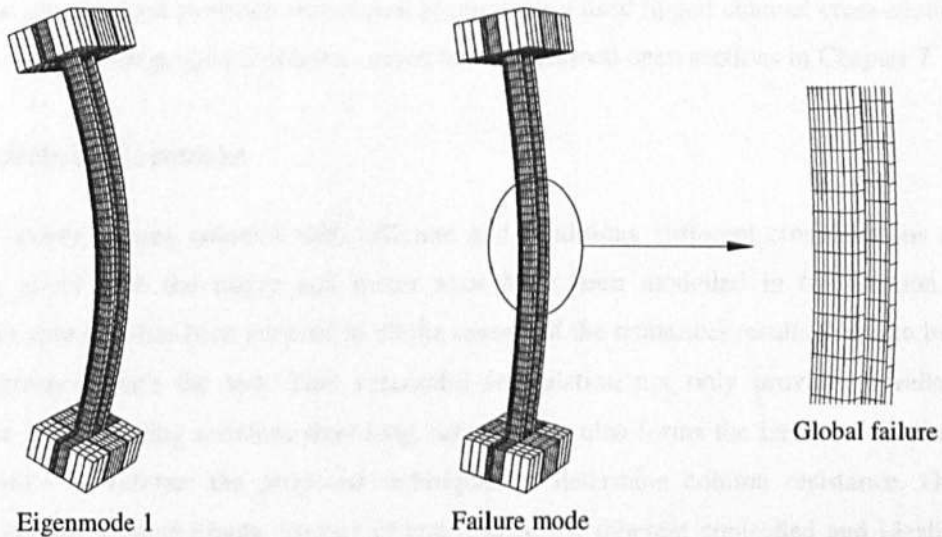
Figure 5.21: Initial imperfection shape and failure mode for 0.322m long lipped channel column with a cross-section of $28 \times 14.88 \times 7.45 \times 2.43$.

Table 5.12: FE results for pin-ended lipped channel columns subject to minor axis buckling.

Cross-section Designation	Cross-section slenderness β	Member slenderness $\bar{\lambda}$	Test F_u (kN)	FE F_u / Test F_u [L/1000]	FE F_u / Test F_u [L/2000]
		3.58	4.36	1.06	1.09
		3.29	4.69	1.17	1.20
		3.00	6.82	0.96	0.99
		2.70	7.83	1.02	1.05
$28 \times 14.88 \times 7.45 \times 2.43$	0.50	2.41	8.79	1.13	1.16
		2.12	11.16	1.13	1.17
		1.82	15.55	1.05	1.10
		1.53	19.10	1.15	1.20
		1.24	28.39	1.04	1.09
		0.94	38.64	1.01	1.05
		0.65	52.64	0.98	1.00
All Sections			**Average**	**1.06**	**1.10**
			COV	**0.07**	**0.07**

The FE results show that an imperfection magnitude of L/1000 gives better prediction in this case. Since the tested cross-sections were very small it is likely that the initial out-of-straightness could easily be more than the values obtained for the previously analysed hollow sections and I sections. If a long member represents a small cross-section, the chance of experiencing higher out-of-straightness is quite obvious. However the performance of the developed FE models are in good agreement with the reported test results and hence the same technique may be used to obtain resistances of commonly used lipped channel cross-sections and thus to verify the proposed column curves for cold-formed open sections in Chapter 7.

5.4.5 Concluding remarks

A wide variety of long columns with different end conditions, different cross-sections and buckling about both the major and minor axes have been modelled in this section. A consistent approach has been adopted in all the cases and the numerical results found to be in good agreement with the test. This successful formulation not only provides a reliable technique for modelling stainless steel long columns but also forms the basis for obtaining extra results to validate the proposed techniques to determine column resistance. Once verified against a considerable number of test results, the inherent controlled and idealised environment offered by the FE models could be used to reduce the uncertainties associated with the testing procedures. Appropriate parametric studies may be employed to verify the applicability of a proposed technique over its full range even for cases where test results are not available.

5.5 MODELLING OF I-SECTION BEAM-COLUMNS

Beam-columns are members subjected to a simultaneous combination of axial load and bending moments. The resistance of such members is generally predicted by the superposition of axial strength and bending strength with some additional interaction factors. As part of the current study, FE models for I section beam-columns tested by Stangenberg (2000b) were developed. The aim is, first, to validate the models against test results and then to obtain extra sets of results to investigate beam-column behaviour.

5.5.1 Development of FE models

A total of six beam-column tests were performed by Stangenberg (2000b) on two I sections produced from austenitic Grade 1.4301. The test setup was the same as that adopted for major axis buckling as shown in Figure 5.16 except that the groove for load application was positioned along the centreline of one of the flanges. All the FE techniques adopted for the

beam-column models are the same as those used for the pin-ended I columns buckling about the major axis as described in Section 5.4.3.1. Figure 5.22 shows how the position of the constrained nodes, used both for defining boundary conditions and for load application, has been moved to the centreline of one of the flanges.

Nodes constrained at top and bottom along the centerline of a flange for

Lateral supports provided to avoid buckling against minor axis.
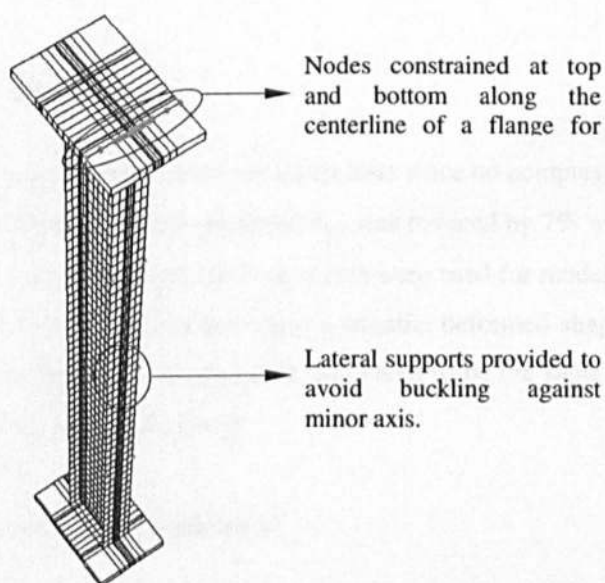
Figure 5.22: Typical position of load application for the beam-column models.

5.5.2 Results and analysis

Table 5.13 compares the ultimate loads obtained from FE analysis to the test results. It is worth mentioning that the global and local imperfections were taken as L/2000 and $0.023(\sigma_{cr}/\sigma_{0.2})t$ respectively where appropriate. The results obtained are in very good agreement with test results and hence they may be used to generate further results to validate the performance of the existing Eurocode and the method proposed in Chapter 7.

Table 5.13: FE results obtained for I section beam-columns.

Cross-section designation	Cross-section slenderness β	Member slenderness $\bar{\lambda}$	Eigenmode No (Type)	Test F_u (kN)	FE F_u / Test F_u
	0.82	0.38	7 (Local)	338	0.94
160×80×10×6	0.82	0.62	2 (Global)	270	0.96
	0.83	0.93	1 (Global)	222	0.92
	0.86	0.35	4 (Local)	540	1.01
160×160×10×6	0.85	0.58	10 (Local)	454	1.00
	0.85	0.90	1 (Global)	356	1.01
All Sections				**Average**	**0.98**
				COV	**0.04**

5.6 MODELLING OF I SECTION BEAMS

Stangenberg (2000b) performed 4 four-point-bending tests on welded I sections produced form austenitic Grade 1.4301 and duplex Grade 1.4462. Four different cross-sections were tested to fail in pure bending.

5.6.1 Basic parameters for FE models

The material properties were taken from the tension coupon tests since no compression results were available. For austenitic Grade 1.4301 the reported $\sigma_{0.2}$ was reduced by 7% while for the duplex Grade 1.4462 $\sigma_{0.2}$ was used unchanged. Shell elements were used for modelling with a relatively fine mesh. Imperfections were included using a suitable deformed shape obtained from elastic analysis. The local imperfection amplitude was taken to be the same as for stub columns and long columns i.e. $\omega_0 = 0.023(\sigma_{0.2}/\sigma_{cr})t$.

5.6.2 Boundary conditions and load application

The beams were simply supported allowing free rotations at the ends. Owing to the high shear forces between the points of load application and supports, two 6 mm thick extra webs were welded to that region. In addition, 6 mm thick stiffeners were welded at each of the supports and at the points of load application. The span between the loads was thus loaded to fail under pure bending, whilst any local failures due to shear near the supports were prevented. Some extra lateral supports were provided at the points of load application and at the mid span to prevent the chance of any lateral movement. Figure 5.23 shows all necessary arrangements adopted for the testing of I beams.

Free against rotation about 1 and translation along 3

Free only against rotation about 1

Extra 6 mm web welded to prevent web buckling due to high shear

One of 12 lateral supports provided to prevent lateral movements
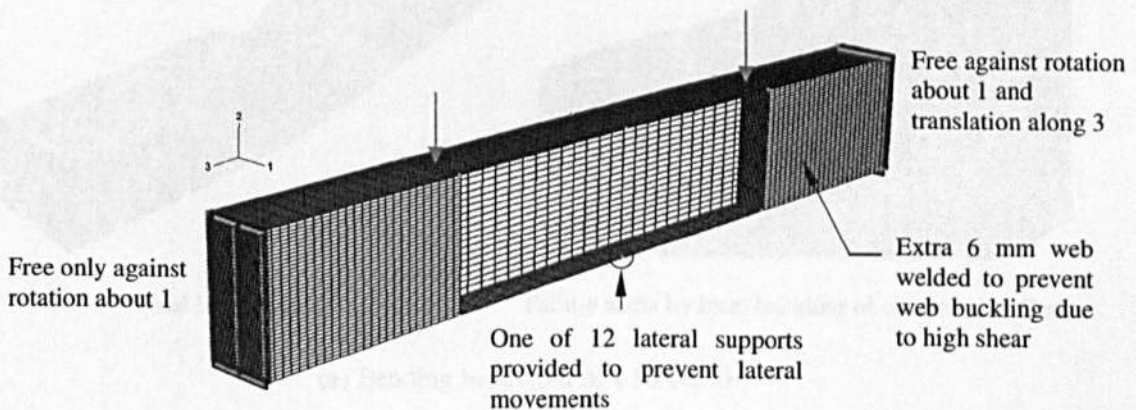
Figure 5.23: Boundary conditions and other special arrangements adopted for the FE modelling of I beams.

5.6.3 Results and analysis

Deformed shapes obtained from the elastic analysis produced similar local deformations for all 4 sections considered. Typical first 2 Eigenmodes are given in Figure 5.24. Between these two the 2nd Eigenmode has been adopted since it affects the critical compression flange.

Eigenmode 1   Eigenmode 2
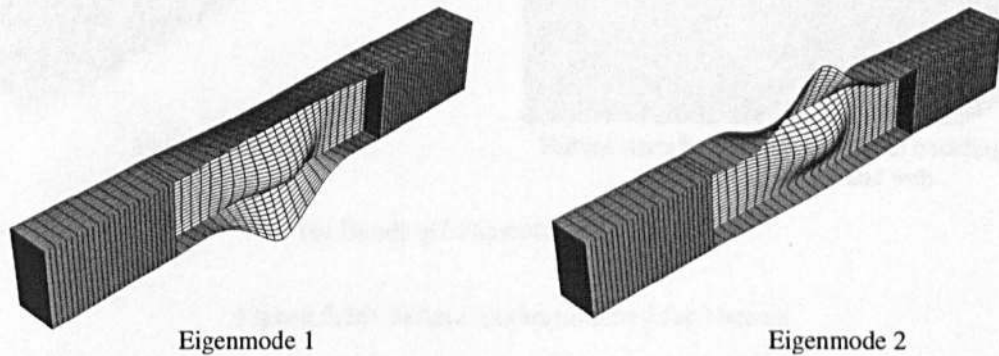
Figure 5.24: Typical Eigenmodes obtained for I beams.

In the case of the I 160×160 beams failure was initiated by local failure of the compression flange, whilst for the relatively deeper sections, I 160×80 and I 320×160, almost simultaneous local failures occurred at both the compression flange and the web. Figure 5.25 shows the final failure mode and the initiation of failure for these two cases.

Final failure mode   Failure starts by local buckling of compression flange
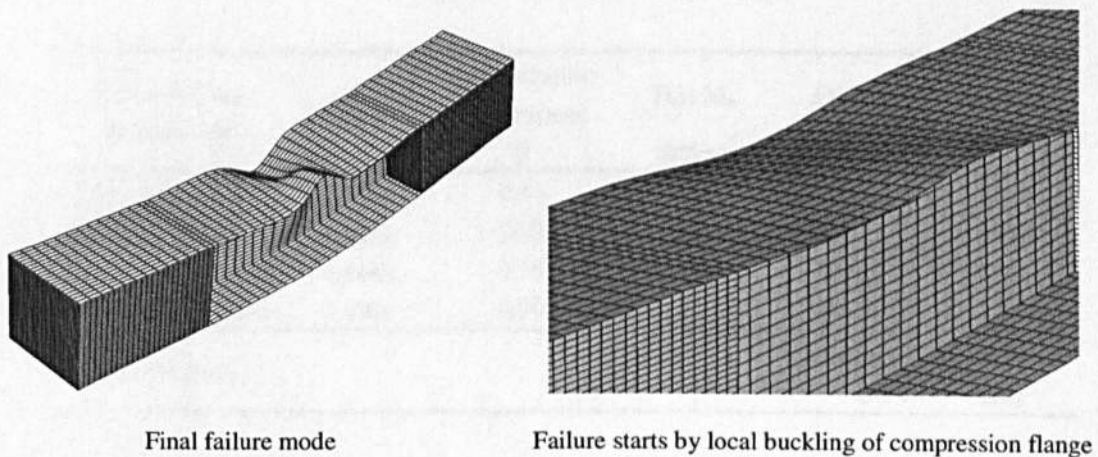
(a) Bending behaviour of I 160×160

Figure 5.25: Failure modes obtained for I beams.

Final failure mode	Failure starts by simultaneous local buckling of compression flange and web

(b) Bending behaviour of I 320×160
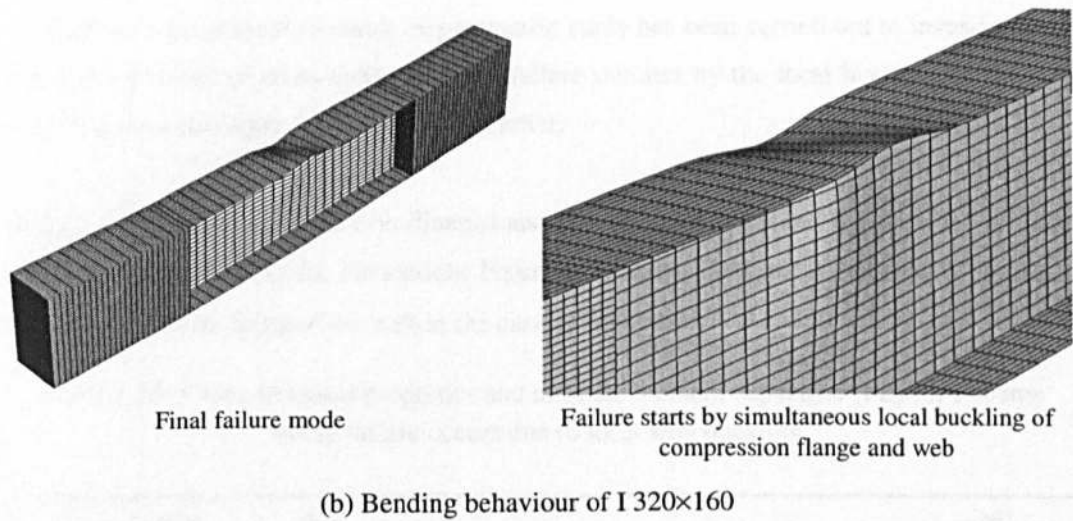
Figure 5.25: Failure modes obtained for I beams.

Table 5.14 compares the ultimate bending capacities obtained from the FE models with those of the tested values. Except for the I 160×80 cross-section the other FE predictions are almost identical to the test results. The load vs displacement curve for I 160×80 section as reported by Stangenberg (2000b) does not seem to have reached the ultimate value; rather it exhibits an upward trend indicating capabilities to withstand further moment. It is believed that the test might have been stopped before reaching the ultimate capacity. When this FE result is compared to the prediction of the proposed technique in Chapter 6, it shows good agreement along with all other results.

Table 5.14: FE results for I beams.

Cross-section designation	Grade	Cross-section slenderness β	Test M_u (kNm)	FE M_u (kNm)	FE M_u / Test M_u
$160 \times 80 \times 10 \times 6$	1.4301	0.44	54.7	70.2	0.78
$160 \times 160 \times 10 \times 6$	1.4301	0.88	89.5	91.7	0.98
$160 \times 160 \times 10 \times 6$	1.4462	1.15	162.5	164.3	0.99
$320 \times 160 \times 10 \times 6$	1.4301	0.90	212.7	209.6	1.01
All Sections				**Average**	**0.94**
				COV	**0.12**

5.6.4 I beams subjected to local buckling of web

The successful modelling technique for stainless steel beams will be used to investigate the behaviour of deep beams where failure is initiated by the local failure of web. The cross-section strength was limited by the compression flange in all available bending tests so far

considered in the present research. A parametric study has been carried out to investigate the bending behaviour of cross-sections where failure initiates by the local buckling of the web following the same approach as described earlier.

Table 5.15 gives the cross-section dimensions, material properties and the obtained ultimate moment capacities using the FE models. Figure 5.26 shows the typical evidence of initiation of failure due to buckling of the web in the case of I 180×60.

Table 5.15: Cross-sectional properties and ultimate moment capacities (FE) for I beams where failure occurs due to local web buckling.

Cross-section designation	$\sigma_{0.2}$ (N/mm²)	E_0 (N/mm²)	β_{flange}	β_{web}	β	M_u (kNm)
I $160 \times 80 \times 10 \times 4$	300	200000	0.45	0.53	0.53	64.3
I $240 \times 80 \times 9 \times 6$	300	200000	0.45	0.57	0.57	97.6
I $160 \times 160 \times 16 \times 3$	300	200000	0.56	0.64	0.64	140.7
I $200 \times 70 \times 5 \times 3$	300	200000	0.72	0.97	0.97	32.0
I $180 \times 60 \times 4 \times 2.2$	300	200000	0.76	1.20	1.20	18.4

Final failure mode   Failure initiates by local buckling of web
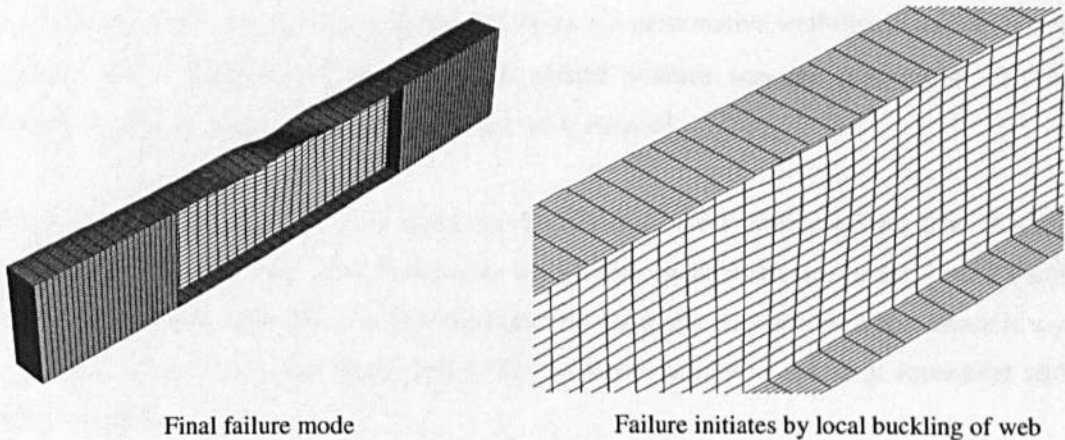
Figure 5.26: Local buckling of web for the developed I 180×60 beam.

5.7 CONCLUSIONS

FE modelling techniques for stainless steel cross-sections and members have been described in this chapter. These cover modelling different types of cross-sections including hollow and open sections, and also the special techniques required to apply different types of loading. Performance of the developed FE models has been evaluated against available test results and showed good agreement in all cases considered.

The material properties were included using the compound Ramberg-Osgood model taking the proposed coefficients for different grades. Appropriate recognition of the strength enhancements at corner regions was made by using the proposed models for the prediction of $\sigma_{0.2,c}$ using the virgin or flat material behaviour. The present research shows that for the press-braked sections the corner strength should be used up to t beyond the corner, whilst for the roll-formed sections Gardner's (2002) proposed 2t is appropriate.

Initial geometric imperfections were incorporated using the appropriate Eigenmode obtained from elastic analysis. In the case of stub columns, adoption of the first Eigenmode with an amplitude of $0.023(\sigma_{0.2}/\sigma_{cr})t$ as proposed by Gardner and Nethercot (2004c) produced the best results when compared with the amplitude originally proposed for carbon steel by Schafer and Peköz (1998). For long columns careful investigation is required to select the appropriate Eigenmode. If a global buckling mode is available within the first few Eigenmodes, an amplitude of L/2000 may be used as a general guideline. In the cases of open sections L/1000 may be taken as a lower bound if there is a possibility of excessive initial out-of-straightness. The column strength is generally dominated by the global buckling mode; superposition of local imperfections did not seem to produce any significant changes. However, in cases, where Eigenmodes are dominated by local failures, a representative well-distributed deformed shape with an amplitude of $0.023(\sigma_{0.2}/\sigma_{cr})t$ should produce accurate predictions. For the beam-columns and beams similar approaches were adopted.

No residual stress pattern is yet available for stainless steel cross-sections. The existing guidelines for carbon steel were followed to incorporate residual stresses in the welded I stub columns. No significant effect on the compression resistance was observed and hence it was neglected in the subsequent FE models which, however, produced excellent agreement with the test results.

A consistent approach has been followed to develop FE models for stainless steel members. This approach is believed to be capable of producing dependable results through careful parametric studies.

CHAPTER - SIX

DESIGN OF STAINLESS STEEL CROSS-SECTIONS

6.1 INTRODUCTION

Steel sections are mostly formed from thin plates which are either welded together or cold-formed to produce the desired geometrical shape. In the case of stainless steel these constituent parts are often thinner than those used for ordinary carbon steel because of the obvious high cost. When such a cross-section is subjected to compression its failure is initiated either by local buckling of thin plates or by yielding of the material. The local buckling of a thin plate is affected by a number of factors such as geometrical dimensions, boundary conditions, type of loading and material properties. For moderately stocky plates the buckling phenomenon becomes more complex since it takes place beyond the elastic range. With stocky plates failure is initiated by material yielding although the cross-section does not fail instantly because of the pronounced strain hardening of stainless steel. Load is shed to the corners as a result of the earlier local failure of the flat material and hence the cross-section resistance goes well beyond the basic design resistance as defined by the existing design codes. For very slender plates post-buckling effects may well be pronounced.

This chapter investigates the behaviour of stainless steel cross-sections under compression, bending and their combined effects taking appropriate account of strain hardening by using an accurate material model and hence proposes a design method based on the deformation capacity of cross-sections to obtain the corresponding resistance.

6.2 COMPRESSION RESISTANCE

The load-deformation behaviour of a cross-section formed from a number of thin plates depends on the geometrical dimensions and orientations of the individual plates. Stub columns are tested to investigate the response of individual plate elements as well as behaviour of the cross-section as a whole. Back in 1924, Basquin used stub columns to obtain

stress-strain behaviour to determine the relationship between tangent modulus and average column stress. The added advantage of using stub columns over material coupons is that the former include the effects of work-hardening and residual stresses which are recognised to have significant effects on the behaviour of a cross-section. Stub column tests follow a common practice to establish the available limits used for section classification; especially to define the boundary between the Class 3 and the Class 4 cross-sections.

As a new structural material, stainless steel is gaining wider usage day by day (Gardner, 2005). The initial guidelines on stainless steel were based on analogies with the section classification approach adopted for carbon steel. Classification limits have been modified depending on tests performed on cross-sections. But the absence of any well-defined yield point and the resulting nonlinearity exhibited by stainless steel makes this section classification technique inappropriate. Gardner and Nethercot (2004d) used a different approach whereby the deformation capacity of a cross-section, obtained from the load-deformation behaviour, was used to determine its compression resistance. He developed a design method for stainless steel hollow sections based on available test results using an exact material model. The development of this 'new approach' is explained briefly in the following section since this technique formed the basis for the present research.

6.2.1 Design method proposed by Gardner and Nethercot for hollow sections

A laboratory testing programme was carried out to investigate the behaviour of austenitic stainless steel cross-sections and members as discussed in Sections 3.3 and 3.5. Stub column tests were conducted on SHS, RHS and CHS to develop a relationship between cross-section slenderness β and the corresponding deformation capacity ε_{LB} and hence to determine ultimate load carrying capacities. The definition of β has been explained in Chapter 3 and is given by Equation 3.4. Since the proposed method is based on this parameter, that expression is reintroduced in Equation 6.1 to avoid referring back to Chapter 3.

$$\beta = \frac{b}{t}\sqrt{\frac{\sigma_{0.2}}{E_0}}\sqrt{\frac{4.0}{k}}$$

(6.1)

6.2.1.1 Development of the design method for hollow sections

The cross-section resistance of stainless steel members is currently assessed (in published design documents) on a similar basis to the cross-section resistance of carbon steel members. The cross-section is initially placed into one of a number of possible behavioural classes (with

the number depending on the particular design code), and subsequently its resistance is limited by either material yielding of the gross section, with either a plastic or elastic distribution of stresses, or yielding of an effective section (to account for local buckling) with an elastic stress distribution. This classification approach is valid for materials having elastic, perfectly-plastic behaviour such as ordinary carbon steel. But in the case of stainless steel the rounded nature of the stress-strain behaviour makes this approach inefficient since the significance of strain hardening is neglected as shown in Figure 6.1. The shaded portion shown in this figure is not considered when an elastic, perfectly-plastic material model is used for stainless steel.
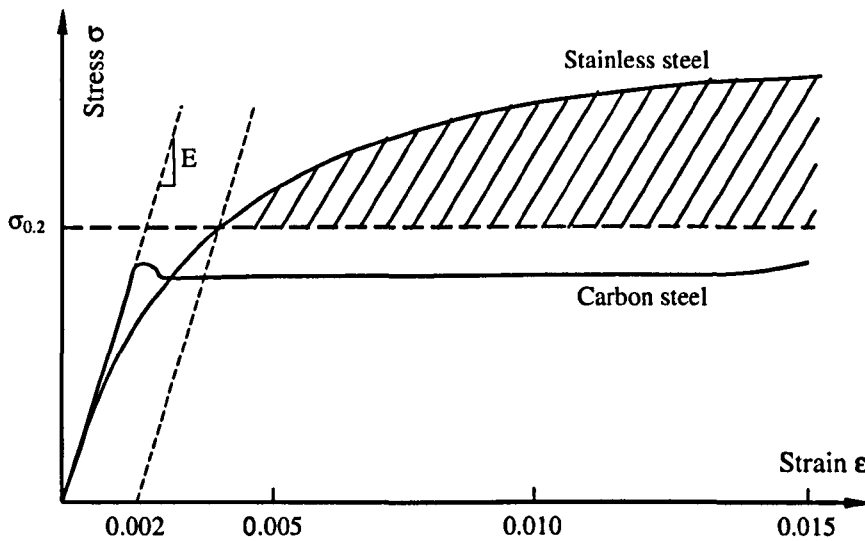
Figure 6.1: Elastic, perfectly-plastic material model vs stainless steel.

All available stub column test results were used to develop a relationship between cross-section slenderness β and normalised cross-section deformation capacity $\varepsilon_{LB}/\varepsilon_0$. The results from tests on SHS were assumed to relate approximately to plate elements with simply-supported boundary conditions, since the four elements of the cross-section provide equal restraint to one another (Timoshenko and Gere, 1985). In the case of rectangular hollow sections, however, greater edge restraint is applied to the more slender sides of the cross-section by the less slender sides. As a result, higher buckling curves can be applied to the more slender sides of rectangular hollow sections, and clearly an increase in aspect ratio produces an increase in edge restraint. A modification factor involving the aspect ratio χ was incorporated into the basic relationship obtained for the SHS to arrive at a general expression for the hollow sections as given in Equation 6.2. Figure 6.2 compares the proposed curves obtained using Equation 6.1 with the test results available to Gardner (2002).

$$\frac{\varepsilon_{LB}}{\varepsilon_0} = \frac{7.07}{\beta^{2.13+0.21\beta}} \chi^{-0.30\beta^{0.5}} \qquad (6.2)$$

The local buckling strain of a cross-section was, thus, obtained from the proposed equations, and the compound Ramberg-Osgood model, as given by Equations 5.3 and 5.11 was used to obtain the corresponding local buckling stress σ_{LB}. It is worth mentioning that their adopted material model has recently been modified by Gardner and Ashraf (2006), as explained in Section 5.2.1.5, to eliminate an observed minor inconsistency. Since this material model is a key parameter in the proposed method it is reintroduced in Equations 6.3 and 6.4. Compression resistance is thus defined as the product of the local buckling strength σ_{LB} and the gross area of the cross-section A_g.

$$\varepsilon = \frac{\sigma_{0.2}}{E_0} + 0.002\left(\frac{\sigma}{\sigma_{0.2}}\right)^n \quad \text{for } \sigma \le \sigma_{0.2} \qquad (6.3)$$

$$\varepsilon = \frac{(\sigma - \sigma_{0.2})}{E_{0.2}} + \left(\varepsilon_{t1.0} - \varepsilon_{t0.2} - \frac{\sigma_{1.0} - \sigma_{0.2}}{E_{0.2}}\right)\left(\frac{\sigma - \sigma_{0.2}}{\sigma_{1.0} - \sigma_{0.2}}\right)^{n'_{0.2,1.0}} + \varepsilon_{t0.2} \quad \text{for } \sigma > \sigma_{0.2} \qquad (6.4)$$
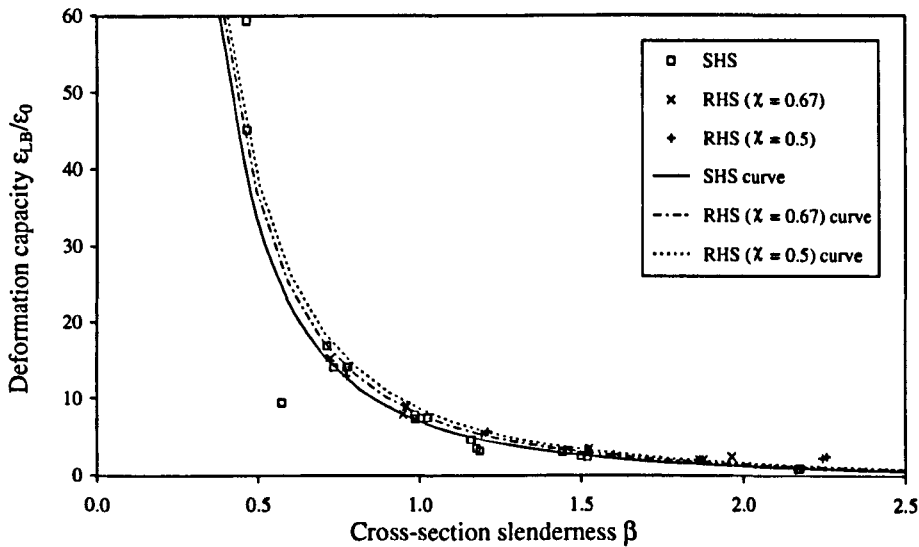
Figure 6.2: Test results and design curves proposed by Gardner (2002) for hollow sections.

6.2.1.2 Validation of the method proposed for hollow sections

Results for the ultimate strength F_u from the proposed method were compared to the Eurocode ENV 1993-1-4 (1996) predictions for all available test results on austenitic stainless steel hollow sections and the summary is given in Table 6.1.

Table 6.1: Performance of the method proposed by Gardner and Nethercot (2004d) for hollow sections.

Cross-section type	No. of stub columns	ENV F_u / Test F_u		Proposed F_u / Test F_u		Proposed F_u / ENV F_u
		Mean	COV	Mean	COV	
SHS ($\chi = 1.00$)	20	0.77	0.19	0.96	0.10	1.25
RHS ($\chi = 0.67$)	10	0.79	0.17	0.95	0.04	1.20
RHS ($\chi = 0.50$)	8	0.77	0.14	0.92	0.07	1.19
All sections	**38**	**0.78**	**0.17**	**0.95**	**0.08**	**1.22**

The comparison showed that the proposed method gives excellent prediction of the test results, and offers a considerable benefit over the Eurocode approach. For SHS and RHS compression resistance, the Eurocode design method predicts, on average, 78% of the test failure load with a coefficient of variation (COV) of 0.17, whereas the proposed design method predicts 95% of the test failure load with a COV of 0.08, resulting in a 22% increase, on average, in cross-sectional resistance .

6.2.2 Modification of the proposed method for open sections

The success of the proposed method for hollow sections opens the way for its extension to cover all types of sections. All available test results on stainless steel open and hollow sections as reported in Chapter 3 have been analysed with a view to obtaining a generalised method for all types of stainless steel cross-sections.

6.2.2.1 Deformation capacity curve from test results

Following the same concept as for the hollow sections, a generalised relationship was established for all the cross-section types containing flat plate elements. Table 3.7 lists the cross-section slenderness β and normalised deformation capacity $\varepsilon_{LB}/\varepsilon_0$ for all types of stainless steel cross-sections considered in the present study. For some stub columns only the ultimate compression resistances of cross-sections were available and hence these were not used in the design formulation. However all tests have been used for verification of the proposed method later in this chapter. All test results with known deformation capacities are plotted in Figure 6.3 to investigate the relationship between β and $\varepsilon_{LB}/\varepsilon_0$.
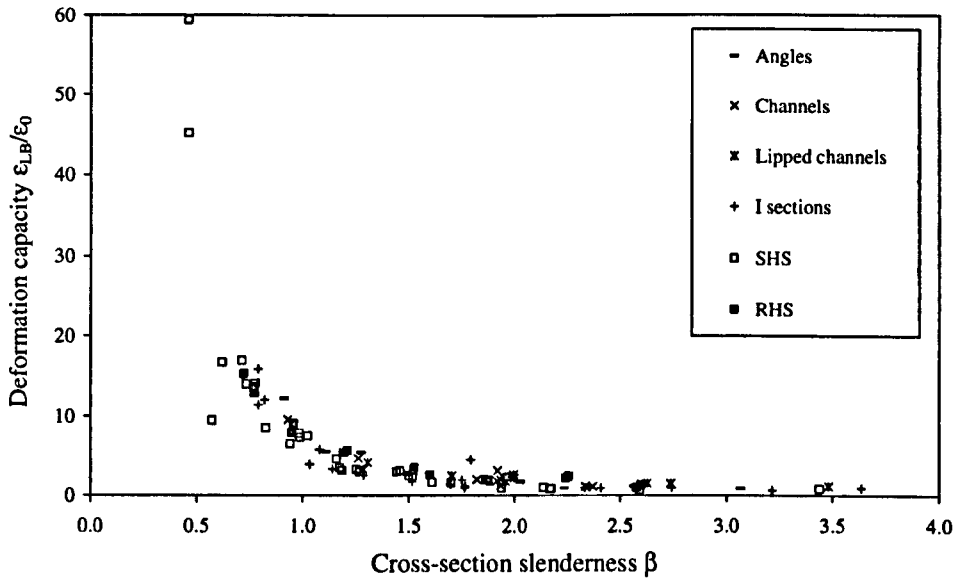
Figure 6.3: Slenderness β vs deformation capacity $\varepsilon_{LB}/\varepsilon_0$ for all available stub column tests.

From Figure 6.3 it is observed that all cross-sections follow a common trend when the slenderness β of the most slender element within a cross-section is calculated using the appropriate buckling coefficient k. For outstand elements in pure compression the buckling coefficient is taken as 0.43, whilst for all internal compression elements, including the flanges of lipped channels, its value is taken as 4.0. It should be noted that the size of a lip is believed to affect the value of k, with its value falling between 0.43 and 4.0. This effect is briefly explained in section 6.2.4, although detailed investigation on this filed has not been considered in the present research.

All considered test results were simulated using sophisticated FE models, as explained in Chapter 5, that include the effects of corner enhancement and predicted initial imperfections following the proposed guidelines. Although test points cover almost the complete range of cross-section slenderness, some additional results were generated using the validated FE technique for low β values to fill in the gap observed in Figure 6.4. The generated points also follow the same path shown in Figure 6.3. A regression analysis was performed to obtain a generalised relationship between $\varepsilon_{LB}/\varepsilon_0$ and β as given by Equation 6.5. Figure 6.4 compares Equation 6.5 to all the stub column results.

$$\frac{\varepsilon_{LB}}{\varepsilon_0} = \frac{6.44}{\beta^{2.85-0.39\beta}} \tag{6.5}$$
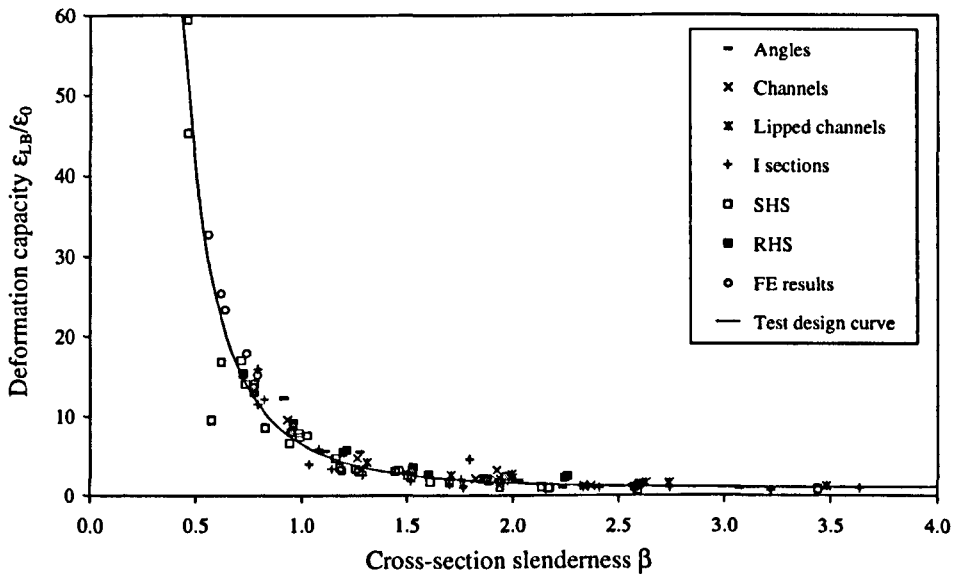
Figure 6.4: Relationship between $\varepsilon_{LB}/\varepsilon_0$ and β as obtained from test results.

6.2.2.2 Local buckling stress σ_{LB} using the material stress-strain behaviour

The cross-section slenderness β is obtained using the material properties and geometric dimensions of the cross-section and hence Equation 6.2 gives the corresponding deformation capacity ε_{LB}. Once ε_{LB} is known the corresponding local buckling stress σ_{LB} can be obtained using the material stress-strain relationship. The material properties for different grades of stainless steel have already been investigated in Chapter 3 and specific values for compound Ramberg-Osgood parameters have been proposed in Table 3.5 which recognise not only the differences among the grades but also the effect of manufacturing process on the most commonly used grade, austenitic 1.4301. The coefficients may be used to obtain the complete material stress-strain behaviour and thus to provide the stress corresponding to ε_{LB}.

The compound Ramberg-Osgood material model, as expressed by Equations 6.3 and 6.4, may be used to model stainless steel behaviour very accurately, but relates strain as a function of stress and hence stress cannot be obtained directly from this model. For practical cases it is preferable to establish a stress-strain relationship such that the stress can be directly obtained from the strain. Hence the material stress-strain behaviour can be presented in tabular form as shown in Table 6.2 which gives the proposed local buckling stress table for roll-formed sections produced from austenitic Grade 1.4301. Appendix A presents similar tables for other considered stainless steel grades. These tables permit designers to obtain σ_{LB} directly from ε_{LB} without the need for iteration.

Abdella (2006) recently proposed inversions of compound Ramberg-Osgood formulations i.e. stress is expressed in terms of strain, which enables obtaining local buckling stresses directly with knowledge of deformation capacity. Use of this formulation in the proposed method has recently been demonstrated by Nethercot et al (2006), although this has not been included in this thesis.

Table 6.2: Local buckling stresses for roll-formed sections produced from austenitic Grade 1.4301 ($n = 4.3$, $n'_{0.2,1.0} = 2.7$, $\sigma_{1.0}/\sigma_{0.2} = 1.25$, $E_0 = 200500$ N/mm^2)

ε_{LB}	$\sigma_{0.2}$ (N/mm^2)								
	200	250	300	350	400	450	500	550	600
0.0005	88	94	96	98	98	99	99	99	99
0.0010	132	153	167	177	184	189	193	195	195
0.0020	175	210	242	270	294	313	330	344	357
0.0030	200	243	284	320	356	387	415	443	465
0.0040	215	265	313	358	400	439	475	509	540
0.0050	224	277	330	380	429	476	520	562	600
0.0060	230	286	340	394	446	498	547	596	642
0.0070	235	292	349	404	459	513	565	617	668
0.0080	239	297	355	412	469	524	579	633	686
0.0090	243	302	361	419	477	534	591	646	701
0.0100	246	306	366	426	484	543	600	657	714
0.0120	252	313	375	436	497	557	617	676	734
0.0140	256	320	383	445	507	569	630	691	752
0.0160	261	325	389	453	516	579	642	704	766
0.0180	265	330	395	460	525	589	653	716	779
0.0200	268	334	401	466	532	597	662	727	791
0.0240	274	342	410	478	545	612	679	745	812
0.0280	280	350	419	488	557	625	694	762	830
0.0320	285	356	426	497	567	637	707	776	846
0.0360	290	362	433	505	576	648	719	789	860
0.0400	294	367	440	513	585	657	730	802	873
0.0500	303	379	454	529	604	679	754	828	903
0.0600	312	389	467	544	621	698	775	852	928
0.0700	319	398	478	557	636	715	794	872	951
0.0800	326	407	488	569	649	730	811	891	971
0.0900	332	414	497	579	662	744	826	908	990
0.1000	337	421	506	589	673	757	841	924	1007

Once the σ_{LB} value is obtained, the cross-section compression resistance can be determined by multiplying this value by the gross-sectional area A_g. It is worth mentioning that the proposed method does not require any calculation for 'effective areas' for slender sections; rather the corresponding 'loss of effectiveness' for such sections is automatically reflected on

σ_{LB} due to the reduced deformation capacity. This method, thus, reduces the amount of calculation by avoiding the traditional cross-section classification which may not be quite justified for a nonlinear material like stainless steel.

6.2.2.3 Validation of the test design curve

The proposed technique for the determination of compressive resistance involves the following steps:

(i)   Determination of the cross-section slenderness β for the most slender element using Equation 6.1

(ii) Computing the local buckling strain ε_{LB} using Equation 6.5

(iii) Obtaining the local buckling stress σ_{LB} using either the compound Ramberg-Osgood Equation in conjunction with the appropriate parameters as proposed in Table 3.5 or using the appropriate table from Appendix A.

(iv) Compression resistance of the cross-section $N_{c,Rd}$ (or F_u) is given by the multiple of σ_{LB} and the gross cross-sectional area A_g

The compression resistances of considered 136 stub columns obtained from 8 different testing programmes involving 4 different grades and 6 different cross-section types manufactured through all possible processes have been determined following these steps and the results are compared to the test results in Figure 6.5. A summary of the predictions is given in Table 6.3.

Table 6.3: Summary of the predictions obtained using the design curve given by Equation 6.5.

Cross-section type	Production process	No. of sources	No. of stub columns	Predicted F_u / Test F_u	
				Mean	COV
Angle	Press-braking	1	12	1.00	0.14
Channel	Press-braking	1	11	1.00	0.17
Lipped Channel	Press-braking	2	22	1.00	0.08
I section	Welded	2	20	1.15	0.18
SHS	Roll-forming & Press-braking	6	42	1.06	0.21
RHS	Roll forming & Press-braking	4	29	0.91	0.06
All sections	**All possible processes**	**8**	**136**	**1.02**	**0.18**
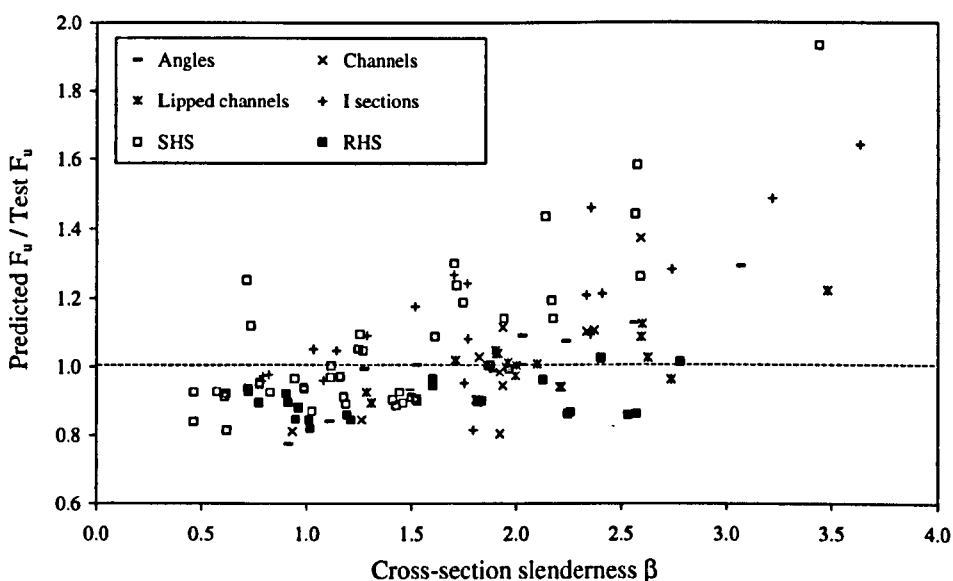
Figure 6.5: Comparison between test results to the predicted compressive resistances obtained using the design curve given by Equation 6.5.

From these comparisons it is observed that the predictions are somewhat scattered, the overall COV being 0.18 with a mean of 1.02 although a large number of predictions, especially those for hollow sections, are lower than the corresponding test result. For the relatively slender sections with $\beta > 1.5$ most of the predictions are rather high when compared to the test results. This comparison clearly suggests that some modifications are required to make the predictions more accurate so as to represent the actual test results.

6.2.2.4 Reasons for the obtained scatter in predictions

The proposed approach directly uses the flat material stress-strain behaviour to obtain the local buckling stress for the stub columns. In reality, stub column stress-strain curves differ from that of the basic material coupon due to the presence of residual stresses, imperfections, local buckling and enhanced strength at the corners. Thermal residual stresses, in the case of hollow and I sections, have been shown to have little influence on stub column behaviour as explained in Chapter 5 and also presented by Gardner and Nethercot (2004c) and Ashraf et al (2005d). Bending residual stresses are re-introduced into the coupons in the process of testing (Rasmussen, 1993 and Gardner, 2002). Enhanced corner strength, on the other hand, plays a very significant role in the case of relatively stocky sections and the use of only the basic material stress-strain curve underestimates the compression resistance. As the section becomes more slender, the corner region gradually loses its significance and local plate buckling at stresses below $\sigma_{0.2}$ dominates failure. However, post-buckling behaviour has been

found to be significant in the case of slender cross-sections as mentioned by Gardner (2002), causing the stub column stress-strain behaviour to deviate from that of the coupon before reaching the peak stress. This causes significant overestimation in compression resistance for the relatively slender cross-sections with β >1.5. These features are illustrated in Figure 6.6.
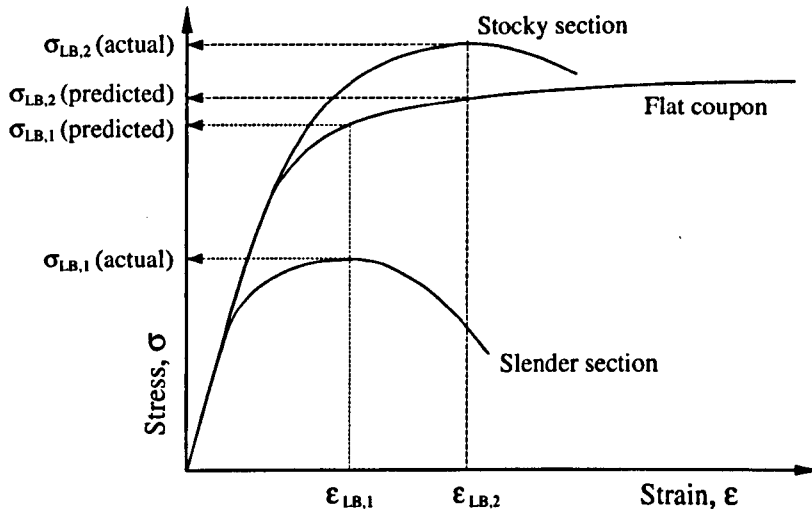
Figure 6.6: Behaviour of slender and stocky stub columns showing differences with the behaviour of flat material.

6.2.2.5 Proposed corrections for sections with enhanced corner strength

Stainless steel exhibits pronounced strain hardening, resulting in the corner regions of cold-formed sections having 0.2% proof strengths much higher than that of the flat material as already shown in Chapter 4. Failure to allow for these enhanced strength regions in design leads to under-predictions of load carrying capacity. This effect has been found to be very important in the case of stocky sections since they normally contain a larger proportion of corner area and the buckling stress goes beyond the 0.2% proof stress $\sigma_{0.2}$ of the flat material. A correction factor is therefore required to explicitly include the effects of corner enhancements and to bring the predictions closer to the test results.

In Chapter 4, models have been proposed to predict the 0.2% proof strength and ultimate strength of corner regions based on a comprehensive investigation of all available test results. Separate models have been proposed to allow for the difference between the roll-forming and press-braking processes. Two different correction factors are proposed herein, considering the difference in manufacturing processes, to include the effect of cold-worked corner regions on the compression resistance of cross-sections.

(a) Correction for roll-formed sections

The material properties of the flat region of roll-formed sections are different from those of the virgin material because of the cold-work done during the roll-forming process. The following expressions hold true for a roll-formed section (considering strength enhancement to be restricted within the corner only),

$$F_u = A_f.\sigma_{0.2,f} + A_c.\sigma_{0.2,c}$$
$$= A_g [A_f/A_g. \sigma_{0.2,f} + A_c/A_g. \sigma_{0.2,c}]$$
$$= A_g [(1 - k_{cor}).\sigma_{0.2,f} + k_{cor} (0.82\sigma_{u,f})]$$
$$= A_g [(1 - k_{cor}).\sigma_{0.2,f} + k_{cor} (0.82 \times 1.61\sigma_{0.2,f})]$$
$$= A_g.\sigma_{0.2,f} (1 + 0.32k_{cor})$$

where, F_u is the peak load of the stub column

A_f is the area of the flat region

A_c is the area of the corner region

A_g is the gross area, $A_f + A_c$

k_{cor} is the proportion of the corner region, A_c/A_g

$\sigma_{0.2,f}$ is the 0.2% proof stress of the flat material

$\sigma_{0.2,c}$ is the 0.2% proof stress of the corner material (= $0.82\sigma_{u,f}$ as given by Equation 4.10)

$\sigma_{u,f}$ is the ultimate strength of the flat material (= $1.61\sigma_{0.2,f}$) [Gardner, 2002]

(b) Correction for press-braked sections

In the case of press-braked sections, the material properties of the flat region can be taken to be the same as the virgin material, with increases in the 0.2% proof strength only at the corners. Thus the resistance of a press-braked section can be expressed as follows,

$$F_u = A_f \sigma_{0.2,v} + A_c \sigma_{0.2,c}$$
$$= A_g [A_f/A_g \sigma_{0.2,v} + A_c/A_g \sigma_{0.2,c}]$$
$$= A_g \left[(1 - k_{cor})\sigma_{0.2,v} + k_{cor} \frac{1.881}{(r_i/t)^{0.194}} \sigma_{0.2,v} \right]$$
$$= A_g \sigma_{0.2,v} \left[1 + \left\{ \frac{1.881}{(r_i/t)^{0.194}} - 1 \right\} k_{cor} \right]$$

where, $\sigma_{0.2,v}$ is the 0.2% proof stress of the flat (virgin) material

Thus the cross-section resistance of a stainless steel section with corners should be multiplied by the following factor ϕ_c to account for the localised corner strength enhancements.

$$\phi_c = 1 + 0.32 k_{cor} \quad \text{for roll-formed sections} \tag{6.6}$$

$$= 1 + \left[\frac{1.881}{(r_i/t)^{0.194}} - 1 \right] k_{cor} \quad \text{for press-braked sections} \tag{6.7}$$

6.2.2.6 Corrections required for the post-buckling effect of slender sections

Relatively slender cross-sections with $\beta > 1.5$ appeared to exhibit significant amounts of post-buckling resistance, which causes the stub-column stress-strain curve to deviate from that of the material, making the proposed predictions significantly in excess of the actual resistances. This is clearly explained in Figure 6.6. Gardner (2002) observed the same effect for hollow sections and made adjustments for hollow sections with $\beta > 1.6$ by modifying the deformation capacities to account for the post-buckling effect.

An explicit correction factor to incorporate this effect has previously been reported by Ashraf et al (2006). The proposal was to multiply the obtained σ_{LB} by a factor of $(-0.154\beta + 1.186)$ as obtained by a regression analysis. The alternative to this is to modify the deformation capacity ε_{LB}, instead, as was done by Gardner (2002), and hence to obtain a modified design curve which includes the post-buckling effect for slender sections. The obvious advantage of the latter approach is that the required adjustment is implicit within the deformation capacity. Thus the designer need not apply any correction for slender sections, leading to a reduced amount of calculation.

An approach similar to Gardner (2002) was, therefore, followed herein by adjusting the deformation capacity of slender sections and thus proposing a modified design curve which includes the post-buckling effect. The modified deformation capacities for slender sections were computed based on the test resistances. Once the required local buckling stress was obtained, the corresponding strain was calculated using the proposed material model. Figure 6.7 shows the modified deformation capacities for slender sections and compares the proposed design curve with the previously obtained curve using test results. The expression for the proposed design curve is given by Equation 6.8. Figure 6.7 does not clearly show the differences because the slender section points lie almost along the horizontal axis. Hence a clearer picture is presented given in Figure 6.8. The visible small difference between these two curves actually affects the compression resistance by a significant margin since these sections fail, in most cases, within the elastic range.

Proposed design equation, $\dfrac{\varepsilon_{LB}}{\varepsilon_0} = \dfrac{6.44}{\beta^{2.85-0.27\beta}}$ (6.8)
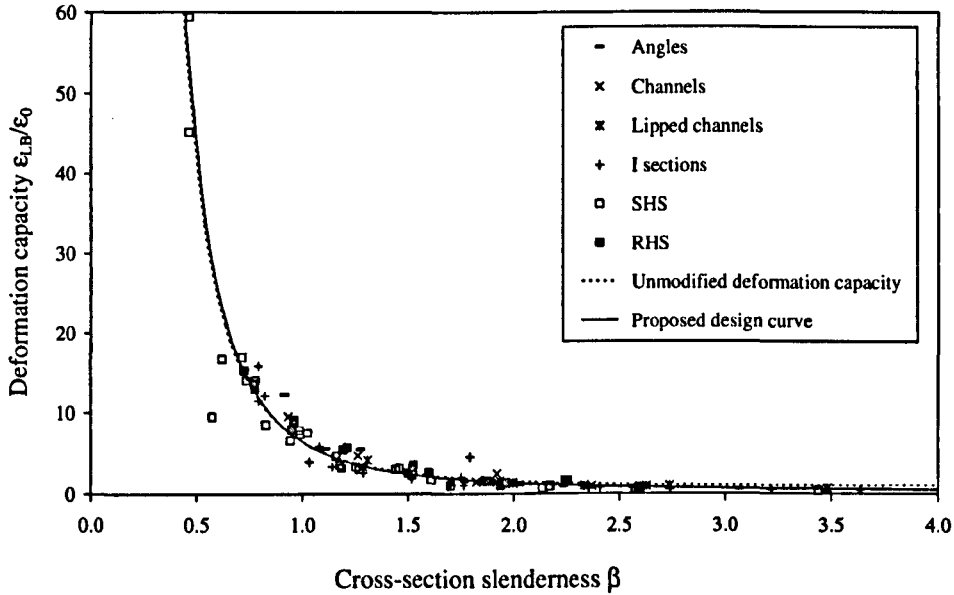
Figure 6.7: Modified deformation capacities and the proposed design curve.
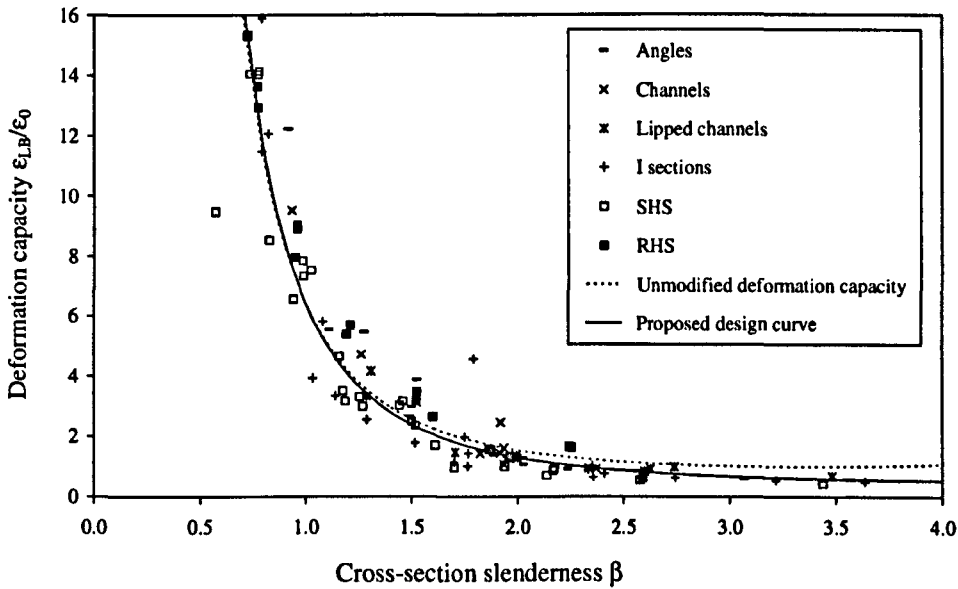
Figure 6.8: Comparison between the proposed design curve and unmodified deformation capacities for slender sections with $\beta > 1.5$.

The modified design steps required to compute the compression resistance of a stainless steel cross-section are given below:

(i) Determine the cross-section slenderness β for the most slender element

(ii) Compute the local buckling strain ε_{LB} using Equation 6.8

(iii) Obtain the local buckling stress σ_{LB} using either the compound Ramberg-Osgood model as given by Equations 6.3 and 6.4 or from the appropriate table given in Appendix A.

(iv) If the cross-section contains any cold-worked corners, an appropriate correction factor ϕ_c needs to be incorporated using Equation 6.6 or 6.7 depending on the manufacturing process. For sections without cold-worked corners $\phi_c = 1.0$.

(v) Compression resistance of a stainless steel cross-section $N_{c,Rd}$ is thus given by the Equation 6.9.

$$N_{c,Rd} = \phi_c \sigma_{LB} A_g \qquad (6.9)$$

6.2.3 Detailed comparisons

Resistances of all the stub columns have been predicted using the proposed method with appropriate corrections for the cold-worked corners and the detailed results are given in Table 6.4. The predicted resistances have been compared to the test results and the corresponding FE results. A summary of the comparisons is given in Table 6.5, whereas Figures 6.9 and 6.10 re-present the comparisons to provide clearer views.

Table 6.4: Predictions for the stub column resistances and comparisons with test and FE results.

Reference	Section type (Grade)	β	A_g (mm^2)	$\sigma_{0.2}$ (N/mm^2)	E_0 (N/mm^2)	Test F_u (kN)	ε_{LB}	σ_{LB} (N/mm^2)	ϕ_c	$N_{c,Rd}$ / Test F_u	$N_{c,Rd}$ / FE F_u
Kuwamura (2003)	Angle (1.4301)	0.91	129.7	279	200000	55.9	0.0113	333	1.14	0.88	0.98
		1.11	158.3	279	200000	59.4	0.0069	314	1.12	0.94	0.97
		1.50	217.4	279	200000	66.9	0.0033	274	1.09	0.97	0.97
		1.49	217.2	279	200000	65.6	0.0034	277	1.09	1.00	0.97
		1.89	275.7	279	200000	68.7	0.0020	235	1.07	1.01	0.98
		2.24	335.5	279	200000	69.6	0.0015	202	1.05	1.03	0.97
	Angle (1.4318)	1.27	135.2	508	187000	79.7	0.0095	577	1.14	1.11	1.00
		1.53	162.0	508	187000	89.8	0.0062	548	1.12	1.11	1.01
		2.03	225.4	508	187000	108.7	0.0034	441	1.08	0.99	0.94
		2.03	225.4	508	187000	100.2	0.0034	441	1.09	1.08	0.96
		2.56	286.3	508	187000	108.7	0.0023	356	1.07	1.00	0.94
		3.07	347.0	508	187000	106.4	0.0018	301	1.06	1.04	1.01
Kuwamura (2003)	Channel (1.4301)	0.93	257.5	279	190000	106.0	0.0114	333	1.15	0.93	0.98
		1.53	431.2	279	190000	134.2	0.0034	277	1.09	0.97	0.96
		1.94	555.5	279	190000	146.2	0.0020	235	1.06	0.95	0.94
		1.92	555.2	279	190000	140.4	0.0021	238	1.06	1.00	0.94
		1.94	698.7	279	190000	156.0	0.0020	235	1.05	1.11	1.11
		1.92	403.7	279	190000	125.0	0.0021	238	1.10	0.84	0.83

Table 6.4 (contd.): Predictions for the stub column resistances and comparisons with test and FE results.

Reference	Section type (Grade)	β	A_g (mm^2)	$\sigma_{0.2}$ (N/mm^2)	E_0 (N/mm^2)	Test F_u (kN)	ε_{LB}	σ_{LB} (N/mm^2)	ϕ_c	$N_{c,Rd}$ / Test F_u	$N_{c,Rd}$ / FE F_u
Kuwamura (2003)	Channel (1.4318)	1.26	267.4	508	180000	186.2	0.0101	580	1.15	0.96	0.99
		1.82	450.5	508	180000	229.7	0.0044	496	1.08	1.05	0.99
		2.34	571.2	508	180000	233.8	0.0028	399	1.07	1.04	0.98
		2.37	570.4	508	180000	229.6	0.0027	390	1.07	1.03	0.96
		2.59	721.0	508	180000	228.2	0.0023	356	1.06	1.19	1.11
Kuwamura (2003)	Lipped channel (1.4301)	1.29	641.2	279	186000	211.4	0.0051	302	1.11	1.02	1.00
		1.95	791.0	279	186000	197.0	0.0020	235	1.09	1.03	1.02
		1.96	873.1	279	186000	214.8	0.0020	235	1.08	1.03	0.98
		2.63	1104.2	279	186000	232.8	0.0012	182	1.06	0.92	0.90
		1.31	69.8	279	187500	23.7	0.0049	300	1.11	0.98	1.01
		2.00	88.4	279	187500	21.7	0.0019	228	1.08	1.00	0.96
		2.00	96.1	279	187500	24.3	0.0019	228	1.08	0.97	0.97
		2.74	120.3	279	187500	26.1	0.0011	176	1.06	0.86	0.82
	Lipped channel (1.4318)	1.71	659.0	508	180000	350.2	0.0051	526	1.11	1.10	1.02
		2.60	807.2	508	180000	317.9	0.0023	356	1.10	1.00	0.92
		2.60	898.1	508	180000	342.3	0.0023	356	1.08	1.01	0.90
		3.48	1139.2	508	180000	377.8	0.0017	287	1.07	0.92	0.81

Table 6.4 (contd.): Predictions for the stub column resistances and comparisons with test and FE results.

Reference	Section type (Grade)	β	A_g (mm²)	$\sigma_{0.2}$ (N/mm²)	E_0 (N/mm²)	Test F_u (kN)	ε_{LB}	σ_{LB} (N/mm²)	ϕ_c	$N_{c,Rd}$ / Test F_u	$N_{c,Rd}$ / FE F_u
Lecce and Rasmussen (2004a)	Lipped channel (1.4301)	1.92	565.0	242	187000	116.0	0.0018	199	1.07	1.04	1.04
		1.91	565.0	242	187000	116.0	0.0018	199	1.07	1.04	1.04
		1.90	565.0	242	187000	116.0	0.0019	204	1.07	1.06	1.07
		1.90	565.0	242	187000	116.0	0.0019	204	1.07	1.06	1.07
	1.4462	2.21	211.0	271	193000	50.0	0.0015	197	1.06	0.88	0.93
		2.21	211.0	271	193000	50.0	0.0015	197	1.06	0.88	0.93
		1.82	188.0	271	193000	51.0	0.0022	235	1.07	0.93	0.95
		1.81	188.0	271	193000	51.0	0.0022	235	1.07	0.93	0.95
	1.4003	2.10	555.0	339	208000	162.0	0.0019	274	1.07	1.01	1.07
		2.10	555.0	339	208000	162.0	0.0019	274	1.07	1.01	1.06
Kuwamura (2003)	Welded I sections (1.4301)	0.79	427.1	279	200000	152.8	0.0166	348	1.00	0.97	1.10
		1.75	709.3	279	200000	192.8	0.0024	248	1.00	0.91	0.98
		1.14	571.2	279	200000	171.1	0.0064	311	1.00	1.04	1.14
		1.29	721.8	279	200000	199.9	0.0048	299	1.00	1.08	1.12
		1.77	862.6	279	200000	203.4	0.0023	245	1.00	1.04	1.01
		1.76	1011.5	279	200000	207.7	0.0023	245	1.00	1.19	1.11
		2.41	1156.8	279	200000	206.1	0.0013	189	1.00	1.06	1.04
		2.74	1460.3	279	200000	231.4	0.0011	176	1.00	1.11	1.08

Table 6.4 (contd.): Predictions for the stub column resistances and comparisons with test and FE results.

Reference	Section type (Grade)	β	A_g (mm²)	$\sigma_{0.2}$ (N/mm²)	E_0 (N/mm²)	Test F_u (kN)	ε_{LB}	σ_{LB} (N/mm²)	ϕ_c	$N_{c,Rd}$ / Test F_u	$N_{c,Rd}$ / FE F_u
Kuwamura (2003)	Welded I sections (1.4318)	1.03	435.4	508	194000	253.4	0.0155	603	1.00	1.04	0.98
		2.35	729.6	508	194000	289.7	0.0025	373	1.00	0.94	0.86
		1.52	591.2	508	194000	279.5	0.0061	547	1.00	1.16	1.03
		1.70	738.9	508	194000	309.9	0.0047	510	1.00	1.22	1.06
		2.33	887.8	508	194000	323.4	0.0026	382	1.00	1.05	0.94
		2.36	1041.4	508	194000	310.1	0.0025	373	1.00	1.25	1.08
		3.22	1194.3	508	194000	311.5	0.0017	287	1.00	1.10	0.97
		3.64	1491.1	508	194000	359.7	0.0015	259	1.00	1.07	0.88
Stangenberg (2000a)	Welded I sections (1.4301)	0.79	2430.2	279	200000	885.0	0.0167	348	1.00	0.96	0.97
		0.82	4074.4	279	198000	1440.0	0.0152	344	1.00	0.97	0.98
		1.79	4569.6	279	200000	1430.0	0.0023	245	1.00	0.78	0.84
	(1.4462)	1.08	4094.1	524	202000	2590.0	0.0137	604	1.00	0.95	0.97
Young and Lui (2005)	SHS (Duplex)	1.11	288.0	707	216000	245.3	0.0160	825	1.04	1.01	1.07
		1.12	289.0	707	216000	238.0	0.0159	825	1.04	1.04	1.06
		1.71	295.0	622	200000	175.7	0.0055	640	1.02	1.10	1.19
		1.74	289.0	622	200000	177.6	0.0053	631	1.02	1.05	1.16
	(1.4301)	2.57	1607.0	448	189000	408.6	0.0020	312	1.02	1.25	1.21
		1.25	3382.0	497	194000	1927.4	0.0095	592	1.03	1.07	1.05

Table 6.4 (contd.): Predictions for the stub column resistances and comparisons with test and FE results.

Reference	Section type (Grade)	β	A_g (mm²)	$\sigma_{0.2}$ (N/mm²)	E_0 (N/mm²)	Test F_u (kN)	ε_{LB}	σ_{LB} (N/mm²)	ϕ_c	$N_{c,Rd}$ / Test F_u	$N_{c,Rd}$ / FE F_u
Liu and Young (2003)	SHS (1.4301)	1.43	512.0	313	195000	194.0	0.0043	330	1.02	0.89	1.00
		1.41	516.0	313	195000	193.1	0.0044	332	1.02	0.91	1.00
		0.62	1213.0	413	194000	825.3	0.0498	623	1.05	0.96	0.95
		0.61	1223.0	413	194000	843.9	0.0515	626	1.03	0.94	0.94
Kuwamura (2003)	SHS (1.4301)	0.62	515.1	279	190500	241.0	0.0337	379	1.18	0.96	0.83
		0.94	813.7	279	190500	282.4	0.0110	332	1.10	1.06	0.92
		1.27	1104.4	279	190500	323.2	0.0052	303	1.08	1.12	0.95
		1.61	1399.7	279	190500	353.8	0.0030	268	1.06	1.12	1.03
		1.94	1686.0	279	190500	363.9	0.0020	235	1.05	1.15	1.11
		2.59	2264.8	279	190500	364.8	0.0012	182	1.04	1.17	1.13
	SHS (1.4318)	0.83	542.2	508	184000	377.5	0.0292	635	1.15	1.05	1.06
		1.25	855.2	508	184000	459.4	0.0101	580	1.09	1.18	1.06
		1.70	1132.5	508	184000	468.7	0.0050	524	1.07	1.36	1.12
		2.14	1450.7	508	184000	480.5	0.0032	429	1.05	1.36	1.19
		2.58	1760.3	508	184000	483.0	0.0023	356	1.05	1.36	1.18
		3.44	2346.1	508	184000	511.9	0.0017	287	1.03	1.36	1.15

Table 6.4 (contd.): Predictions for the stub column resistances and comparisons with test and FE results.

Reference	Section type (Grade)	β	A_g (mm^2)	$\sigma_{0.2}$ (N/mm^2)	E_0 (N/mm^2)	Test F_u (kN)	ε_{LB}	σ_{LB} (N/mm^2)	ϕ_c	$N_{c,Rd}$ / Test F_u	$N_{c,Rd}$ / FE F_u
Gardner (2002)	SHS (1.4301)	1.02	1080.0	457	186600	727.0	0.0148	582	1.04	0.90	1.02
		0.99	1124.0	457	186600	714.0	0.0163	589	1.04	0.97	1.03
		0.99	1125.0	457	186600	711.0	0.0164	590	1.04	0.97	1.03
		0.71	1105.0	261	206300	309.0	0.0199	349	1.00	1.25	0.93
		0.73	1080.0	261	206300	335.0	0.0184	345	1.00	1.11	0.94
		2.18	743.0	370	207100	197.0	0.0020	279	1.01	1.06	1.05
		2.17	739.0	370	207100	187.0	0.0020	279	1.01	1.12	1.05
		1.44	1101.0	379	208800	489.0	0.0047	401	1.02	0.92	0.99
		1.46	1089.0	379	208800	496.0	0.0046	398	1.02	0.89	1.00
		1.16	1431.0	437	203400	779.0	0.0095	523	1.03	0.99	0.94
		1.16	1426.0	437	203400	774.0	0.0095	523	1.03	1.00	0.94
		0.77	2147.0	473	197900	1513.0	0.0302	664	1.05	0.99	1.03
		0.78	2153.0	473	197900	1507.0	0.0298	662	1.05	0.99	1.03
		0.46	2785.0	330	205200	1630.0	0.0836	540	1.07	0.99	1.07
		0.46	2781.0	330	205200	1797.0	0.0841	541	1.07	0.90	1.07
		1.50	2167.0	294	195400	726.0	0.0036	296	1.03	0.91	0.91
		1.52	2139.0	294	195400	713.0	0.0035	293	1.03	0.90	0.91
Talja and Salmi (1995)	(1.4301)	0.57	999.0	463	186500	801.0	0.0714	738	1.06	0.97	1.12
Rasmussen and Hancock (1993)	SHS (1.4306)	1.19	908.0	415	196000	485.0	0.0088	470	1.05	0.92	0.87
		1.18	900.0	415	196000	471.0	0.0090	472	1.05	0.94	0.87

Table 6.4 (contd.): Predictions for the stub column resistances and comparisons with test and FE results.

Reference	Section type (Grade)	β	A_g (mm^2)	$\sigma_{0.2}$ (N/mm^2)	E_0 (N/mm^2)	Test F_u (kN)	ε_{LB}	σ_{LB} (N/mm^2)	ϕ_c	$N_{c,Rd}$ / Test F_u	$N_{c,Rd}$ / FE F_u
Young and Lui (2005)	RHS (Duplex)	2.13	1258.0	486	212000	558.2	0.0026	384	1.04	0.90	1.00
		2.78	1305.0	536	208000	537.3	0.0019	335	1.03	0.84	0.93
	(1.4301)	2.40	2291.0	503	200000	957.0	0.0024	365	1.04	0.91	0.90
Young and Liu (2003)	RHS (1.4301)	2.53	598.0	350	198000	187.8	0.0015	223	1.03	0.73	0.85
		2.57	590.0	350	198000	184.7	0.0015	223	1.03	0.73	0.85
		1.01	1523.0	424	194000	969.8	0.0137	535	1.04	0.88	0.90
		1.02	1515.0	424	194000	994.7	0.0135	535	1.04	0.85	0.91
		1.83	1056.0	366	193000	404.6	0.0029	326	1.03	0.87	1.00
		1.82	1066.0	366	193000	413.1	0.0030	326	1.03	0.86	0.99
		0.91	2159.0	443	194000	1414.1	0.0187	583	1.05	0.94	0.96
		0.90	2172.0	443	194000	1387.8	0.0192	585	1.05	0.96	0.96
Gardner (2002)	RHS (1.4301)	0.72	675.0	469	193100	492.0	0.0370	677	1.05	0.98	1.02
		0.72	675.0	469	193100	497.0	0.0368	677	1.05	0.97	1.02
		1.86	1109.0	429	197300	452.0	0.0032	384	1.03	0.97	0.92
		1.88	1100.0	429	197300	447.0	0.0032	384	1.03	0.98	0.92
		0.96	2107.0	466	192300	1459.0	0.0174	606	1.06	0.92	0.98
		0.96	2108.0	466	192300	1465.0	0.0173	606	1.06	0.92	0.98
		1.53	1799.0	319	200300	660.0	0.0037	320	1.03	0.90	0.85
		1.52	1805.0	319	200300	659.0	0.0037	320	1.03	0.90	0.84
		2.24	529.0	370	205900	182.0	0.0019	269	1.02	0.80	0.83
		2.26	529.0	370	205900	181.0	0.0019	269	1.02	0.80	0.84

Table 6.4 (contd.): Predictions for the stub column resistances and comparisons with test and FE results.

Reference	Section type (Grade)	β	A_g (mm^2)	$\sigma_{0.2}$ (N/mm^2)	E_0 (N/mm^2)	Test F_u (kN)	ε_{LB}	σ_{LB} (N/mm^2)	ϕ_c	$N_{c,Rd}$ / Test F_u	$N_{c,Rd}$ / FE F_u
Gardner (2002)	RHS (1.4301)	1.60	811.0	455	200900	407.0	0.0047	469	1.03	0.96	0.94
		1.60	811.0	455	200900	415.0	0.0047	469	1.03	0.95	0.94
		1.19	1026.0	439	203900	626.0	0.0089	521	1.04	0.89	0.91
		1.21	1014.0	439	203900	627.0	0.0085	517	1.04	0.87	0.91
		0.77	1558.0	494	206300	1217.0	0.0303	693	1.07	0.95	1.01
		0.77	1559.0	494	206300	1217.0	0.0305	694	1.07	0.95	1.01
Talja and Salmi (1995)	RHS (1.4301)	1.97	1397.0	305	206600	372.0	0.0020	252	1.05	0.99	0.94
		0.95	2683.0	345	240800	1292.0	0.0106	407	1.10	0.93	0.90

Table 6.5: Summary of the predictions for compression resistance using the proposed method.

Cross-section type	Production process	Grade	No. of Stub Columns	$N_{C,Rd}$ / Test F_u		$N_{c,Rd}$ / FE F_u	
				Mean	COV	Mean	COV
Angle	Press-braking	1.4301, 1.4318	12	1.01	0.07	0.98	0.02
Channel	Press-braking	1.4301, 1.4318	11	1.01	0.09	0.98	0.08
Lipped channel	Press-braking	1.4301, 1.4318	22	0.99	0.07	0.97	0.08
I section	Welding	1.4301, 1.4318, 1.4462	20	1.04	0.11	1.01	0.09
SHS	Roll-forming & Press-braking	1.4301, 1.4318, 1.4306, Duplex	42	1.05	0.13	1.03	0.09
RHS	Roll forming & Press-braking	1.4301, Duplex	29	0.90	0.08	0.93	0.06
All sections	**All possible processes**	**1.4301, 1.4318, 1.4306, Duplex**	**136**	**1.00**	**0.12**	**0.99**	**0.09**
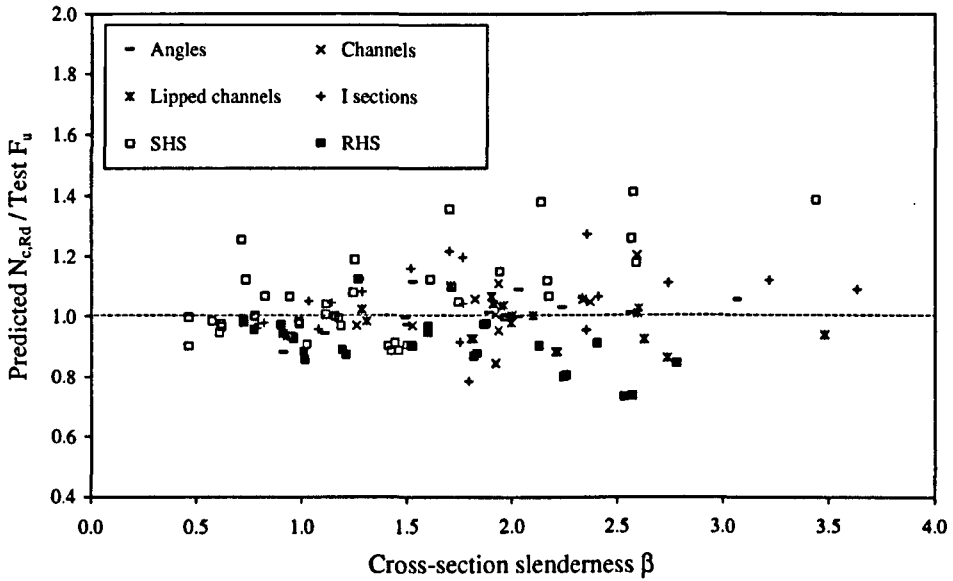
Figure 6.9: Comparison between the predicted compression resistance and test results.
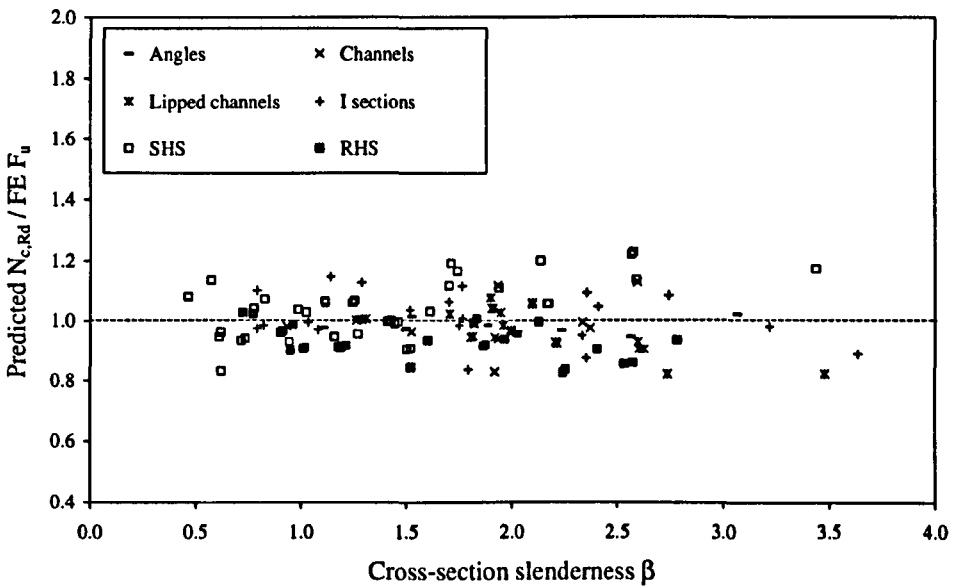
Figure 6.10: Comparison between the predicted compression resistance and FE results.

From Table 6.5 it is observed that using the proposed design curve in conjunction with the exact material model, the compression resistance of stainless steel cross-sections can be predicted very accurately. The overall average for the predicted resistances to test results for 136 stub columns is 1.00 with a COV of 0.12. These two figures were 1.02 and 0.18 respectively when the unmodified design curve (Equation 6.5) was used. The significant

reduction in scatter is quite obvious if Figure 6.9 is compared with Figure 6.5. This improvement in prediction clearly confirms the importance of appropriate recognition of the corner strength enhancement as well as the post-buckling effect for slender sections.

Figure 6.10 compares the predictions with the corresponding FE results. The FE simulation technique reduces the inevitable uncertainties associated with test results and hence significantly better agreement was attained with the overall mean prediction being 0.99 with a COV of 0.09. This improvement is clearly observed when Figures 6.9 and 6.10 are compared.

The reasons for the obtained scatter, although not significant given the variability of the cases considered, were carefully investigated and the following sections explain some of the possible features.

6.2.3.1 Predicted material behaviour

Test results were collected from all available sources; it is worth mentioning that full details were not available is many cases. A significant number of test results were reported by Kuwamura (2003) on two grades of austenitic stainless steel. For a total of 63 stub columns only one coupon test result for each grade has been reported. Although the sections were press-braked, it is believed that variability of resistance among the stainless steel cross-sections is very likely. Among 136 stub columns only in 48 cases, as reported by Lecce and Rasmussen (2004a), Gardner (2002), Talja and Salmi (1995) and Rasmussen and Hancock (1993), the compression coupon tests were available. It has been shown in Chapter 3 that the resistance of stainless steel may vary significantly in tension and compression. After analysing a considerable amount of material test data, it was therefore proposed to take the compressive 0.2% proof strength, if unavailable, as 93% of the tension 0.2% proof strength for austenitic Grade 1.4301, whereas for other grades the compression behaviour has been assumed to be the same as that for tension. These guidelines should be verified against more test results to obtain a general acceptability since in some cases the compression strength has been observed to be very close or even higher than the tension strength. Table 6.6 gives a comparison showing the importance of using appropriate material strength to determine compression resistance of cross-sections. Using the compression property reduces the scatter and also makes the predictions closer to the test results and also reduces the chances of overprediction.

Table 6.6: Comparison between the predictions using compression and tensile material properties.

Available material property	No. of stub columns	$N_{c,Rd}$ / Test F_u		$N_{c,Rd}$ / FE F_u	
		Mean	COV	Mean	COV
Compression	48	0.96	0.084	0.98	0.076
Tension	88	1.03	0.128	1.00	0.090

6.2.3.2 Welded cross-sections tested by Kuwamura (2003)

Among the 63 stub column tests reported by Kuwamura (2003), 28 sections are welded. I sections were welded by laser beam and TIG welding. SHS sections were formed in a rather unusual fashion - two press-braked channel sections were welded tip-to-tip using laser beam. Welding processes often cause significant reduction in material strength. Young and Lui (2005), in a recent study, collected material coupons from different parts within cross-sections of two roll-formed RHS. In the case of duplex RHS 160×80×3 the average flat material strength was 543 N/mm², whereas the strength near a weld was only 484 N/mm², showing 11% reduction in localised material strength. For the second section of high strength austenitic RHS 200×110×4 this reduction was 26%. Almost half of Kuwamura's (2003) tested cross-sections were produced from heat treated high strength austenitic Grade 1.4318, which is very likely to be significantly affected by welding on opposite faces. A more representative material property should reduce the significant overpredictions observed for these sections. The developed FE models used uniform material property and hence the obtained results have been found to be closer to the predictions. Table 6.7 compares the results for the welded sections reported by Kuwamura (2003) with those for his other tested sections.

Table 6.7: Predictions for the stub columns tested by Kuwamura (2003).

Production process	Cross-section types	No. of stub columns	$N_{c,Rd}$ / Test F_u		$N_{c,Rd}$ / FE F_u	
			Mean	COV	Mean	COV
Press-braked	Angles, Channels, Lipped Channels	35	1.01	0.075	0.97	0.065
Welded	I sections, SHS	28	1.13	0.116	1.05	0.093

6.2.3.3 Slender sections with β>2.0

Relatively slender sections have been observed to be very sensitive, very minor changes in the deformation capacity can affect the resistance by a significant margin. The effect has been

carefully investigated and the deformation capacities for slender sections were modified to obtain the proposed design curve which uses different coefficients than those previously reported by Ashraf (2005) and Gardner and Ashraf (2006). The performance of the proposed design curve, as given by Equation 6.8, for slender sections is closer and more consistent with the test results.

The local buckling stress tables given in Appendix A are based on average material properties obtained by analysing available material test results in Chapter 3. These properties are believed to be representative values for the grades specified. But when a cross-section fails within the elastic limit, then σ_{LB} is directly proportional to the Young's modulus E_0. If the exact value for E_0 is available and is significantly different from the value used in the local buckling stress table, using the exact value should produce more accurate predictions.

6.2.4 Distortional buckling

Distortional buckling mode is a unique mode for thin steel sections with outstands or partially restrained elements. In the case of stainless steel the sections are generally formed from even thinner elements making the possibility of distortional buckling more likely. This section briefly describes the behaviour observed for open sections used in the present research and investigates the effect of such a mode on the compression resistance.

6.2.4.1 Open sections tested by Kuwamura (2003)

Kuwamura (2003), in his extensive testing programme involving 63 open sections, investigated the local buckling behaviour of stainless steel sections. No observation of distortional buckling has been reported and no evidence is available to indicate whether the failure modes were dominated by local or distortional buckling in the case of lipped channel sections. However, deformed shapes were studied using the developed FE models which had been previously verified against available load-deformation behaviour as explained in Chapter 5. In most of the cases the onset of the stub column failure occurred at the tip of the outstands and was followed by a local buckling mode. Some of the sections possessed very thin webs, where the failure started by obvious local buckling. However the overall failure pattern was, in most of the cases, dominated by the local buckling with a simultaneous distortion at the outstands or partially restrained elements. Figure 6.11 illustrates some typical failure modes showing local buckling of the cross-sections.

C 80 × 40 × 3   CL 200 × 75 × 25 × 3   I 50 × 50 × 3 × 3
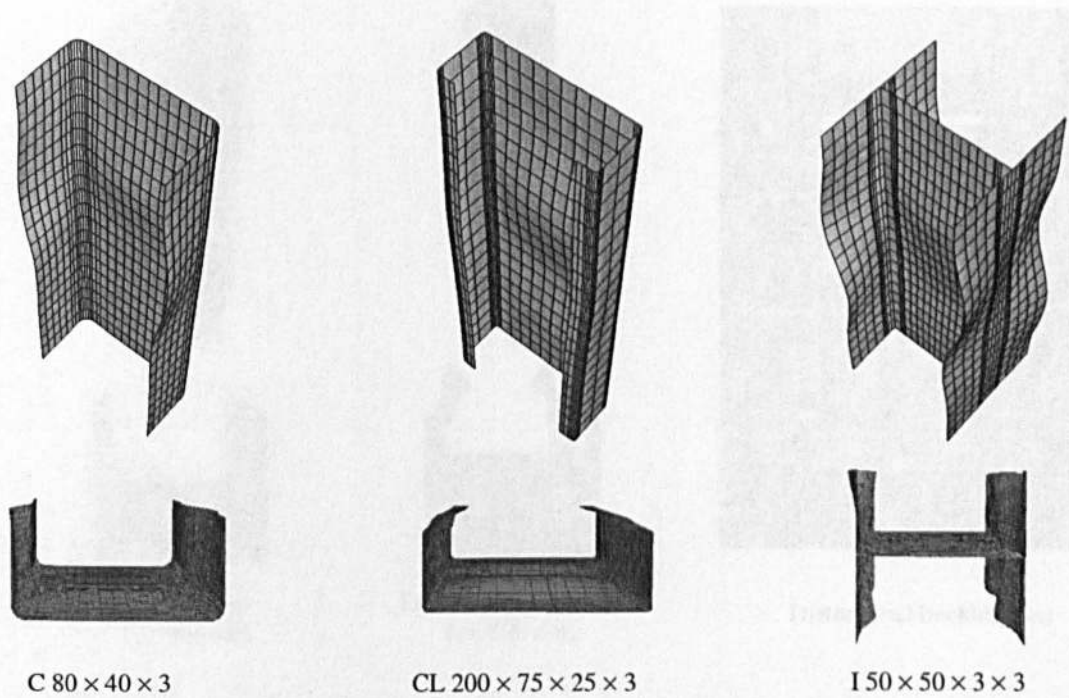
Figure 6.11: Typical failure modes observed in the FE models for open sections
tested by Kuwamura (2003)

6.2.4.2 Lipped channels tested by Lecce and Rasmussen (2004a)

Lecce and Rasmussen (2004a) tested 10 lipped channel sections specially designed to fail by
distortional buckling and the results for both stub column tests and distortional buckling tests
have been reported. The compression resistances for these cross-sections have been predicted
considering both the webs and the flanges to be simply supported, as given in Table 6.4, and
were compared to the test and FE results. All the predictions have shown excellent agreement
with the reported resistances.

Both the stub column tests and distortional buckling tests have been modelled using
ABAQUS. The lengths of the stub columns were not available, although, it has been reported
that the sections were made to lengths in accordance with the recommendations in Galambos
(1998) between 3d and 20r, where d is the web depth and r is the least radius of gyration.
Figure 6.12 compares the simulated deformed shapes obtained for the stub column test
(assumed L = 400mm) and the distortional buckling test for CL 105×90×12.5×2 (304D2a).
Excellent agreement is observed between the obtained and reported failure mode in the case
of distortional buckling.

Stub column
L = 400 mm

Distortional buckling
L = 600 mm

Distortional buckling test
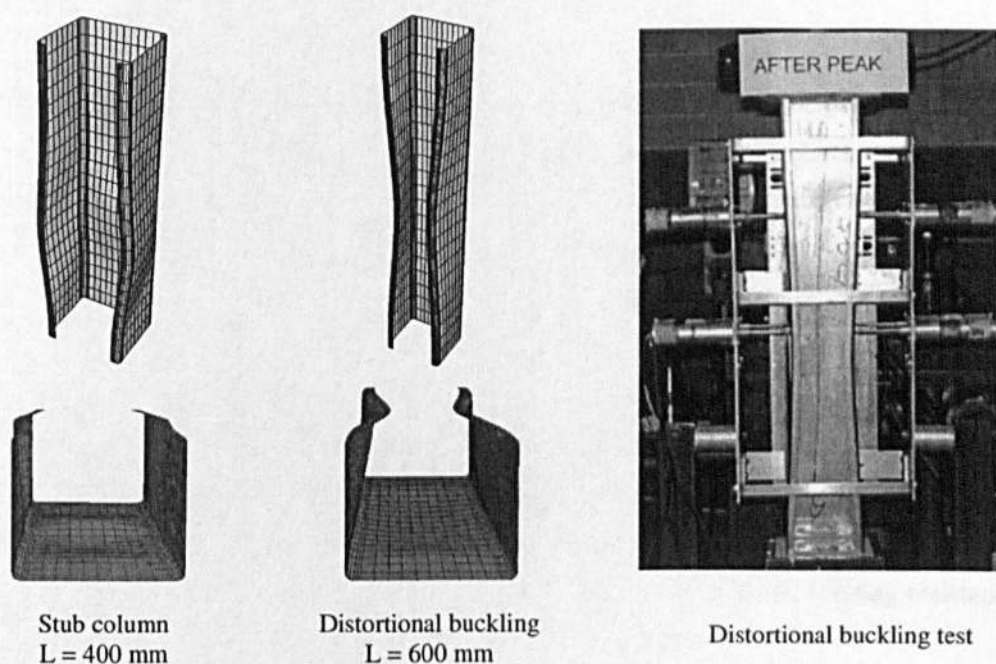
Figure 6.12: Distortional buckling mode reported in test and observed in the developed FE model for CL 105×90×12.5×2 (304D2a) tested by Lecce and Rasmussen (2004a).

The differences in the deformed shapes observed for the stub column test and the distortional buckling test are significant. In the case of the stub column, local buckling dominates even in these specially designed sections and hence the proposed method produced good predictions for the cross-section compression resistance. As the length increases, the partial restraint offered by the lips comes into play and hence the expected distortional buckling mode dominates. Even more severe cases are expected when such sections are subjected to bending. However, the absence of test results, at this stage, has prevented the exploration of such cases.

6.2.4.3 Summary and proposals

The compression resistances of the considered lipped channel cross-sections have been predicted using the proposed method, without any special considerations for the partial restraint, and the predictions have been found in good agreement with the test results. It is, however, understood that assuming the partially restrained flanges to be 'simply supported' plates may produce overpredictions and hence modifications are required to evaluate appropriate buckling coefficients k for such elements whereby the slenderness factor β should be modified. Parametric investigations on the bending behaviour of stainless steel lipped channel sections with varying lip sizes could provide answers to this phenomenon. Although numerical modelling may be employed, this should only be done once sufficient test results become available for validation.

6.2.5 Concluding remarks

The formulation of the basic design curve to determine the deformation capacity of a stainless steel cross-section has been explained and the performance of this proposed method has also been verified against all available stub column test results. For an expensive material such as stainless steel, it is important to exploit its special features such as sensitivity to cold-working and significant strain hardening, to obtain accurate predictions. An exact material model has been proposed with specific parameters to be used for different grades. Predictions using FE models have been used to investigate the inevitable uncertainties associated with test results and the obtained comparisons have been analysed to identify the reasons for the obtained scattered predictions, which, however, is considerably smaller than that exists in the case of Eurocode prEN 1993-1-4 (2004) predictions (compared in Chapter 8). The proposed design curve will be used in the remainder of the thesis to obtain not only the bending resistance of cross-sections but also the resistance of stainless steel members.

6.3 BENDING RESISTANCE

The behaviour of stainless steel cross-sections in bending is quite similar to that in compression. The compression flange behaves in the same way as a plate element interacts in a stub column. Moreover, the in-plane bending resistance of a cross-section formed from thin plates is most likely to be limited either by the local buckling the compression flange or the compressed portion of the web. The method proposed for stub columns is believed to be suitable to predict the bending resistance of cross-sections failing by local buckling. Gardner and Nethercot (2004d) proposed and verified this approach for SHS and RHS beams. The present research adopts the same technique using the proposed design curve (Equation 6.8) to include all types of sections and thus to establish a general procedure to determine the in-plane bending resistance of stainless steel cross-sections.

6.3.1 Guidelines proposed by Gardner (2002) to determine bending resistance

This section explains the methodology proposed by Gardner (2002) to obtain the in-plane bending resistance of stainless steel SHS and RHS. The design steps are explained herein, step-by-step, to demonstrate the special features that must be considered when analysing a stainless steel cross-section subjected to bending.

(i) Determine the cross-section slenderness for the most slender element in bending. It should be noted that the stress conditions are different for flange and web elements and hence both the edge restraints and the stress distribution will affect the plate buckling

coefficient k. Gardner (2002) proposed that the theoretical buckling coefficients presently given in Tables 4.1 and 4.2 of Eurocode 3 Part 1.5, prEN 1993-1-5 (2003), may be adopted. Thus for SHS and RHS the k value for flange and web are 4.0 and 23.9 respectively, whereas for an I section subjected to major axis bending the buckling coefficients for flange and web will be 0.43 and 23.9 respectively.

(ii) Once the most slender element is identified, determine the deformation capacity ε_{LB} of the cross-section using the proposed design curve. This is assumed to be the strain at the outermost fibre at the initiation of failure and thus may be used to define the stress distribution over the depth of the cross-section using the proposed compound Ramberg-Osgood material model. Figure 6.13 shows the actual nonlinear bending stress distribution for a stainless steel cross-section. The nonlinearity of this stress distribution makes it complex yet necessary to produce in a way which is different to the linear distributions adopted for carbon steel.

Bending stress (N/mm^2)
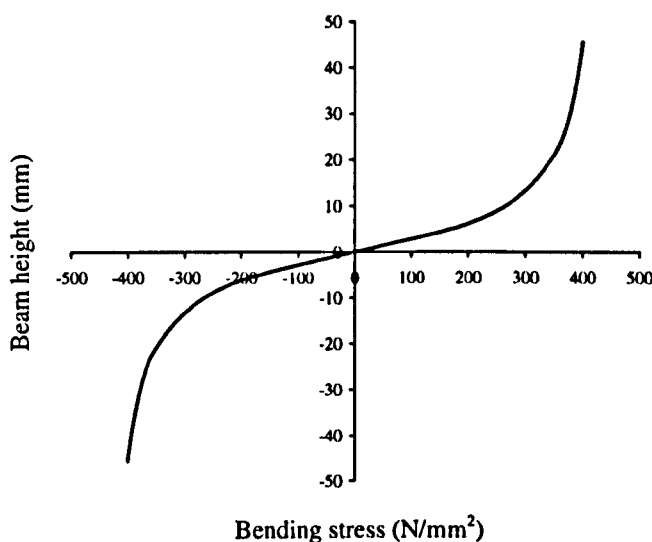
Figure 6.13: Typical bending stress distribution for a stainless steel cross-section.

(iii) The concept of a generalised shape factor, first proposed by Mazzolani (1995) for aluminium cross-sections, has been successfully exploited by Gardner (2002) for stainless steel. Generalised shape factor a_g includes both the material and the geometrical properties of a cross-section and thus provides a useful technique to include material nonlinearity contributed by stainless steel. Equation 6.10 gives the general expression which relates ultimate moment capacity M_u of a cross-section to its generalised shape factor a_g.

$$M_u = a_g \, \sigma_{0.2} \, W_{el} \qquad (6.10)$$

Generalised shape factor a_g depends on the geometric shape factor of a cross-section a_p, the elastic strain at $\sigma_{0.2}$ of the material ε_0 (which is defined as $\varepsilon_0 = \sigma_{0.2}/E_0$) and the total strain at the outermost fibre of the cross-section given by the deformation capacity ε_{LB}. For a specific value of ε_{LB}, the generalised shape factor a_g may be expressed by Equation 6.11, as proposed by Gardner (2002), which expresses a_g as a function a_p and ε_0.

$$a_g = A_1 + A_2\, \varepsilon_0 + A_3\, a_p + A_4\, \varepsilon_0\, a_p \qquad (6.11)$$

These constants may be obtained by numerical integration of the proposed compound Ramberg-Osgood material model over the depth of the beam. To facilitate this, tables similar to those for local buckling stresses have been developed for determining a_g. Table 6.8 shows the table proposed for roll-formed sections produced from austenitic Grade 1.4301. Geometric shape factor constant tables for all the considered grades are given in Appendix B. Linear interpolation is believed to be adequate for any intermediate values of ε_{LB}.

Table 6.8: Generalised shape factor constants for roll-formed sections produced from austenitic Grade 1.4301.

ε_{LB}	A_1	A_2	A_3	A_4
0.0005	0.462	-105.54	0.132	-53.23
0.0010	0.392	-10.74	0.437	-167.51
0.0015	0.323	53.85	0.610	-212.45
0.0020	0.299	77.29	0.701	-215.86
0.0025	0.296	82.52	0.757	-205.44
0.0030	0.302	80.99	0.796	-191.94
0.0035	0.290	85.03	0.842	-185.09
0.0040	0.212	116.02	0.933	-199.52
0.0045	0.154	138.59	0.998	-205.70
0.0050	0.116	152.17	1.040	-204.24
0.0060	0.134	107.09	1.043	-147.72
0.0070	0.149	76.92	1.048	-111.56
0.0080	0.157	59.74	1.057	-90.03
0.0090	0.160	49.82	1.069	-76.65
0.0100	0.165	42.15	1.078	-66.40
0.0120	0.157	38.26	1.108	-57.46
0.0140	0.182	21.19	1.108	-39.61
0.0160	0.184	21.30	1.126	-37.37
0.0180	0.188	19.35	1.140	-33.75
0.0200	0.192	17.38	1.152	-30.61
0.0240	0.202	14.21	1.172	-25.76
0.0280	0.213	10.79	1.188	-21.32

Table 6.8 (contd.): Generalised shape factor constants for roll-formed sections produced from austenitic Grade 1.4301.

ε_{LB}	A_1	A_2	A_3	A_4
0.0320	0.219	10.39	1.206	-19.86
0.0360	0.228	9.31	1.220	-18.04
0.0400	0.237	7.19	1.231	-15.58
0.0500	0.249	8.39	1.265	-15.29
0.0600	0.267	6.26	1.287	-12.64
0.0700	0.282	4.75	1.309	-10.70
0.0800	0.291	5.35	1.331	-10.71
0.0900	0.305	4.13	1.348	-9.28
0.1000	0.315	4.39	1.365	-9.17
0.1500	0.364	2.27	1.434	-6.34
0.2000	0.396	5.18	1.496	-8.17

6.3.2 Significance of generalised shape factor a_g

Generalised shape factor a_g is believed to be an intelligent and efficient method for incorporating material nonlinearity. The absence of a well-defined yield point makes it inappropriate to use the traditional concept of using plastic modulus for stainless steel sections. Generalised shape factor uses an accurate material model and hence provides very accurate predictions for the bending resistance of cross-sections. Two typical cases for stocky and slender sections are explained herein to illustrate the added benefits of using a_g.

Stocky cross-sections, which deform well beyond the material elastic limit when stressed, are generally evaluated using the plastic section modulus W_{pl} instead of the elastic section modulus W_{el} to account for the added resistance due to plasticity. In the case of stainless steel, the outer fibre strain ε_{LB} often exceeds the strain corresponding to material $\sigma_{0.2}$ by a significant margin for such sections. In these cases considerable underpredictions will occur even if the plastic modulus of the cross-section W_{pl} is used since it does not consider the extra deformation and hence the additional resistance offered by stainless steel.

On the other hand for slender cross-sections, where local buckling occurs below $\sigma_{0.2}$, the geometric shape factor adopts a value of less than 1.0 and thus considers the 'loss of effectivess' for such sections without going into the traditional sectional classification, which requires a lengthy process of calculating of effective cross-sectional properties. Figure 6.14 explains these two cases.

Plastic vs actual bending stress distribution
for a stainless steel stocky cross-section

Elastic vs actual bending stress distribution
for a stainless steel slender cross-section
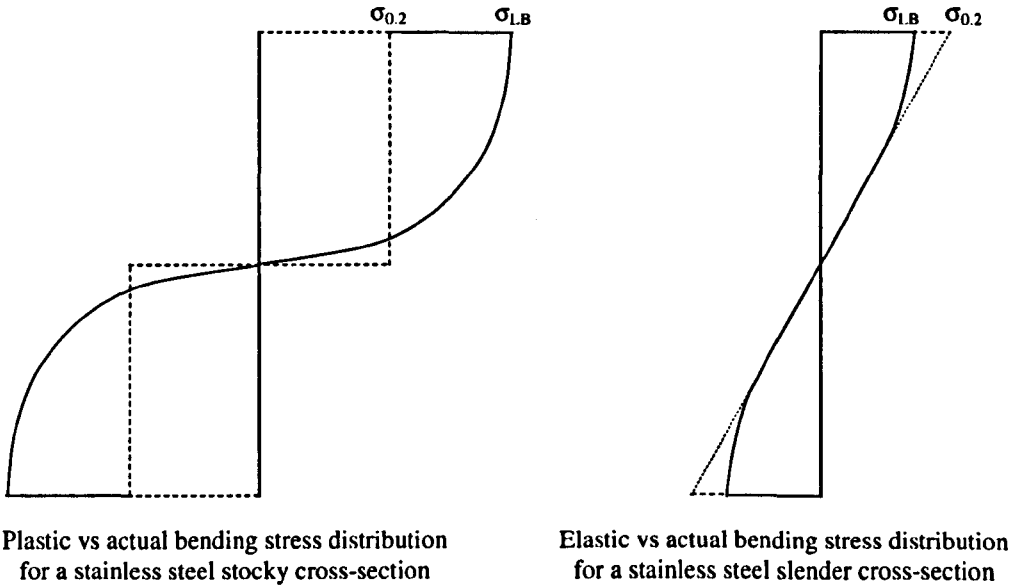
Figure 6.14: Typical bending stress distributions for stocky and slender sections showing the significance of generalised shape factor a_g.

In addition to the method proposed by Gardner (2002), a simpler approach will be discussed in the following section which will clearly show the importance of using the exact nonlinear shape of the bending stress distribution based on the compound Ramberg-Osgood model. It is worth mentioning that the method proposed in the present research includes the additional resistance offered by the cold-worked corner regions.

6.3.3 Proposed methods for bending resistance

6.3.3.1 Local buckling stress approach

This approach is very similar to that adopted for stub columns. It involves determination of ε_{LB} using the proposed design curve, Equation 6.8, and hence obtaining the local buckling stress for the cross-section using the appropriate table of Appendix A. The bending resistance of a cross-section is given by the following equation.

$$M_{c,Rd} = \phi_c \, \sigma_{LB} \, W_{el} \qquad (6.12)$$

where ϕ_c is the corner enhancement factor as explained in section 6.2.2.5. Equation 6.12 uses the material definition only to obtain σ_{LB} but considers a linear bending stress distribution neglecting the exact nonlinear behaviour.

6.3.3.2 Generalised shape factor approach

This approach has already been explained in section 6.3.1. However the steps involved in this technique for obtaining bending resistance are summarised below:

(i) Determine the cross-section slenderness β considering the most slender element.

(ii) Compute the local buckling strain ε_{LB} using the proposed design curve (Equation 6.8).

(iii) Determine the geometric shape factor a_p, obtain the coefficients using the appropriate table as given in Appendix B, and hence compute a_g using Equation 6.11.

(iv) Determine the elastic modulus W_{el} for the cross-section.

(v) If the cross-section contains any cold-worked corner, the appropriate correction factor ϕ_c needs to be incorporated using Equation 6.6 or 6.7 depending on the manufacturing process. For sections without cold-worked corners $\phi_c = 1.0$.

(vi) Bending resistance of a cross-section $M_{c.Rd}$ is given by Equation 6.13.

$$M_{c.Rd} = \phi_c \, a_g \, \sigma_{0.2} \, W_{el} \qquad\qquad (6.13)$$

6.3.4 Detailed comparisons against test results and analysis

Both the proposed methods have been used to determine the bending resistances for all available stainless steel cross-sections. A total of 36 stainless steel beam tests are obtainable from 6 different sources and involve SHS, RHS and I sections produced by welding, roll-forming and press-braking processes. The cross-sections were manufactured from 5 different grades of austenitic, ferritic and duplex categories. Moreover, different test arrangement were adopted such as 3 point bending with a moment gradient and 4 and 6 point bending tests with pure bending at the midspan. The cases considered cover almost all common variations. Table 6.9 compares the predictions for each of the individual test results, whilst Table 6.10 presents a summary of the performance of the proposed approaches. Figure 6.15 shows the bending resistance predictions using the proposed methods.

Table 6.9: Comparison of bending resistance predictions to test results.

Reference	Section type (Grade)	β_{flange}	β_{web}	ε_{LB}	σ_{LB} (N/mm²)	W_{el} (mm³)	ϕ_c	a_g	Test M_u (kNm)	$M_{c,Rd}$/Test M_u [using a_g]	$M_{c,Rd}$/Test M_u [using σ_{LB}]
Stangenberg (2000a)	I section (1.4301)	0.43	0.35	0.0920	439	130012	1.00	1.75	54.7	1.16	1.04
		0.85	0.34	0.0139	341	236959	1.00	1.33	89.5	0.98	0.90
		0.86	0.75	0.0134	340	559016	1.00	1.33	212.7	0.97	0.89
	(1.4462)	1.15	0.41	0.0118	598	246772	1.00	1.24	162.5	0.99	0.91
Mirambell and Real (2000)	I section (1.4306)	0.84	0.21	0.0267	514	74507	1.00	1.40	44.1	0.98	0.87
		0.84	0.21	0.0267	514	74507	1.00	1.40	46.5	0.93	0.82
Gardner (2002)	SHS (1.4301)	0.92	0.37	0.0165	538	25990	1.04	1.48	17.5	0.95	0.83
		2.25	0.92	0.0019	269	22730	1.01	0.78	8.0	0.83	0.77
		1.46	0.60	0.0046	398	33960	1.02	1.14	17.2	0.86	0.80
		1.17	0.48	0.0092	521	42860	1.03	1.33	24.5	1.06	0.94
		0.47	0.19	0.0823	539	76670	1.07	1.93	44.2	1.18	1.00
Mirambell and Real (2000)	SHS (1.4301)	1.30	0.53	0.0079	459	21277	1.03	1.32	13.5	0.84	0.74
		1.30	0.53	0.0079	459	21277	1.03	1.32	13.1	0.87	0.77
Talja and Salmi (1995)	SHS (1.4301)	0.57	0.24	0.0718	698	16200	1.06	1.79	15.0	0.94	0.80
		0.55	0.23	0.0786	708	16220	1.05	1.81	13.5	1.06	0.90
		0.57	0.24	0.0722	699	16140	1.05	1.79	15.2	0.92	0.78
Hyttinen (1994)	SHS (1.4301)	0.65	0.27	0.0446	645	1883	1.04	1.79	1.7	0.91	0.76
		0.85	0.35	0.0197	522	3553	1.03	1.56	2.8	0.81	0.69
		0.58	0.24	0.0679	762	15874	1.07	2.01	17.1	0.97	0.76

Table 6.9 (contd.): Comparison of bending resistance predictions to test results.

Reference	Section type (Grade)	β_{flange}	β_{web}	ε_{LB}	σ_{LB} (N/mm^2)	W_{el} (mm^3)	ϕ_c	a_g	Test M_u (kNm)	$M_{c,Rd}$/Test M_u [using a_g]	$M_{c,Rd}$/Test M_u [using σ_{LB}]
Hyttinen (1994)	SHS (1.4512)	0.69	0.28	0.0411	633	1881	1.04	1.56	1.2	1.21	0.99
		0.91	0.37	0.0185	551	3568	1.03	1.42	2.2	1.12	0.94
	SHS (1.4003)	0.68	0.28	0.0449	665	1956	1.04	1.53	1.5	1.08	0.88
		0.91	0.37	0.0198	599	3629	1.03	1.40	2.6	1.04	0.87
Rasmussen and Hancock (1993)	SHS (1.4306)	1.22	0.50	0.0087	497	21960	1.03	1.27	15.4	0.82	0.73
Gardner (2002)	RHS (1.4301)	0.47	0.30	0.1226	785	9927	1.05	2.09	10.5	0.98	0.78
		1.14	0.95	0.0083	437	13480	1.02	1.37	7.1	0.99	0.85
		0.78	0.66	0.0282	633	20530	1.03	1.66	15.4	1.04	0.87
		0.58	0.50	0.0593	680	24990	1.04	1.87	21.6	0.99	0.82
Mirambell and Real (2000)	RHS (1.4301)	1.04	0.65	0.0147	524	45873	1.03	1.51	31.9	0.92	0.78
		1.04	0.65	0.0147	524	45873	1.03	1.51	31.5	0.93	0.79
Talja and Salmi (1995)	RHS (1.4301)	1.29	0.80	0.0050	328	59750	1.05	1.21	26.3	0.88	0.78
		1.30	0.80	0.0050	328	59680	1.05	1.21	26.3	0.88	0.78
		1.29	0.80	0.0050	328	59750	1.05	1.21	26.3	0.88	0.78
		0.61	0.38	0.0347	471	109100	1.10	1.62	70.5	0.95	0.80
		0.61	0.38	0.0347	471	109100	1.10	1.62	70.4	0.95	0.80
		0.61	0.38	0.0348	471	109100	1.10	1.62	70.2	0.95	0.80

Table 6.10: Summary of the bending resistance predictions.

Cross-section type	Testing process	Grades	Control element	No. of beams	Equation 6.13 using a_g		Equation 6.12 using σ_{LB}	
					Mean	COV	Mean	COV
I section	4 point bending	1.4301, 1.4462	Flange	4	1.02	0.09	0.94	0.08
	3 point bending	1.4306	Flange	2	0.95	0.04	0.85	0.04
SHS	6 point bending	1.4301, 1.4512, 1.4003	Flange	7	1.02	0.13	0.84	0.13
	4 point bending	1.4306	Flange	1	0.82	-	0.73	-
	3 point bending	1.4301	Flange	10	0.95	0.12	0.83	0.10
RHS	3 point bending	1.4301	Flange	12	0.95	0.05	0.80	0.04
	All sections		Flange	36	0.97	0.10	0.83	0.10

(a) Predictions using generalised shape factor a_g (b) Predictions using local buckling stress σ_{LB}
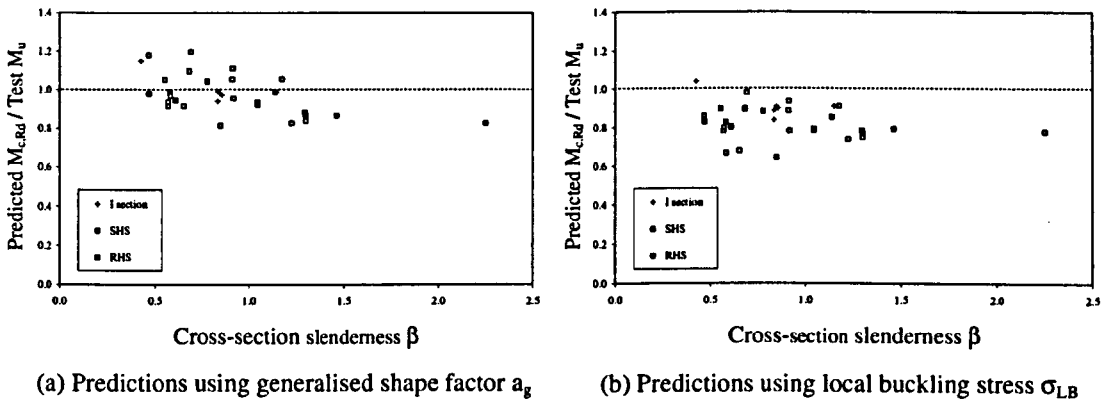
Figure 6.15: Predictions for the bending resistance using the proposed methods.

Table 6.10 clearly shows the importance of considering the nonlinear behaviour of the bending stress distribution, especially for the relatively stocky sections. Figure 6.16 compares the predictions of the proposed methods and gives an indication on how the effect of a_g varies with the cross-section slenderness β.
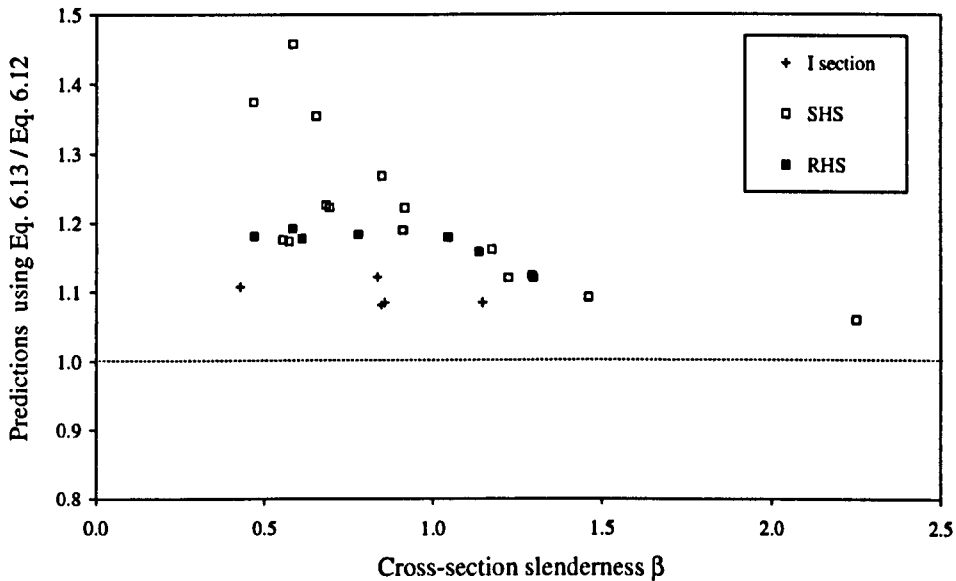
Figure 6.16: Variation of the effect of generalised shape factor a_g with cross-section slenderness β.

Appropriate use of generalised shape factors made the predictions very close to the test results - mean prediction for 36 beams is 0.97 with a COV of 0.10. This scatter is mostly contributed by the overpredictions for ferritic beams tested by Hyttinen (1994) for which compression coupon results were not available. The other significant overprediction for the I 160×80 beam tested by Stangenberg (2000a) is explained by comparing with the FE result in the following section.

One of the important points to note is that all available tested beams failed due to local buckling of the flange. This is believed to be the usual case for typical cross-sections used in bending. However to justify the general applicability of the proposed approach, FE models have been developed with very slender webs so that the bending resistance is limited by local buckling of the web. The obtained results and comparisons are described in the following section.

6.3.5 Investigation of local buckling of web in bending using FE models

Stangenberg's (2000a) reported 4 point bending tests have been modelled using ABAQUS as explained in Chapter 5. The FE results for these beams were very close to the tested capacities and hence formed the basis for undertaking parametric analysis to investigate the behaviour of relatively deep beams with slender webs.

The results of the FE models were compared against the test results in Table 5.14. They are now compared against both the test and the predicted resistances in Table 6.11.

Table 6.11: Performance of the FE models for I beams tested by Stangenberg (2000a).

Cross-section designation	Grade	β	Test M_u (kNm)	FE M_u (kNm)	$M_{c,Rd}$ (kNm)	$M_{c,Rd}$ / Test M_u	$M_{c,Rd}$ / FE M_u
$160 \times 80 \times 10 \times 6$	1.4301	0.44	54.7	70.2	62.8	1.15	0.95
$160 \times 160 \times 10 \times 6$	1.4301	0.88	89.5	91.7	87.6	0.98	0.96
$160 \times 160 \times 10 \times 6$	1.4462	1.15	162.5	164.3	160.1	0.99	0.97
$320 \times 160 \times 10 \times 6$	1.4301	0.90	212.7	209.6	206.8	0.97	0.99
All sections					**Mean**	**1.02**	**0.97**
					COV	**0.08**	**0.02**

The observed excellent agreement between the predicted $M_{c,Rd}$ and the FE results indicates that the test result for I 160×80 beam may have been understated since the reported load-deformation curve did not seem to reach its ultimate point.

In addition to the 5 beams reported in Chapter 5, two very slender sections have also been modelled and results for all 7 sections are reported herein. These additional sections were modelled using different material properties for web and flange to verify the proposed method for a more general case. The webs for I 100×40 and I 200×60 beams were modelled using $\sigma_{0.2}$ = 450 and 350 N/mm^2 respectively, whilst $\sigma_{0.2}$ = 300 N/mm^2 was used for the flanges.

Material properties considered for the other sections are given in Table 5.15. Table 6.12 compares the FE results for web bending with those obtained using the proposed method.

Table 6.12: Predictions for the beams where failure occurs due to local buckling of web.

Cross-section designation	β	FE M_u (kNm)	$M_{c,Rd}$ (kNm)	$M_{c,Rd}$ / FE M_u
I 160 × 80 × 10 × 4	0.53	64.3	58.6	0.91
I 240 × 80 × 9 × 6	0.57	97.6	97.8	1.00
I 160 × 160 × 16 × 3	0.64	140.7	149.6	1.06
I 200 × 70 × 5 × 3	0.97	32.0	32.8	1.02
I 180 × 60 × 4 × 2.2	1.20	18.4	18.7	1.02
I 100 × 40 × 1 × 3	1.79	4.8	4.5	0.93
I 200 × 60 × 1.5 × 3	2.19	13.2	11.5	0.87
All sections			**Mean**	**0.97**
			COV	**0.07**

The overall agreement for the beams failing due to local buckling of web is very accurate showing the applicability of the proposed method in such cases. Thus equation 6.13 is believed to be suitable to predict the bending resistance of stainless steel cross-sections when appropriate generalised shape factors are used to account for the extra deformation capacity offered by stainless steel.

6.3.6 Concluding remarks

Two different methods have been proposed for the prediction of bending resistance of stainless steel cross-sections and their performance have been compared against all available test results. The introduction of the concept of a generalised shape factor a_g has been observed to work well in exploiting the special feature of material nonlinearity quite accurately. FE models have been verified and later were used where test results have been scarce, especially, to investigate local buckling of web subjected to bending. The performance of the proposed method has been found to be excellent in this case and thus proves its general applicability.

6.4 CROSS-SECTION RESISTANCE AGAINST COMPRESSION PLUS BENDING

The combined action of compression and bending on a stainless steel cross-section may be evaluated based on the methods proposed for individual actions. Thus such a section should satisfy Equation 6.14.

$$\frac{N_{Ed}}{N_{c,Rd}} + \frac{M_{y,Ed}}{M_{y,c,Rd}} + \frac{M_{z,Ed}}{M_{z,c,Rd}} \leq 1 \qquad (6.14)$$

where, N_{Ed} is the applied axial compression

$M_{y,Ed}$ is the applied bending moment about the y-axis

$M_{z,Ed}$ is the applied bending moment about the z axis

$N_{c,Rd}$ is the compression resistance (= $\phi_c \sigma_{LB} A_g$), as given by Equation 6.9

$M_{y,c,Rd}$ is the bending resistance about y axis (= $a_{g,y} W_{el,y} \sigma_{0.2}$), as given by Equation 6.13

$M_{z,c,Rd}$ is the bending resistance about z axis (= $a_{g,z} W_{el,z} \sigma_{0.2}$), as given by Equation 6.13

Available test results on eccentrically loaded stub columns have been reported by Stangenberg (2000a). Two welded I section stub columns, produced from austenitic Grade 1.4301, were subjected to compression along the centreline of one of the flanges and thus combined action of compression and bending was investigated. The cross-sectional and material properties were the same as those for similar stub columns tested by Stangenberg (2000a), which have already been reported in Chapter 3. Hence only the basic parameters are reported and the obtained results are compared to the test values in Table 6.13.

Table 6.13: Predictions for I sections subjected to combined compression and bending.

Section designation	Compression resistance			Bending resistance			Test F_u (kN)	Pred F_u / Test F_u
	β	σ_{LB} (N/mm²)	$N_{c,Rd}$ (kN)	β	a_g	$M_{c,Rd}$ (kNm)		
I 160 × 80	0.83	344	847	0.41	1.76	64.1	503	0.85
I 160 × 160	0.85	341	1375	0.85	1.33	90.7	711	0.90

The comparisons given in Table 6.13 suggest that the proposed method can predict the combined actions on stainless steel cross-sections within acceptable limits. However, to justify its general applicability, more results on eccentric stub columns are required.

6.5 CONCLUSION

This chapter explains the development of a proposed design curve to obtain the deformation capacities of stainless steel cross-sections and hence proposes a method to obtain the cross-section resistances using the exact material behaviour based on a compound Ramberg-Osgood formulation. The predictions for both compression and bending resistances have been

compared with all available test results. The average prediction for 136 stub columns is 1.00 with a COV of 0.12, whereas for 36 beams the average is 0.97 with a COV of 0.10. Given the variability in testing procedures, specimens, grades and cross-sections, these variations may be considered acceptable. However, when the predictions for stub columns have been compared to FE results, which are believed to reduce experimental uncertainties to some extent, both the average and the COV improved giving values of 0.97 and 0.09 respectively. The performances of the proposed methods will be compared against the existing Eurocode prEN 1993-1-4 (2004) in Chapter 8.

The proposed methods make explicit recognition of the enhanced strength at the cold-worked corner regions within a cross-section, giving special emphasis to the manufacturing processes. In the case of bending the additional resistance arising due to the nonlinear bending stress distribution has been incorporated through the introduction of a generalised shape factor. Its effect has also been demonstrated showing its importance.

Accurate prediction of the extra deformation and the resulting strain hardening offered by stainless steel forms the basis of the proposed technique. The cross-section resistances for individual actions such as compression and bending have been accurately predicted and their combined action has also been demonstrated in this chapter. The following chapter investigates the behaviour of stainless steel members and proposes methods for obtaining member resistances exploiting the design curve proposed for determining cross-section resistances.

CHAPTER - SEVEN

DESIGN OF STAINLESS STEEL MEMBERS

7.1 INTRODUCTION

The nonlinear behaviour of stainless steel requires appropriate recognition when designing structural members so as to exploit its special features in a similar way as has already been done for cross-sections in Chapter 6. Introduction of the global effects makes the design procedure for members much more complex than those for cross-sections. This chapter investigates the behaviour of stainless steel columns subjected to both concentric and eccentric loading. All available test results have been used to examine the column behaviour and on the basis of which new sets of column curves are proposed that include effects of material nonlinearity and cold-working. The basic form of the proposed column curves has been retained as the Perry-Robertson format adopted in Eurocode 3. The obvious advantage of this format is the absence of iteration required with the tangent modulus method used by American and Australian codes. Appropriate imperfection factors have been proposed by analysing the flexural behaviour of stainless steel columns. Developed FE models have been used to investigate the uncertainties associated with tests and hence to verify the performance of the proposed methods.

The behaviour of stainless steel columns subjected to eccentric loads has been investigated so as to explore the interaction between axial load and bending moment. The existing interaction formulas given in prEN 1993-1-4 (2004) produce very conservative predictions in such cases. However the conservatism is significantly reduced when the resistances against individual actions such as compression, bending and flexural buckling are determined using the methods proposed in Chapters 6 and 7. Interaction coefficients have been observed to be a function of column slenderness and hence specific proposals have been made to obtain appropriate magnitudes for beam-column interaction coefficient instead of considering a constant value as in prEN 1993-1-4 (2004). Unavailability of test results for lateral torsional buckling prohibited the making of any proposals in such cases.

7.2 FLEXURAL BUCKLING OF STAINLESS STEEL COLUMNS

7.2.1 Background

Two different approaches – Tangent stiffness method and Perry-Robertson format – are generally adopted for obtaining the flexural buckling resistance of steel columns. The former approach is followed in American and Australian codes, which are based on the Euler formula proposed in 1744. In Europe, on the other hand, the latter approach which was originally proposed by Ayrton and Perry (1886) has been adopted. The tangent stiffness method involves a simple equation but the process is iterative, whereas Eurocode 3 approach uses a direct method involving separate curves for different cross-sections considering the differences in initial imperfections.

Gardner (2002) investigated the performance of the ENV 1993-1-4 (1996) column curves against the test results available at the time. The basic flexural strength was modified using appropriate factors of the ratio of local buckling stress and material 0.2% proof stress $\sigma_{LB}/\sigma_{0.2}$ and new sets of values for the imperfection factor α and the limiting slenderness ratio $\bar{\lambda}_0$ for hollow sections were proposed. The availability of more test results on different cross-sections has now made it possible to reinvestigate the column curves in a similar fashion to obtain rational explanations for the observed behaviour and hence to propose generalised column curves for stainless steel alloys. Two different sets of column curves with the same Perry type format have been proposed herein with a view to obtaining accurate predictions of flexural buckling resistance.

7.2.2 Eurocode 3 guidelines for flexural buckling

Column curves in Eurocode 3 are based on the Perry type format, both for carbon and for stainless steel, with different coefficients for different sections, although the basic formulation is the same. Following are the basic equations for obtaining the flexural buckling resistance of a stainless column (without the inclusion of partial safety factors).

$$N_{b,Rd} = \chi A_g \sigma_{0.2} \quad \text{for Class 1, 2 and 3 cross-sections} \tag{7.1}$$

$$N_{b,Rd} = \chi A_{eff} \sigma_{0.2} \quad \text{for Class 4 cross-sections} \tag{7.2}$$

where χ is the reduction factor for relevant buckling mode.

The appropriate value of χ for the corresponding non-dimensional member slenderness $\bar{\lambda}$ should be determined using the following relationships:

$$\chi = \frac{1}{\phi + \sqrt{\phi^2 - \bar{\lambda}^2}} \leq 1.0 \qquad (7.3)$$

with $\phi = 0.5\left[1 + \alpha\left(\bar{\lambda} - \bar{\lambda}_0\right) + \bar{\lambda}^2\right]$ $\qquad (7.4)$

where $\bar{\lambda} = \sqrt{\dfrac{A_g \sigma_{0.2}}{N_{cr}}}$ for Class 1, 2 and 3 cross-sections $\qquad (7.5)$

$\bar{\lambda} = \sqrt{\dfrac{A_{eff} \sigma_{0.2}}{N_{cr}}}$ for Class 4 cross-sections $\qquad (7.6)$

$$N_{cr} = \frac{\pi^2 EI}{L_e^2} \qquad (7.7)$$

α is an imperfection factor

$\bar{\lambda}_0$ is the limiting slenderness ratio

N_{cr} is the elastic critical buckling force for the relevant buckling mode based on the gross cross-sectional area A_g.

L_e is the effective length of the column about the relevant buckling axis.

Appropriate values for α and $\bar{\lambda}_0$ corresponding to a specific buckling curve should be obtained from Table 7.1, which is a reproduction of Table 5.2 of prEN 1993-1-4 (2004).

Table 7.1: Values of α and $\bar{\lambda}_0$ for flexural, torsional and torsional-flexural buckling.

Buckling mode	Type of member	α	$\bar{\lambda}_0$
Flexural	Cold-formed open sections	0.49	0.40
	Hollow sections (welded and seamless)	0.49	0.40
	Welded open sections (major axis)	0.49	0.20
	Welded open sections (minor axis)	0.76	0.20
Torsional and torsional-flexural	All members	0.34	0.20

7.2.3 Perry type curves using local buckling stress σ_{LB}

Local buckling stress σ_{LB} is the basic key parameter of the methods proposed in Chapter 6 to determine cross-section resistances. This parameter considers the effects of material nonlinearity as well as the effect of cold working and also takes appropriate account of the interaction among the constituent elements within a cross-section. Hence accurate predictions for cross-section resistances were achieved by using the local buckling stress σ_{LB} instead of material 0.2% proof stress $\sigma_{0.2}$. Efforts have been made herein to obtain column curves using σ_{LB} with appropriate reduction for global buckling.

7.2.3.1 Development of the design method

Keeping the same basic form as in Eurocode 3, the expressions for non-dimensional slenderness $\bar{\lambda}$ and flexural buckling strength $N_{b,Rd}$ have been modified to include the local buckling stress σ_{LB}. Hence no section classification is required as the loss of effectiveness for relatively slender cross-sections is accounted for by σ_{LB}. Apart from $N_{b,Rd}$ and $\bar{\lambda}$, expressions for all other parameters remain the same as in Eurocode 3. Equations 7.8 and 7.9 give the proposed expressions for $N_{b,Rd}$ and $\bar{\lambda}$.

$$N_{b,Rd} = \chi \phi_c A_g \sigma_{LB} \quad \text{for all cross-sections} \tag{7.8}$$

$$\bar{\lambda} = \sqrt{\frac{A_g \sigma_{LB}}{N_{cr}}} \tag{7.9}$$

where ϕ_c is the corner enhancement factor as explained in Section 6.2.2.5. A total of 97 long columns, listed in Tables 3.9 and 3.10, tested in 8 different laboratories with different cross-section types, material grades and end conditions representing all practical cases, have been considered in the present research. The proposals made herein have been developed based on these test results and the best fit column curves for different cross-sections have been proposed. Table 7.2 gives specific values for the imperfection factor α and the limiting slenderness ratio $\bar{\lambda}_0$, which were determined using regression analysis. Figures 7.1 to 7.3 compare the test results with the proposed column curves for different cross-sections.

Table 7.2: Values of α and $\bar{\lambda}_0$ for flexural buckling curves based on local buckling stress σ_{LB}.

Type of member	Buckling axis	α	$\bar{\lambda}_0$
Welded I sections	Minor	0.90	0.20
	Major	0.73	0.20
Square hollow sections SHS	-	0.75	0.35
Rectangular hollow sections RHS	All	0.55	0.40
Lipped channels	Minor	0.85	0.20
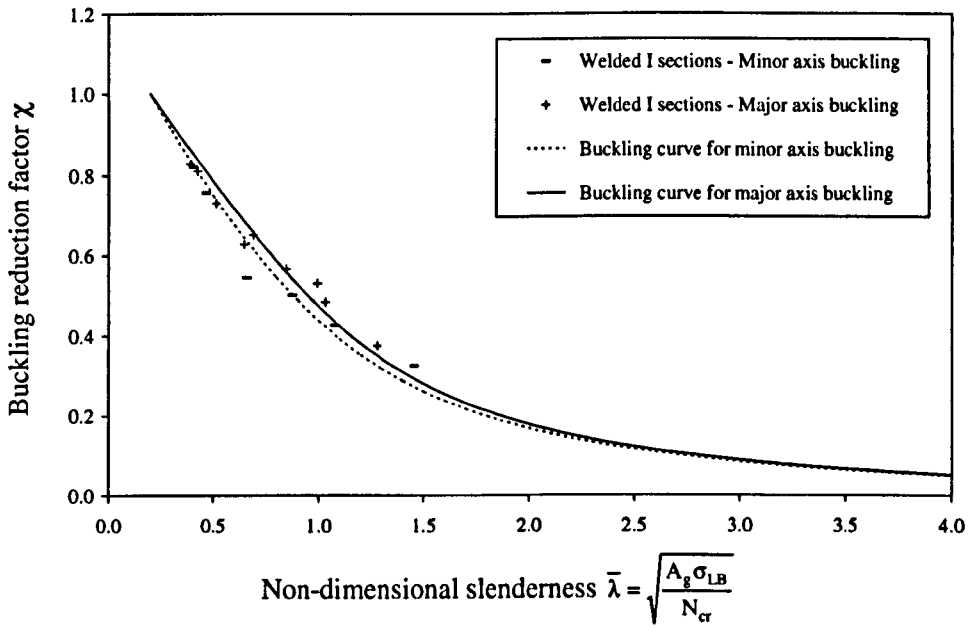
Figure 7.1: Proposed buckling curves for welded I sections based on local buckling stress σ_{LB}.
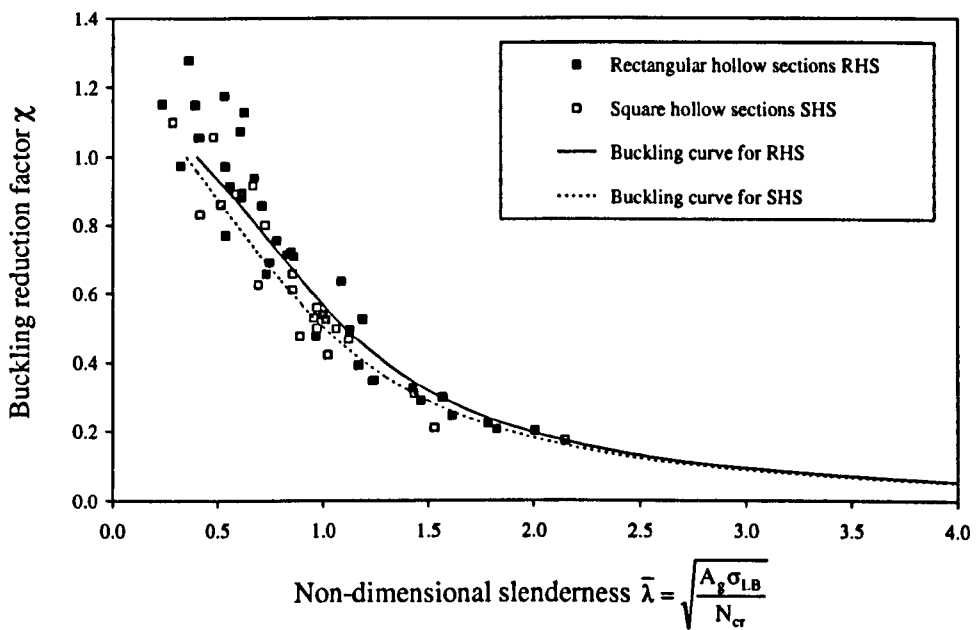
Figure 7.2: Proposed buckling curves for hollow sections based on local buckling stress σ_{LB}.
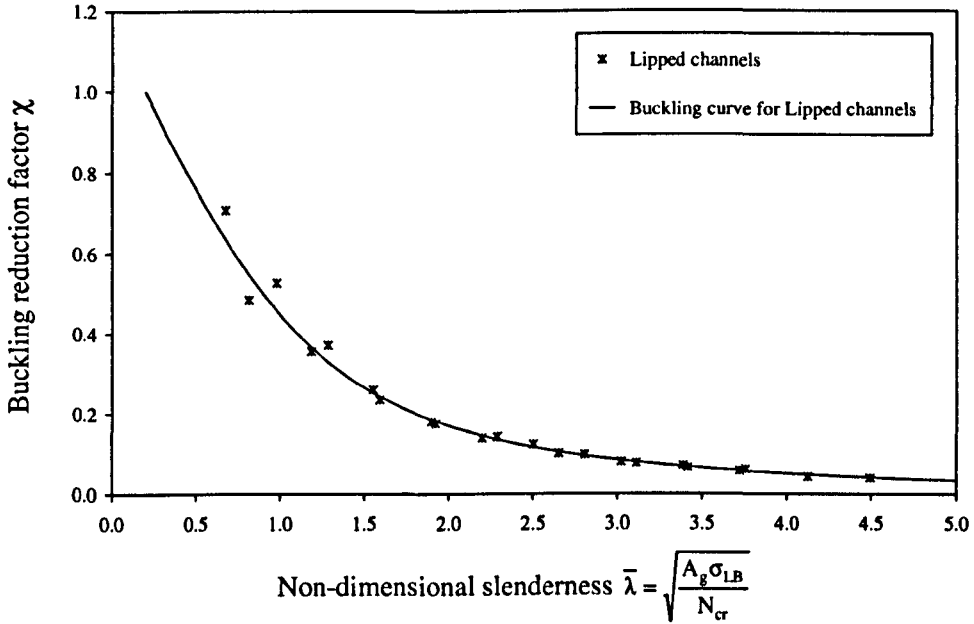
Figure 7.3: Proposed buckling curve for lipped channels based on local buckling stress σ_{LB}.

The buckling strengths of all these columns have been predicted using the proposed curves and the predictions are compared to test and FE results in Figures 7.4 and 7.5 respectively.
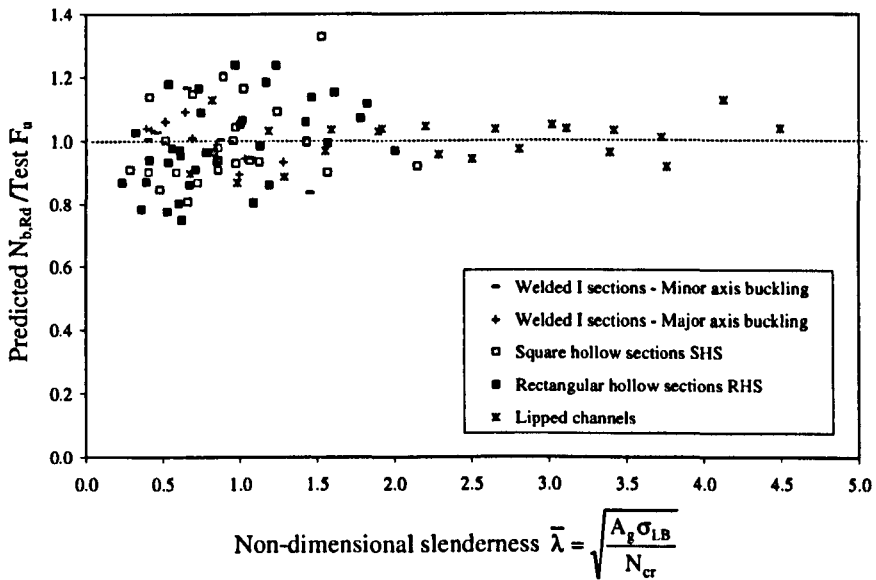
Figure 7.4: Comparison of the test results and predictions of the flexural buckling resistances for columns using the proposed curves based on local buckling stress σ_{LB}.

Legend:
- ▪ Welded I sections - Minor axis buckling
- + Welded I sections - Major axis buckling
- □ Square hollow sections SHS
- ■ Rectangular hollow sections RHS
- x Lipped channels

$$\text{Non-dimensional slenderness } \bar{\lambda} = \sqrt{\frac{A_g \sigma_{LB}}{N_{cr}}}$$
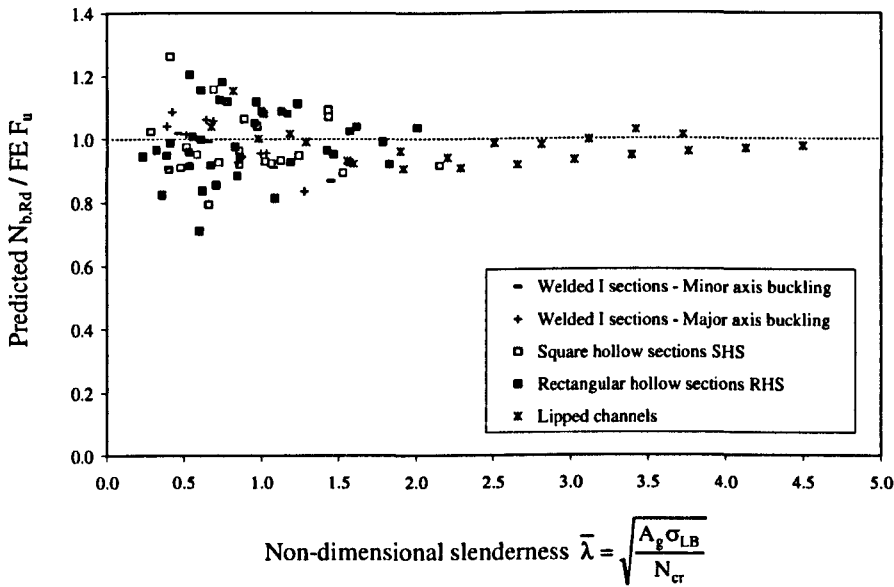
Figure 7.5: Comparison of the FE results and predictions of the flexural buckling resistances for columns using the proposed curves based on local buckling stress σ_{LB}.

7.2.3.2 Analysis of results

Figures 7.1 to 7.3 show that the proposed column curves roughly follow the trends taken by the test results although substantial deviation is observed for hollow sections in Figure 7.2. The flexural buckling resistances of the columns have been predicted using the proposed column curves. The average prediction was 99% of the test strength with a considerably high scatter of 11% as measured by the coefficient of variation (COV), which is quite obvious in Figure 7.4. Since the tests were obtained from a wide variety of sources, the possibility of some experimental errors cannot be ignored. To identify these uncertainties associated with testing, Figure 7.5 compares the predictions with the FE results which were validated in Chapter 5. This comparison provides better agreement with an average of 0.98 and a reduced COV of 0.10. The improvement in scatter is clear when Figure 7.4 is compared to Figure 7.5 although considerable amount of scatter is observed for columns with low slenderness ratio $\bar{\lambda}$. Hence the results indicate that local buckling stress σ_{LB}, although it can accurately predict cross-sectional resistances, may not be used directly when considering flexural buckling. In pure compression or bending the capacity of a cross-section is generally limited by the local buckling of the most slender element within a cross-section. Whereas, in the case of a column, the overall flexural buckling induces extra moments which makes this interaction more complex and the member resistance is not controlled only by the local buckling stress σ_{LB} of the cross-section. The predictions have been plotted against the cross-section slenderness β in Figure 7.6 to identify different aspects of flexural buckling.
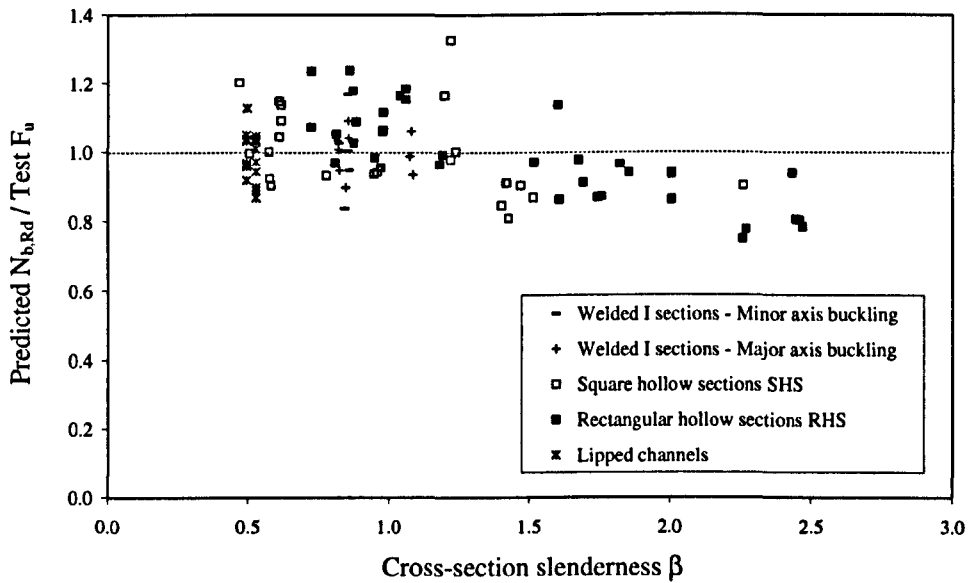
Figure 7.6: Variation in predictions for column buckling resistances using σ_{LB} with cross-section slenderness β.

From Figure 7.6 it is observed that for relatively slender cross-sections, for which $\sigma_{LB} \leq \sigma_{0.2}$, the predictions are generally below the test results; on the other hand, for stocky cross-sections, for which $\sigma_{LB} \geq \sigma_{0.2}$, the predictions are higher than the test results. This suggests σ_{LB}, which has successfully been used to predict cross-section resistances, requires some modifications for appropriate prediction of the flexural buckling.

For relatively stocky sections, direct use of σ_{LB}, which in such cases is always higher than $\sigma_{0.2}$, provides over predictions for column buckling resistance. The maximum column stress may reach σ_{LB}, because of the excessive lateral deformation, although the average stress will be lower. On the other hand, for slender cross-sections, for which σ_{LB} is less then $\sigma_{0.2}$, local buckling occurs in a very localized zone – ideally on the compressed face at mid-height. Despite this local failure, additional resistance may be achieved due to post-buckling strength. Also the existence of the cold-worked corners may provide further resistance, resulting in the column to fail at a stress higher than σ_{LB}.

Hence the concept of an 'effective buckling stress σ_{eff}', which includes corner enhancement factor ϕ_c, material 0.2% proof stress $\sigma_{0.2}$ and cross-section local buckling stress σ_{LB}, is proposed herein to make appropriate account of the flexural buckling.

7.2.4 Perry type curves using effective buckling stress σ_{eff}

7.2.4.1 Formulation of the proposed method

A new parameter, effective buckling stress σ_{eff}, is introduced herein to account for the effects of strain hardening in flexural buckling. Effective buckling stress considers following three parameters – the basic material strength $\sigma_{0.2}$, the element interactions at the cross-section level expressed by σ_{LB} and the effects of corner strength enhancement measured by ϕ_c. The effective buckling stress σ_{eff} is thus given by Equation 7.10.

$$\sigma_{eff} = \sqrt{\phi_c \sigma_{0.2} \sigma_{LB}} \qquad (7.10)$$

The definition of non-dimensional slenderness $\overline{\lambda}$ has also been changed accordingly and is given by Equation 7.11.

$$\overline{\lambda} = \sqrt{\frac{A_g \sigma_{eff}}{N_{cr}}} \qquad (7.11)$$

The flexural buckling resistance of a column is thus given by Equation 7.12.

$$N_{b,Rd} = \chi \, A_g \, \sigma_{eff} \qquad (7.12)$$

where χ is the buckling reduction factor which is to be determined from the buckling curves using σ_{eff}. However the expressions for χ and ϕ remain the same as given by Equations 7.3 and 7.4.

7.2.4.2 Development of column curves using effective buckling stress σ_{eff}

Regression analysis was carried out to obtain best-fit column buckling curves for different cross-sections as shown in Figures 7.7 to 7.9 using effective buckling stress σ_{eff}.

The values of imperfection factor α and limiting slenderness ratio $\overline{\lambda}_0$ used in the proposed column curve formulations are given in Table 7.3, in which the cross-section types have been generalised. The factors proposed for cold-formed open sections are based on lipped channel sections only and hence should be verified against other cross-sections when test results are available. The predictions have been compared against both the test and the FE results in Figures 7.10 and 7.11. Significant reduction in scatter is observed if these figures are compared with Figures 7.4 and 7.5, in which the column resistances were determined using

local buckling stress σ_{LB}. This comparison suggests that σ_{eff}, which considers both material and cross-section strength, may be used to represent the flexural behaviour of stainless steel columns.
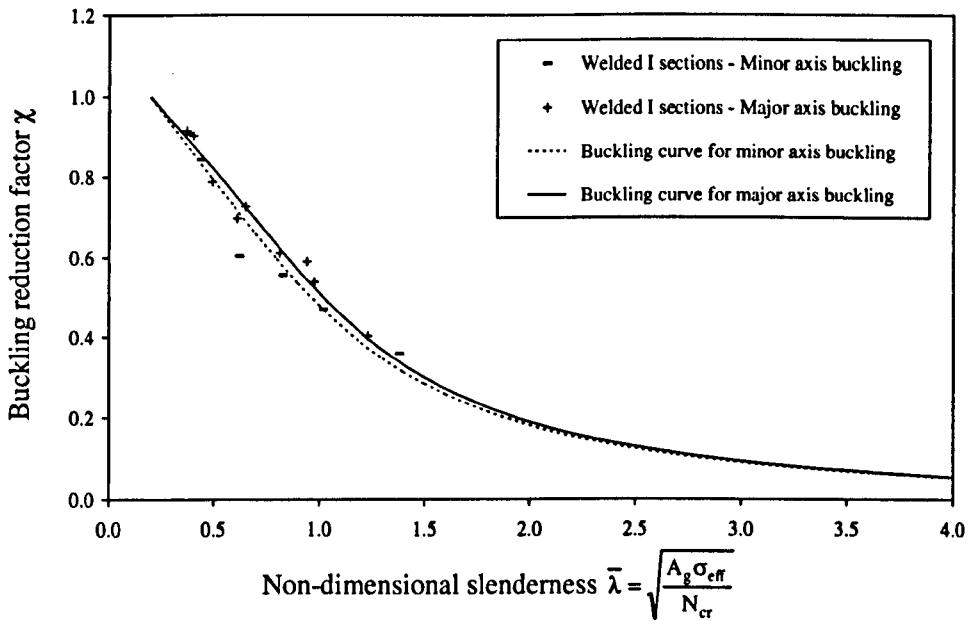
Figure 7.7: Proposed buckling curves for welded I sections based on effective buckling stress σ_{eff}.
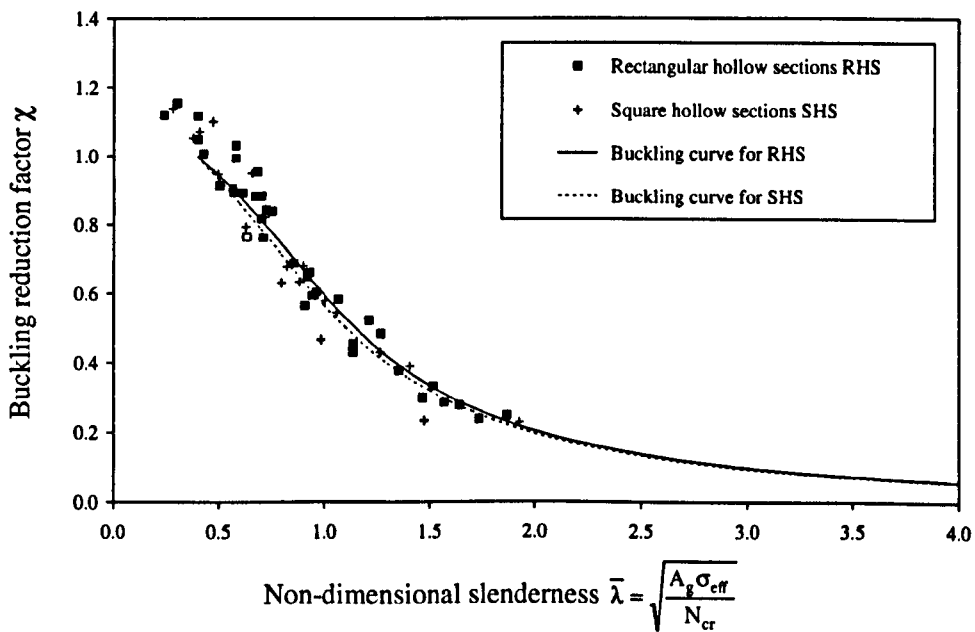
Figure 7.8: Proposed buckling curves for hollow sections based on effective buckling stress σ_{eff}.

$$\text{Non-dimensional slenderness } \bar{\lambda} = \sqrt{\frac{A_g \sigma_{eff}}{N_{cr}}}$$
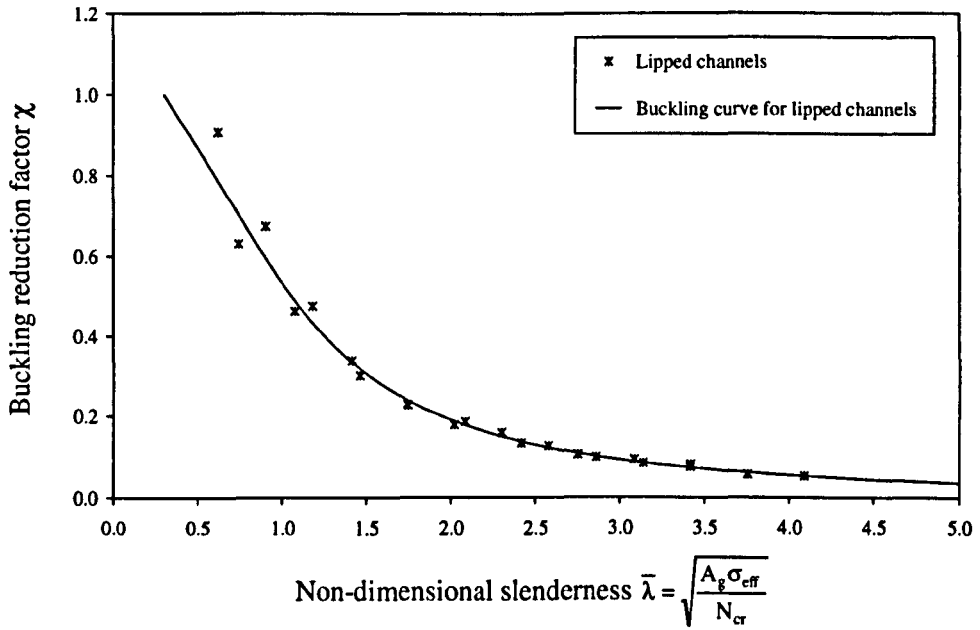
Figure 7.9: Proposed buckling curves for lipped channels based on effective buckling stress σ_{eff}.

Table 7.3: Values of α and $\bar{\lambda}_0$ for flexural buckling curves based on effective buckling stress σ_{eff}.

Type of member	Buckling axis	α	$\bar{\lambda}_0$
Welded I sections	Minor	0.70	0.20
	Major	0.58	0.20
Square hollow sections SHS	-	0.55	0.40
Rectangular hollow sections RHS	All	0.45	0.40
Cold-formed open sections	All	0.58	0.30

Figure 7.10: Comparison of the test results and predictions of the column flexural buckling resistances using the proposed curves based on effective buckling stress σ_{eff}.
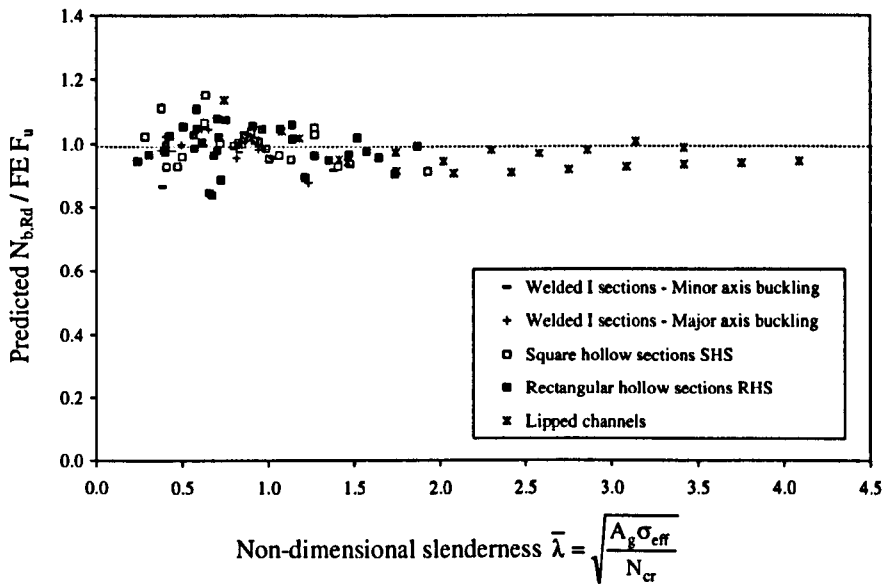
Figure 7.11: Comparison of the FE results and predictions of the column flexural buckling resistances using the proposed curves based on effective buckling stress σ_{eff}.

7.2.5 Detailed comparisons

The flexural buckling resistances of all 97 columns considered in the present research have been determined using the proposed methods and are compared against the test and the corresponding FE results in Table 7.4. These comparisons are summarised in Tables 7.5 and 7.6.

Table 7.4: Predictions for the flexural buckling resistances of stainless steel columns using the proposed methods.

Reference [Buckling axis]	Cross-section	A_g mm^2	$\sigma_{0.2}$ (N/mm^2)	E_0 (N/mm^2)	β	ϕ_c	Buckling resistance using σ_{LB}				Buckling resistance using σ_{eff}			
							σ_{LB} (N/mm^2)	$\bar{\lambda}$	$N_{b,Rd}$ / Test F_u	$N_{b,Rd}$ / FE F_u	σ_{eff} (N/mm^2)	$\bar{\lambda}$	$N_{b,Rd}$ / Test F_u	$N_{b,Rd}$ / FE F_u
Satngenberg (2000b) Minor axis	I 160×80×10×6	2397	279	200000	0.82	1.00	344	0.46	1.03	1.02	310	0.44	0.99	0.98
	I 160×80×10×6	2445	279	200000	0.85	1.00	341	0.87	1.00	0.94	308	0.83	1.04	0.98
	I 160×80×10×6	2424	279	200000	0.84	1.00	341	1.45	0.84	0.87	308	1.38	0.89	0.92
	I 160×160×10×6	3965	281	200000	0.85	1.00	343	0.40	1.00	0.91	310	0.38	0.96	0.86
	I 160×160×10×6	3990	280	199000	0.86	1.00	341	0.66	1.17	0.99	309	0.63	1.17	1.00
	I 160×160×10×6	3981	281	200000	0.86	1.00	342	1.08	0.95	0.91	310	1.02	1.00	0.96
Satngenberg (2000b) Major axis	I 160×80×10×6	2381	279	200000	0.82	1.00	344	0.42	1.03	1.09	310	0.40	0.97	1.02
	I 160×80×10×6	2374	279	200000	0.82	1.00	344	0.69	1.01	1.06	310	0.65	1.00	1.04
	I 160×80×10×6	2403	279	200000	0.83	1.00	343	1.03	0.95	0.96	309	0.97	0.97	0.98
	I 160×160×10×6	3999	279	198000	0.86	1.00	340	0.39	1.04	1.04	308	0.37	0.98	0.98
	I 160×160×10×6	3996	279	198000	0.85	1.00	340	0.65	1.09	1.06	308	0.61	1.07	1.04
	I 160×160×10×6	3981	279	199000	0.85	1.00	341	0.99	0.90	0.95	308	0.94	0.92	0.98
	I 160×160×10×7	4350	523	201000	1.08	1.00	604	0.51	1.06	1.01	562	0.49	1.04	1.00
	I 160×160×10×7	4335	523	201000	1.08	1.00	604	0.84	0.99	0.93	562	0.81	1.02	0.95
	I 160×160×10×7	4360	523	201000	1.09	1.00	603	1.28	0.93	0.83	561	1.23	0.98	0.88
Rasmussen and Hancock (1993)	SHS 80×80×3	900	415	194000	1.24	1.03	467	0.52	1.00	0.97	447	0.49	0.97	0.94
	SHS 80×80×3	900	415	194000	1.20	1.03	470	1.02	1.17	0.93	448	0.97	1.22	0.98
	SHS 80×80×3	900	415	194000	1.22	1.03	468	1.53	1.33	0.89	447	1.46	1.40	0.94

Table 7.4(contd.): Predictions for the flexural buckling resistances of stainless steel columns using the proposed methods.

Reference [Buckling axis]	Cross-section	A_g mm²	$\sigma_{0.2}$ (N/mm²)	E_0 (N/mm²)	β	ϕ_c	Buckling resistance using σ_{LB}				Buckling resistance using σ_{eff}			
							σ_{LB} (N/mm²)	$\bar{\lambda}$	$N_{b,Rd}$/ Test F_u	$N_{b,Rd}$/ FE F_u	σ_{eff} (N/mm²)	$\bar{\lambda}$	$N_{b,Rd}$/ Test F_u	$N_{b,Rd}$/ FE F_u
Talja and Salmi (1995)	SHS 60×60×5	999	463	185500	0.58	1.05	737	0.96	1.00	1.05	599	0.86	0.96	1.01
	SHS 60×60×5	999	463	181000	0.58	1.05	736	1.57	0.90	0.93	599	1.40	0.90	0.93
	SHS 60×60×5	999	463	184000	0.58	1.05	737	2.15	0.92	0.92	599	1.92	0.92	0.91
Ala-outinen (1997)	SHS 40×40×4	519	592	197980	0.51	1.09	1049	1.43	1.00	1.07	822	1.27	0.96	1.03
	SHS 40×40×4	519	592	197980	0.51	1.09	1049	1.43	1.00	1.09	822	1.27	0.96	1.05
Gardner (2002)	SHS 80×80×4	1093	416	186600	0.96	1.04	536	1.06	0.94	0.92	482	1.00	0.97	0.95
	SHS 80×80×4	1106	416	186600	0.95	1.04	538	1.12	0.94	0.93	483	1.06	0.97	0.96
	SHS 100×100×2	723	370	201300	2.26	1.01	269	0.59	0.90	0.95	317	0.63	1.09	1.15
	SHS 100×100×3	1089	379	195800	1.51	1.02	395	0.72	0.87	0.93	390	0.72	0.94	1.00
	SHS 100×100×4	1410	437	191300	1.22	1.03	518	0.85	0.98	0.96	484	0.82	1.02	1.00
	SHS 100×100×6	2145	473	198400	0.78	1.05	662	0.97	0.93	1.04	573	0.90	0.93	1.04
	SHS 100×100×8	2778	330	202400	0.47	1.07	538	0.89	1.20	1.06	436	0.80	1.12	0.99
	SHS 150×150×4	2159	294	206000	1.47	1.03	296	0.41	0.90	0.90	299	0.41	0.93	0.93
Liu and Young (2003)	SHS 70×70×2	513	313	195000	1.42	1.02	330	0.28	0.91	1.02	325	0.28	0.91	1.02
	SHS 70×70×2	522	313	195000	1.40	1.02	334	0.48	0.85	0.91	327	0.47	0.86	0.93
	SHS 70×70×2	515	313	195000	1.43	1.02	330	0.66	0.81	0.79	325	0.66	0.86	0.85
	SHS 70×70×2	516	313	195000	1.42	1.02	332	0.85	0.91	0.92	326	0.85	0.99	1.00
	SHS 70×70×5	1212	413	194000	0.62	1.05	623	0.41	1.14	1.26	520	0.38	1.05	1.11
	SHS 70×70×5	1223	413	194000	0.61	1.05	626	0.69	1.15	1.16	522	0.63	1.05	1.06
	SHS 70×70×5	1222	413	194000	0.61	1.05	626	0.97	1.04	1.04	522	0.88	1.02	1.02
	SHS 70×70×5	1212	413	194000	0.62	1.05	623	1.24	1.09	0.95	520	1.13	1.09	0.95

Table 7.4 (contd.): Predictions for the flexural buckling resistances of stainless steel columns using the proposed methods.

Reference [Buckling axis]	Cross-section	A_g mm^2	$\sigma_{0.2}$ (N/mm^2)	E_0 (N/mm^2)	β	ϕ_c	Buckling resistance using σ_{LB}				Buckling resistance using σ_{eff}			
							σ_{LB} (N/mm^2)	$\bar{\lambda}$	$N_{b,Rd}$ / Test F_u	$N_{b,Rd}$ / FE F_u	σ_{eff} (N/mm^2)	$\bar{\lambda}$	$N_{b,Rd}$ / Test F_u	$N_{b,Rd}$ / FE F_u
Talja and Salmi (1995) [Major]	RHS 150×100×3	1394	305	197200	2.01	1.05	252	0.53	0.93	0.91	284	0.58	1.02	1.00
	RHS 150×100×3	1394	305	197200	2.01	1.05	252	0.86	0.94	0.94	284	0.93	1.01	1.02
	RHS 150×100×3	1394	305	197200	2.01	1.05	252	1.19	0.86	0.93	284	1.28	0.90	0.97
	RHS 150×100×6	2708	345	193600	1.04	1.10	406	0.73	1.16	1.12	393	0.70	1.04	1.01
	RHS 150×100×6	2678	345	193600	1.06	1.10	404	1.17	1.18	1.08	392	1.13	1.11	1.01
	RHS 150×100×6	2678	345	193600	1.06	1.10	404	1.61	1.15	1.04	392	1.56	1.08	0.97
Gardner [Major]	RHS 60×40×4	675	469	192800	0.72	1.05	677	1.78	1.07	0.99	579	1.64	1.03	0.96
	RHS 100×50×2	524	370	208000	2.26	1.02	259	0.62	0.75	0.84	313	0.68	0.86	0.96
Gardner (2002) [Minor]	RHS 100×50×3	807	455	203600	1.60	1.03	465	1.47	1.14	0.95	467	1.47	1.16	0.97
	RHS 100×50×4	1018	439	208000	1.19	1.04	519	1.57	0.99	1.02	487	1.51	0.99	1.02
	RHS 100×50×6	1559	494	187200	0.81	1.07	691	2.01	0.97	1.04	603	1.86	0.93	0.99
	RHS 120×80×3	1101	429	209300	1.82	1.03	384	0.83	0.97	0.97	412	0.86	1.02	1.03
	RHS 120×80×6	2115	466	194500	0.95	1.06	607	1.13	0.98	1.09	546	1.07	0.94	1.05
	RHS 150×100×4	1787	319	205800	1.52	1.03	317	0.61	0.97	1.00	323	0.62	0.98	1.01
	RHS 60×40×4	673	469	192800	0.72	1.05	677	1.23	1.24	1.11	579	1.13	1.18	1.06
	RHS 100×50×2	522	370	208000	2.27	1.02	259	0.53	0.78	0.96	313	0.58	0.90	1.11
	RHS 100×50×3	804	455	203600	1.61	1.03	465	0.67	0.86	0.92	467	0.74	0.98	1.04
	RHS 100×50×4	1028	439	208000	1.18	1.04	521	0.78	0.96	1.12	488	0.75	0.93	1.07
	RHS 100×50×6	1555	494	187200	0.81	1.07	690	1.00	1.05	1.09	603	0.93	0.97	1.01
	RHS 120×80×3	1083	429	209300	1.85	1.03	379	0.41	0.94	0.99	410	0.43	0.98	1.02

Table 7.4 (contd.): Predictions for the flexural buckling resistances of stainless steel columns using the proposed methods.

Reference [Buckling axis]	Cross-section	A_g mm²	$\sigma_{0.2}$ (N/mm²)	E_0 (N/mm²)	β	ϕ_c	Buckling resistance using σ_{LB}				Buckling resistance using σ_{eff}			
							σ_{LB} (N/mm²)	$\bar{\lambda}$	$N_{b,Rd}/$ Test F_u	$N_{b,Rd}/$ FE F_u	σ_{eff} (N/mm²)	$\bar{\lambda}$	$N_{b,Rd}/$ Test F_u	$N_{b,Rd}/$ FE F_u
	RHS120×40×2	593	326	198000	2.47	1.03	214	0.36	0.78	0.82	267	0.40	0.95	1.00
	RHS 120×40×2	596	326	198000	2.46	1.03	214	0.60	0.80	0.71	267	0.67	0.94	0.84
	RHS 120×40×2	602	326	198000	2.43	1.03	214	0.85	0.94	0.88	267	0.94	1.07	1.01
	RHS 120×40×2	599	326	198000	2.45	1.03	214	1.09	0.80	0.81	267	1.21	0.88	0.89
	RHS 120×40×5.3	1524	394	194000	0.97	1.04	500	0.61	0.95	1.15	454	0.58	0.86	1.04
	RHS 120×40×5.3	1516	394	194000	0.98	1.04	499	1.01	1.06	1.08	453	0.96	1.03	1.04
Young	RHS 120×40×5.3	1521	394	194000	0.98	1.04	499	1.42	1.06	0.96	453	1.35	1.04	0.95
and Liu	RHS 120×40×5.3	1516	394	194000	0.98	1.04	499	1.82	1.12	0.92	453	1.73	1.10	0.91
(2003)	RHS 120×80×3	1071	340	193000	1.74	1.03	313	0.23	0.87	0.94	331	0.24	0.87	0.94
[Minor]	RHS 120×80×3	1063	340	193000	1.76	1.03	313	0.39	0.87	0.95	331	0.40	0.89	0.97
	RHS 120×80×3	1103	340	193000	1.68	1.03	324	0.56	0.98	1.01	337	0.57	1.00	1.03
	RHS 120×80×3	1099	340	193000	1.69	1.03	320	0.71	0.91	0.85	335	0.72	0.94	0.89
	RHS 120×80×6	2165	412	194000	0.87	1.05	545	0.32	1.03	0.96	486	0.30	1.02	0.96
	RHS 120×80×6	2171	412	194000	0.87	1.05	546	0.54	1.18	1.21	487	0.50	1.03	1.05
	RHS 120×80×6	2156	412	194000	0.88	1.05	544	0.75	1.09	1.18	486	0.70	0.99	1.08
	RHS 120×80×6	2203	412	194000	0.86	1.05	549	0.97	1.24	1.12	488	0.91	1.17	1.05

Table 7.4 (contd.): Predictions for the flexural buckling resistances of stainless steel columns using the proposed methods.

Reference [Buckling axis]	Cross-section	A_g mm²	$\sigma_{0.2}$ (N/mm²)	E_0 (N/mm²)	β	ϕ_c	Buckling resistance using σ_{LB}				Buckling resistance using σ_{eff}			
							σ_{LB} (N/mm²)	$\bar{\lambda}$	$N_{b,Rd}$/ Test F_u	$N_{b,Rd}$/ FE F_u	σ_{eff} (N/mm²)	$\bar{\lambda}$	$N_{b,Rd}$/ Test F_u	$N_{b,Rd}$/ FE F_u
Rhodes et al (2000) [Minor]	CL 28×15×8×2.5	143.27	446	200000	0.50	1.08	704	4.49	1.04	0.98	582	4.09	1.00	0.94
	CL 28×15×8×2.5	143.27	446	200000	0.50	1.08	704	4.13	1.13	0.97	582	3.76	1.09	0.94
	CL 28×15×8×2.5	143.27	446	200000	0.50	1.08	704	3.76	0.92	0.96	582	3.42	0.89	0.93
	CL 28×15×8×2.5	143.27	446	200000	0.50	1.08	704	3.39	0.96	0.95	582	3.09	0.94	0.93
	CL 28×15×8×2.5	143.27	446	200000	0.50	1.08	704	3.02	1.05	0.93	582	2.75	1.03	0.92
	CL 28×15×8×2.5	143.27	446	200000	0.50	1.08	704	2.66	1.04	0.92	582	2.42	1.03	0.91
	CL 28×15×8×2.5	143.27	446	200000	0.50	1.08	704	2.29	0.96	0.91	582	2.08	0.96	0.91
	CL 28×15×8×2.5	143.27	446	200000	0.50	1.08	704	1.92	1.04	0.90	582	1.75	1.05	0.91
	CL 28×15×8×2.5	143.27	446	200000	0.50	1.08	704	1.55	0.97	0.93	582	1.41	0.99	0.95
	CL 28×15×8×2.5	143.27	446	200000	0.50	1.08	704	1.18	1.03	1.02	582	1.08	1.05	1.04
	CL 28×15×8×2.5	143.27	446	200000	0.50	1.08	704	0.82	1.13	1.15	582	0.74	1.12	1.14
	CL 38×17×10×3	228.65	428	200000	0.53	1.08	652	3.72	1.01	1.01	549	3.42	0.98	0.99
	CL 38×17×10×3	228.65	428	200000	0.53	1.08	652	3.42	1.03	1.03	549	3.14	1.01	1.01
	CL 38×17×10×3	228.65	428	200000	0.53	1.08	652	3.11	1.04	1.00	549	2.86	1.02	0.98
	CL 38×17×10×3	228.65	428	200000	0.53	1.08	652	2.81	0.97	0.98	549	2.58	0.96	0.97
	CL 38×17×10×3	228.65	428	200000	0.53	1.08	652	2.50	0.94	0.99	549	2.30	0.94	0.98
	CL 38×17×10×3	228.65	428	200000	0.53	1.08	652	2.20	1.05	0.94	549	2.02	1.05	0.94
	CL 38×17×10×3	228.65	428	200000	0.53	1.08	652	1.90	1.03	0.96	549	1.74	1.04	0.97
	CL 38×17×10×3	228.65	428	200000	0.53	1.08	652	1.59	1.03	0.92	549	1.46	1.06	0.94
	CL 38×17×10×3	228.65	428	200000	0.53	1.08	652	1.29	0.89	0.99	549	1.18	0.91	1.02
	CL 38×17×10×3	228.65	428	200000	0.53	1.08	652	0.98	0.87	1.00	549	0.90	0.88	1.02
	CL 38×17×10×3	228.65	428	200000	0.53	1.08	652	0.68	0.90	1.04	549	0.62	0.87	1.00

Table 7.5: Summary of comparisons with test results for flexural buckling resistance.

Cross-section type	Buckling axis	No. of columns	Predictions using σ_{LB}		Predictions using σ_{eff}	
			Mean	COV	Mean	COV
I section	Minor	6	1.00	0.11	1.01	0.10
	Major	9	1.00	0.06	1.00	0.04
SHS	-	24	0.99	0.13	1.00	0.12
RHS	Minor	28	0.98	0.13	0.99	0.09
	Major	8	1.01	0.16	1.01	0.08
Lipped C	Minor	22	1.00	0.07	1.00	0.07
All sections	**-**	**97**	**0.99**	**0.11**	**1.00**	**0.09**

Table 7.6: Summary of comparisons with FE results for flexural buckling resistance.

Cross-section type	Buckling axis	No. of columns	Predictions using σ_{LB}		Predictions using σ_{eff}	
			Mean	COV	Mean	COV
I section	Minor	6	0.94	0.06	0.95	0.05
	Major	9	0.99	0.08	0.99	0.05
SHS	-	24	0.98	0.10	0.99	0.07
RHS	Minor	28	0.99	0.12	1.00	0.06
	Major	8	0.98	0.10	0.99	0.02
Lipped C	Minor	22	0.98	0.06	0.97	0.06
All sections	**-**	**97**	**0.98**	**0.09**	**0.99**	**0.06**

The comparisons clearly show that the proposed method using the effective buckling stress σ_{eff} is able to predict the flexural buckling resistances of stainless steel columns quite accurately. The overall performance of the proposed method has been compared against the existing Eurocode prEN 1993-1-4 (2004) in Chapter 8.

7.2.6 Concluding remarks

Two different sets of column curves have been proposed herein by analysing all available tests on stainless steel columns. Instead of using the traditional 0.2% proof stress of the flat material the proposed techniques use different key parameters – local buckling stress σ_{LB} and effective buckling stress σ_{eff} - yet retain the Perry-Robertson formulation. The performance of these methods has been verified against considered test results. The first technique, which uses σ_{LB}, produces a mean of 0.99 with a COV of 0.11, whilst the second method using σ_{eff} provides more accurate predictions with a mean and a COV of 1.00 and 0.09 respectively.

The extent of experimental uncertainties was investigated by comparing the predictions with the developed FE models, which produced significantly better agreement by reducing the overall COV from 0.09 to 0.06. Once the proposed methods are validated for all practical cases, they should perform well in determining the flexural buckling resistance of stainless steel columns and thus could turn into a useful practical design tool.

7.3 BEAM-COLUMN INTERACTIONS IN STAINLESS STEEL

7.3.1 Introduction

The combined action of axial load and bending moment is the most general type of loading applied to structures. All available test results have been used to investigate the performance of the existing Eurocode prEN 1993-1-4 (2004) that has been observed to provide inconsistent results, mostly because of under-prediction of the cross-sectional resistances but also because of using a fixed value for the beam-column interaction factor κ (Greiner et al 2005). The design methods proposed in Chapter 6 produce accurate predictions for the cross-sectional resistances and hence the initial notion was to determine the individual resistances using the proposed method retaining the basic formulations. This technique produced better predictions, although the scatter was relatively high. This observation leads to the proposed formulations to determine the appropriate values for κ which has been expressed as a function of the non-dimensional member slenderness $\overline{\lambda}$.

7.3.2 Eurocode guidelines on beam-column interaction

To determine the resistance of stainless steel members subjected to combined compression and bending, Gardner (2002) used the provisions given in ENV 1993-1-3 (1996) as directed by ENV 1993-1-4 (1996). When the individual resistances were determined using the methods proposed by Gardner (2002) for hollow sections, the adopted formulations produced reasonably accurate predictions for the available SHS and RHS beam-column test results (Talja and Salmi, 1995). The latest version of Eurocode for stainless steel prEN 1993-1-4 (2004) simplified the interaction equations by adopting a constant value of 1.5 for the interaction factor κ. This simplification is, however, noted by Greiner et al (2005) who stated that this may lead to very conservative predictions for small slenderness and, on the other hand, non-conservative results for high slenderness since interaction factors are generally dependent on the column slenderness.

In the present research, the guidelines proposed in both ENV 1993-1-4 (1996) and prEN 1993-1-4 (2004) were compared with the test results. As mentioned earlier the former approach uses empirical relationships to obtain the interaction factor κ, which in most of the cases is governed by the specified maximum limit of 1.5. prEN 1993-1-4 (2004) states that all stainless steel members subjected to axial compression and biaxial bending should satisfy Equation 7.13.

$$\frac{N_{Ed}}{(N_{b,Rd})_{min}} + \frac{1.5M_{y,Ed} + N_{Ed}e_{Ny}}{\beta_{w,y}W_{pl,y}f_y} + \frac{1.5M_{z,Ed} + N_{Ed}e_{Nz}}{\beta_{w,z}W_{pl,z}f_y} \leq 1 \qquad (7.13)$$

where N_{Ed}, $M_{y,Ed}$ and $M_{z,Ed}$ are the design values of the compression force and the maximum moments about the y-y and z-z axis along the member, respectively

$(N_{b,Rd})_{min}$ is the smallest value of $N_{b,Rd}$ for the following four buckling modes: flexural buckling about the y axis, flexural buckling about the z axis, torsional buckling and torsional-flexural buckling

e_{Ny} and e_{Nz} are the shifts in the neutral axes when the cross-section is subjected to uniform compression.

$\beta_{w,y}$ and $\beta_{w,z}$ are the values of β_w determined for the y and z axes respectively in which

$\beta_w = 1$ for Class 1 and 2 cross-sections

$\quad = W_{el}/W_{pl}$ for Class 3 cross-sections

$\quad = W_{eff}/W_{pl}$ for Class 4 cross-sections

$W_{pl,y}$ and $W_{pl,z}$ are the plastic moduli for the y and z axes respectively.

A total of 61 beam-column tests, summarised in Table 3.11, have been used in the present study. Figures 7.12 and 7.13 shows the interaction diagrams, whereas Figures 7.14 and 7.15 compare the predictions obtained following two versions of Eurocode guidelines considered for stainless steel with the corresponding test results.

Predictions obtained from both the versions of Eurocode are almost the same as seen from Figures 7.12 – 7.15. ENV 1993-1-4 (1996) predictions produce an average of 0.91 with COV 0.20, whereas prEN 1993-1-4 (2004) gives an average of 0.90 with COV 0.21. Using a

constant interaction factor 1.5 has made the predictions rather more inconsistent. Figures 7.14 and 7.15 show that the predictions are very conservative for small slenderness and become non-conservative for slender sections as stated by Greiner et al (2005). Hence specific proposals have been made to obtain appropriate values for κ in the following section.
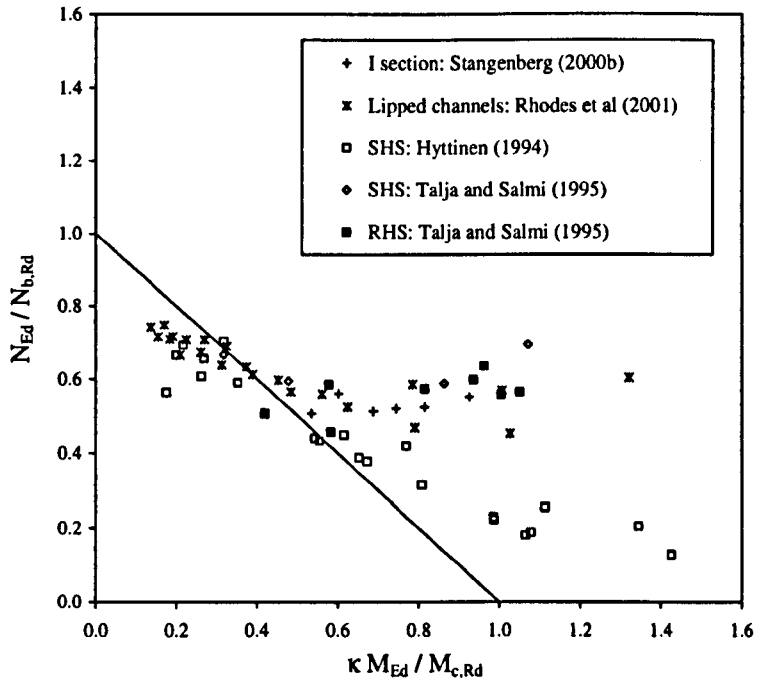
Figure 7.12: Beam-column interactions obtained using ENV 1993-1-4 (1996).
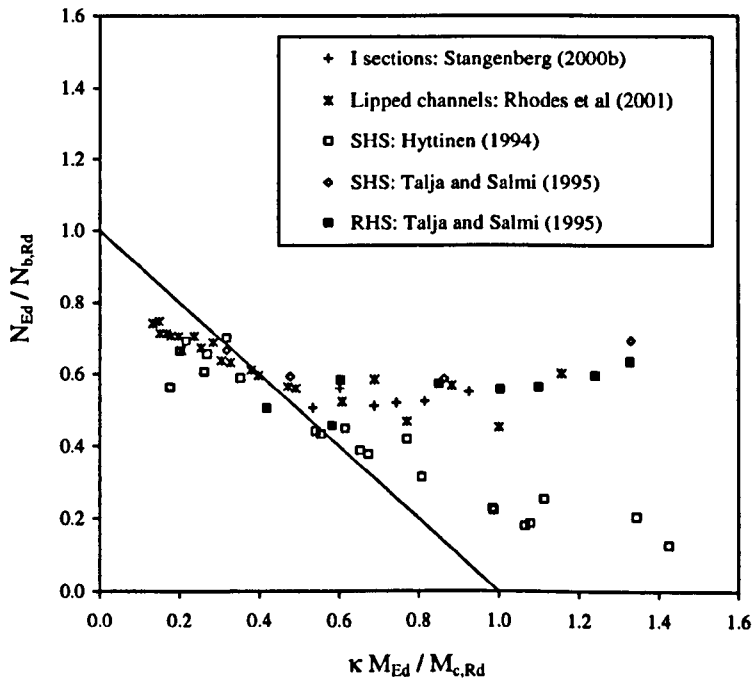
Figure 7.13: Beam-column interactions obtained using prEN 1993-1-4 (2004).
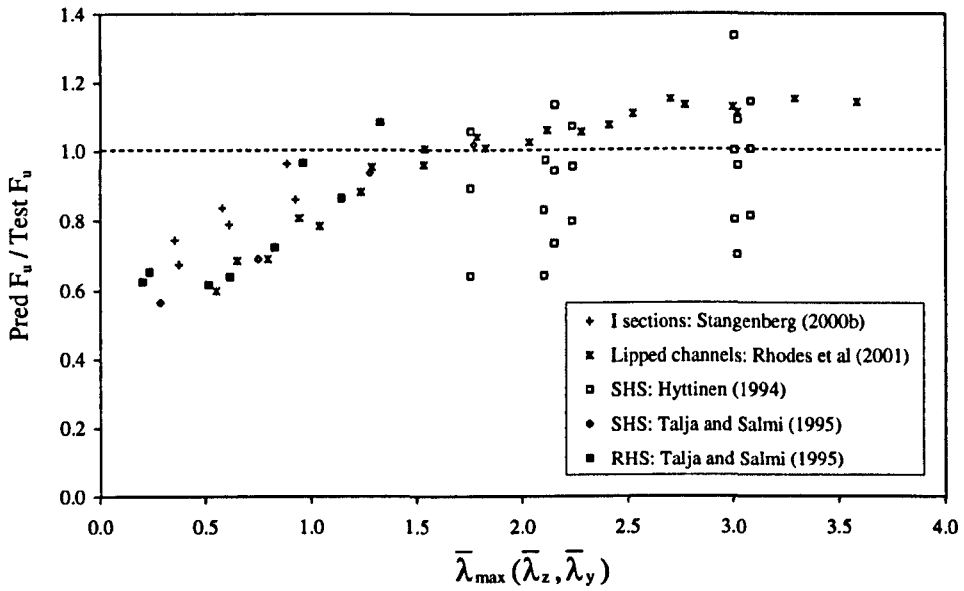
Figure 7.14: Ultimate load predictions for beam-columns using ENV 1993-1-4 (1996).
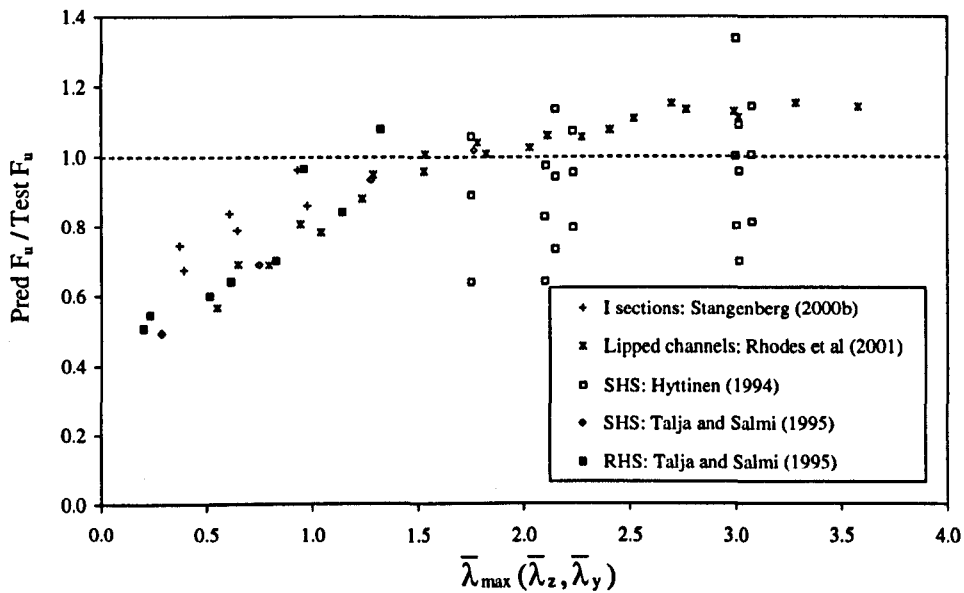
Figure 7.15: Ultimate load predictions for beam-columns using prEN 1993-1-4 (2004).

7.3.3 Proposed formulations for beam-column interaction

Gardner (2002) determined the individual resistances for hollow sections using his proposed techniques and later adopted the interaction formulas given in ENV 1993-1-3 (1996) as directed by the ENV 1993-1-4 (1996). This method produced considerably more accurate predictions for the available hollow sections, although the number of test results was very

limited. In the present research a similar technique has been adopted to investigate its performance against currently available wider variety of test results. The basic interaction equation, in which the parameters have been harmonised with the proposals made for individual actions, is given by Equation 7.14.

$$\frac{N_{Ed}}{\chi_{min}\sigma_{eff}A_g} + \frac{1.5M_{y,Ed}}{a_{g,y}W_{el,y}\sigma_{0.2}} + \frac{1.5M_{z,Ed}}{a_{g,z}W_{el,z}\sigma_{0.2}} \leq 1 \qquad (7.14)$$

where $a_{g,y}$ and $a_{g,z}$ are the generalised shape factors for the y and z axes respectively.

χ_{min} is the smallest value of buckling reduction factor χ for the following two buckling modes: flexural buckling about the y axis and flexural buckling about the z axis. It should be noted that flexural-torsional buckling has not been considered in the present research due the unavailability of test results.

σ_{eff} is the effective buckling stress as given by Equation 7.10.

$W_{el,y}$ and $W_{el,z}$ are the elastic moduli for the y and z axes respectively.

The obtained interactions and predictions following these formulations are given in Figures 7.16 and 7.17.
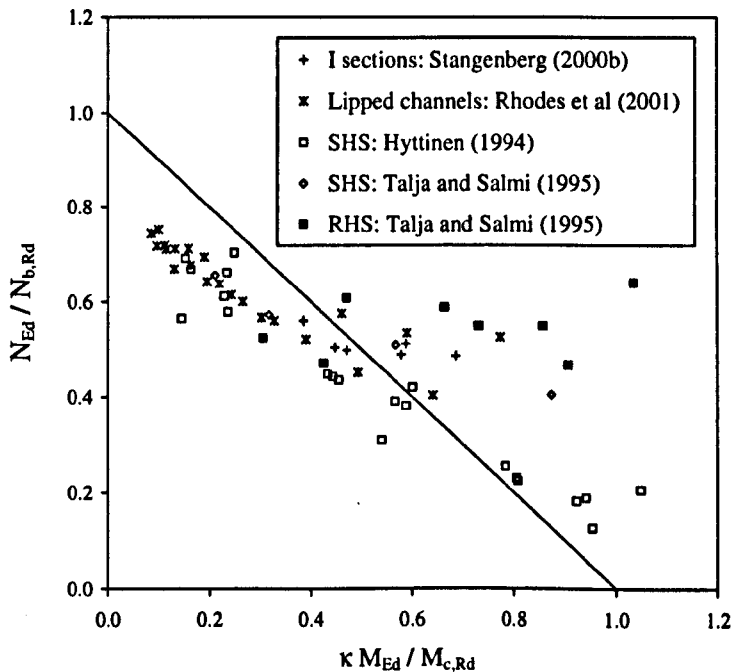
Figure 7.16: Beam-column interactions obtained using the proposed method with $\kappa = 1.5$.
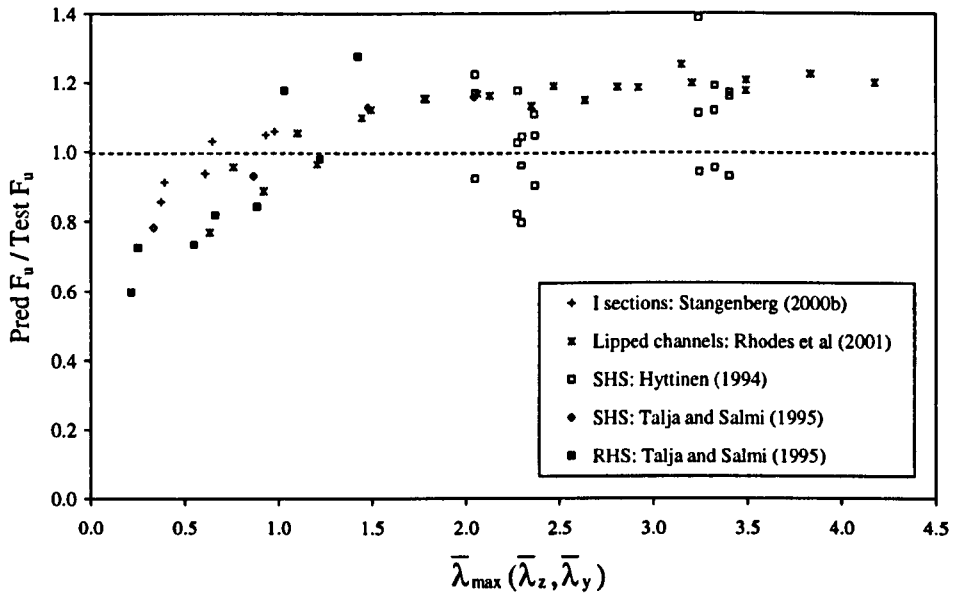
Figure 7.17: Ultimate load predictions for beam-columns using the proposed method with $\kappa = 1.5$

The average of the obtained predictions is 1.04 with a COV of 0.16. These results suggest that the stainless steel beam-column interactions cannot be accurately predicted using a constant value of 1.5 for κ even when the individual actions are determined accurately. Hence all the test results have been predicted accurately considering κ as a variable. The obtained values for κ are plotted against the maximum non-dimensional slenderness $\overline{\lambda}_{max}$ in Figure 7.18.
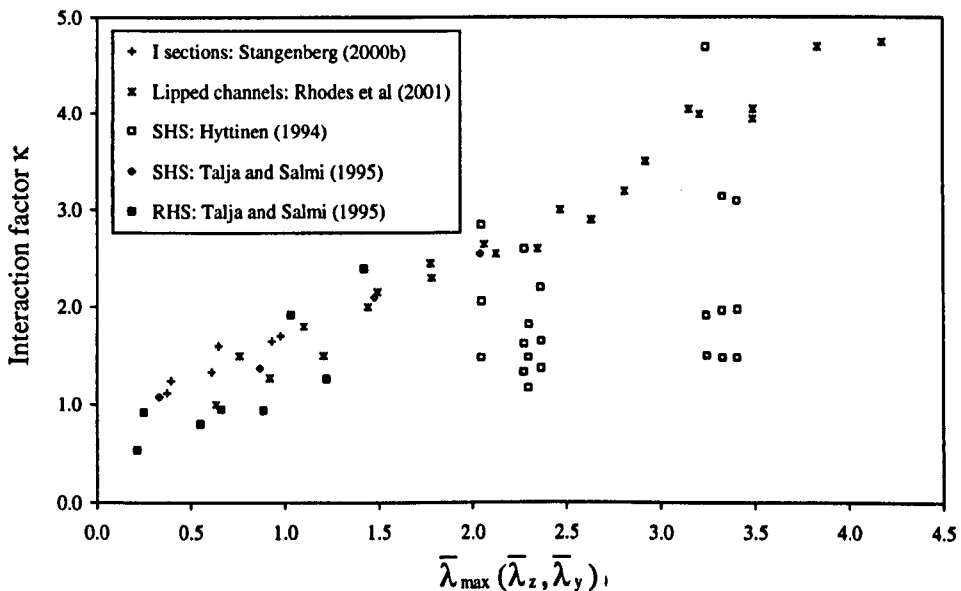
Figure 7.18: Predicted beam-column interaction factors κ for different slenderness $\overline{\lambda}_{max}$.

Figure 7.18 clearly shows that there is an obvious trend for κ to increase with increasing $\overline{\lambda}_{max}$ except for some specimens tested by Hyttinen (1994). Slender members undergo higher lateral deformation which, in turn, reduces the effective bending resistance of the cross-section, and hence a higher value for the interaction factor κ is required to obtain accurate predictions. Hyttinen (1994) tested a total of 21 beams with the moment to the axial load ratio M_{Ed}/N_{Ed} varying from 0.024 to 0.649 m. Among 61 tests considered in the present study, only 14 specimens, shown by the hollow squares in Figure 7.18, for which M_{Ed}/N_{Ed} were very close to or more than 0.1 m offered a considerably different trend than the others. Hence it may be considered that κ is a function of $\overline{\lambda}_{max}$ for lower values of M_{Ed}/N_{Ed}, but as this ratio increases the member slenderness starts to lose its significance and resistances become more dependent on the cross-sectional properties. It should be noted that this study is limited to uniaxial bending and also the flexural-torsional buckling mode was not considered. Hence the proposals made herein must be verified against more test results, when they become available, to attain general applicability. However this may be considered as a step forward towards the development of a rational beam-column interaction formulation, which is based on proposals made for accurate prediction of cross-sectional and flexural resistances.

Regression analysis was carried out to obtain a linear relationship between beam-column interaction factor κ for stainless steel members subjected to compression and uniaxial bending. This relationship is valid up to M_{Ed}/N_{Ed} = 0.075 m and beyond that κ should be taken as 1.5 as proposed by prEN 1993-1-4 (2004). Equation 7.14 gives the relationship obtained between κ and $\overline{\lambda}_{max}$.

$$\kappa = \overline{\lambda}_{max} + 0.55 \qquad \text{for } M_{Ed}/N_{Ed} \leq 0.075 \text{ m} \qquad (7.14)$$
$$\kappa = 1.50 \qquad \text{for } M_{Ed}/N_{Ed} > 0.075 \text{ m}$$

These values for κ should be used in interaction formula given in Equation 7.15.

$$\frac{N_{Ed}}{\chi_{min}\sigma_{eff}A_g} + \frac{\kappa_y M_{y,Ed}}{a_{g,y}W_{el,y}\sigma_{0.2}} + \frac{\kappa_z M_{z,Ed}}{a_{g,z}W_{el,z}\sigma_{0.2}} \leq 1 \qquad (7.15)$$

7.3.4 Verification of the proposed formulations

All considered test results have been analysed using the proposals made in the preceding section. The detailed calculations are given in Table 7.7. The obtained average for all these predictions is 1.00 with a COV of 0.09, which marks a significant improvement both in terms of average and scatter. The interaction diagram and the predictions are plotted in Figures 7.19 and 7.20 respectively.

Table 7.7: Predictions for the ultimate load of stainless steel beam-columns considered in the present research.

Ref.	Section	A_g (mm^2)	$\sigma_{0.2}$ (N/mm^2)	E_0 (N/mm^2)	$N_{c,Rd}$ (kN)	$N_{b,Rd}$ (kN)	$M_{c,Rd}$ (kN-m)	M_{Ed}/N_{Ed} (m)	$\bar{\lambda}_{max}$	κ	Pred F_u (kN)	Test F_u (kN)	Pred F_u/ Test F_u
Stangenberg (2000b)	I 160×80×10×6	2411	279	200000	827.6	660.7	64.96	0.075	0.39	0.94	385.0	338.0	1.14
	I 160×80×10×6	2397	279	200000	826.0	541.3	64.15	0.075	0.65	1.20	312.0	270.0	1.16
	I 160×80×10×6	2429	279	200000	837.1	396.1	64.43	0.074	0.98	1.53	236.0	222.0	1.06
	I 160×160×10×6	4009	279	200000	1369.1	1110.9	88.15	0.075	0.37	0.92	600.0	540.0	1.11
	I 160×160×10×6	3992	279	200000	1365.6	927.2	87.63	0.074	0.61	1.16	490.0	454.0	1.08
	I 160×160×10×6	4140	279	198000	1418.7	706.1	89.31	0.075	0.93	1.48	382.0	356.0	1.07
Rhodes et al (2000)	CL 28×15×8×2.5	143	446	200000	109.2	4.4	0.49	0.008	4.18	4.73	3.3	3.3	1.01
	CL 28×15×8×2.5	143	446	200000	109.2	5.1	0.49	0.008	3.84	4.39	3.8	3.7	1.02
	CL 28×15×8×2.5	143	446	200000	109.2	6.1	0.49	0.008	3.49	4.04	4.4	4.4	1.00
	CL 28×15×8×2.5	143	446	200000	109.2	7.4	0.49	0.008	3.15	3.70	5.1	5.0	1.03
	CL 28×15×8×2.5	143	446	200000	109.2	9.1	0.49	0.008	2.81	3.36	6.1	6.2	0.99
	CL 28×15×8×2.5	143	446	200000	109.2	11.5	0.49	0.008	2.47	3.02	7.3	7.4	0.99
	CL 28×15×8×2.5	143	446	200000	109.2	15.0	0.49	0.008	2.13	2.68	9.1	9.2	0.99
	CL 28×15×8×2.5	143	446	200000	109.2	20.2	0.49	0.008	1.78	2.33	11.4	11.5	0.99
	CL 28×15×8×2.5	143	446	200000	109.2	28.3	0.49	0.008	1.44	1.99	14.8	14.8	1.00
	CL 28×15×8×2.5	143	446	200000	109.2	41.4	0.49	0.008	1.10	1.65	19.5	18.7	1.04
	CL 28×15×8×2.5	143	446	200000	109.2	60.2	0.49	0.008	0.76	1.31	26.3	24.3	1.08
	CL 38×17×10×3	229	428	200000	162.2	9.2	0.90	0.008	3.49	4.04	7.0	6.9	1.00
	CL 38×17×10×3	229	428	200000	162.2	10.8	0.90	0.008	3.21	3.76	8.0	7.8	1.02
	CL 38×17×10×3	229	428	200000	162.2	12.8	0.90	0.008	2.92	3.47	9.2	9.1	1.01
	CL 38×17×10×3	229	428	200000	162.2	15.4	0.90	0.008	2.64	3.19	10.8	11.0	0.98

Table 7.7 (contd.): Predictions for the ultimate load of stainless steel beam-columns considered in the present research.

Ref.	Section	A_g (mm²)	$\sigma_{0.2}$ (N/mm²)	E_0 (N/mm²)	$N_{c,Rd}$ (kN)	$N_{b,Rd}$ (kN)	$M_{c,Rd}$ (kN-m)	M_{Ed}/N_{Ed} (m)	$\bar{\lambda}_{max}$	κ	Pred F_u (kN)	Test F_u (kN)	Pred F_u/ Test F_u
Rhodes et al (2000)	CL 38×17×10×3	229	428	200000	162.2	18.9	0.90	0.008	2.35	2.90	12.8	13.2	0.97
	CL 38×17×10×3	229	428	200000	162.2	23.8	0.90	0.008	2.06	2.61	15.4	15.2	1.01
	CL 38×17×10×3	229	428	200000	162.2	30.6	0.90	0.008	1.78	2.33	18.8	18.4	1.02
	CL 38×17×10×3	229	428	200000	162.2	40.6	0.90	0.008	1.49	2.04	23.4	22.7	1.03
	CL 38×17×10×3	229	428	200000	162.2	55.4	0.90	0.008	1.21	1.76	29.8	31.9	0.93
	CL 38×17×10×3	229	428	200000	162.2	76.5	0.90	0.008	0.92	1.47	38.4	40.9	0.94
	CL 38×17×10×3	229	428	200000	162.2	102.1	0.90	0.008	0.63	1.18	49.0	53.6	0.91
Hyttinen (1994)	SHS 30×30×2	219	468	196000	160.4	9.8	1.64	0.025	3.41	3.96	6.1	6.8	0.91
	SHS 30×30×2	221	468	196000	161.2	9.8	1.64	0.100	3.41	1.50	5.2	4.4	1.17
	SHS 30×30×2	221	468	196000	161.2	9.8	1.65	0.350	3.40	1.50	2.4	2.5	0.95
	SHS 40×40×2	301	423	198000	175.2	23.2	2.43	0.025	2.30	2.85	13.9	16.3	0.85
	SHS 40×40×2	307	423	198000	179.7	23.8	2.50	0.100	2.30	1.50	9.8	10.0	0.98
	SHS 40×40×2	307	423	198000	180.0	23.8	2.51	0.350	2.30	1.50	4.0	4.9	0.81
	SHS 60×60×5	975	518	194000	873.8	129.7	17.86	0.035	2.05	2.60	78.5	75.2	1.04
	SHS 60×60×5	977	518	194000	876.3	129.8	17.90	0.150	2.05	1.50	49.3	40.2	1.23
	SHS 60×60×5	976	518	194000	873.7	129.9	17.86	0.650	2.05	1.50	16.0	16.3	0.98
	SHS 30×30×2	217	498	208000	141.3	10.3	1.50	0.025	3.24	3.79	6.3	5.8	1.07
	SHS 30×30×2	217	498	208000	141.3	10.3	1.50	0.100	3.24	1.50	5.1	4.5	1.12
	SHS 30×30×2	218	498	208000	142.2	10.4	1.51	0.350	3.24	1.50	2.3	2.3	0.97
	SHS 40×40×2	295	462	204000	165.2	23.7	2.36	0.025	2.28	2.83	13.9	14.5	0.95
	SHS 40×40×2	293	462	204000	164.2	23.6	2.34	0.100	2.27	1.50	9.4	9.0	1.04
	SHS 40×40×2	293	462	204000	164.3	23.6	2.35	0.350	2.27	1.50	3.8	4.5	0.84

187

Table 7.7: Predictions for the ultimate load of stainless steel beam-columns considered in the present research.

Ref.	Section	A_g (mm^2)	$\sigma_{0.2}$ (N/mm^2)	E_0 (N/mm^2)	$N_{c,Rd}$ (kN)	$N_{b,Rd}$ (kN)	$M_{c,Rd}$ (kN-m)	M_{Ed}/N_{Ed} (m)	$\bar{\lambda}_{max}$	κ	Pred F_u (kN)	Test F_u (kN)	Pred F_u/ Test F_u
Hyttinen (1994)	SHS 30×30×2	225	536	213000	157.5	10.9	1.67	0.025	3.33	3.88	6.7	7.3	0.92
	SHS 30×30×2	224	536	213000	156.7	10.9	1.66	0.100	3.32	1.50	5.5	4.8	1.14
	SHS 30×30×2	225	536	213000	157.6	10.9	1.67	0.350	3.33	1.50	2.5	2.5	0.98
	SHS 40×40×2	302	511	212000	188.5	25.2	2.67	0.025	2.36	2.91	15.0	16.7	0.90
	SHS 40×40×2	305	511	212000	190.6	25.4	2.70	0.100	2.37	1.50	10.5	9.9	1.06
	SHS 40×40×2	306	511	212000	191.7	25.6	2.71	0.350	2.37	1.50	4.3	4.7	0.92
Talja and Salmi (1995)	SHS 60×60×5	1002	463	187000	794.2	622.4	15.99	0.028	0.33	0.88	362.0	322.0	1.12
	SHS 60×60×5	1004	463	187000	795.7	412.6	16.07	0.028	0.87	1.42	207.0	210.0	0.99
	SHS 60×60×5	990	506	184000	846.7	218.2	17.08	0.027	1.48	2.03	127.0	125.0	1.02
	SHS 60×60×5	990	506	184000	846.7	126.5	17.08	0.027	2.04	2.59	83.2	83.0	1.00
	RHS 150×100×3	1394	305	205000	326.0	375.7	22.76	0.074	0.21	0.76	181.0	209.0	0.87
	RHS 150×100×3	1394	305	205000	326.0	314.7	22.76	0.074	0.55	1.10	149.0	173.0	0.86
	RHS 150×100×3	1394	305	205000	326.0	228.0	22.76	0.074	0.89	1.44	111.0	134.0	0.83
	RHS 150×100×3	1394	305	205000	326.0	156.2	22.76	0.074	1.22	1.77	82.6	95.0	0.87
	RHS 150×100×6	2678	356	242000	1217.6	1097.8	70.84	0.072	0.25	0.80	613.0	569.0	1.08
	RHS 150×100×6	2708	309	198000	1073.0	732.9	61.62	0.072	0.66	1.21	360.0	403.0	0.89
	RHS 150×100×6	2678	356	242000	1217.6	566.3	70.84	0.072	1.03	1.58	295.0	267.0	1.10
	RHS 150×100×6	2678	356	242000	1217.6	366.1	70.84	0.072	1.42	1.97	210.0	192.0	1.09
									Average (61 beam-column tests)				**1.00**
									COV				**0.09**
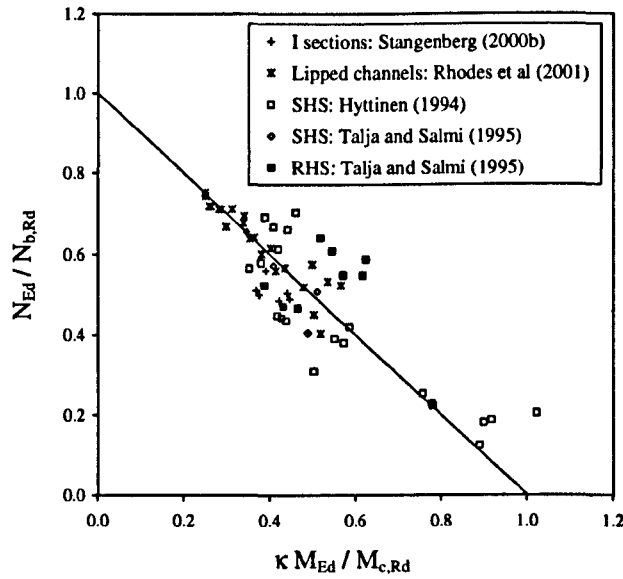
Figure 7.19: Beam-column interactions using the proposed method.
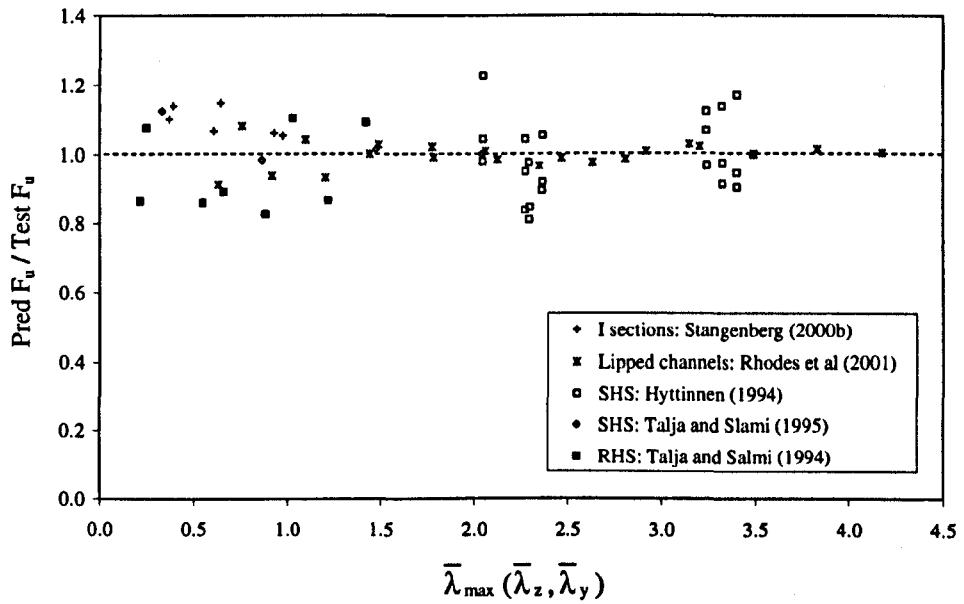
Figure 7.20: Ultimate load predictions for the beam-columns using the proposed method.

7.3.5 Concluding remarks

Beam-column behaviour has been investigated using the currently available test results, all of which represent columns subjected to compression with simultaneous uniaxial bending. The existing Eurocode approach has been observed to provide inconsistent predictions for such behaviour and hence investigations have been made to find appropriate solutions. Regression

analysis has been conducted to establish a relationship between the maximum non-dimensional slenderness $\overline{\lambda}_{max}$ and the beam-column interaction factor κ. When the basic interaction equation, which has a similar form to that specified in the Eurocode, has been used with the member resistances against individual actions determined using the proposed methods along with the proposed values for κ, the ultimate load predictions for the considered beam-column actions were found to be very accurate. The average prediction for 61 beam-column tests was 1.00 with a COV of 0.09. It should be noted that torsional and flexural-torsional buckling modes were not reported in the considered cases and hence no proposals have been made herein to incorporate these buckling modes.

7.4 CONCLUSIONS

Flexural buckling behaviour of stainless steel columns has been investigated using currently available 97 tests on four different cross-section types obtained from six different sources. Two different sets of column curves have been proposed for stainless steel columns subjected to flexural buckling. Instead of using the traditional 0.2% proof stress of the flat material the proposed techniques exploit different key parameters – local buckling stress σ_{LB} and effective buckling stress σ_{eff} - yet retain the basic Perry-Robertson formulation. The performance of these methods has been verified against the test results. The first technique, which uses σ_{LB}, produces a mean of 0.99 with a COV of 0.11, whereas that using σ_{eff} provides more accurate predictions with an average of 1.00 with a COV of 0.09. When the predictions were compared against the FE results, which are believed to reduce the experimental uncertainties to some extent, significantly improved agreements have been achieved reducing the overall COV from 0.09 to 0.06.

Beam-column interactions have been investigated using 61 tests performed on four different cross-section types obtained from four different sources. Stainless steel members were subjected to compression with a simultaneous uniaxial bending moment. Guidelines available in the existing Eurocode were found to produce very inconsistent predictions, largely due to the inaccurate predictions for resistances against individual actions, which was supplemented by the adoption of a constant value of 1.5 for the interaction factor κ. Detailed investigations have been made and hence an empirical relationship has been proposed between κ and non-dimensional member slenderness $\overline{\lambda}_{max}$. The proposed design techniques produced significant improvements in the ultimate load predictions for the considered 61 cases giving an average of 1.00 and a COV of 0.09.

The overall conclusion from this chapter is that the basic Eurocode formulations are acceptable, that their accuracy is significantly improved when used with the cross-sectional approach of Chapter 6 and that further improvements are possible if small modifications are made to the original formats.

CHAPTER - EIGHT

DESIGN METHOD

8.1 INTRODUCTION

Development of the design proposals for stainless steel structures have been discussed in detail in Chapters 6 and 7. This chapter summarises all the proposed design methods in a common format and also compares their performance with the existing Eurocode prEN 1993-1-4 (2004). However, it should be noted that the proposed design expressions currently predict mean failure loads and hence the material safety factors have been omitted from the Eurocode predictions. It is recognised that appropriate load factors and material safety factors need to be incorporated to achieve the required level of reliability, although this has not been addressed as part of the current research.

8.2 DESIGN METHOD

8.2.1 Compression resistance of cross-sections $N_{c,Rd}$

Compression resistance of a cross-section depends on its geometry, basic material properties and the extent of cold-working, if any. The following sections explain the proposed techniques to determine the values for the key parameters required to obtain the compression resistance.

8.2.1.1 Cross-section slenderness β

Cross-section slenderness β shall be the highest among the determined values for all component plate elements using Equation 8.1.

$$\beta = \frac{b}{t}\sqrt{\frac{\sigma_{0.2}}{E_0}}\sqrt{\frac{4}{k}} \qquad (8.1)$$

where   b   is the flat width measured between centrelines of adjacent faces as explained in Table 3.6

t   is the thickness of the plate element

$\sigma_{0.2}$ is the 0.2% proof stress in compression of the flat material

(if compression strength is not available, the corresponding tension strength may be used. In the case of austenitic Grade 1.4301 the tension strength should be reduced by 7%)

E_0 is the material Young's modulus

k   is the plate buckling coefficient, which is equivalent to the buckling factor defined as k_σ for internal and outstand compression elements in Tables 4.1 and 4.2 of prEN 1993-1-5 (2003). Table 8.1 presents a summary of guidelines for the determination of k.

Table 8.1: Buckling coefficients k for compressed plate elements.

$\psi = \sigma_2/\sigma_1$	1	$1 > \psi > 0$	0	$0 > \psi > -1$	-1	$-1 > \psi > -3$
Internal element	4.0	$\dfrac{8.2}{1.05+\psi}$	7.81	$7.81 - 6.29\psi + 9.78\psi^2$	23.9	$5.98\,(1-\psi)^2$
Outstand element	0.43	$\dfrac{0.578}{0.34+\psi}$	1.70	$1.7 - 5\psi + 17.1\psi^2$	23.8	-

Note: ψ is the ratio of end stresses (compression positive) for the compression element.

8.2.1.2 Cross-section deformation capacity ε_{LB}

The deformation capacity of a cross-section is based on β and shall be calculated using Equation 8.2.

$$\frac{\varepsilon_{LB}}{\varepsilon_0} = \frac{6.44}{\beta^{2.85-0.27\beta}}$$

(8.2)

where ε_0 is the elastic strain at 0.2% proof stress = $\sigma_{0.2}/E_0$ of the flat material

8.2.1.3 Local buckling stress σ_{LB}

Local buckling stress σ_{LB} is based on the proposed compound Ramberg-Osgood material model modified for different grades of stainless steel and shall be determined from Tables A.1 to A.6 given in Appendix A.

8.2.1.4 Strength enhancement factor ϕ_c due to the cold-worked corners

The presence of cold-worked corners affects the compression resistance of a cross-section. The strength enhancement factor ϕ_c depends on the manufacturing process and may be determined using Equation 8.3 or 8.4.

For roll-formed sections: $\quad \phi_c = 1 + 0.32 k_{cor}$ $\hfill$ (8.3)

For press-braked sections: $\quad \phi_c = 1 + \left[\dfrac{1.881}{(r_i/t)^{0.194}} - 1 \right] k_{cor}$ $\hfill$ (8.4)

where $\qquad$ k_{cor} $\quad$ is the proportion of corner region $= A_c/A_g$

$\qquad\qquad$ A_c $\quad$ is the area of the corner region

$\qquad\qquad$ A_g $\quad$ is the gross-area of the cross-section

$\qquad\qquad$ r_i $\quad$ is the internal radius of the corner

$\qquad\qquad$ t $\quad$ is the thickness of the plate

For sections without any cold-worked corners, ϕ_c should be taken as 1.0.

8.2.1.5 Compression resistance $N_{c,Rd}$

The compression resistance of a cross-section $N_{c,Rd}$ shall be determined using Equation 8.5.

$$N_{c,Rd} = \phi_c \sigma_{LB} A_g \hfill (8.5)$$

8.2.2 Bending resistance of cross-sections $M_{c,Rd}$

The bending resistance of a stainless steel cross-section is most likely to be limited either by the local buckling of the compression flange or by the compressed portion of the web. Hence the proposed technique to determine the bending resistance is based on the same principles proposed for compression. In-plane bending resistance $M_{c,Rd}$ is given by Equation 8.6.

$$M_{c,Rd} = \phi_c \, a_g \, W_{el} \, \sigma_{0.2} \hfill (8.6)$$

where $\qquad$ ϕ_c $\quad$ is the corner enhancement factor, which should be determined by using either Equation 8.3 or 8.4.

$\qquad\qquad$ W_{el} $\quad$ is the elastic modulus of the cross-section

$\qquad\qquad$ a_g $\quad$ is the generalised shape factor, which is a function of geometric shape factor a_p, material properties and the outer fibre strain expressed by the deformation capacity ε_{LB}. For a specific value of ε_{LB}, generalised

shape factor a_g may be determined using Equation 8.7, where the coefficients A_1 to A_4 should be obtained from Tables B1 to B6 given in Appendix B.

$$a_g = A_1 + A_2\varepsilon_0 + A_3 a_p + A_4 \varepsilon_0 a_p \qquad (8.7)$$

where ε_0 is the elastic strain at 0.2% proof stress $= \sigma_{0.2}/E_0$

8.2.3 Cross-section resistance against combined compression and bending

The combined action of compression and bending on a stainless steel cross-section may be evaluated based on the methods proposed for individual actions. Thus such a section should satisfy Equation 8.8.

$$\frac{N_{Ed}}{N_{c,Rd}} + \frac{M_{y,Ed}}{M_{y,c,Rd}} + \frac{M_{z,Ed}}{M_{z,c,Rd}} \le 1 \qquad (8.8)$$

where

N_{Ed} is the applied axial compression

$M_{y,Ed}$ is the applied bending moment about the y-axis

$M_{z,Ed}$ is the applied bending moment about the z axis

$N_{c,Rd}$ is the compression resistance $(= \phi_c \sigma_{LB} A_g)$, as given by Equation 8.5

$M_{y,c,Rd}$ is the bending resistance about the y axis $(= \phi_c a_g W_{el,y} \sigma_{0.2})$, as given by Equation 8.6

$M_{z,c,Rd}$ is the bending resistance about the z axis $(= \phi_c a_g W_{el,z} \sigma_{0.2})$, as given by Equation 8.6

8.2.4 Flexural buckling resistance of members $N_{b,Rd}$

The proposed method to determine the flexural buckling resistance $N_{b,Rd}$ of stainless steel members is based on an effective buckling stress σ_{eff} rather than the traditional 0.2% material proof stress $\sigma_{0.2}$. Column curves have been proposed based on σ_{eff}, yet retaining the basic Perry type format, to determine appropriate buckling reduction factors χ.

8.2.4.1 Effective buckling stress σ_{eff}

Effective buckling stress σ_{eff} may be determined using Equation 8.9.

$$\sigma_{eff} = \sqrt{\phi_c \sigma_{0.2} \sigma_{LB}} \qquad (8.9)$$

where	ϕ_c	is the corner enhancement factor which may be determined by using either Equation 8.3 or 8.4.
	$\sigma_{0.2}$	is the 0.2% proof stress of material in compression
	σ_{LB}	is the local buckling stress of the cross-section as explained in Section 8.2.1.3

8.2.4.2 Buckling reduction factor χ

Buckling reduction factors χ for different cross-sections should be determined using the following Equations

$$\chi = \frac{1}{\phi + \sqrt{\phi^2 - \bar{\lambda}^2}} \leq 1.0 \qquad (8.10)$$

with

$$\phi = 0.5\left[1 + \alpha\left(\bar{\lambda} - \bar{\lambda}_0\right) + \bar{\lambda}^2\right] \qquad (8.11)$$

$$\bar{\lambda} = \sqrt{\frac{A_g \sigma_{eff}}{N_{cr}}} \qquad (8.12)$$

$$N_{cr} = \frac{\pi^2 EI}{L_e^2} \qquad (8.13)$$

where	ϕ	is a coefficient to define imperfection
	α	is the imperfection factor, which depends on the cross-section type and should be taken from the proposed Table 8.2.
	$\bar{\lambda}_0$	is the limiting slenderness ratio, which depends on the cross-section type and should be taken from the proposed Table 8.2.
	N_{cr}	is the elastic critical buckling force for the relevant buckling mode based on the gross cross-sectional area A_g.
	L_e	is the effective length of the column about the relevant buckling axis.

Table 8.2: Values of α and $\bar{\lambda}_0$ for flexural buckling curves based on σ_{eff}.

Type of member	Buckling axis	α	$\bar{\lambda}_0$
Welded I sections	Minor	0.70	0.20
	Major	0.58	0.20
Square hollow sections SHS	-	0.55	0.40
Rectangular hollow sections RHS	All	0.45	0.40
Cold-formed open sections	All	0.58	0.30

Alternatively the buckling reduction factors may be obtained using the buckling curves given in Figure 8.1.
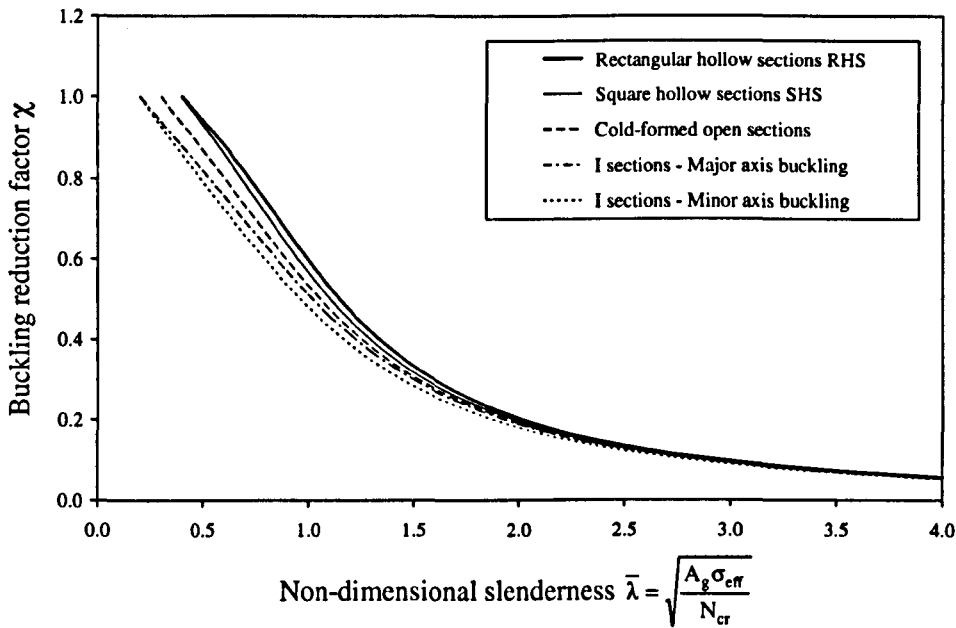
Figure 8.1: Proposed flexural buckling curves for stainless steel members based on σ_{eff}.

8.2.4.3 Flexural buckling resistance $N_{b,Rd}$

The flexural buckling resistance $N_{b,Rd}$ of a stainless steel member may be determined using Equation 8.14.

$$N_{b,Rd} = \chi \, A_g \, \sigma_{eff} \tag{8.14}$$

where A_g is the gross area of the cross-section

8.2.5 Member resistance against combined axial load plus bending

Members subjected to simultaneous compression and bending should satisfy Equation 8.15.

$$\frac{N_{Ed}}{\chi_{min}\sigma_{eff}A_g} + \frac{\kappa_y M_{y,Ed}}{a_{g,y}W_{el,y}\sigma_{0.2}} + \frac{\kappa_z M_{z,Ed}}{a_{g,z}W_{el,z}\sigma_{0.2}} \le 1 \tag{8.15}$$

where N_{Ed}, $M_{y,Ed}$ and $M_{z,Ed}$ are the design values of the compression force and the maximum moments about the y-y and z-z axis along the member, respectively.

κ_y and κ_z are the beam-column interaction factors about the y-y and z-z axis which may be obtained using Equation 8.16 and 8.17.

$$\kappa = \overline{\lambda}_{max} + 0.55 \qquad \text{for } M_{Ed}/N_{Ed} \leq 0.075 \text{ m} \tag{8.16}$$

$$\kappa = 1.50 \qquad \text{for } M_{Ed}/N_{Ed} > 0.075 \text{ m} \tag{8.17}$$

χ_{min} is the smallest value of buckling reduction factor χ for the following two buckling modes: flexural buckling about the y axis and flexural buckling about the z axis. It should be noted that flexural-torsional buckling has not been considered in the present research due to the unavailability of test results.

$a_{g,y}$ and $a_{g,z}$ are the generalised shape factors for the y and z axes respectively, which should be determined following Equation 8.7.

$W_{el,y}$ and $W_{el,z}$ are the elastic moduli for the y and z axes respectively.

σ_{eff} is the effective buckling stress as given by Equation 8.9.

$\sigma_{0.2}$ is the 0.2% material proof stress in compression.

A_g is the gross area of the cross-section.

8.3 COMPARISON OF THE PROPOSED DESIGN METHOD WITH prEN 1993-1-4 (2004)

The proposed design methods have already been verified against the test results in Chapters 6 and 7. This section compares the performance with the existing Eurocode for stainless steel prEN 1993-1-4 (2004). For comparison purposes, measured geometric and material properties have been used and all safety factors and load factors are taken as unity.

8.3.1 Cross-section resistance

8.3.1.1 Compression resistance $N_{c,Rd}$

Table 8.3 presents a detailed comparison between the predictions obtained following the proposed guidelines and those of prEN 1993-1-4 (2004) for all stub column tests considered in the present research. A summary of the comparisons is given in Table 8.4. The comparisons show that the proposed method can predict the compression resistance of cross-sections more accurately than the existing Eurocode. The reasons for the obtained higher scatter for the welded I and square hollow sections have already been explained in Section 6.2.3.2. Overall the proposed method provides a 25% increase in compression resistance with less scatter.

Table 8.3: Comparison between prEN 1993-1-4 (2004) and the proposed design method for stub columns.

Reference	Cross-section designation	Test F_u (kN)	$\sigma_{0.2}$ (N/mm^2)	E_0 (N/mm^2)	Class (1 – 4)	prEN F_u (kN)	prEN F_u / Test F_u	$\varepsilon_{LB}/\varepsilon_0$	Prop F_u (kN)	Prop F_u / Test F_u	Prop F_u / prEN F_u
Kuwamura (2003)	L 25 × 25 × 3	55.9	279	200000	4	36.18	0.65	8.13	49.2	0.88	1.36
	L 30 × 30 × 3	59.4	279	200000	4	44.16	0.74	4.94	55.8	0.94	1.26
	L 40× 40 × 3	66.9	279	200000	4	53.96	0.81	2.39	64.9	0.97	1.20
	L 40 × 40 × 3	65.6	279	200000	4	54.10	0.82	2.42	65.6	1.00	1.21
	L 50 × 50 × 3	68.7	279	200000	4	59.81	0.87	1.46	69.4	1.01	1.16
	L 60 × 60 × 3	69.6	279	200000	4	64.99	0.93	1.06	71.4	1.03	1.10
	L 25 × 25 × 3	79.7	508	187000	4	65.68	0.82	3.51	88.6	1.11	1.35
	L 30 × 30 × 3	89.8	508	187000	4	72.55	0.81	2.30	99.7	1.11	1.37
	L 40× 40 × 3	108.7	508	187000	4	84.69	0.78	1.27	107.7	0.99	1.27
	L 40 × 40 × 3	100.2	508	187000	4	85.47	0.85	1.26	108.4	1.08	1.27
	L 50 × 50 × 3	108.7	508	187000	4	91.50	0.84	0.84	108.6	1.00	1.19
	L 60 × 60 × 3	106.4	508	187000	4	97.85	0.92	0.67	110.6	1.04	1.13
Kuwamura (2003)	C 50 × 25 × 3	106.0	279	190000	1	71.84	0.68	7.73	98.7	0.93	1.37
	C 80 × 40 × 3	134.2	279	190000	4	112.48	0.84	2.30	130.2	0.97	1.16
	C 100 × 50 × 3	146.2	279	190000	4	126.03	0.86	1.39	139.0	0.95	1.10
	C 100 × 50 × 3	140.4	279	190000	4	126.04	0.90	1.41	140.7	1.00	1.12
	C 150 × 50 × 3	156.0	279	190000	4	134.73	0.86	1.38	172.6	1.11	1.28
	C 50 × 50 × 3	125.0	279	190000	4	95.11	0.76	1.40	105.3	0.84	1.11
	C 50 × 25 × 3	186.2	508	180000	4	133.21	0.72	3.59	178.7	0.96	1.34
	C 80 × 40 × 3	229.7	508	180000	4	178.65	0.78	1.56	242.2	1.05	1.36
	C 100 × 50 × 3	233.8	508	180000	4	193.45	0.83	0.98	243.6	1.04	1.26
	C 100 × 50 × 3	229.6	508	180000	4	191.80	0.84	0.96	237.1	1.03	1.24
	C 150 × 50 × 3	228.2	508	180000	4	205.63	0.90	0.83	271.2	1.19	1.32

Table 8.3 (contd.): Comparison between prEN 1993-1-4 (2004) and the proposed design method for stub columns.

Reference	Cross-section designation	Test F_u (kN)	$\sigma_{0.2}$ (N/mm^2)	E_0 (N/mm^2)	Class (1 – 4)	prEN F_u (kN)	prEN F_u / Test F_u	$\varepsilon_{LB}/\varepsilon_0$	Prop F_u (kN)	Prop F_u / Test F_u	Prop F_u / prEN F_u
Kuwamura (2003)	CL 100 × 50 × 20 × 3	211.4	279	186000	4	168.11	0.80	3.43	215.4	1.02	1.28
	CL 150 × 50 × 20 × 3	197.0	279	186000	4	178.12	0.90	1.37	202.8	1.03	1.14
	CL 150 × 65 × 20 × 3	214.8	279	186000	4	201.09	0.94	1.35	222.0	1.03	1.10
	CL 200 × 75 × 25 × 3	232.8	279	186000	4	229.59	0.99	0.81	213.9	0.92	0.93
	CL 100 × 33 × 18 × 1	23.7	279	187500	4	18.28	0.77	3.30	23.2	0.98	1.27
	CL 150 × 50 × 17 × 1	21.7	279	187500	4	19.79	0.91	1.30	21.7	1.00	1.09
	CL 150 × 50 × 22 × 1	24.3	279	187500	4	22.06	0.91	1.30	23.7	0.97	1.07
	CL 200 × 68 × 25 × 1	26.1	279	187500	4	24.63	0.94	0.77	22.5	0.86	0.91
	CL 100 × 50 × 20 × 3	350.2	508	180000	4	292.59	0.84	1.80	386.3	1.10	1.32
	CL 150 × 50 × 20 × 3	317.9	508	180000	4	302.96	0.95	0.83	316.4	1.00	1.04
	CL 150 × 65 × 20 × 3	342.3	508	180000	4	337.93	0.99	0.83	346.5	1.01	1.03
	CL 200 × 75 × 25 × 3	377.8	508	180000	4	368.91	0.98	0.59	348.5	0.92	0.94
Lecce and Rasmussen (2004a)	CL 105 × 90 × 13 × 2	116.0	242	187000	4	99.62	0.86	1.41	120.2	1.04	1.21
	CL 105 × 90 × 13 × 2	116.0	242	187000	4	99.96	0.86	1.43	120.2	1.04	1.20
	CL 105 × 90 × 13 × 2	116.0	242	187000	4	100.08	0.86	1.44	123.2	1.06	1.23
	CL 105 × 90 × 13 × 2	116.0	242	187000	4	99.97	0.86	1.43	123.2	1.06	1.23
	CL 67 × 57 × 8 × 1.13	50.0	271	193000	4	38.14	0.76	1.08	44.2	0.88	1.16
	CL 67 × 57 × 8 × 1.13	50.0	271	193000	4	38.14	0.76	1.08	44.2	0.88	1.16
	CL 55 × 55 × 8 × 1.13	51.0	271	193000	4	36.29	0.71	1.58	47.3	0.93	1.30
	CL 55 × 55 × 8 × 1.13	51.0	271	193000	4	36.32	0.71	1.59	47.3	0.93	1.30
	CL 105 × 85 × 15 × 2	162.0	339	208000	4	132.02	0.81	1.18	163.0	1.01	1.23
	CL 105 × 85 × 15 × 2	162.0	339	208000	4	132.12	0.82	1.18	163.0	1.01	1.23

Table 8.3 (contd.): Comparison between prEN 1993-1-4 (2004) and the proposed design method for stub columns.

Reference	Cross-section designation	Test F_u (kN)	$\sigma_{0.2}$ (N/mm^2)	E_0 (N/mm^2)	Class (1–4)	prEN F_u (kN)	prEN F_u / Test F_u	$\varepsilon_{LB}/\varepsilon_0$	Prop F_u (kN)	Prop F_u / Test F_u	Prop F_u / prEN F_u
	I 50 × 50 × 3 × 3	152.8	279	200000	1	119.17	0.78	11.89	148.6	0.97	1.25
	I 50 × 100 × 3 × 3	192.8	279	200000	4	165.57	0.86	1.70	175.9	0.91	1.06
	I 100 × 50 × 3 × 3	171.1	279	200000	4	149.02	0.87	4.61	177.6	1.04	1.19
	I 100 × 75 × 3 × 3	199.9	279	200000	4	184.58	0.92	3.43	215.8	1.08	1.17
	I 100 × 100 × 3 × 3	203.4	279	200000	4	196.73	0.97	1.67	211.3	1.04	1.07
	I 150 × 100 × 3 × 3	207.7	279	200000	4	206.53	0.99	1.67	247.8	1.19	1.20
	I 200 × 100 × 3 × 3	206.1	279	200000	4	210.16	1.02	0.93	218.6	1.06	1.04
Kuwamura	I 200 × 150 × 3 × 3	231.4	279	200000	4	223.66	0.97	0.77	257.0	1.11	1.15
(2003)	I 50 × 50 × 3 × 3	253.4	508	194000	3	221.18	0.87	5.91	262.5	1.04	1.19
	I 50 × 100 × 3 × 3	289.7	508	194000	4	265.46	0.92	0.97	272.1	0.94	1.03
	I 100 × 50 × 3 × 3	279.5	508	194000	4	256.58	0.92	2.33	323.4	1.16	1.26
	I 100 × 75 × 3 × 3	309.9	508	194000	4	287.97	0.93	1.81	376.8	1.22	1.31
	I 100 × 100 × 3 × 3	323.4	508	194000	4	302.81	0.94	0.98	339.1	1.05	1.12
	I 150 × 100 × 3 × 3	310.1	508	194000	4	312.73	1.01	0.96	388.5	1.25	1.24
	I 200 × 100 × 3 × 3	311.5	508	194000	4	315.66	1.01	0.64	342.8	1.10	1.09
	I 200 × 150 × 3 × 3	359.7	508	194000	4	326.22	0.91	0.58	386.2	1.07	1.18
	I 160 × 80 × 10 × 6	885.0	279	200000	1	678.03	0.77	11.95	845.7	0.96	1.25
Stangenberg	I 160 × 160 × 10 × 6	1440.0	279	198000	1	1136.76	0.79	10.78	1401.6	0.97	1.23
(2000a)	I 320 × 160 × 10 × 6	1430.0	279	200000	4	1195.39	0.84	1.61	1119.6	0.78	0.94
	I 160 × 160 × 10 × 6	2590.0	524	202000	3	2145.31	0.83	5.29	2472.8	0.95	1.15

Table 8.3 (contd.): Comparison between prEN 1993-1-4 (2004) and the proposed design method for stub columns.

Reference	Cross-section designation	Test F_u (kN)	$\sigma_{0.2}$ (N/mm²)	E_0 (N/mm²)	Class (1 – 4)	prEN F_u (kN)	prEN F_u / Test F_u	$\varepsilon_{LB}/\varepsilon_0$	Prop F_u (kN)	Prop F_u / Test F_u	Prop F_u / prEN F_u
	SHS 80 × 80 × 4	727.0	457	186600	1	493.56	0.68	6.04	656.3	0.90	1.33
	SHS 80 × 80 × 4	714.0	457	186600	1	513.67	0.72	6.64	690.6	0.97	1.34
	SHS 80 × 80 × 4	711.0	457	186600	1	514.13	0.72	6.69	692.4	0.97	1.35
	SHS 80 × 80 × 4	309.0	261	206300	1	288.41	0.93	15.73	385.6	1.25	1.34
	SHS 80 × 80 × 4	335.0	261	206300	1	281.88	0.84	14.58	372.6	1.11	1.32
	SHS 100 × 100 × 2	197.0	370	207100	4	165.83	0.84	1.11	209.7	1.06	1.26
	SHS 100 × 100 × 2	187.0	370	207100	4	165.11	0.88	1.12	208.6	1.12	1.26
	SHS 100 × 100 × 3	489.0	379	208800	4	344.61	0.70	2.61	448.3	0.92	1.30
Gardner (2002)	SHS 100 × 100 × 3	496.0	379	208800	4	338.21	0.68	2.55	440.1	0.89	1.30
	SHS 100 × 100 × 4	779.0	437	203400	3	625.35	0.80	4.44	774.3	0.99	1.24
	SHS 100 × 100 × 4	774.0	437	203400	3	623.16	0.81	4.42	771.6	1.00	1.24
	SHS 100 × 100 × 6	1513.0	473	197900	1	1015.53	0.67	12.63	1495.1	0.99	1.47
	SHS 100 × 100 × 6	1507.0	473	197900	1	1018.37	0.68	12.47	1494.3	0.99	1.47
	SHS 100 × 100 × 8	1630.0	330	205200	1	919.05	0.56	52.00	1607.6	0.99	1.75
	SHS 100 × 100 × 8	1797.0	330	205200	1	917.73	0.51	52.32	1608.4	0.90	1.75
	SHS 150 × 150 × 4	726.0	294	195400	4	515.63	0.71	2.39	658.8	0.91	1.28
	SHS 150 × 150 × 4	713.0	294	195400	4	505.26	0.71	2.32	644.1	0.90	1.27
Talja and Salmi (1995)	SHS 60 × 60 × 5	801.0	463	186500	1	462.54	0.58	28.78	778.9	0.97	1.68
Rasmussen and Hancock (1993)	SHS 80 × 80 × 3	485.0	415	196000	3	376.82	0.78	4.14	446.6	0.92	1.19
	SHS 80 × 80 × 3	471.0	415	196000	3	373.50	0.79	4.23	444.7	0.94	1.19
	SHS 50 × 50 × 3	241.0	279	190500	1	143.71	0.60	23.03	231.2	0.96	1.61
Kuwamura (2003)	SHS 75 × 75 × 3	282.4	279	190500	1	227.03	0.80	7.51	298.4	1.06	1.31
	SHS 100 × 100 × 3	323.2	279	190500	4	279.18	0.86	3.55	360.7	1.12	1.29

Table 8.3 (contd.): Comparison between prEN 1993-1-4 (2004) and the proposed design method for stub columns.

Reference	Cross-section designation	Test F_u (kN)	$\sigma_{0.2}$ (N/mm^2)	E_0 (N/mm^2)	Class (1 – 4)	prEN F_u (kN)	prEN F_u / Test F_u	$\varepsilon_{LB}/\varepsilon_0$	Prop F_u (kN)	Prop F_u / Test F_u	Prop F_u / prEN F_u
Kuwamura (2003)	SHS 125 × 125 × 3	353.8	279	190500	4	301.51	0.85	2.03	397.7	1.12	1.32
	SHS 150 × 150 × 3	363.9	279	190500	4	317.12	0.87	1.38	416.7	1.15	1.31
	SHS 200 × 200 × 3	364.8	279	190500	4	337.64	0.93	0.83	428.1	1.17	1.27
	SHS 50 × 50 × 3	377.5	508	184000	1	275.45	0.73	10.59	396.1	1.05	1.44
	SHS 75 × 75 × 3	459.4	508	184000	4	398.89	0.87	3.65	541.3	1.18	1.36
	SHS 100 × 100 × 3	468.7	508	184000	4	430.14	0.92	1.81	635.7	1.36	1.48
	SHS 125 × 125 × 3	480.5	508	184000	4	458.79	0.95	1.14	654.5	1.36	1.43
	SHS 150 × 150 × 3	483.0	508	184000	4	480.90	1.00	0.84	655.3	1.36	1.36
	SHS 200 × 200 × 3	511.9	508	184000	4	501.92	0.98	0.60	696.6	1.36	1.39
Young and Lui (2005)	SHS 40 × 40 × 2	245.3	707	216000	3	203.62	0.83	4.90	246.7	1.01	1.21
	SHS 40 × 40 × 2	238.0	707	216000	3	204.32	0.86	4.86	247.6	1.04	1.21
	SHS 50 × 50 × 1.5	175.7	622	200000	4	134.68	0.77	1.78	192.9	1.10	1.43
	SHS 50 × 50 × 1.5	177.6	622	200000	4	130.24	0.73	1.72	186.3	1.05	1.43
	SHS 150 × 150 × 3	408.6	448	189000	4	385.09	0.94	0.84	511.2	1.25	1.33
	SHS 150 × 150 × 6	1927.4	497	194000	4	1550.53	0.80	3.70	2067.5	1.07	1.33
Liu and Young (2003)	SHS 70 × 70 × 2	194.0	313	195000	4	134.07	0.69	2.68	172.6	0.89	1.29
	SHS 70 × 70 × 2	193.1	313	195000	4	136.04	0.70	2.75	175.0	0.91	1.29
	SHS 70 × 70 × 5	825.3	413	194000	1	500.87	0.61	23.39	795.4	0.96	1.59
	SHS 70 × 70 × 5	843.9	413	194000	1	505.00	0.60	24.21	789.4	0.94	1.56
Gardner (2002)	RHS 60 × 40 × 4	492.0	469	193100	1	316.58	0.64	15.25	482.1	0.98	1.52
	RHS 60 × 40 × 4	497.0	469	193100	1	316.58	0.64	15.13	482.0	0.97	1.52
	RHS 120 × 80 × 3	452.0	429	197300	4	375.18	0.83	1.49	439.6	0.97	1.17
	RHS 120 × 80 × 3	447.0	429	197300	4	370.44	0.83	1.47	436.0	0.98	1.18
	RHS 120 × 80 × 6	1459.0	466	192300	1	981.86	0.67	7.16	1347.6	0.92	1.37
	RHS 120 × 80 × 6	1465.0	466	192300	1	982.33	0.67	7.15	1348.2	0.92	1.37

Table 8.3 (contd.): Comparison between prEN 1993-1-4 (2004) and the proposed design method for stub columns.

Reference	Cross-section designation	Test F_u (kN)	$\sigma_{0.2}$ (N/mm^2)	E_0 (N/mm^2)	Class (1 – 4)	prEN F_u (kN)	prEN F_u/ Test F_u	$\varepsilon_{LB}/\varepsilon_0$	Prop F_u (kN)	Prop F_u/ Test F_u	Prop F_u/ prEN F_u
Gardner (2002)	RHS 150 × 100 × 4	660.0	319	200300	4	504.47	0.76	2.30	594.1	0.90	1.18
	RHS 150 × 100 × 4	659.0	319	200300	4	506.72	0.77	2.31	596.1	0.90	1.18
	RHS 100 × 50 × 2	182.0	370	205900	4	141.35	0.78	1.05	145.5	0.80	1.03
	RHS 100 × 50 × 2	181.0	370	205900	4	140.96	0.78	1.04	145.5	0.80	1.03
	RHS 100 × 50 × 3	407.0	455	200900	4	312.77	0.77	2.06	392.7	0.96	1.26
	RHS 100 × 50 × 3	415.0	455	200900	4	312.77	0.75	2.06	392.7	0.95	1.26
	RHS 100 × 50 × 4	626.0	439	203900	4	432.48	0.69	4.12	555.9	0.89	1.29
	RHS 100 × 50 × 4	627.0	439	203900	4	424.85	0.68	3.97	545.0	0.87	1.28
	RHS 100 × 50 × 6	1217.0	494	206300	1	769.65	0.63	12.65	1150.7	0.95	1.50
	RHS 100 × 50 × 6	1217.0	494	206300	1	770.15	0.63	12.75	1152.4	0.95	1.50
Talja and Salmi (1995)	RHS 150 × 100 × 3	372.0	305	206600	4	319.13	0.86	1.34	369.7	0.99	1.16
	RHS 150 × 100 × 6	1292.0	345	240800	1	925.64	0.72	7.38	1203.2	0.93	1.30
Young and Lui (2005)	RHS 140 × 80 × 3	558.2	486	212000	4	458.30	0.82	1.15	503.2	0.90	1.10
	RHS 160 × 80 × 3	537.3	536	208000	4	441.50	0.82	0.75	451.8	0.84	1.02
	RHS 200 × 110 × 4	957.0	503	200000	4	798.35	0.83	0.93	868.6	0.91	1.09
Young and Liu (2003)	RHS 120 × 40 × 2	187.8	350	198000	4	136.38	0.73	0.86	136.9	0.73	1.00
	RHS 120 × 40 × 2	184.7	350	198000	4	133.61	0.72	0.84	135.1	0.73	1.01
	RHS 120 × 40 × 5.3	969.8	424	194000	3	645.75	0.67	6.28	851.0	0.88	1.32
	RHS 120 × 40 × 5.3	994.7	424	194000	3	642.36	0.65	6.18	846.4	0.85	1.32
	RHS 120 × 80 × 3	404.6	366	193000	4	307.14	0.76	1.55	353.9	0.87	1.15
	RHS 120 × 80 × 3	413.1	366	193000	4	311.63	0.75	1.57	357.3	0.86	1.15
	RHS 120 × 80 × 6	1414.1	443	194000	1	956.44	0.68	8.17	1325.2	0.94	1.39
	RHS 120 × 80 × 6	1387.8	443	194000	1	962.20	0.69	8.42	1338.1	0.96	1.39

Table 8.4: Summary of comparison between prEN 1993-1-4 (2004) and the proposed design method for compression resistance.

Cross-section type	No. of stub columns	prEN F_u / Test F_u		Proposed F_u / Test F_u		Prop F_u / prEN F_u
		Mean	COV	Mean	COV	
Angle	12	0.82	0.09	1.01	0.07	1.24
Channel	11	0.81	0.09	1.01	0.09	1.24
Lipped channel	22	0.86	0.10	0.99	0.07	1.15
I section	20	0.91	0.09	1.04	0.11	1.16
SHS	42	0.77	0.16	1.05	0.13	1.37
RHS	29	0.73	0.10	0.90	0.08	1.24
All sections	**136**	**0.81**	**0.14**	**1.00**	**0.12**	**1.25**
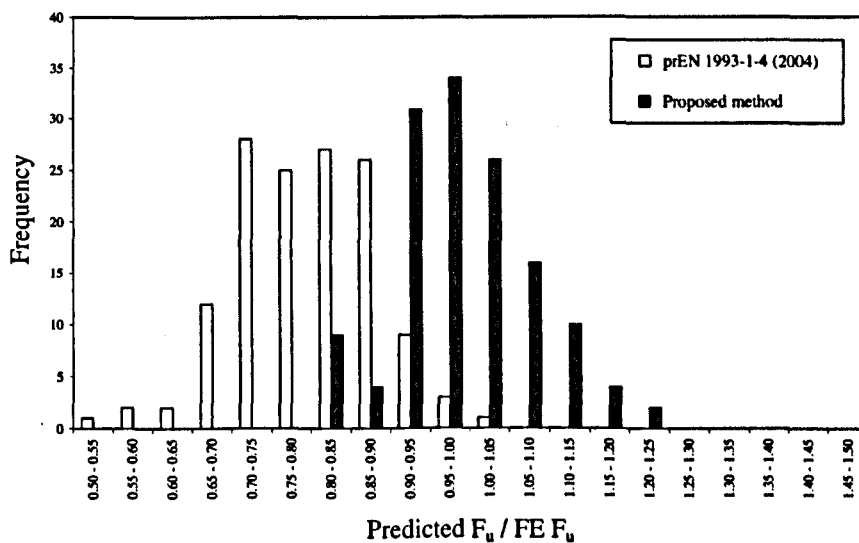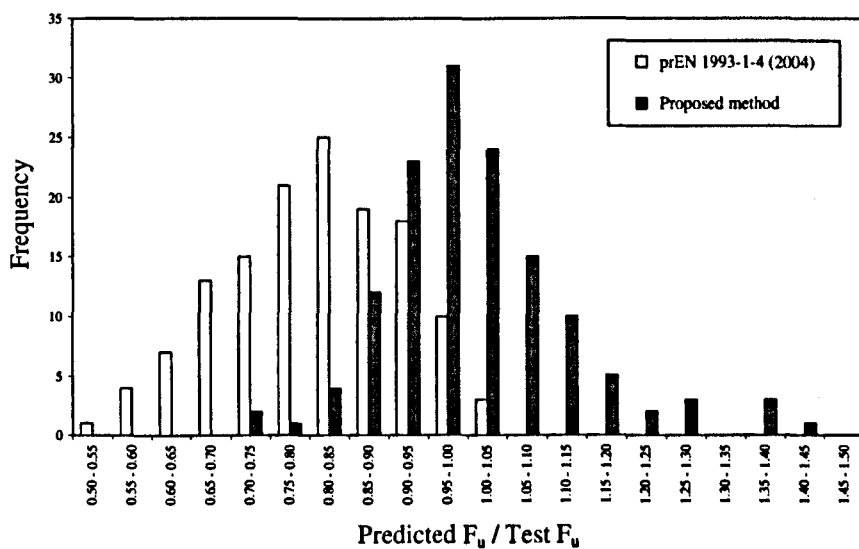
Figure 8.2: Frequency distributions for the predictions of compression resistance using prEN 1993-1-4 (2004) and the proposed design method.

Figure 8.2 presents the frequency distribution for the predictions of the compression resistance using prEN 1993-1-4 (2004) and the proposed design method. This graph clearly shows that most of the Eurocode predictions are lower than the test results, whereas the predictions of the proposed are mostly between the range of 0.90 – 1.10. The scattered overpredictions are significantly reduced when the predicted resistances are compared to the FE results, which are believed to reduce the suspected inconsistencies with some test results as has been explained in Section 6.3.3.

8.3.1.2 Bending resistance $M_{c,Rd}$

Bending resistances of 36 cross-sections have been predicted using the proposed design method and the Eurocode. Table 8.5 presents a detailed comparison between the predictions obtained using prEN 1993-1-4 (2004) and proposed method followed by a summary in Table 8.6. Eurocode predicts the bending resistance with an average of 0.73 and a COV of 0.14, whereas the proposed method predictions are very close to the test results with an average and COV of 0.97 and 0.10 respectively. By adopting the proposed method, an overall increase of 34% in bending resistance has been achieved for the cases considered.

Figure 8.3 represents the frequency distributions of the predictions for bending resistance. Most of the predictions obtained using the proposed method lie within the range of 0.90 – 1.00. The possible reasons for the observed overpredictions have already been discussed in Section 6.3.4.

8.3.1.3 Combined compression plus bending

Only a very limited number of tests – utilising two I sections reported by Stangenberg (2000a) – are available for cross-sections subjected to eccentric compression. Table 8.7 shows a comparison for the predicted ultimate load using prEN 1993-1-4 (2004) and the proposed method. The average predictions using Eurocode and the proposed method are 0.68 and 0.88, which suggests that the proposed method can provide significant material saving in such cases as well. However, this is too limited a comparison to make any general comment on the extent of achievable saving.

Table 8.5: Comparison between prEN 1993-1-4 (2004) and the proposed design method for beams.

Reference	Cross-section designation	Test M_u (kN-m)	$\sigma_{0.2}$ (N/mm²)	E_0 (N/mm²)	Class (1 – 4)	prEN M_u (kN-m)	prEN M_u / Test M_u	$\varepsilon_{LB}/\varepsilon_0$	Prop M_u (kN-m)	Prop M_u / Test M_u	Prop M_u / prEN M_u
Stangenberg (2000a)	I 160x80	54.70	279	200000	1	44.81	0.82	65.97	63.58	1.16	1.42
	I 160x 160	89.50	279	200000	1	78.51	0.88	9.95	87.68	0.98	1.12
	I 320x160	212.70	279	200000	1	188.58	0.89	9.62	206.85	0.97	1.10
	I 160x160	162.50	524	202000	3	129.06	0.79	4.54	160.13	0.99	1.24
Real (2001)	H 100x100	44.10	414	160110	1	35.64	0.81	10.33	43.21	0.98	1.21
	H 100x100	46.50	414	160110	1	35.64	0.77	10.33	43.21	0.93	1.21
Rasmussen and Hancock (1993)	SHS 80×80×3	15.40	440	196000	4	9.56	0.62	3.87	12.66	0.82	1.32
Hyttinen (1994)	SHS 30 x 30 x 2	1.67	435	196000	1	1.11	0.67	20.07	1.52	0.91	1.37
	SHS 40 x 40 x 2	2.75	393	198000	1	1.84	0.67	9.91	2.24	0.81	1.22
	SHS 60 x 60 x 5	17.07	482	194000	1	11.09	0.65	27.36	16.53	0.97	1.49
	SHS 30 x 30 x 2	1.25	498	208000	1	1.18	0.95	17.16	1.51	1.21	1.28
	SHS 40 x 40 x 2	2.15	462	204000	1	2.02	0.94	8.19	2.41	1.12	1.19
	SHS 30 x 30 x 2	1.54	536	213000	1	1.33	0.86	17.83	1.66	1.08	1.25
	SHS 40 x 40 x 2	2.56	511	212000	1	2.27	0.89	8.23	2.67	1.04	1.17
Talja and Salmi (1995)	SHS 60×60×5	15.00	463	186500	1	9.27	0.62	28.93	14.15	0.94	1.53
	SHS 60×60×5	13.50	463	186500	1	9.31	0.69	31.67	14.34	1.06	1.54
	SHS 60×60×5	15.20	463	186500	1	9.23	0.61	29.07	14.04	0.92	1.52
Real (2001)	SHS 80×80×3	13.50	392	165570	4	8.81	0.65	3.35	11.31	0.84	1.28
	SHS 80×80×3	13.05	392	165570	4	8.81	0.68	3.35	11.31	0.87	1.28

Table 8.5 (contd.): Comparison between prEN 1993-1-4 (2004) and the proposed design method for beams.

Reference	Cross-section designation	Test M_u (kN-m)	$\sigma_{0.2}$ (N/mm^2)	E_0 (N/mm^2)	Class (1 – 4)	prEN M_u (kN-m)	prEN M_u / Test M_u	$\varepsilon_{LB}/\varepsilon_0$	Prop M_u (kN-m)	Prop M_u / Test M_u	Prop M_u / prEN M_u
Gardner (2002)	SHS 80×80×4	17.50	416	203200	1	12.85	0.73	8.08	16.70	0.95	1.30
	SHS 100×100×2	8.00	370	207100	4	6.32	0.79	1.04	6.60	0.83	1.05
	SHS 100×100×3	17.20	379	208800	4	11.63	0.68	2.53	14.88	0.86	1.28
	SHS 100×100×4	24.50	437	203200	3	18.73	0.76	4.28	25.86	1.06	1.38
	SHS 100×100×8	44.20	330	205200	1	31.21	0.71	51.17	52.15	1.18	1.67
Talja and Salmi (1995)	RHS 150×100×3	26.30	305	206600	4	17.43	0.66	3.38	23.17	0.88	1.33
	RHS 150×100×3	26.30	305	206600	4	17.41	0.66	3.37	23.14	0.88	1.33
	RHS 150×100×3	26.30	305	206600	4	17.43	0.66	3.38	23.17	0.88	1.33
	RHS 150×100×6	70.50	345	240800	1	46.16	0.65	24.23	66.77	0.95	1.45
	RHS 150×100×6	70.40	345	240800	1	46.16	0.66	24.23	66.77	0.95	1.45
	RHS 150×100×6	70.20	345	240800	1	46.16	0.66	24.30	66.80	0.95	1.45
Real (2001)	RHS 120×80×4	31.85	411	161160	1	24.60	0.77	5.76	29.40	0.92	1.20
	RHS 120×80×4	31.50	411	161160	1	24.60	0.78	5.76	29.40	0.93	1.20
Gardner (2002)	RHS 60×40×4	10.50	469	193100	1	5.90	0.56	50.46	10.27	0.98	1.74
	RHS 100×50×2	7.10	370	205900	3	4.99	0.70	4.65	7.01	0.99	1.41
	RHS 100×50×3	15.40	455	200900	1	11.68	0.76	12.47	16.07	1.04	1.38
	RHS 100×50×4	21.60	439	203900	1	13.88	0.64	27.56	21.34	0.99	1.54

Table 8.6: Summary of comparison between prEN 1993-1-4 (2004) and the proposed design method for bending resistance.

Cross-section type	No. of beams	prEN M_u / Test M_u		Proposed M_u / Test M_u		Prop M_u / prEN M_u
		Mean	COV	Mean	COV	
I section	6	0.83	0.06	1.00	0.08	1.22
SHS	18	0.73	0.15	0.97	0.13	1.34
RHS	12	0.68	0.09	0.95	0.05	1.40
All sections	**36**	**0.73**	**0.14**	**0.97**	**0.10**	**1.34**
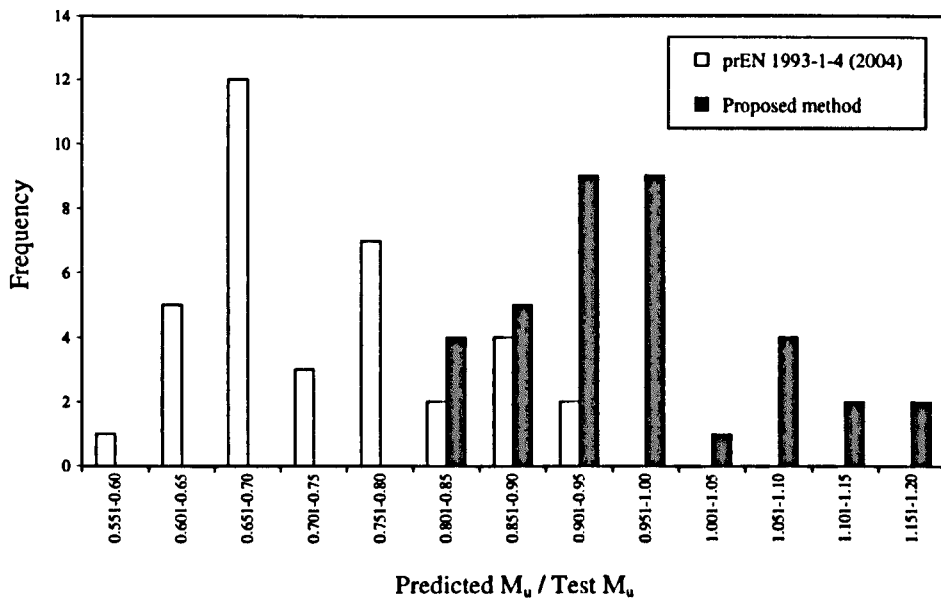
Figure 8.3: Frequency distributions for the predictions of bending resistance using prEN 1993-1-4 (2004) and the proposed design method.

Table 8.7: Comparison between prEN 1993-1-4 (2004) and the proposed design method for cross-sections subjected to combined axial load plus bending.

Cross-section designation	Test F_u (kN)	$\sigma_{0.2}$ (kN/mm^2)	E_0 (kN/mm^2)	prEN F_u / Test F_u	Prop F_u / Test F_u	Prop F_u / prEN F_u
I 160 × 80	503	300	200000	0.62	0.85	1.37
I 160 × 160	711	300	198000	0.75	0.90	1.20
			Average	**0.68**	**0.88**	**1.28**
			COV	**0.13**	**0.04**	

8.3.2 Member resistance

8.3.2.1 Flexural buckling resistance $N_{b,Rd}$

Table 8.8 presents a comparison between the flexural buckling resistances predicted by the Eurocode procedure and the proposed method for all available tests performed on 97 columns with different cross-section types, material grades and boundary conditions. It should be noted that for the pin-ended and the fixed ended columns effective lengths have been taken as 1.0 and 0.5 times the actual length respectively. Table 8.9 provides a summary to compare the performance of prEN 1993-1-4 (2004) and the proposed method in predicting the flexural buckling resistance of stainless steel columns.

The proposed method predicts the test results with an average of 1.00 and a COV of 0.09, whereas prEN 1993-1-4 (2004) gives an average of 0.93 with a COV of 0.12. Figure 8.4 shows the frequency distributions of the predictions compared against test and FE results. Significant reduction in scatter is obvious when the predictions are compared with the FE results, reducing the COV from 0.09 to 0.06. These comparisons suggest that the proposed method could offer, on average, an 8% increase in flexural buckling resistance when compared with the Eurocode approach.

8.3.2.2 Member resistance against combined axial load plus bending

Table 8.10 presents comparisons for the ultimate failure loads predicted by the proposed method and prEN1993-1-4 (2004) with the test results. A total of 61 beam-column tests performed on 4 different cross-section types have been considered. A summary of the comparisons is also given in Table 8.11.

The proposed method, for all the cases considered, produces an average of 0.99 with a COV of 0.09, whereas the existing Eurocode approach gives an average of 0.90 with a very high COV of 0.21. Figure 8.5 gives a clear representation of the performance of the developed method and prEN 1993-1-4 (2004). The observed scatter clearly suggests that the existing Eurocode approach requires modifications to accurately predict the beam-column interaction. The performance of the proposed method, on the other hand, shows that further research could establish this technique into a rational approach for understanding the beam-column interactions in stainless steel.

Table 8.8: Comparison between prEN 1993-1-4 (2004) and the proposed design method for flexural buckling of columns.

Reference [axis of buckling]	Cross-section designation	Test F_u (kN)	Effective length (mm)	$\sigma_{0.2}$ (N/mm^2)	E_0 (N/mm^2)	Class (1 – 4)	$\bar{\lambda}$	prEN F_u / Test F_u	$\varepsilon_{LB}/\varepsilon_0$	$\bar{\lambda}$	Prop F_u / Test F_u	Prop F_u / prEN F_u
Stangenberg (2000b) [Minor]	I 160×80×10×6	627	650	279	200000	1	0.42	0.89	10.75	0.44	0.99	1.10
	I 160×80×10×6	420	1248	279	200000	2	0.79	0.95	9.99	0.83	1.04	1.09
	I 160×80×10×6	270	2046	279	200000	2	1.31	0.84	10.05	1.38	0.89	1.06
	I 160×160×10×6	1120	1248	281	200000	1	0.37	0.87	9.71	0.38	0.96	1.10
	I 160×160×10×6	745	2049	280	199000	1	0.60	1.07	9.70	0.63	1.17	1.10
	I 160×160×10×6	582	3347	281	200000	1	0.97	0.92	9.55	1.02	1.00	1.08
Stangenberg (2000b) [Major]	I 160×80×10×6	668	2048	279	200000	1	0.38	0.90	10.95	0.40	0.97	1.08
	I 160×80×10×6	535	3343	279	200000	1	0.62	0.96	10.81	0.65	1.00	1.04
	I 160×80×10×6	402	5031	279	200000	1	0.93	0.97	10.62	0.97	0.97	1.00
	I 160×160×10×6	1130	2025	279	198000	1	0.35	0.91	9.68	0.37	0.98	1.08
	I 160×160×10×6	860	3348	279	198000	2	0.58	1.03	9.72	0.61	1.07	1.04
	I 160×160×10×6	725	5145	279	199000	1	0.90	0.92	9.91	0.94	0.92	1.00
	I 160×160×10×7	1930	2050	523	201000	3	0.48	1.01	5.31	0.49	1.04	1.03
	I 160×160×10×7	1490	3348	523	201000	3	0.78	1.02	5.34	0.81	1.02	1.00
	I 160×160×10×7	990	5046	523	201000	3	1.19	1.01	5.20	1.23	0.98	0.97
Rasmussen and Hancock (1993)	SHS 80×80×3	390	1001	415	194000	4	0.46	0.87	3.77	0.49	0.97	1.11
	SHS 80×80×3	193	2000	415	194000	4	0.93	1.21	4.08	0.97	1.22	1.01
	SHS 80×80×3	96	3002	415	194000	4	1.38	1.41	3.91	1.46	1.40	0.99
Talja and Salmi (1995)	SHS 60×60×5	417	1050	463	185500	1	0.75	0.85	28.42	0.86	0.96	1.13
	SHS 60×60×5	235	1700	463	181000	1	1.23	0.87	27.47	1.40	0.90	1.03
	SHS 60×60×5	137	2350	463	184000	1	1.69	0.91	28.10	1.92	0.92	1.01

Table 8.8 (contd.): Comparison between prEN 1993-1-4 (2004) and the proposed design method for flexural buckling of columns.

Reference	Cross-section designation	Test F_u (kN)	Effective length (mm)	$\sigma_{0.2}$ (N/mm^2)	E_0 (N/mm^2)	Class (1 – 4)	$\bar{\lambda}$	prEN F_u / Test F_u	$\varepsilon_{LB}/\varepsilon_0$	$\bar{\lambda}$	Prop F_u / Test F_u	Prop F_u / prEN F_u
Ala-outinen (1997)	SHS 40×40×4	184	889	592	197980	1	1.08	0.89	40.52	1.27	0.96	1.07
	SHS 40×40×4	184	888	592	197980	1	1.08	0.89	40.52	1.27	0.96	1.07
Gardner (2002)	SHS 80×80×4	307	1900	416	186600	1	0.93	0.94	7.15	1.00	0.97	1.03
	SHS 80×80×4	293	2001	416	186600	1	0.98	0.94	7.39	1.06	0.97	1.03
	SHS 100×100×2	176	2000	370	201300	4	0.53	0.84	1.04	0.63	1.09	1.29
	SHS 100×100×3	350	2000	379	195800	4	0.65	0.83	2.34	0.72	0.94	1.13
	SHS 100×100×4	464	2000	437	191300	3	0.78	0.99	3.90	0.82	1.02	1.03
	SHS 100×100×6	842	2000	473	198400	1	0.82	0.87	12.40	0.90	0.93	1.08
	SHS 100×100×8	770	2000	330	202400	1	0.69	0.96	50.19	0.80	1.12	1.17
	SHS 150×150×4	692	2000	294	206000	4	0.37	0.78	2.51	0.41	0.93	1.19
Liu and Young (2003)	SHS 70×70×2	190	600	313	195000	4	0.26	0.72	2.70	0.28	0.91	1.27
	SHS 70×70×2	188	1000	313	195000	4	0.43	0.73	2.80	0.47	0.86	1.18
	SHS 70×70×2	159	1400	313	195000	4	0.60	0.75	2.69	0.66	0.86	1.14
	SHS 70×70×2	115	1800	313	195000	4	0.77	0.91	2.73	0.85	0.99	1.09
	SHS 70×70×5	669	600	413	194000	1	0.33	0.75	23.39	0.38	1.05	1.41
	SHS 70×70×5	510	1000	413	194000	1	0.56	0.89	24.11	0.63	1.05	1.18
	SHS 70×70×5	407	1400	413	194000	1	0.78	0.92	24.11	0.88	1.02	1.11
	SHS 70×70×5	281	1800	413	194000	1	1.00	1.04	23.39	1.13	1.09	1.05

Table 8.8 (contd.): Comparison between prEN 1993-1-4 (2004) and the proposed design method for flexural buckling of columns.

Reference	Cross-section designation	Test F_u (kN)	Effective length (mm)	$\sigma_{0.2}$ (N/mm²)	E_0 (N/mm²)	Class (1 – 4)	$\bar{\lambda}$	prEN F_u / Test F_u	$\varepsilon_{LB}/\varepsilon_0$	$\bar{\lambda}$	Prop F_u / Test F_u	Prop F_u / prEN F_u
Talja and Salmi (1995) [Major]	RHS 150×100×3	349	2700	305	197200	4	0.53	0.87	1.29	0.58	1.02	1.17
	RHS 150×100×3	254	4350	305	197200	4	0.85	0.91	1.29	0.93	1.01	1.12
	RHS 150×100×3	189	6000	305	197200	4	1.17	0.84	1.29	1.28	0.90	1.07
	RHS 150×100×6	830	2700	345	193600	1	0.66	0.94	5.84	0.70	1.04	1.11
	RHS 150×100×6	488	4350	345	193600	1	1.06	1.04	5.55	1.13	1.11	1.07
	RHS 150×100×6	306	6000	345	193600	1	1.46	1.04	5.55	1.56	1.08	1.04
Gardner [Major]	RHS 60×40×4	109	2000	469	192800	1	1.47	0.98	15.22	1.64	1.03	1.06
	RHS 100×50×2	157	2000	370	208000	4	0.64	0.77	1.04	0.68	0.86	1.12
Gardner (2002) [Minor]	RHS 100×50×3	113	2000	455	203600	4	1.35	1.09	2.06	1.47	1.16	1.06
	RHS 100×50×4	165	2000	439	208000	4	1.43	0.95	4.13	1.51	0.99	1.04
	RHS 100×50×6	234	2000	494	187200	1	1.69	0.89	11.19	1.86	0.93	1.05
	RHS 120×80×3	313	1999	429	209300	4	0.80	0.92	1.57	0.86	1.02	1.10
	RHS 120×80×6	677	2000	466	194500	1	0.98	0.87	7.32	1.07	0.94	1.09
	RHS 150×100×4	515	2000	319	205800	4	0.58	0.89	2.33	0.62	0.98	1.10
	RHS 60×40×4	169	1000	469	192800	1	1.02	1.07	15.17	1.13	1.18	1.10
	RHS 100×50×2	163	1000	370	208000	4	0.54	0.80	1.03	0.58	0.90	1.13
	RHS 100×50×3	304	1000	455	203600	4	0.68	0.86	2.05	0.74	0.98	1.14
	RHS 100×50×4	422	1000	439	208000	4	0.71	0.84	4.22	0.75	0.93	1.10
	RHS 100×50×6	624	1000	494	187200	1	0.84	0.86	11.09	0.93	0.97	1.13
	RHS 120×80×3	448	1001	429	209300	4	0.40	0.86	1.51	0.43	0.98	1.14

Table 8.8 (contd.): Comparison between prEN 1993-1-4 (2004) and the proposed design method for flexural buckling of columns.

Reference	Cross-section designation	Test F_u (kN)	Effective length (mm)	$\sigma_{0.2}$ (N/mm^2)	E_0 (N/mm^2)	Class (1 – 4)	$\bar{\lambda}$	prEN F_u / Test F_u	$\varepsilon_{LB}/\varepsilon_0$	$\bar{\lambda}$	Prop F_u / Test F_u	Prop F_u / prEN F_u
Young and Liu (2003) [Minor]	RHS 120×40×2	167	1199	326	198000	4	0.36	0.77	0.89	0.40	0.95	1.23
	RHS 120×40×2	141	2000	326	198000	4	0.61	0.80	0.90	0.67	0.94	1.18
	RHS 120×40×2	96	2800	326	198000	4	0.85	0.95	0.92	0.94	1.07	1.13
	RHS 120×40×2	84	3600	326	198000	4	1.09	0.81	0.91	1.21	0.88	1.09
	RHS 120×40×5.3	717	1200	394	194000	3	0.54	0.77	6.95	0.58	0.86	1.13
	RHS 120×40×5.3	417	2000	394	194000	3	0.90	0.94	6.80	0.96	1.03	1.09
	RHS 120×40×5.3	261	2801	394	194000	3	1.26	0.99	6.86	1.35	1.04	1.06
	RHS 120×40×5.3	164	3600	394	194000	3	1.62	1.06	6.80	1.73	1.10	1.04
	RHS 120×80×3	398	1200	340	193000	4	0.22	0.77	1.72	0.24	0.87	1.12
	RHS 120×80×3	394	2000	340	193000	4	0.37	0.77	1.69	0.40	0.89	1.16
	RHS 120×80×3	337	2799	340	193000	4	0.53	0.88	1.87	0.57	1.00	1.13
	RHS 120×80×3	311	3598	340	193000	4	0.68	0.85	1.83	0.72	0.94	1.12
	RHS 120×80×6	1222	1200	412	194000	1	0.28	0.73	9.13	0.30	1.02	1.39
	RHS 120×80×6	970	2000	412	194000	1	0.46	0.89	9.18	0.50	1.03	1.16
	RHS 120×80×6	860	2800	412	194000	1	0.65	0.87	8.88	0.70	0.99	1.14
	RHS 120×80×6	612	3600	412	194000	1	0.83	1.05	9.54	0.91	1.17	1.12
Rhodes et al (2000) [Minor]	CL 28×15×8×2.5	4	1222	446	200000	1	3.58	1.01	42.97	4.09	1.00	0.99
	CL 28×15×8×2.5	5	1122	446	200000	1	3.29	1.10	42.97	3.76	1.09	0.99
	CL 28×15×8×2.5	7	1022	446	200000	1	3.00	0.90	42.97	3.42	0.89	0.99

Table 8.8 (contd.): Comparison between prEN 1993-1-4 (2004) and the proposed design method for flexural buckling of columns.

Reference	Cross-section designation	Test F_u (kN)	Effective length (mm)	$\sigma_{0.2}$ (N/mm^2)	E_0 (N/mm^2)	Class (1 – 4)	$\bar{\lambda}$	prEN F_u / Test F_u	$\varepsilon_{LB}/\varepsilon_0$	$\bar{\lambda}$	Prop F_u / Test F_u	Prop F_u / prEN F_u
	CL 28×15×8×2.5	8	922	446	200000	1	2.70	0.95	42.97	3.09	0.94	0.99
	CL 28×15×8×2.5	9	822	446	200000	1	2.41	1.04	42.97	2.75	1.03	0.99
	CL 28×15×8×2.5	11	722	446	200000	1	2.12	1.04	42.97	2.42	1.03	0.99
	CL 28×15×8×2.5	16	622	446	200000	1	1.82	0.97	42.97	2.08	0.96	0.99
	CL 28×15×8×2.5	19	522	446	200000	1	1.53	1.06	42.97	1.75	1.05	0.99
	CL 28×15×8×2.5	28	422	446	200000	1	1.24	0.99	42.97	1.41	0.99	0.99
	CL 28×15×8×2.5	39	322	446	200000	1	0.94	1.03	42.97	1.08	1.05	1.02
	CL 28×15×8×2.5	53	222	446	200000	1	0.65	1.02	42.97	0.74	1.12	1.09
Rhodes et al (2000) [Minor]	CL 38×17×10×3	9	1222	428	200000	1	3.02	0.99	35.92	3.42	0.98	0.99
	CL 38×17×10×3	11	1122	428	200000	1	2.77	1.02	35.92	3.14	1.01	0.99
	CL 38×17×10×3	13	1022	428	200000	1	2.52	1.03	35.92	2.86	1.02	0.99
	CL 38×17×10×3	16	922	428	200000	1	2.28	0.97	35.92	2.58	0.96	0.99
	CL 38×17×10×3	20	822	428	200000	1	2.03	0.95	35.92	2.30	0.94	0.99
	CL 38×17×10×3	23	722	428	200000	1	1.78	1.07	35.92	2.02	1.05	0.99
	CL 38×17×10×3	29	622	428	200000	1	1.54	1.06	35.92	1.74	1.04	0.99
	CL 38×17×10×3	38	522	428	200000	1	1.29	1.07	35.92	1.46	1.06	0.99
	CL 38×17×10×3	60	422	428	200000	1	1.04	0.91	35.92	1.18	0.91	1.00
	CL 38×17×10×3	85	322	428	200000	1	0.80	0.85	35.92	0.90	0.88	1.04
	CL 38×17×10×3	114	222	428	200000	1	0.55	0.78	35.92	0.62	0.87	1.11

Table 8.9: Summary of comparisons between prEN 1993-1-4 (2004) and the proposed design method for flexural buckling resistance.

Cross-section type	No. of columns	prEN F_u / Test F_u		Proposed F_u / Test F_u		Prop F_u / prEN F_u
		Mean	COV	Mean	COV	
I section	15	0.95	0.07	1.00	0.07	1.05
SHS	24	0.91	0.17	1.00	0.12	1.12
RHS	36	0.89	0.11	0.99	0.08	1.12
Lipped channel	22	0.99	0.08	1.00	0.07	1.00
All sections	**97**	**0.93**	**0.12**	**1.00**	**0.09**	**1.08**

Figure 8.4: Frequency distributions for the predictions of flexural buckling resistance using prEN 1993-1-4 (2004) and the proposed design method.

Table 8.10: Comparison between prEN 1993-1-4 (2004) and the proposed design method for members subjected to combined axial load plus bending.

Reference [buckling axis]	Cross-section designation	Test F_u (kN)	Effective length (mm)	$\sigma_{0.2}$ (N/mm²)	E_0 (N/mm²)	$\bar{\lambda}$	κ	prEN F_u / Test F_u	$\bar{\lambda}$	κ	Prop F_u / Test F_u	Prop F_u / prEN F_u
Satngenberg (2000b) [Major]	I 160×80×10×6	338	2045	279	198000	0.37	1.50	0.67	0.39	0.94	1.14	1.69
	I 160×80×10×6	270	3339	279	198000	0.61	1.50	0.79	0.65	1.20	1.15	1.46
	I 160×80×10×6	222	5041	279	198000	0.93	1.50	0.86	0.98	1.53	1.05	1.23
	I 160×160×10×6	540	2048	279	198000	0.35	1.50	0.74	0.37	0.92	1.10	1.48
	I 160×160×10×6	454	3345	279	198000	0.58	1.50	0.84	0.61	1.16	1.07	1.28
	I 160×160×10×6	356	5043	279	198000	0.88	1.50	0.96	0.93	1.48	1.06	1.10
Rhodes et al (2000) [Minor]	CL 28×15×8×2.5	3.26	1222	446.4	200000	3.58	1.50	1.14	4.18	4.73	1.01	0.88
	CL 28×15×8×2.5	3.69	1122	446.4	200000	3.29	1.50	1.15	3.84	4.39	1.02	0.88
	CL 28×15×8×2.5	4.35	1022	446.4	200000	3.00	1.50	1.13	3.49	4.04	1.00	0.89
	CL 28×15×8×2.5	4.95	922	446.4	200000	2.70	1.50	1.15	3.15	3.70	1.03	0.89
	CL 28×15×8×2.5	6.18	822	446.4	200000	2.41	1.50	1.08	2.81	3.36	0.99	0.92
	CL 28×15×8×2.5	7.40	722	446.4	200000	2.12	1.50	1.06	2.47	3.02	0.99	0.93
	CL 28×15×8×2.5	9.22	622	446.4	200000	1.82	1.50	1.01	2.13	2.68	0.99	0.98
	CL 28×15×8×2.5	11.46	522	446.4	200000	1.53	1.50	0.96	1.78	2.33	0.99	1.03
	CL 28×15×8×2.5	14.76	422	446.4	200000	1.24	1.50	0.88	1.44	1.99	1.00	1.14
	CL 28×15×8×2.5	18.70	322	446.4	200000	0.94	1.50	0.81	1.10	1.65	1.04	1.29
	CL 28×15×8×2.5	24.30	222	446.4	200000	0.65	1.50	0.69	0.76	1.31	1.08	1.57
	CL 38×17×10×3	6.93	1222	427.8	200000	3.02	1.50	1.11	3.49	4.04	1.00	0.90
	CL 38×17×10×3	7.77	1122	427.8	200000	2.77	1.50	1.13	3.21	3.76	1.02	0.90
	CL 38×17×10×3	9.12	1022	427.8	200000	2.52	1.50	1.11	2.92	3.47	1.01	0.91
	CL 38×17×10×3	10.99	922	427.8	200000	2.28	1.50	1.06	2.64	3.19	0.98	0.93

Table 8.10 (contd): Comparison between prEN 1993-1-4 (2004) and the proposed design method for members subjected to combined axial load plus bending.
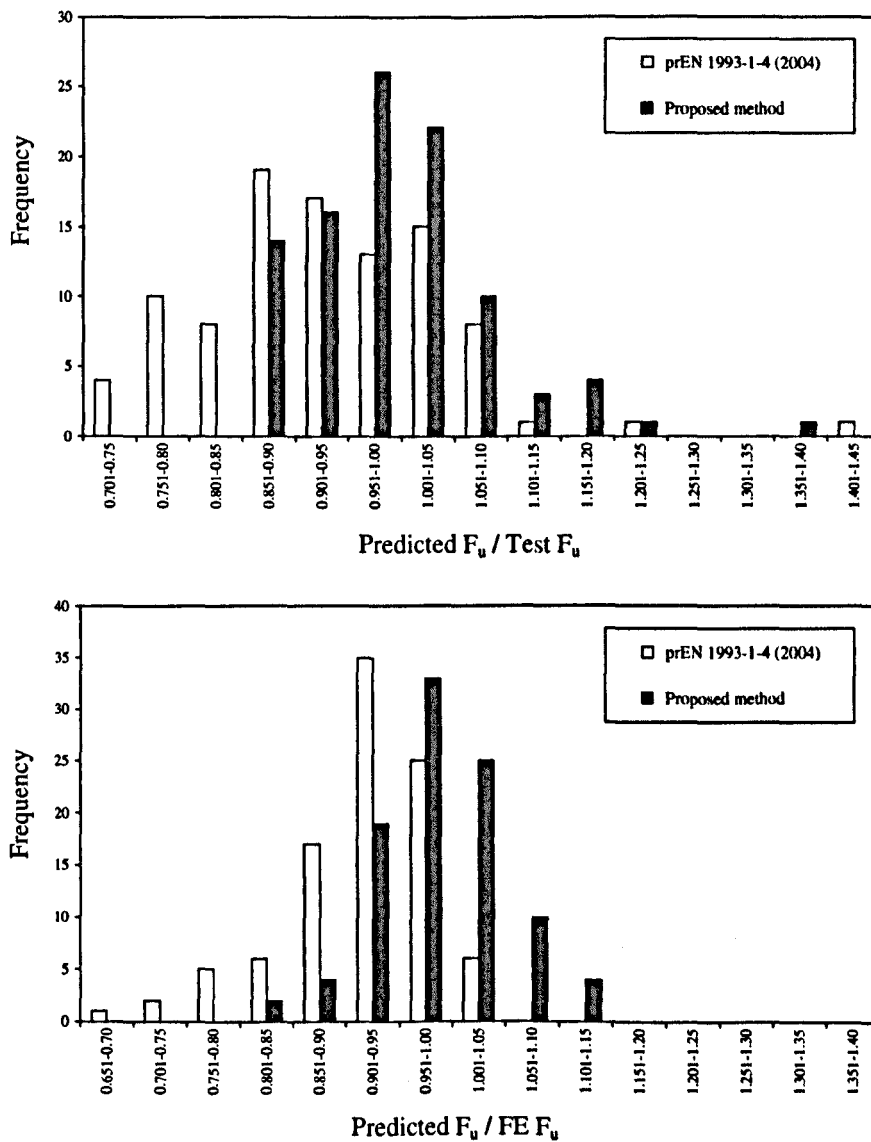
Reference	Cross-section designation	Test F_u (kN)	Effective length (mm)	$\sigma_{0.2}$ (N/mm²)	E_0 (N/mm²)	$\bar{\lambda}$	κ	prEN F_u / Test F_u	$\bar{\lambda}$	κ	Prop F_u / Test F_u	Prop F_u / prEN F_u
Rhodes et al (2000) [Minor]	CL 38×17×10×3	13.16	822	427.8	200000	2.03	1.50	1.03	2.35	2.90	0.97	0.94
	CL 38×17×10×3	15.18	722	427.8	200000	1.78	1.50	1.04	2.06	2.61	1.01	0.97
	CL 38×17×10×3	18.39	622	427.8	200000	1.54	1.50	1.01	1.78	2.33	1.02	1.02
	CL 38×17×10×3	22.75	522	427.8	200000	1.29	1.50	0.95	1.49	2.04	1.03	1.08
	CL 38×17×10×3	31.89	422	427.8	200000	1.04	1.50	0.78	1.21	1.76	0.93	1.19
	CL 38×17×10×3	40.85	322	427.8	200000	0.80	1.50	0.69	0.92	1.47	0.94	1.36
	CL 38×17×10×3	53.60	222	427.8	200000	0.55	1.50	0.57	0.63	1.18	0.91	1.61
Hyttinen (1994)	SHS 30×30×2	6.75	2203	468	196000	3.02	1.50	1.09	3.41	3.96	0.91	0.83
	SHS 30×30×2	4.40	2203	468	196000	3.02	1.50	0.96	3.41	1.50	1.17	1.22
	SHS 30×30×2	2.50	2202	468	196000	3.02	1.50	0.70	3.40	1.50	0.95	1.35
	SHS 40×40×2	16.31	2215	423	198000	2.11	1.50	0.97	2.30	2.85	0.85	0.87
	SHS 40×40×2	10.00	2211	423	198000	2.10	1.50	0.83	2.30	1.50	0.98	1.18
	SHS 40×40×2	4.90	2215	423	198000	2.10	1.50	0.64	2.30	1.50	0.81	1.26
	SHS 60×60×5	75.19	2351	518	194000	1.75	1.50	1.06	2.05	2.60	1.04	0.99
	SHS 60×60×5	40.16	2351	518	194000	1.75	1.50	0.89	2.05	1.50	1.23	1.38
	SHS 60×60×5	16.29	2350	518	194000	1.75	1.50	0.64	2.05	1.50	0.98	1.53
	SHS 30×30×2	5.84	2203	498	208000	3.00	1.50	1.34	3.24	3.79	1.07	0.80
	SHS 30×30×2	4.50	2203	498	208000	3.00	1.50	1.00	3.24	1.50	1.12	1.12
	SHS 30×30×2	2.32	2205	498	208000	3.01	1.50	0.80	3.24	1.50	0.97	1.21

Table 8.10 (contd): Comparison between prEN 1993-1-4 (2004) and the proposed design method for members subjected to combined axial load plus bending.

Reference	Cross-section designation	Test F_u (kN)	Effective length (mm)	$\sigma_{0.2}$ (N/mm²)	E_0 (N/mm²)	$\bar{\lambda}$	κ	prEN F_u / Test F_u	$\bar{\lambda}$	κ	Prop F_u / Test F_u	Prop F_u / prEN F_u
Hyttinen (1994)	SHS 40×40×2	14.54	2210	462	204000	2.15	1.50	1.13	2.28	2.83	0.95	0.84
	SHS 40×40×2	9.00	2210	462	204000	2.15	1.50	0.94	2.27	1.50	1.04	1.11
	SHS 40×40×2	4.46	2210	462	204000	2.15	1.50	0.74	2.27	1.50	0.84	1.14
	SHS 30×30×2	7.31	2212	536	213000	3.08	1.50	1.14	3.33	3.88	0.92	0.80
	SHS 30×30×2	4.83	2210	536	213000	3.08	1.50	1.00	3.32	1.50	1.14	1.13
	SHS 30×30×2	2.52	2211	536	213000	3.08	1.50	0.81	3.33	1.50	0.98	1.20
	SHS 40×40×2	16.69	2209	511	212000	2.23	1.50	1.07	2.36	2.91	0.90	0.84
	SHS 40×40×2	9.94	2209	511	212000	2.24	1.50	0.96	2.37	1.50	1.06	1.11
	SHS 40×40×2	4.66	2209	511	212000	2.24	1.50	0.80	2.37	1.50	0.92	1.16
Talja and Salmi (1995)	SHS 60×60×5	322	400	463	187000	0.29	1.50	0.49	0.33	0.88	1.12	2.28
	SHS 60×60×5	210	1050	463	187000	0.75	1.50	0.69	0.87	1.42	0.99	1.43
	SHS 60×60×5	125	1700	506	184000	1.28	1.50	0.94	1.48	2.03	1.02	1.09
	SHS 60×60×5	83	2350	506	184000	1.77	1.50	1.02	2.04	2.59	1.00	0.98
Talja and Salmi (1995) [Major]	RHS 150×100×3	209	1050	305	205000	0.20	1.50	0.51	0.21	0.76	0.87	1.71
	RHS 150×100×3	173	2700	305	205000	0.51	1.50	0.60	0.55	1.10	0.86	1.43
	RHS 150×100×3	134	4350	305	205000	0.83	1.50	0.70	0.89	1.44	0.83	1.18
	RHS 150×100×3	95	6000	305	205000	1.14	1.50	0.84	1.22	1.77	0.87	1.03
	RHS 150×100×6	569	1050	356	242000	0.23	1.50	0.54	0.25	0.80	1.08	1.98
	RHS 150×100×6	403	2700	309	198000	0.62	1.50	0.64	0.66	1.21	0.89	1.39
	RHS 150×100×6	267	4350	356	242000	0.96	1.50	0.97	1.03	1.58	1.10	1.14
	RHS 150×100×6	192	6000	356	242000	1.33	1.50	1.08	1.42	1.97	1.09	1.01

Table 8.11: Summary of comparisons between prEN 1993-1-4 (2004) and the proposed design method for member resistance against combined axial load plus bending.

Cross-section type	No of members	prEN F_u / Test F_u		Proposed F_u / Test F_u		Prop F_u / prEN F_u
		Mean	COV	Mean	COV	
I section	6	0.81	0.12	1.10	0.04	1.37
Lipped channel	22	0.98	0.17	1.00	0.04	1.06
SHS	25	0.91	0.21	1.00	0.11	1.15
RHS	8	0.74	0.28	0.95	0.13	1.36
All sections	**61**	**0.90**	**0.21**	**1.00**	**0.09**	**1.17**
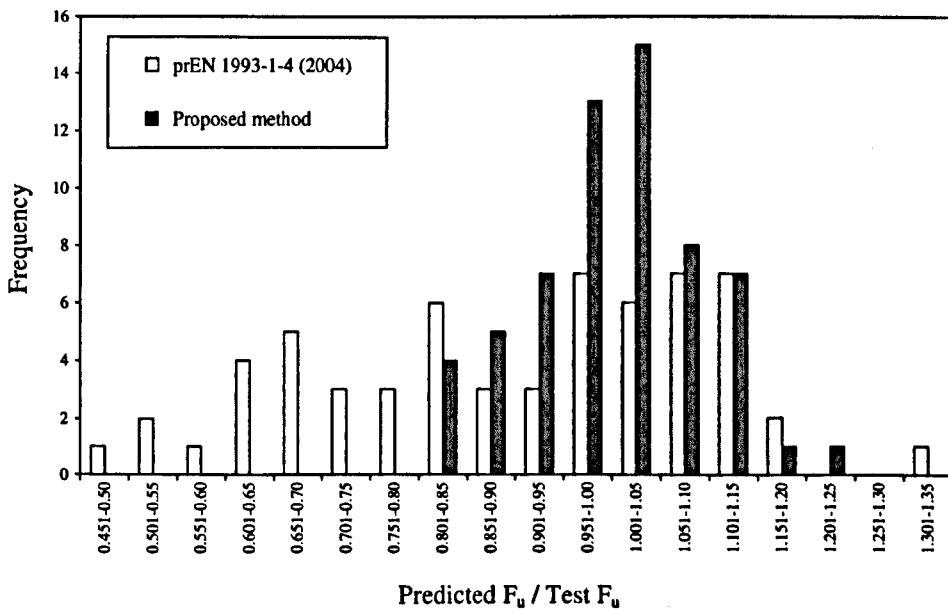
Figure 8.5: Frequency distributions for the predictions of member resistance against combined axial load plus bending using prEN 1993-1-4 (2004) and the proposed design method.

8.4 WORKED EXAMPLES

This section presents some worked examples to demonstrate the application of the proposed design method for different types of cross-sections and loading conditions. Detailed calculations are shown herein to make clear the various steps in each case. For the Design Example 07, which represents the most general case of beam-column interaction, calculations have been provided using both the proposed method and prEN 1993-1-4 (2004) guidelines to demonstrate a comparison of the volume of calculations required.

8.4.1 Compression resistance

Two different examples have been chosen to explain the method for angle and lipped channel sections produced from two different grades of stainless steel.

DESIGN EXAMPLE 01

Compression resistance of an angle section L 40×40×3 tested by Kuwamura (2003).

Cross- section properties:
Press-braked cross-section
B = $40.05\,mm$
t = $2.93\,mm$ $\qquad r_i$ = $4.1\,mm$ $\qquad r_o$ = $7.03\,mm$
A_g = $217.40\,mm^2$ $\qquad A_c$ = $\pi/4\,(7.03^2\text{-}4.1^2) = 25.30\,mm^2$

Material properties:
Austenitic Grade 1.4301
$\sigma_{0.2} = 279\,N/mm^2$ $\qquad E_0 = 200000\,N/mm^2$ $\qquad \varepsilon_0 = 279/200000 = 0.0014$

Cross-section slenderness β:

$$\beta = \left(\frac{b}{t}\right)\sqrt{\frac{\sigma_{0.2}}{E_0}}\sqrt{\frac{4.0}{k}} = \frac{\left(40.05-2.93/2\right)}{2.93}\times\sqrt{\frac{279}{200000}}\times\sqrt{\frac{4.0}{0.43}} = 1.50$$

Deformation capacity ε_{LB}:

$$\frac{\varepsilon_{LB}}{\varepsilon_0} = \frac{6.44}{\beta^{2.85-0.27\beta}} = \frac{6.44}{1.50^{2.85-0.27\times1.50}} = 2.39$$

$$\therefore \varepsilon_{LB} = 2.39 \times 0.0014 = 0.0033$$

Local buckling stress σ_{LB}:
For austenitic Grade 1.4301 and press-braked cross-sections, the compound Ramberg-Osgood parameters are:
$n = 5.3$ $\qquad n'_{0.2,1.0} = 2.5$ $\qquad \sigma_{1.0}/\sigma_{0.2} = 1.20$
Using this material definition, $\sigma_{LB} = 274\,N/mm^2$
Alternatively, σ_{LB} can be directly obtained using Table A.1 by linear interpolation.

Corner enhancement factor ϕ_c:
For press braked sections

$$\phi_c = 1+\left[\frac{1.881}{(r_i/t)^{0.194}}-1\right]k_{cor} = 1+\left[\frac{1.881}{(4.1/2.93)^{0.194}}-1\right]\times\left(\frac{25.30}{217.40}\right) = 1.09$$

Compression resistance $N_{c,Rd}$:
$N_{c,Rd} = \phi_c\,A_g\,\sigma_{LB} = 1.09 \times 217.40 \times 274 \times 10^{-3} = 64.92\,kN$

[Test ultimate load = 66.90 kN
 prEN 1993-1-4 (2004) predicted compression resistance = 53.96 kN]

DESIGN EXAMPLE 02

Compression resistance of a lipped channel section CL 105×85×15×2 tested by Lecce and Rasmussen (2004a).

Cross- section properties:
Press-braked cross-section

D	=	105.00 mm	B = 85.40 mm		Lip	= 14.80 mm
t	=	1.98 mm	r_i = 4.0 mm		r_o	= 5.98 mm

A_g = 555.00 mm² $\qquad A_c = \pi(5.98^2 - 4.0^2) = 62.08$ mm²

Material properties
Ferritic Grade 1.4003

$\sigma_{0.2} = 339$ N/mm² $\qquad E_0 = 208000$ N/mm² $\qquad \varepsilon_0 = 339/208000 = 0.0016$

Cross-section slenderness β:

$$\beta_{web} = \left(\frac{b}{t}\right)\sqrt{\frac{\sigma_{0.2}}{E_0}}\sqrt{\frac{4.0}{k}} = \frac{(105-1.98)}{1.98}\times\sqrt{\frac{339}{208000}}\times\sqrt{\frac{4.0}{4.0}} = 2.08$$

$$\beta_{flange} = \left(\frac{b}{t}\right)\sqrt{\frac{\sigma_{0.2}}{E_0}}\sqrt{\frac{4.0}{k}} = \frac{(85.4-1.98)}{1.98}\times\sqrt{\frac{339}{208000}}\times\sqrt{\frac{4.0}{4.0}} = 1.69$$

$$\beta_{lip} = \left(\frac{b}{t}\right)\sqrt{\frac{\sigma_{0.2}}{E_0}}\sqrt{\frac{4.0}{k}} = \frac{(14.8-1.98/2)}{1.98}\times\sqrt{\frac{339}{208000}}\times\sqrt{\frac{4.0}{0.43}} = 0.85$$

∴ *Cross-section slenderness β = 2.08*

Deformation capacity ε_{LB}:

$$\frac{\varepsilon_{LB}}{\varepsilon_0} = \frac{6.44}{\beta^{2.85-0.27\beta}} = \frac{6.44}{2.08^{2.85-0.27\times2.08}} = 1.21$$

∴ $\varepsilon_{LB} = 1.21 \times 0.0016 = 0.0019$

Local buckling stress σ_{LB}:
For ferritc Grade 1.4003 and press-braked cross-sections, the compound Ramberg-Osgood parameters are:

$n = 7.3$ $\qquad\qquad n'_{0.2,1.0} = 3.3$ $\qquad\qquad \sigma_{1.0}/\sigma_{0.2} = 1.14$

Using this material definition, $\sigma_{LB} = 274$ N/mm²

[alternatively, σ_{LB} can be directly obtained using Table A..4 by linear interpolation.]

Corner enhancement factor ϕ_c:
For press braked sections

$$\phi_c = 1 + \left[\frac{1.881}{(r_i/t)^{0.194}} - 1\right]k_{cor} = 1 + \left[\frac{1.881}{(4.0/1.98)^{0.194}} - 1\right]\times\left(\frac{62.08}{555}\right) = 1.07$$

Compression resistance $N_{c,Rd}$:
$N_{c,Rd} = \phi_c A_g \sigma_{LB} = 1.07 \times 555 \times 274 \times 10^{-3} = 162.71$ kN

[Test ultimate load = 162 kN
prEN 1993-1-4 (2004) predicted compression resistance = 132.12 kN]

8.4.2 Bending resistance (in-plane) $M_{c,Rd}$

DESIGN EXAMPLE 03

Bending resistance of an I section I 160×160×10×6 tested by Stangenberg (2000a).

Cross- section properties:
Welded cross-section
D = $159.2\,mm$ B = $161.7\,mm$
t_f = $10.06\,mm$ t_w = $6.8\,mm$ $a\ (weld\text{-}size) = 3.0\,mm$
A_g = $4199\,mm^2$

Material properties
Duplex Grade 1.4462
$\sigma_{0.2}$ = $523\,N/mm^2$ $E_0 = 202000\,N/mm^2$ $\varepsilon_0 = 523/202000 = 0.0026$

Cross-section slenderness β:

$$\beta_{web} = \left(\frac{b}{t}\right)\sqrt{\frac{\sigma_{0.2}}{E_0}}\sqrt{\frac{4.0}{k}} \quad = \frac{(159.2 - 2\times10.06 - 2\times3.0)}{6.8}\times\sqrt{\frac{523}{202000}}\times\sqrt{\frac{4.0}{23.9}} = 0.41$$

$$\beta_{flange} = \left(\frac{b}{t}\right)\sqrt{\frac{\sigma_{0.2}}{E_0}}\sqrt{\frac{4.0}{k}} \quad = \frac{(161.7-6.8)/2 - 3.0}{10.06}\times\sqrt{\frac{523}{202000}}\times\sqrt{\frac{4.0}{0.43}} = 1.15$$

∴ *Cross-section slenderness* β = 1.15

Deformation capacity ε_{LB}:

$$\frac{\varepsilon_{LB}}{\varepsilon_0} = \frac{6.44}{\beta^{2.85-0.27\beta}} = \frac{6.44}{1.15^{2.85-0.27\times1.15}} = 4.52$$

∴ $\varepsilon_{LB} = 4.52\times0.0026 = 0.0117$

Geometric shape factor a_g:
W_{el} = $246772\,mm^3$ W_{pl} = $275490\,mm^3$ ∴ $a_p = 275490/246772 = 1.12$
Using Table B.6, for ε_{LB} = 0.0117 the constants for generalised shape factor a_g are:
$A_1 = 0.071$ $A_2 = 29.09$ $A_3 = 1.081$ $A_4 = -39.36$
∴ a_g = $A_1 + A_2\varepsilon_0 + A_3 a_p + A_4\varepsilon_0 a_p$
        = $0.071 + 29.09\times0.0026 + 1.081\times1.12 - 39.36\times0.0026\times1.12 = 1.24$

Corner enhancement factor ϕ_c:
For I sections, $\phi_c = 1.0$

Bending resistance $M_{c,Rd}$:
$M_{c,Rd} = \phi_c\,a_g\,W_{el}\,\sigma_{0.2} = 1.0\times1.24\times246772\times523\times10^{-6} = 160.04\,kN\,m$

[Test ultimate load = 162.50 kN m
prEN 1993-1-4 (2004) predicted bending resistance = 129.06 kN m]

DESIGN EXAMPLE 04

Bending resistance of a Rectangular hollow section RHS 150×100×6 tested by Talja and Salmi (1995).

Cross- section properties:
Press-braked cross-section

D = 149.8 mm $\qquad$ B = 100.1 mm

t = 5.85 mm $\qquad$ r_i = 4.5 mm $\qquad$ r_o = 10.35 mm

A_g = 2713 mm² $\qquad$ A_c = $\pi(10.35^2 - 4.5^2) = 272.92$ mm²

Material properties
Austenitic Grade 1.4301

$\sigma_{0.2}$ = 345 N/mm² $\qquad$ $E_0 = 240800$ N/mm² $\qquad$ ε_0 = 345/240800 = 0.0014

Cross-section slenderness β:

$$\beta_{web} = \left(\frac{b}{t}\right)\sqrt{\frac{\sigma_{0.2}}{E_0}}\sqrt{\frac{4.0}{k}} = \frac{(149.8-5.85)}{5.85} \times \sqrt{\frac{345}{240800}} \times \sqrt{\frac{4.0}{23.9}} = 0.38$$

$$\beta_{flange} = \left(\frac{b}{t}\right)\sqrt{\frac{\sigma_{0.2}}{E_0}}\sqrt{\frac{4.0}{k}} = \frac{(100.1-5.85)}{5.85} \times \sqrt{\frac{345}{240800}} \times \sqrt{\frac{4.0}{4.0}} = 0.60$$

∴ *Cross-section slenderness* β = 0.60

Deformation capacity ε_{LB}:

$$\frac{\varepsilon_{LB}}{\varepsilon_0} = \frac{6.44}{\beta^{2.85-0.27\beta}} = \frac{6.44}{0.60^{2.85-0.27\times0.60}} = 25.42$$

∴ ε_{LB} = 25.42 × 0.0014 = 0.0356

Geometric shape factor a_g:

W_{el} = 109100 mm³ $\qquad$ W_{pl} = 133800 mm³ $\qquad$ ∴ a_p = 133800/109100 = 1.23

Using Table B.1, for ε_{LB} = 0.0356 *the constants for generalised shape factor* a_g *are:*

$A_1 = 0.203$ $\qquad$ $A_2 = 7.35$ $\qquad$ $A_3 = 1.168$ $\qquad$ A_4 = -14.94

∴ a_g = $A_1 + A_2\varepsilon_0 + A_3a_p + A_4\varepsilon_0a_p$

$\qquad$ = $0.203 + 7.35\times0.0014 + 1.168\times1.23 - 14.94\times0.0014\times1.23 = 1.62$

Corner enhancement factor ϕ_c:
For press braked sections

$$\phi_c = 1 + \left[\frac{1.881}{(r_i/t)^{0.194}} - 1\right]k_{cor} = 1 + \left[\frac{1.881}{(4.5/5.85)^{0.194}} - 1\right]\times\left(\frac{272.92}{2713}\right) = 1.10$$

Bending resistance $M_{c,Rd}$:

$M_{c,Rd}$ = $\phi_c\, a_g\, W_{el}\, \sigma_{0.2}$ = $1.10 \times 1.62 \times 109100 \times 345 \times 10^{-6} = 67.07$ kN m

[Test ultimate load = 70.2 kN m
prEN 1993-1-4 (2004) predicted bending resistance = 46.16 kN m]

8.4.3 Combined compression plus bending resistance of a cross-section

DESIGN EXAMPLE 05

Resistance of an I section I 160×80×10×6 subjected to combined axial load plus uniaxial bending tested by Stangenberg (2000a).

Cross- section properties:

Welded cross-section

D	=	$158.3\ mm$	B	= $82.8\ mm$
t_f	=	$9.86\ mm$	t_w	= $6.0\ mm$
A_g	=	$2463.3\ mm^2$		

$a\ (weld\text{-}size) = 3.0\ mm$

Material properties

Austenitic Grade 1.4301

$\sigma_{0.2} = 279\ N/mm^2$ $\qquad E_0 = 200000\ N/mm^2$ $\qquad \varepsilon_0 = 279/200000 = 0.0014$

Compression resistance $N_{c,Rd}$:

$$\beta_{web} = \left(\frac{b}{t}\right)\sqrt{\frac{\sigma_{0.2}}{E_0}}\sqrt{\frac{4.0}{k}} = \frac{(158.3 - 2\times9.86 - 2\times3.0)}{6.0}\times\sqrt{\frac{279}{200000}}\times\sqrt{\frac{4.0}{4.0}} = 0.83$$

$$\beta_{flange} = \left(\frac{b}{t}\right)\sqrt{\frac{\sigma_{0.2}}{E_0}}\sqrt{\frac{4.0}{k}} = \frac{(82.8 - 9.86)/2 - 3.0}{9.86}\times\sqrt{\frac{279}{200000}}\times\sqrt{\frac{4.0}{0.43}} = 0.39$$

∴ *Cross-section slenderness* $\beta = 0.41$

$$\frac{\varepsilon_{LB}}{\varepsilon_0} = \frac{6.44}{\beta^{2.85-0.27\beta}} = \frac{6.44}{0.83^{2.85-0.27\times0.83}} = 10.50$$

∴ $\varepsilon_{LB} = 10.50 \times 0.0014 = 0.0147$

ForAustenitic Grade 1.4301 and welded cross-sections, the compound Ramberg-Osgood parameters are: $n = 5.3$, $n'_{0.2,1.0} = 2.5$ and $\sigma_{1.0}/\sigma_{0.2} = 1.20$.

Using this material definition, $\sigma_{LB} = 343.80\ N/mm^2$

[alternatively, σ_{LB} can be directly obtained using Table A..1 by linear interpolation.]

For I sections, Corner enhance factor $\phi_c = 1.0$

$N_{c,Rd} = \phi_c A_g\ \sigma_{LB} = 1.0 \times 2463.3 \times 343.8 \times 10^{-3} = 846.9\ kN$

Bending resistance $M_{c,Rd}$:

$$\beta_{web} = \left(\frac{b}{t}\right)\sqrt{\frac{\sigma_{0.2}}{E_0}}\sqrt{\frac{4.0}{k}} = \frac{(158.3 - 2\times9.86 - 2\times3.0)}{6.0}\times\sqrt{\frac{279}{200000}}\times\sqrt{\frac{4.0}{23.9}} = 0.34$$

$$\beta_{flange} = \left(\frac{b}{t}\right)\sqrt{\frac{\sigma_{0.2}}{E_0}}\sqrt{\frac{4.0}{k}} = \frac{(82.8 - 9.86)/2 - 3.0}{9.86}\times\sqrt{\frac{279}{200000}}\times\sqrt{\frac{4.0}{0.43}} = 0.39$$

∴ *Cross-section slenderness* $\beta = 0.39$

$$\frac{\varepsilon_{LB}}{\varepsilon_0} = \frac{6.44}{\beta^{2.85-0.27\beta}} = \frac{6.44}{0.39^{2.85-0.27\times0.39}} = 85.37$$

$\therefore \varepsilon_{LB} = 85.37 \times 0.0014 = 0.1195$

$W_{el} = 130550\,mm^3$ $\qquad W_{pl} = 149921\,mm^3$ $\qquad \therefore a_p = 149921/130550 = 1.15$

Using Table B.1, for $\varepsilon_{LB} = 0.1195$ the constants for generalised shape factor a_g are:

$A_1 = 0.312$ $\qquad\qquad A_2 = 3.06$ $\qquad\qquad A_3 = 1.319$ $\qquad\qquad A_4 = -7.00$

$$\therefore a_g = A_1 + A_2\varepsilon_0 + A_3 a_p + A_4\varepsilon_0 a_p$$
$$= 0.312 + 3.06 \times 0.0014 + 1.319 \times 1.15 - 7.00 \times 0.0014 \times 1.15 = 1.82$$

$M_{c,Rd} = \phi_c\, a_g\, W_{el}\, \sigma_{0.2} = 1.0 \times 1.82 \times 130550 \times 279 \times 10^{-6} = 66.29\,kN\,m$

Interaction between axial load and bending
Trial design value of axial load $N_{Ed} = 431\,kN$
$\therefore$ Design moment $M_{Ed} = 431 \times (158.3 - 9.86)/2 \times 10^{-3} = 31.99\,kN\,m$

The following interaction equation should be satisfied:

$$\frac{N_{Ed}}{N_{c,Rd}} + \frac{M_{Ed}}{M_{c,Rd}} \le 1$$

Here, for the trial values $\dfrac{431}{846.9} + \dfrac{31.99}{66.29} = 0.991$

$\therefore$ Proposed ultimate load $= 431\,kN$

[Test ultimate load $= 503\,kN$
prEN 1993-1-4 (2004) predicted ultimate load $= 311\,kN$]

8.4.4 Flexural buckling resistance $N_{b,Rd}$

DESIGN EXAMPLE 06

Flexural buckling resistance of a pin-ended column with a Square hollow cross-section SHS 60×60×5 tested by Talja and Salmi (1995).

Cross- section properties:
Roll-formed cross-section

D	=	$59.8\,mm$	B	=	$59.6\,mm$

$t = 4.77\,mm$ $\qquad\qquad r_i = 3.0\,mm$ $\qquad\qquad r_o = 7.77\,mm$

$A_g = 999\,mm^2$ $\qquad\qquad A_c = \pi(7.77^2 - 3.0^2) = 161.39\,mm^2$

Material properties
Austenitic Grade 1.4301

$\sigma_{0.2} = 463\,N/mm^2$ $\qquad\qquad E_0 = 185500\,N/mm^2$ $\qquad\qquad \varepsilon_0 = 463/185500 = 0.0025$

Cross-section slenderness β:

$$\beta = \left(\frac{b}{t}\right)\sqrt{\frac{\sigma_{0.2}}{E_0}}\sqrt{\frac{4.0}{k}} = \frac{(59.6 - 4.77)}{4.77} \times \sqrt{\frac{463}{185500}} \times \sqrt{\frac{4.0}{4.0}} = 0.57$$

Deformation capacity ε_{LB}:

$$\frac{\varepsilon_{LB}}{\varepsilon_0} = \frac{6.44}{\beta^{2.85-0.27\beta}} = \frac{6.44}{0.57^{2.85-0.27\times0.57}} = 29.31$$

$$\therefore \varepsilon_{LB} = 29.31 \times 0.0025 = 0.0733$$

Local buckling stress σ_{LB}:

ForAustenitic Grade 1.4301 and roll-formed cross-sections, the compound Ramberg-Osgood parameters are:

$n = 4.3$ $\qquad\qquad n'_{0.2,1.0} = 2.7$ $\qquad\qquad \sigma_{1.0}/\sigma_{0.2} = 1.25$

Using this material definition, $\sigma_{LB} = 737 \ N/mm^2$

[alternatively, σ_{LB} can be directly obtained by linear interpolation using Table A..2.]

Corner enhancement factor ϕ_c:

For roll-formed sections

$$\phi_c = 1 + 0.32 k_{cor} = 1 + 0.32 \times \left(\frac{161.39}{999}\right) = 1.05$$

Effcetive buckling stress σ_{eff}:

$$\sigma_{eff} = \sqrt{\phi_c \sigma_{LB} \sigma_{0.2}} = \sqrt{1.05 \times 737 \times 463} = 599 \ N/mm^2$$

Non-dimensional column slenderness $\overline{\lambda}$:

Pin-ended column with length L = 1050 mm

$\therefore$ Effective length $L_e = 1.0 \times 1050 = 1050 \ mm$

Elastic critical buckling load $N_{cr} = \dfrac{\pi^2 E_0 I}{L_e^2} = \dfrac{\pi^2 \times 185500 \times 493205}{1050^2} \times 10^{-3} = 819 \ kN$

Non-dimensional slenderness $\overline{\lambda} = \sqrt{\dfrac{A_g \sigma_{eff}}{N_{cr}}} = \sqrt{\dfrac{999 \times 599}{819 \times 10^3}} = 0.86$

Buckling reduction factor χ:

For SHS sections

Imperfection factor $\alpha = 0.55$ $\qquad\qquad$ *Limiting slenderness ratio $\overline{\lambda}_0 = 0.40$*

$$\therefore \phi = 0.5\left[1 + \alpha\left(\overline{\lambda} - \overline{\lambda}_0\right) + \overline{\lambda}^2\right] = 0.5[1 + 0.55(0.86 - 0.40) + 0.86^2] = 0.996$$

$$\therefore \chi = \frac{1}{\phi + \sqrt{\phi^2 - \overline{\lambda}^2}} = \frac{1}{0.996 + \sqrt{0.996^2 - 0.86^2}} = 0.67$$

Flexural buckling resistance $N_{b,Rd}$:

$N_{b,Rd} = \chi A_g \sigma_{eff} = 0.67 \times 999 \times 599 \times 10^{-3} = 400.93 \ kN$

[Test ultimate load = 417 kN

prEN 1993-1-4 (2004) predicted buckling resistance = 354.62 kN]

8.4.5 Combined compression plus bending resistance of a member

DESIGN EXAMPLE 07

Resistance of a pin-ended column with a Square hollow cross-section SHS 40×40×2 subjected to combined axial load plus bending tested by Hyttinen (1994).

Cross- section properties:
Roll-formed cross-section

D	$=$	$40.29\,mm$	B	$=$	$40.14\,mm$

$t = 1.97\,mm$ $\qquad r_i = 1.03\,mm$ $\qquad r_o = 3.0\,mm$

$A_g = 294.54\,mm^2$ $\qquad A_c = \pi(3.0^2-1.03^2) = 24.94\,mm^2$

Material properties
Ferritic Grade 1.4512

$\sigma_{0.2} = 462\,N/mm^2$ $\qquad E_0 = 204000\,N/mm^2$ $\qquad \varepsilon_0 = 462/204000 = 0.0023$

8.4.5.1 Calculations using the proposed method

Compression resistance of the cross-section $N_{c,Rd}$:

$$\beta = \left(\frac{b}{t}\right)\sqrt{\frac{\sigma_{0.2}}{E_0}}\sqrt{\frac{4.0}{k}} = \frac{(40.14-1.97)}{1.97}\times\sqrt{\frac{462}{204000}}\times\sqrt{\frac{4.0}{4.0}} = 0.93$$

$$\frac{\varepsilon_{LB}}{\varepsilon_0} = \frac{6.44}{\beta^{2.85-0.27\beta}} = \frac{6.44}{0.93^{2.85-0.27\times0.93}} = 7.78$$

$$\therefore \varepsilon_{LB} = 7.78\times0.0023 = 0.0179$$

Using Table A..4 (since 1.4512 shows similar behaviour as 1.4003), $\sigma_{LB} = 539.20\,N/mm^2$

For roll-formed sections $\phi_c = 1+0.32k_{cor} = 1+0.32\times\left(\frac{24.94}{294.54}\right) = 1.03$

$\therefore$ *Compression resistance* $N_{c,Rd} = \phi_c\,\sigma_{LB}\,A_g = 1.03\times539.2\times294.54\times10^{-3} = 163.58\,kN$

Bending resistance of the cross-section $M_{c,Rd}$:

$$\beta_{web} = \left(\frac{b}{t}\right)\sqrt{\frac{\sigma_{0.2}}{E_0}}\sqrt{\frac{4.0}{k}} = \frac{(40.29-1.97)}{1.97}\times\sqrt{\frac{462}{204000}}\times\sqrt{\frac{4.0}{23.9}} = 0.38$$

$$\beta_{flange} = \left(\frac{b}{t}\right)\sqrt{\frac{\sigma_{0.2}}{E_0}}\sqrt{\frac{4.0}{k}} = \frac{(40.14-1.97)}{1.97}\times\sqrt{\frac{462}{204000}}\times\sqrt{\frac{4.0}{4.0}} = 0.93$$

$\therefore$ *Cross-section slenderness* $\beta = 0.93$ *(same as compression)*

$\therefore \varepsilon_{LB} = 0.0179$

$W_{el} = 3536\,mm^3$ $\qquad W_{pl} = 4332\,mm^3$ $\qquad \therefore a_p = 4332/3536 = 1.23$

Using Table B.4, for $\varepsilon_{LB} = 0.0179$ the constants for the generalised shape factor a_g are:

$A_1 = 0.086$ $\qquad A_2 = 12.14$ $\qquad A_3 = 1.086$ $\qquad A_4 = -18.78$

$\therefore a_g = A_1 + A_2\varepsilon_0 + A_3a_p + A_4\varepsilon_0 a_p$

$\qquad = 0.086 + 12.14\times0.0023 + 1.086\times1.23 - 18.78\times0.0023\times1.23 = 1.40$

$M_{c,Rd} = \phi_c\,a_g\,W_{el}\,\sigma_{0.2} = 1.03\times1.40\times3536\times462\times10^{-6} = 2.36\,kN\,m$

Flexural buckling resistance $N_{b,Rd}$:

$$\sigma_{eff} = \sqrt{\phi_c \sigma_{LB} \sigma_{0.2}} = \sqrt{1.03 \times 539.2 \times 462} = 506.54 \ N/mm^2$$

Pin-ended member with length L = 2210 mm

$\therefore$ *Effective length $L_e = 1.0 \times 1050 = 2210 \ mm$*

Elastic critical buckling load $N_{cr} = \dfrac{\pi^2 E_0 I}{L_e^2} = \dfrac{\pi^2 \times 204000 \times 71236}{2210^2} \times 10^{-3} = 29.37 \ kN$

Non-dimensional slenderness $\overline{\lambda} = \sqrt{\dfrac{A_g \sigma_{eff}}{N_{cr}}} = \sqrt{\dfrac{294.54 \times 506.54}{29.37 \times 10^3}} = 2.25$

For SHS sections,   *Imperfection factor $\alpha = 0.55$*   *Limiting slenderness ratio $\overline{\lambda}_0 = 0.40$*

$\therefore \phi = 0.5\left[1 + \alpha(\overline{\lambda} - \overline{\lambda}_0) + \overline{\lambda}^2\right] = 0.5[1 + 0.55(2.25 - 0.40) + 2.25^2] = 3.54$

$\therefore \chi = \dfrac{1}{\phi + \sqrt{\phi^2 - \overline{\lambda}^2}} = \dfrac{1}{3.54 + \sqrt{3.54^2 - 2.25^2}} = 0.16$

$N_{b,Rd} = \chi A_g \sigma_{eff} = 0.16 \times 294.54 \times 506.54 \times 10^{-3} = 23.87 \ kN$

Interaction between axial load and bending:

For the considered member $M_{Ed}/N_{Ed} = 0.025m < 0.075 \ m$

$\therefore$ *Beam-column interaction factor* $\kappa = \overline{\lambda} + 0.55 = 2.25 + 0.55 = 2.80$

Trial design value of axial load $N_{Ed} = 13.85 \ kN$

$\therefore$ *Design moment $M_{Ed} = 13.85 \times 0.025 = 0.35 \ kN \ m$*

The following interaction equation should be satisfied:

$$\dfrac{N_{Ed}}{N_{b,Rd}} + \dfrac{\kappa M_{Ed}}{M_{c,Rd}} \leq 1$$

Here, for the trial values $\dfrac{13.85}{23.87} + \dfrac{2.80 \times 0.35}{2.36} = 0.995$

$\therefore$ *Proposed ultimate load = 13.85 kN*

[Test ultimate load = 14.54 kN]

8.4.5.2 Calculations using the guidelines proposed in prEN 1993-1-4 (2004)

Compression resistance of the cross-section $N_{c,Rd}$:

$$\varepsilon = \left[\dfrac{235}{\sigma_{0.2}} \times \dfrac{E_0}{210000}\right]^{0.5} = \left[\dfrac{235}{462} \times \dfrac{204000}{210000}\right]^{0.5} = 0.933$$

Classification of the cross-section when subjected to compression:

Class 1 limit = $25.7\varepsilon = 25.7 \times 0.933 = 23.98$

Class 2 limit = $26.7\varepsilon = 26.7 \times 0.933 = 24.91$

Class 3 limit = $30.7\varepsilon = 30.7 \times 0.933 = 28.64$

Cross-section $c/t = \dfrac{40.29 - 2t - 2r_i}{t} = \dfrac{40.29 - 2 \times 1.97 - 2 \times 1.03}{1.97} = 17.41 < 23.98$

Thus, the cross-section is Class 1 in compression.

$\therefore$ Compression resistance $N_{c,Rd} = \sigma_{0.2} A_g = 462 \times 294.54 \times 10^{-3} = 136.08 \, kN$

Bending resistance of the cross-section $M_{c,Rd}$:
Classification of the cross-section when subjected to bending:

Classification of the compression flange:
Class 1 limit $= 25.7\varepsilon = 25.7 \times 0.933 = 23.98$
Class 2 limit $= 26.7\varepsilon = 26.7 \times 0.933 = 24.91$
Class 3 limit $= 30.7\varepsilon = 30.7 \times 0.933 = 28.64$

Cross-section $c/t = \dfrac{40.14 - 2t - 2r_i}{t} = \dfrac{40.14 - 2 \times 1.97 - 2 \times 1.03}{1.97} = 17.33 < 23.98$

Thus the flange is Class 1

Classification of the web subjected to bending:
Class 1 limit $= 56\varepsilon = 56 \times 0.933 = 52.25$
Class 2 limit $= 58.2\varepsilon = 58.2 \times 0.933 = 54.3$
Class 3 limit $= 74.8\varepsilon = 74.8 \times 0.933 = 69.79$

Cross-section $c/t = \dfrac{40.29 - 2t - 2r_i}{t} = \dfrac{40.29 - 2 \times 1.97 - 2 \times 1.03}{1.97} = 17.41 < 52.25$

Thus the web is Class 1

$\therefore$ the cross-section is Class 1 in bending.

$W_{pl} = 4332 \, mm^3$
For Class 1 cross-sections:
$M_{c,Rd} = W_{pl} \, \sigma_{0.2} = 4332 \times 462 \times 10^{-6} = 2.00 \, kN \, m$

Flexural buckling resistance $N_{b,Rd}$:
Pin-ended member with length $L = 2210 \, mm$
$\therefore$ Effective length $L_e = 1.0 \times 1050 = 2210 \, mm$

Elastic critical buckling load $N_{cr} = \dfrac{\pi^2 E_0 I}{L_e^2} = \dfrac{\pi^2 \times 204000 \times 71236}{2210^2} \times 10^{-3} = 29.37 \, kN$

For Class 1 cross-sections:

Non-dimensional slenderness $\bar{\lambda} = \sqrt{\dfrac{A\sigma_{0.2}}{N_{cr}}} = \sqrt{\dfrac{294.54 \times 462}{29.37 \times 10^3}} = 2.15$

For SHS sections,   Imperfection factor $\alpha = 0.49$ Limiting slenderness ratio $\bar{\lambda}_0 = 0.40$

$\therefore \phi = 0.5\left[1 + \alpha\left(\bar{\lambda} - \bar{\lambda}_0\right) + \bar{\lambda}^2\right] = 0.5[1 + 0.49(2.15 - 0.40) + 2.25^2] = 3.24$

$$\therefore \chi = \frac{1}{\phi + \sqrt{\phi^2 - \overline{\lambda}^2}} = \frac{1}{3.54 + \sqrt{3.54^2 - 2.25^2}} = 0.177$$

For Class 1 cross-sections:
$N_{b,Rd} = \chi A\, \sigma_{0.2} = 0.177 \times 294.54 \times 462 \times 10^{-3} = 24.09\ kN$

Interaction between axial load and bending:
Beam-column interaction factor $\kappa = 1.5$

Trial design value of axial load $N_{Ed} = 16.5\ kN$
$\therefore$ *Design moment* $M_{Ed} = 16.5 \times 0.025 = 0.41\ kN\,m$

The following interaction equation should be satisfied:

$$\frac{N_{Ed}}{N_{b,Rd}} + \frac{\kappa M_{Ed}}{M_{c,Rd}} \le 1$$

Here, for the trial values $\dfrac{16.5}{24.09} + \dfrac{1.5 \times 0.41}{2.00} = 0.992$

$\therefore$ *Proposed ultimate load* = 16. 5 kN

[Test ultimate load = 14.54 kN]

8.5 CONCLUDING REMARKS

A new design method based on the deformation capacity of cross-sections for structural stainless steel has been presented in this chapter. The scope of the proposed design method covers cross-section resistance against compression, bending and combined action of compression plus bending, and member resistance against flexural buckling and combination of compression and flexural buckling. No guidelines have been proposed for the torsional, distortional and flexural-torsional buckling modes – primarily because of the unavailability of test results.

All the proposed techniques have been verified against the test results and also their performance has been compared to that of the existing Eurocode prEN 1993-1-4 (2004). A summary of these comparisons is given in Table 8.12. The comparisons show that the proposed method provides accurate and consistent predictions when compared with the Eurocode. Moreover considerable material savings may be achieved by adopting the proposed method.

Table 8.12: Summary of comparisons between prEN 1993-1-4 (2004) and the proposed design method for all types of loading.

	Configuration	No of tests	prEN / Test	Proposed / Test	Proposed / prEN
Cross-section resistance	Compression	136	0.81 (0.14)	1.00 (0.12)	1.25
	Bending	36	0.73 (0.14)	0.97 (0.10)	1.34
	Compression plus bending	2	0.68 (0.13)	0.88 (0.04)	1.28
Member resistance	Flexural buckling	97	0.93 (0.12)	1.00 (0.09)	1.08
	Flexural buckling plus bending	61	0.90 (0.21)	1.00 (0.09)	1.17

Note: the values within brackets are coefficient of variation (COV).

A number of worked examples have been presented to demonstrate the application of the developed method under different types of loading. Different types of cross-sections and materials have been used to provide a general understanding of how the cross-section deformation capacity instead of the traditional cross-section classification may be exploited to obtain accurate member resistances for stainless steel structures. Design examples show that the proposed method requires similar volumes of calculation when compared with prEN 1993-1-4 (2004). It is worth mentioning that for Class 4 cross-sections, which is a very common case for stainless steel cross-sections, the volume of calculations for prEN 1993-1-4 (2004) will significantly increase, requiring the lengthy procedure to calculate effective cross-sectional properties, whilst the proposed method will remain unchanged. In such cases the proposed method provides significantly improved predictions following a rational procedure, which does not require any more calculations.

CHAPTER - NINE

CONCLUSIONS AND RECOMMENDATIONS

9.1 CONCLUSIONS

9.1.1 General

Owing to its combination of strength, stiffness, ductility and relative economy, carbon steel has been the most widely used structural metallic material for the past century and this dominance is set to continue. However, advances in materials and production techniques and an increased emphasis on durability, efficiency and whole-life costing have recently prompted more use of high alloy metals such as stainless steel in structural applications. Hence, the last 15 years have seen developments in design guidance for structural stainless steel all around the world. Current design codes have been developed on the basis of bi-linear (elastic, perfectly-plastic) material behaviour, which is synonymous with structural carbon steel. Use of such a material model and the concept of the cross-section classification ensures both convenience in structural design calculations and harmonisation of treatment between materials. Experimental investigations have now established that stainless steel exhibits significantly different nonlinear material behaviour, which makes adoption of an elastic, perfectly-plastic material model inappropriate. The primary objective of this study has therefore been to develop a more rational and efficient design method for stainless steel structures exploiting its special features, whilst providing designer friendly guidance by optimising the required volume of calculations.

A review of the relevant literature has been the first step in the process of developing the proposed design method. A brief overview of the subject areas covered within this thesis has been presented in Chapter 2, whilst a detailed review of the related literature is presented in the following chapters as appropriate. Investigations into all available laboratory testing programmes provided invaluable information on the behaviour of different material grades, different cross-section types and members subjected to different types of loading. Since no

laboratory testing was undertaken as a part of the present research, these investigations formed the core of the whole project.

9.1.2 Material modelling

Accurate material modelling is the foremost condition needed to develop a rational and accurate design method. A total of 88 coupon tests, 55 in tension and 33 in compression, from 12 different sources have been considered in the present study. Material coupons were collected either from the virgin sheet or from the finished cross-sections, representing 6 different shapes including open and hollow sections, produced from 5 different grades, which belong to the following 3 categories: austenitic, ferritic and duplex. These diverse material stress-strain curves have been used to obtain compound Ramberg-Osgood coefficients for the considered grades of stainless steel. The proposed material model has been observed to provide excellent agreement with the reported experimental behaviour. Load-deformation responses for stub columns have been studied to formulate the behaviour of cross-sections when subjected to compression. Members subjected to bending, flexural buckling and compression plus bending were also investigated to propose design methods for each case. Chapter 3 lists all necessary details of the test results considered in the present research. The considered laboratory tests have been used for the following three purposes – developing and verifying the numerical models, developing the proposed design method and comparing the performance of the proposed method against the existing Eurocode ENV 1993-1-4 (2004).

Mechanical properties of stainless steel are changed due to cold working of the virgin material because of its response to deformation. Stainless steel exhibits pronounced strain hardening, resulting in the corner regions of cold-formed sections having 0.2% proof strengths much higher than that of the virgin material. In Chapter 4, a total of 65 corner material coupon tests obtained from 6 different sources have been analysed to establish rational relationships between the material strength at corner regions and that of the virgin sheet or flat regions. The effects of manufacturing processes – roll-forming and press-braking – on the extent of strength enhancement were also investigated. Hence two power models have been proposed to predict the 0.2% proof strength of corner material using the geometry of the corner and the properties of the virgin material. The proposed models have been verified against all available test data for corner properties and have been found to give accurate predictions – the average and COV for the predictions using a simple power model (using 0.2% proof strength of virgin material) are 1.00 and 0.06, whilst those for the power model using the ultimate strength of virgin material are 1.00 and 0.04.

A simplified model to predict the 0.2% proof strength of corner material in roll-formed sections from a knowledge of only the ultimate strength of flat material has been recalibrated. Once the 0.2% proof strength is known, a further model has been proposed to predict the ultimate strength of corner material and thus to provide a complete view of the changes in stress-strain behaviour due to cold-working.

9.1.3 Numerical modelling

Numerical modelling of the structural response of stainless steel structural elements has been explained in Chapter 4. Numerical models for stub columns, beams, columns and beam-columns have been developed using the FE package ABAQUS. Six different types of cross-section including both open and hollow sections were considered. The material properties were incorporated using the compound Ramberg-Osgood model taking the proposed coefficients for different grades. Appropriate recognition of the strength enhancements at corner regions were made by using the models proposed for the prediction of the 0.2% proof strength of corner region. Previous studies on corner properties showed that the strength enhancement should not be limited only to the corner, rather these need to be extended up to a certain distance to obtain accurate load-deformation predictions. Parametric studies have been carried out to determine a representative limit for this extension in the case of stainless steel cross-sections. The developed numerical models showed that for the press-braked sections the corner strength should be used up to t, where t is the plate thickness, beyond the corner, whilst for the roll-formed sections Gardner's (2002) proposed 2t is appropriate.

Geometric imperfections are an inseparable property of real steel members, with the potential to significantly influence their structural behaviour. Despite their importance, there are no general guidelines for the shape and the magnitude of geometric imperfections to be used in numerical models. Predictions are normally conducted by either modelling the structure with an assumed initial out-of-plane deflection or by using assumed small transverse forces. Parametric studies were performed to obtain appropriate distributions and magnitudes for initial imperfections in the case of stainless steel members. Elastic analysis was performed to obtain Eigenmodes, which were used in the subsequent nonlinear analysis with an appropriate amplitude. Each of the stub columns was analysed with combinations of the first 3 Eigenmodes obtained from the elastic analysis and 2 amplitudes proposed by Gardner (2002) and Schafer and Pekoz (1998). Adoption of the first Eigenmode with an amplitude of $0.023(\sigma_{0.2}/\sigma_{cr})t$, where $\sigma_{0.2}$ and σ_{cr} are 0.2% proof strength of the material and elastic critical buckling stress of the plate respectively, as proposed by Gardner (2002) produced the closest agreement with the test results. For long columns careful investigation is required to select the

appropriate Eigenmode. If a global buckling mode is available, an amplitude of L/2000 may be used as a general guideline. In the case of open sections L/1000 should be taken as a lower bound if there is a possibility of excessive initial out-of-straightness. The column strength is always dominated by the global buckling mode and superposition of local imperfections did not seem to produce any significant changes. However, in cases, where Eigenmodes are dominated by local failures without showing any global mode, a representative well-distributed deformed shape with an amplitude of $0.023(\sigma_{0.2}/\sigma_{cr})t$ should produce accurate predictions. Similar techniques have been adopted for the beams and the beam-columns considered in the present study.

Since there is no established residual stress pattern available for stainless steel cross-sections, the existing guidelines for carbon steel were followed to incorporate residual stresses in the welded I stub columns. No significant effect was observed and hence it was neglected in the subsequent FE models which, however, produced excellent agreement with the test results.

9.1.4 Design method

The development of the method for designing stainless steel cross-sections subjected to compression, bending and combined compression plus bending has been explained in Chapter 6. The new approach proposed by Gardner and Nethercot (2004d) for stainless steel hollow sections has led to a new technique for designing nonlinear metallic materials without using the traditional section classification system based on the bi-linear elastic, perfectly-plastic material definition. The present research has been aimed at providing a generalised design method for structural stainless steel exploiting its special features.

The key parameters of the proposed method are: cross-section slenderness parameter β and cross-section deformation capacity ε_{LB}. The proposed slenderness β is a continuous parameter, which does not involve any discrete section classification and hence avoids the lengthy calculation processes involved with the effective areas for slender sections. Deformation capacity ε_{LB}, on the other hand, is the strain of a compressed plate at the onset of local buckling. Stub column test results obtained from six different sources have been analysed to obtain a relationship between β and ε_{LB}, which is actually the proposed design equation to determine cross-section resistances. Once the cross-section slenderness β is known, the design equation is used to obtain the deformation capacity ε_{LB} and, finally, the proposed material model may be used to determine the cross-section resistance. Design tables have been presented in Appendix A to obtain stresses corresponding to ε_{LB} without going into iteration.

Explicit recognition of the enhanced strength at the cold-worked corner regions has been made by the proposed strength enhancement factor ϕ_c. Effects of the manufacturing process on ϕ_c have been considered and distinct formulations have been proposed for the press-braked and the roll-formed sections using the models proposed for predicting corner strength in Chapter 4.

The analogy between the compression flange of a beam and that of a plate within a stub column has been used to extend this method for predicting bending resistance. The concept of plastic modulus is no longer valid in the proposed method since the elastic, perfectly-plastic model has not been adopted. The actual nonlinear bending stress distribution has been incorporated by introducing the concept of a generalised shape factor a_g. For a specific value of ε_{LB}, generalised shape factor a_g is a function of geometric shape factor a_p and 0.2% elastic strain ε_0. Design tables have been provided in Appendix B to determine generalised shape factors with the knowledge of ε_{LB}, a_p and ε_0. The proposed method has also been verified for beams where failure occurs due to the local buckling of the web subjected to pure bending.

Finally, ultimate loads for two available eccentric cross-section test results were predicted using the combination of the proposals made for compression and bending resistance. The obtained predictions, though very limited in number, were in good agreement with the test results.

The predictions obtained using the proposed techniques for both compression and bending resistances have been compared with all available test results. The average prediction for the considered 136 stub columns is 1.00 with a COV of 0.12, whereas for the 36 beams considered the average is 0.97 with a COV of 0.10. Given the variability in testing procedures, specimens, grades and cross-section types, these variations may be considered as acceptable. However, when the predictions for stub columns have been compared to FE results, which are believed to reduce experimental uncertainties to some extent, the scatter reduced by giving a COV of 0.09.

Once the cross-section resistances have been predicted successfully, Chapter 7 has investigated the behaviour of stainless steel members. Flexural buckling behaviour of stainless steel columns has been studied using the currently available 97 tests on four different cross-section types obtained from six different sources. Two different sets of column curves have been proposed for stainless steel columns subjected to flexural buckling. Instead of using the traditional 0.2% proof stress of the flat material the proposed techniques exploit

different key parameters – local buckling stress σ_{LB} and effective buckling stress σ_{eff} - yet retain the basic Perry-Robertson formulation. The performance of these methods has been verified against available test results. The first technique, which uses σ_{LB}, produces a mean of 0.99 with a COV of 0.11, whereas that using σ_{eff} provides more accurate predictions with an average of 1.00 with a COV of 0.09. When the predictions were compared against the FE results, which are considered to reduce the uncertainties associated with experiments, significantly improved agreements have been achieved reducing the overall COV from 0.09 to 0.06.

Beam-column interactions have been investigated using 61 tests performed on four different cross-section types obtained from four different sources. Stainless steel members were subjected to compression with a simultaneous uniaxial bending moment. Guidelines available in the existing Eurocode were found to produce very inconsistent predictions, largely due to the inaccurate predictions for resistances against individual actions, which was supplemented by the adoption of a constant value of 1.5 for the interaction factor κ. Detailed investigations have been made and hence an empirical relationship has been proposed between κ and non-dimensional member slenderness $\bar{\lambda}_{max}$. The proposed techniques produced significant improvements in the ultimate load predictions for the considered 61 cases giving an average of 1.00 and a COV of 0.09.

9.1.5 Proposed method vs prEN 1993-1-4 (2004)

The performance of the proposed design method based on the deformation capacity of cross-sections has been compared to that of the Eurocode prEN 1993-1-4 (2004). The comparisons have been made for cross-section resistance against compression, bending and combined action of compression plus bending, and member resistance against flexural buckling and combination of compression and flexural buckling.

In all the cases considered in the present study, the predictions of the proposed method are more accurate and more consistent with the test results when compared to the predictions obtained using prEN 1993-1-4 (2004). Moreover, the proposed method, on average, provides improvements in the compression resistance by 26%, bending resistance by 34%, combined compression plus bending resistance of cross-sections by 28%, flexural buckling resistance by 8% and member resistance subjected to compression plus bending by 17% compared with the Eurocode. Worked examples have been presented to demonstrate the required volume of

calculation, which is normally much less for the relatively slender (Class 4 in Eurocode) cross-sections because of the use of properties based on gross area.

The primary objective of achieving a more rational and a more efficient design method for structural stainless steel has been met. The proposed design method is based on a new concept, whereby the deformation capacity of cross-sections is relied on rather than the traditional material yield stress. This approach recognises the material's nonlinearity and its sensitivity to cold-working and hence produces accurate predictions for cross-section and member resistances when subjected to different types of loading. It is envisaged that the proposed design method will be considered for incorporation into future revisions of Eorocode 3, providing more efficient structural design for stainless steel and hence promoting wider use of a more sustainable material.

9.2 RECOMMENDATIONS

9.2.1 Extension of the proposed design method

The proposed design concept has already been observed to perform very well at the cross-section level. Further research is required to develop an accurate understanding of the member behaviour. The proposed column curves should be validated using more general test data. Laboratory testing schemes as well as FE modelling techniques may be used to investigate the behaviour of angle and channel columns since no test results are available. The physical significance of the proposed limiting slenderness ratios $\overline{\lambda}_0$ for different cross-sections needs to be carefully investigated to provide a rational transition between stub column and long column. Moreover, introduction of an 'effective stress σ_{eff}' concept produced very accurate and consistent predictions in the case of flexural buckling of stainless steel columns, although further investigation is required to evaluate the critical stress at which flexural buckling occurs. Numerical modelling may be employed for such investigations.

Beam-column interaction formulas presented in the current Eurocode prEN 1993-1-4 (2004) are based on a limited set of test results and hence produce inconsistent predictions, which are partly contributed by the inaccurate predictions for individual actions. Since the proposed method can provide accurate predictions for the cross-section and the member resistances, it is believed that appropriate interaction formulas may be attained through extended research. Preliminary studies have shown that the beam-column interaction factor κ depends on the member slenderness and the equivalent eccentricity i.e. M_{Ed}/N_{Ed}. The proposed guidelines for the interaction coefficients produced significant improvements in the predictions and hence it is envisaged that appropriate parametric studies should further develop this. Moreover,

interaction of compression and biaxial bending has not been considered in the present research; this requires even more careful thought. Numerical modelling may be used to carry out well designed parametric studies to identify key parameters and hence to understand these more complex interactions.

Two important buckling modes – distortional buckling and flexural torsional buckling – have not been considered in the present research primarily because of the unavailability of sufficient test data. For cross-sections with outstand elements, these buckling modes must be considered if a complete design guidance is to be developed. Moreover, cross-sections subjected to torsion are another subject, which requires investigation. Laboratory testing programmes, augmented by the numerical models developed based on the test results, could form the basis for relevant formulations. Once all of these cases are properly incorporated, the developed method will be ready to be established as a practical design tool and eventually should be included in the Eurocode.

The present method utilises a compound Ramberg-Osgood material model, in which strain is expressed as a function of stress. This formulation requires either iteration or design tables, as shown in Appendix A, to obtain local buckling stresses corresponding to a specific deformation capacity. Recently, Abdella (2006) has proposed an inversion of this stress-strain formulation. This should make the proposed design method even more designer friendly by providing explicit expressions for local buckling stresses.

9.2.2 Further scope for research in the relevant field

The basic concept of the proposed method may be applied to metallic materials showing similar nonlinear stress-strain behaviour. Preliminary investigations have been carried out by Gardner and Ashraf (2006) for aluminium and high strength steel, which produced improved predictions for the cross-section resistances for hollow sections. This investigation opens the way for further investigation to devise an alternative, rational and generalised design approach for nonlinear metallic materials. Moreover, the stress-strain behaviour of ordinary carbon steel at elevated temperature becomes nonlinear by losing its unique elastic, perfectly-plastic characteristic. Thus the concept of deformation capacity may be employed in such cases with the inclusion of temperature as an additional parameter in material modelling.

Experimental results have now showed that the design strengths for different grades specified in the available codes are significantly under estimated. Effects of strain hardening, which takes place during the rolling of cold-formed sheets into coils and also during the

manufacturing process of cross-sections, should be appropriately taken into account when specifying the design strengths. Special attention should be given to the most commonly used austenitic grades, which are also the most sensitive to cold-working. Different design strengths may be specified for the same grade depending on its prior history of cold-working.

The compound Ramberg-Osgood model has now generally been accepted for modelling the stress-strain behaviour of stainless steel, although minor differences exist among the available formulations. However the basic concept is the same, using two different curves involving two different exponential constants to define the nonlinearity exhibited by stainless steel. Different sets of equations with the corresponding values for the exponential coefficients are now available from different sources, although the end-product i.e. the stress strain curve is almost the same. A comparison of the available material models showing their relative advantages and disadvantages should produce a generally acceptable material model. Moreover, the significance of using slightly different values for the exponential coefficients for different grades should also be investigated, and hence minor discrepancies should be avoided, if possible, without compromising the accuracy.

The present research showed the significance of recognising the strength enhancement in the cold-worked corners. The proposed models have been developed based on the available test results on different grades. However, some of the recent tests performed on corner material obtained from austenitic grades were found to produce significantly different strengths than those predicted using the proposed models. Further investigations could reveal the reasons behind these discrepancies and, if required, separate models should be developed for the austenitic grades since they are the most commonly used type of stainless steel.

Cross-sections with partially stiffened elements such as lipped channels and lipped angles are observed to provide structural responses which are considerably different from the other typical cross-section types such as angles, I sections and hollow sections. The existence of even a relatively small lip adds significant differences to the flange behaviour since, structurally, it lies between the two traditional limits – outstand and internal element. In the proposed design method, the partially restrained elements have been considered as simply supported internal elements, which can lead to rather an optimistic design approach. Careful investigations are required to obtain appropriate plate buckling coefficients for such elements.

Only the static response of stainless steel structural elements has been investigated as part of this Ph.D. research. The high level of ductility offered by stainless steel – austenitic grades often offer as much as 50% – could make this more favourable than carbon steel for dynamic

applications. Recent investigations on the seismic response of building frames showed that stainless steel could be a viable alternative to carbon steel, provided that proper design choices are employed for the structural configuration and material distribution within the members of the adopted systems. Since stainless steel is a relatively new structural material, investigations to reveal its full potential in dynamic applications is still at the preliminary level. Extensive research is required to obtain a complete overview of the response of different types of structural elements when subjected to cyclic loading. Considering the high initial cost, selective use of such metal alloy to enhance the energy absorption capacity should be an interesting field of research.

Sustainability and life-cycle costing are important arguments for selecting stainless steel as a construction material. Currently available research on this field show some qualitative comparisons to establish its overall superiority over ordinary carbon steel recognising its durability, low maintenance cost, corrosion resistance and recyclablity. This general concept should be developed mathematically to promote wider use of stainless steel in construction. Efficient design guidance will add material savings making the equation more favourable towards stainless steel and hence could lead to more sustainable and innovative design solutions for a better world.

REFERENCES

ABAQUS (2003). ABAQUS/ Standard User's Manual Volumes I-III and ABAQUS Post Manual. Version 6.4. Hibbitt, Karlsson & Sorensen, Inc. Pawtucket, USA.

Abdella, K (2006). Inversion of a full-range stress-strain relation for stainless steel alloys. *International Journal of Non-Linear Mechanics.* **41**(3): 456-463.

Abdel-Rahman, N. and Sivakumaran, K. S. (1997). Material properties models for analysis of cold-formed steel members. *Journal of Structural Engineering ASCE.* **123** (9): 1135-1143.

AISI (1974). Stainless Steel Cold-Formed Structural Design Manual. *American Iron ansd Steel Institute.* Washington, D.C.

Ala-Outinen (1999). Stainless steel compression members exposed to fire. *Proceedings of the 4th International Conference on Steel and Aluminium Structures.ICSAS'99.* Edited by Mäkeläinen, P. and Hassinen, P. Espoo, Finland. 523 – 530.

Ala-Outinen, T. and Oksanen, T. (1997). Stainless steel compression members exposed to fire. *Research Note 1864.* VTT Building Technology, Finland.

ASCE (2002). Specifications for the design of cold-formed stainless steel structural members. SEI/ASCE 8-02. *American Society of Civil Engineers.*

AS/NZS:4673 (2001). Cold-Formed Stainless Steel Structures, *Australian Standard/New Zealand Standard 4673:2001.* Standards Australia, Sydney, Australia.

Ashraf, M., Gardner, L. and Nethercot, D. A. (2006). Compression strength of stainless steel cross-sections. *Journal of Constructional Steel Research.* **62**(1-2): 105-115.

Ashraf, M. (2005a). Structural stainless steel design: project. *The Structural Engineer*. **83**: 28-29.

Ashraf, M., Gardner, L. and Nethercot, D. A. (2005b). Strength enhancement of the corner regions of stainless steel cross-sections. *Journal of Constructional Steel Research.* **61**(1): 37-52.

Ashraf, M., Gardner, L. and Nethercot, D. A. (2005c). Geometric imperfections in stainless steel cross-sections. *Proceedings of the ICASS '05 – Fourth International Conference on Advances in Steel Structures*. Shanghai, China. 105-112.

Ashraf, M., Gardner, L. and Nethercot, D. A. (2005d). Numerical modelling of stainless steel open sections. *Proceedings of the Eurosteel 2005 – 4th European Conference on Steel and Composite Structures*. Maastricht, The Netherlands. 197-204.

Ashraf, M., Gardner, L. and Nethercot, D. A. (2004). Numerical modelling of static response of stainless steel sections. *Proceedings of the Colloquium dedicated to the 70th anniversary of Professor Victor GIONCU - Recent Advances and New Trends in Structural Design.*, Timişoara, Romania. 1-10.

ASTM E8 – 93 (1993). Standard test methods for tension testing of metallic materials. American Society for Testing Materials.

Australian Standard (AS) (1991). Methods for tensile testing of metals. AS 1391, Standards Association of Australia. Sydney, Australia.

Basquin, O. H. (1924). Tangent modulus and the strength of steel columns in tests. *Building Standards Technical Paper No. 263*. US Bureau of Standards, Washington D. C.; 18.

Bažant, Z. P. (2000). Structural stability. *International Journal of Solids and Structures*. **37**: 55-67.

Boh, J. W., Louca, L. A. Choo, Y. (2004). Numerical assessment of explosion resistant profiled barriers. *Marine Structures*. **17**: 139-160.

Bredenkamp, P..J., van den Berg, G. J. and van der Merwe, P. (1992). Residual stresses and the strength of stainless steel I-section columns. *Proceedings of the Structural Stability Research Council, Annual Technical Session.* Pittsburg, USA. 69-86.

Bredenkamp, P.J. and van den Berg, G.J. (1995). The strength of stainless steel built-up I-section columns. *Journal of Constructional Steel Research.* 34: 131-144

BS 5950-1 (2000). Structural use of steelwork in buildings – Part 1: Code of practice for design in simple and continuous construction: hot rolled sections. British Standards Institution.

BS EN 10088-1 (1995). Stainless steels – Part 1: List of stainless steels. British Standards Institution.

Burns, T. (2001). Buckling of stiffened stainless steel plates. *BE (Honours) Thesis, Department of Civil Engineering, University of Sydney, Australia.*

Chou, S. M., Chai, G. B. and Ling, L. (2000). Finite element technique for design of stub columns. *Thin-Walled Structures.* 37: 97-112.

Coates, R. C., Coutie, M. G. and Kong, F. K. (1988). Structural analysis. Third Edition. *Chapman and Hall, University and Professional Division.*

Coetzee, J. S., Van den Berg, G. J. and Van der Merwe, P. (1990). The effect of work hardening and residual stresses due to cold-work of forming on the strength of cold-formed stainless steel lipped channel section. *Proceedings of the Tenth International Specialty Conference on Cold-Formed Steel Structures,* St. Louis, Missouri, U.S.A. 143-162.

Dawson, R. G. and Walker, A. C. (1972). Post-buckling of geometrically imperfect plates. *Journal of the Structural Division. ASCE.* 98 (ST1): 75-94.

Dubina, D. and Ungureanu, V. (2002). Effect of imperfections on numerical simulation of instability behaviour of cold-formed steel members. *Thin-Walled Structures.* 40: 239-262.

Ellobody, E. and Young B. (2005). Structural performance of cold-formed high strength stainless steel columns. *Journal of Constructional Steel Research.* 61(12): 1631-1649.

ENV 1993-1-3 (1996), Eurocode 3: Design of steel structures, Part 1.3: General Rules, Supplementary rules for cold formed thin gauge members and sheetings, CEN.

ENV 1999-1-1. (1998). Eurocode 9: Design of Aluminium Structures – Part 1.1: General Rules – General rules and rules for buildings. CEN.

ENV 1993-1-3. (1996). Eurocode 3: Design of Steel Structures – Part 1.3: General Rules – Supplementary rules for cold formed thin gauge members and sheeting. CEN.

ENV 1993-1-4. (1996). Eurocode 3: Design of Steel Structures – Part 1.4: General rules - Supplementary rules for stainless steel. CEN.

European Convention for Constructional Steelwork ECSC (1984). Ultimate limit state calculation of sway frames with rigid joints. Technical Committee 8 – Structural Stability Technical Working Group 8.2 – System. Publication No. 33.

Galambos, T. V., Editor. (1998). Guide to stability design criteria for metal structures. 4th Edition. Structural Stability research Council. John Wiley and Sons, Inc. New York.

Gardner, L. and Ashraf, M. (2006). Structural design for non-linear metallic materials. *Engineering Structures.* **28**: 925-936.

Gardner, L. (2005). The use of stainless steel in structures. *Progress in Structural Engineering Materials.* **7**: 45-55.

Gardner, L. and Nethercot, D. A. (2004a). Experiments on stainless steel hollow sections - Part 1- Material and cross-sectional behaviour. *Journal of Constructional Steel Research.* **60**(9): 1291 – 1318.

Gardner, L. and Nethercot, D. A. (2004b). Experiments on stainless steel hollow sections - Part 2- Member behaviour of columns and beams. *Journal of Constructional Steel Research.* **60**(9): 1319 – 1332.

Gardner, L. and Nethercot, D. A. (2004c). Numerical modelling of stainless steel structural components - A consistent approach. *Journal of Structural Engineering ASCE,* **130**(10): 1586-1601.

Gardner, L. and Nethercot, D. A. (2004d). Structural stainless steel design: A new approach. *Structural Engineer*. 82(21): 21-28

Gardner, L and Talja A. (2003). WP2: Structural Hollow Sections. *ECSC Project: Structural Design of Cold-Worked Austenitic Stainless Steel*. Contract No. 7210 PR318. The Steel Construction Institute.

Gardner, L (2002). A new approach to structural stainless steel design. *Ph.D. Thesis*. Structures Section, Department of Civil and Environmental Engineering. Imperial College London, UK.

Gardner L. and Nethercot D. A. (2001). Numerical modelling of cold-formed stainless steel sections. *Proceedings of the Ninth Nordic Steel Construction Conference*. Edited by Mäkeläinen P, Kesti J, Jutila A and Kautila O. 781-789.

Godfrey, G. B. (1962). The allowable stresses in axially-loaded steel struts. *The Structural Engineer*. 40: 97-112.

Greiner, R., Hörmaier, I., Ofner, R. and Kettler, M. (2005). Buckling behaviour of stainless steel members under bending and axial compression. *Research Report F-5-14/2005*. Technische Universität Graz, Austria.

Grondin, G. Y., Elwi, A. E. and Cheng, J. J. R. (1999). Buckling of stiffened steel plates – a parametric study. *Journal of Constructional Steel Research*. 50: 151-175.

Hill, H. N. (1944). Determination of stress-strain relations from the offset yield strength values. *Technical Note No. 927, National Advisory Committee for Aeronautics*, Washington, D.C.

Hopperstad, O. S., Langseth, M. and Hanssen, L. (1997). Ultimate compressive strength of plate elements in Aluminium: Correlation of Finite Element analyses and tests. *Thin-Walled Structures*. 29: 31-46.

Hyttinen, V. (1994). Design of cold-formed stainless steel SHS beam-columns. *Report 41: Laboratory of Structural Engineering, University of Oulu*. Finland.

Johnston, B. G. (1983). Column buckling theory: Historic highlights. *Journal of Structural Engineering* ASCE. **109** (9): 2086-2096.

Johnson, A. L. and Winter, G. (1966). Behaviour of stainless steel columns and beams. *Journal of the Structural Engineering* ASCE; **92** (ST5): 97-118.

Kaitila, O. (2002). Imperfection sensitivity analysis of lipped channel columns at high temperatures. *Journal of Constructional Steel Research.* **58**: 333-351.

Karren, K. W. (1967). Corner properties of cold-formed steel shapes. *Journal of the Structural Division, ASCE.* 93(ST1): 401-432.

Korvink, S. A., van den Berg, G. J. and van der Merwe, P. (1995). Web crippling of stainless steel cold-formed beams. *Journal of Constructional Steel Research.* **34**: 225-248.

Kuwamura, H. (2003). Local buckling of thin-walled stainless steel members. *Steel Structures.* 3: 191-201.

Lagerqvist, O. and Olsson, A. (2001). Residual stresses in welded I-girders made of stainless steel and structural steel. *Proceedings of the 9th Nordic Steel Construction Conference.* Helsinki, Finland, 737-744.

Laubscher, R. F. and van der Merwe, P. (2003). Structural design in hot-rolled 3CR12 sections. *Proceedings of the International Experts Seminar.* UK. 93-113.

Lecce, M. and Rasmussen, K. J. R. (2005a). Experimental investigation of the distortional buckling of cold-formed stainless steel sections. *Research report No. 844.* Department of Civil Engineering, The University of Sydney.

Lecce, M. and Rasmussen, K. J. R. (2005b). Finite element modelling and design of cold-formed stainless steel sections. *Research report No. 845.* Department of Civil Engineering, The University of Sydney.

Lecce, M. and Rasmussen, K. J. R. (2004). Experimental investigation of distortional buckling of cold-formed stainless steel sections. *Proceedings of the 17th International Specialty Conference on Cold-formed Steel Structures.* Orlando, USA.

Leffler, B. (2000). Stainless steel and their properties, *Technical article*, Outokumpu.

Lin, S. H., Yu, W. W., Galambos, T. V. and Wang, E. (2005). Revised ASCE specification for the design of cold-formed stainless steel structural members. *Engineering Structures*. **27**: 1365-1372.

Lin, S. H., Yen, S. I. and Weng, C. C. (2005). Simplified design approach for cold-formed stainless steel compression members subjected to flexural buckling. *Thin-Walled Structures*. **43**: 1831-1851.

Lecce, M. and Rasmussen, K. J. R. (2005). Finite element modelling and design of cold-formed stainless steel sections. *Research report No. 845*. Department of Civil Engineering, University of Sydney.

Liu, Y. and Young, B. (2003). Buckling of stainless steel square hollow section compression members. *Journal of Constructional Steel Research*. **59**: 165-177.

Macdonald, M., Rhodes, J. and Taylor, G. T. (2000). Mechanical properties of stainless steel lipped channels. *Proceedings of the Fifteenth International Specialty Conference on Cold-Formed Steel Structures*. St. Louis, Missouri, U.S.A. 673-681.

Mateus, A. F. and Witz, J. A. (2001). A parametric study of the post-buckling behaviour of steel plates. *Engineering Structures*. **23**: 172-185.

Mazzolani, F. M. (1995). Aluminum Alloy Structures. 2nd Edition. E & FN Spon, An imprint of Chapman and Hill.

Mirambell, E. and Real, E. (2000). On the calculation of deflections in structural stainless steel beams: an experimental and numerical investigation. *Journal of Constructional Steel Research*. **54** : 109-133.

Nethercot, D. A., Gardner, L. and Ashraf, M. (2006). Improved design of structural stainless steel members. Proceedings of ICMS: Steel- A new and traditional material for building. Timisoara, Romania.

Nethercot, D. A. and Gardner, L. (2004). Exploiting the special features of stainless steel in structural design. *International Journal of Applied Mechanics and Engineering*. 9(1): 7-23.

Olsson, A. (2001). Stainless steel plasticity – material modelling and structural applications. *Ph.D. Thesis, Department of Civil and Mining Engineering, Luleå University of Technology, Sweden.*

prEN 1993-1-4 (2004). Eurocode 3 : Design of Steel Structures. Part 1.4 : General rules - Supplementary rules for stainless steel. CEN.

prEN 1993-1-5 (2003). Eurocode 3 : Design of Steel Structures. Part 1.5 : Plated structural elements. CEN.

prENV 1993-1-4. (1994). Eurocode 3: Design of Steel Structures – Part 1.4: General rules - Supplementary rules for stainless steel. CEN.

Ramberg, W. and Osgood, W. R. (1943). Description of stress-strain curves by three parameters. *Technical Note No. 902, National Advisory Committee for Aeronautics.* Washington, D.C.

Rasmussen, K. J. R. (2003). Full-Range Stress-Strain Curves for Stainless Steel Alloys. *Journal of Constructional Steel Research.* **59**: 47-61.

Rasmussen, K. J. R., Burns, T., Bezkorovainy, P. and Bambach, M. R. (2002). Numerical modelling of stainless steel plates in compression, *Research Report No. 813.* Department of Civil Engineering, University of Sydney.

Rasmussen, K. J. R. (2001). Full-range stress-strain curves for stainless steel alloys. *Research report No. 811.* Department of Civil Engineering, University of Sydney.

Rasmussen, K. J. R. and Hancock, G. J. (1993a). Design of cold-formed stainless steel tubular members. I: Columns. *Journal of the Structural Engineering.* ASCE ;119(8): 2349-2367.

Rasmussen, K. J. R. and Hancock, G. J. (1993b). Design of cold-formed stainless steel tubular members. II: Beams. *Journal of the Structural Engineering.* ASCE ;119(8): 2368-2386.

Rhodes, J., Macdonald, M., McNiff, W. (2000). Buckling of cold-formed stainless steel columns under concentric and eccentric loading, *Fifteenth International Specialty Conference on Cold-formed Steel Structures.* St. Louis, Missouri, USA.

Schafer, B. W. and Peköz, T. (1998). Computational modelling of cold-formed steel: Characterizing geometric imperfections and residual stresses. *Journal of Constructional Steel Research.* **47**: 193-210.

Schafer, B.W. (2002). Design Manual for The Direct Strength Method of Cold-Formed Steel Design. Final Report to the American Iron and Steel Institute, Washington, D.C. available online at www.ce.jhu.edu/bschafer/direct_strength.

Stangenberg, H. (2000a). Development of the use of stainless steel in construction: Work package 2: Cross-sections – Welded I sections and cold formed sheeting. *Report to ECSC.*

Stangenberg, H. (2000b). Development of the use of stainless steel in construction: Work package 3: Beams, columns and beam-columns – Welded I sections. *Report to ECSC.*

Sun, J. and Butterworth, J. W. (1998). Behaviour of steel single angle compression members axially loaded through one leg, *Proceedings of the Australian Structural Engineering Conference.* Auckland, 859-866.

Talja (1997). Test report on welded I and CHS beams, columns and beams-columns. *Report to ECSC.* VTT Building Technology, Finland.

Talja, A. and Salmi, P. (1995). Design of stainless steel RHS beams, columns and beam-columns. *Research Note 1619.* VTT Building Technology, Finland.

Tiomshenko, S. P. and Gere, J. M. (1985). Theory of elastic stability. McGraw – Hill International Book Company, New York.

van den Berg, G. J. and van der Merwe, P. (1992). Prediction of corner mechanical properties for stainless steels due to cold forming. *Proceedings of the Eleventh International Specialty Conference on Cold-Formed Steel Structures,* St. Louis, Missouri, U.S.A. 571-586.

Young, B. and Lui, W. M. (2005). Behaviour of cold-formed high strength stainless steel sections. *Journal of Structural Engineering.* ASCE. **131**(11): 1738-1745.

Young, B. and Liu, Y. (2003). Experimental investigation of cold-formed stainless steel columns. *Journal of Structural Engineering.* ASCE. **129**(2): 169-176.

APPENDIX - A

DESIGN TABLES FOR LOCAL BUCKLING STRESSES

Local buckling stresses σ_{LB} for different grades of stainless steel are presented herein to facilitate obtaining the stress corresponding to a specific deformation capacity ε_{LB}. The proposed tables are based on the compound Ramberg-Osgood material model with the parameters obtained from test results as described in Chapter 3. The material model is reproduced here in Equations A.1 and A.2.

$$\varepsilon = \frac{\sigma}{E_0} + 0.002\left(\frac{\sigma}{\sigma_{0.2}}\right)^n \quad \text{for } \sigma \le \sigma_{0.2} \tag{A.1}$$

$$\varepsilon = \frac{(\sigma - \sigma_{0.2})}{E_{0.2}} + \left(\varepsilon_{t1.0} - \varepsilon_{t0.2} - \frac{\sigma_{1.0} - \sigma_{0.2}}{E_{0.2}}\right)\left(\frac{\sigma - \sigma_{0.2}}{\sigma_{1.0} - \sigma_{0.2}}\right)^{n'_{0.2,1.0}} + \varepsilon_{t0.2} \quad \text{for } \sigma > \sigma_{0.2} \tag{A.2}$$

where σ and ε are the engineering stress and the engineering strain respectively

$\sigma_{0.2}$ and $\sigma_{1.0}$ are the 0.2% and 1% proof stresses respectively

$\varepsilon_{t0.2}$ and $\varepsilon_{t1.0}$ are the total strains corresponding to $\sigma_{0.2}$ and $\sigma_{1.0}$

E_0 and $E_{0.2}$ are the material's Young's modulus and tangent modulus at $\sigma_{0.2}$.

n and $n'_{0.2,1.0}$ are the exponential constants to take appropriate account of the material nonlinearity. (Table 3.5)

Table A.1: Local buckling stresses for the press-braked sections of austenitic Grade 1.4301.

ε_{LB}	$\sigma_{0.2}$ (N/mm^2)								
	200	250	300	350	400	450	500	550	600
0.0005	92	96	98	98	98	99	99	99	99
0.0010	139	160	176	186	190	194	195	195	198
0.0020	178	215	249	278	304	326	343	358	366
0.0030	199	244	285	326	362	394	425	454	477
0.0040	212	262	310	356	398	439	478	514	546
0.0050	218	271	323	373	423	470	516	559	597
0.0060	223	278	331	384	436	487	537	586	633
0.0070	227	283	338	392	446	499	551	603	653
0.0080	231	287	344	399	454	509	562	616	668
0.0090	234	291	348	405	461	517	572	626	680
0.0100	237	295	353	410	467	524	580	635	690
0.0120	241	301	360	419	478	536	593	651	708
0.0140	245	306	367	427	487	546	605	664	722
0.0160	249	311	372	434	494	555	615	675	735
0.0180	253	315	378	440	501	563	624	685	746
0.0200	256	319	382	445	508	570	633	694	756
0.0240	261	326	391	455	520	584	647	711	774
0.0280	266	332	398	464	530	595	660	725	790
0.0320	271	338	405	472	539	606	672	738	804
0.0360	275	343	411	480	547	615	683	750	817
0.0400	279	348	417	486	555	624	693	761	829
0.0500	287	359	430	502	573	644	715	785	856
0.0600	295	368	442	515	588	661	734	806	879
0.0700	302	377	452	527	602	676	751	825	900
0.0800	308	384	461	538	614	690	767	843	919
0.0900	313	392	470	548	626	703	781	858	936
0.1000	319	398	478	557	636	715	794	873	952

Table A.2: Local buckling stresses for the roll-formed sections of austenitic Grade 1.4301.

ε_{LB}	$\sigma_{0.2}$ (N/mm^2)								
	200	250	300	350	400	450	500	550	600
0.0005	88	94	96	98	98	99	99	99	99
0.0010	132	153	167	177	184	189	193	195	195
0.0020	175	210	242	270	294	313	330	344	357
0.0030	200	243	284	320	356	387	415	443	465
0.0040	215	265	313	358	400	439	475	509	540
0.0050	224	277	330	380	429	476	520	562	600
0.0060	230	286	340	394	446	498	547	596	642
0.0070	235	292	349	404	459	513	565	617	668
0.0080	239	297	355	412	469	524	579	633	686
0.0090	243	302	361	419	477	534	591	646	701
0.0100	246	306	366	426	484	543	600	657	714
0.0120	252	313	375	436	497	557	617	676	734
0.0140	256	320	383	445	507	569	630	691	752
0.0160	261	325	389	453	516	579	642	704	766
0.0180	265	330	395	460	525	589	653	716	779
0.0200	268	334	401	466	532	597	662	727	791
0.0240	274	342	410	478	545	612	679	745	812
0.0280	280	350	419	488	557	625	694	762	830
0.0320	285	356	426	497	567	637	707	776	846
0.0360	290	362	433	505	576	648	719	789	860
0.0400	294	367	440	513	585	657	730	802	873
0.0500	303	379	454	529	604	679	754	828	903
0.0600	312	389	467	544	621	698	775	852	928
0.0700	319	398	478	557	636	715	794	872	951
0.0800	326	407	488	569	649	730	811	891	971
0.0900	332	414	497	579	662	744	826	908	990
0.1000	337	421	506	589	673	757	841	924	1007

Table A.3: Local buckling stresses for austenitic Grades 1.4306 and 1.4318.

ε_{LB}	$\sigma_{0.2}$ (N/mm^2)								
	200	250	300	350	400	450	500	550	600
0.0005	87	93	95	95	96	96	96	96	96
0.0010	132	151	165	175	182	187	188	190	192
0.0020	174	209	240	268	292	311	328	341	351
0.0030	199	243	282	320	354	385	413	437	459
0.0040	213	263	311	356	398	437	473	506	537
0.0050	218	271	324	375	424	472	517	558	594
0.0060	222	277	331	384	436	488	538	587	634
0.0070	225	281	336	390	444	497	550	602	653
0.0080	228	284	340	395	450	504	558	612	665
0.0090	230	286	343	399	455	510	565	620	674
0.0100	232	289	346	403	459	515	571	626	681
0.0120	235	293	351	409	466	523	580	637	694
0.0140	237	296	355	414	472	530	588	646	703
0.0160	240	299	359	418	477	536	595	653	712
0.0180	242	302	362	422	482	541	601	660	719
0.0200	244	305	365	426	486	546	606	666	725
0.0240	247	309	370	432	493	554	615	676	736
0.0280	250	313	375	437	499	561	623	685	746
0.0320	253	316	379	442	505	567	630	692	755
0.0360	255	319	383	446	510	573	636	699	762
0.0400	258	322	386	450	514	578	642	706	769
0.0500	262	328	393	459	524	589	655	720	785
0.0600	267	333	400	466	533	599	665	732	798
0.0700	270	338	405	473	540	608	675	742	809
0.0800	274	342	411	479	547	615	683	752	820
0.0900	277	346	415	484	553	622	691	760	829
0.1000	280	350	420	489	559	629	699	768	838

Table A.4: Local buckling stresses for ferritic Grade 1.4003.

ε_{LB}	$\sigma_{0.2}$ (N/mm^2)								
	200	250	300	350	400	450	500	550	600
0.0005	96	96	96	96	96	97	98	98	98
0.0010	149	170	185	191	194	194	195	195	195
0.0020	183	223	258	291	318	340	358	369	378
0.0030	199	245	288	329	368	405	438	468	492
0.0040	209	259	308	354	398	441	480	520	555
0.0050	215	267	319	369	419	466	512	556	597
0.0060	218	272	325	377	429	480	530	579	627
0.0070	221	275	329	383	436	489	541	592	643
0.0080	223	278	333	387	441	495	548	601	653
0.0090	224	280	335	390	445	500	554	608	661
0.0100	226	282	338	393	449	504	559	613	667
0.0120	229	285	342	398	455	511	566	622	677
0.0140	231	288	345	403	459	516	573	629	685
0.0160	233	291	348	406	464	521	578	635	692
0.0180	234	293	351	409	467	525	583	640	698
0.0200	236	295	353	412	470	529	587	645	703
0.0240	239	298	358	417	476	535	594	653	712
0.0280	241	301	361	421	481	541	601	660	720
0.0320	243	304	364	425	485	546	606	666	726
0.0360	245	306	367	428	489	550	611	672	732
0.0400	247	308	370	431	493	554	615	677	738
0.0500	250	313	376	438	501	563	625	687	750
0.0600	254	317	381	444	507	570	634	697	760
0.0700	257	321	385	449	513	577	641	705	769
0.0800	259	324	389	453	518	583	647	712	777
0.0900	262	327	392	458	523	588	653	719	784
0.1000	264	330	396	461	527	593	659	725	790

Table A.5: Local buckling stresses for ferritic Grade 1.4016.

ε_{LB}	$\sigma_{0.2}$ (N/mm^2)								
	200	250	300	350	400	450	500	550	600
0.0005	94	96	96	96	96	97	98	98	98
0.0010	145	166	180	187	192	194	195	195	195
0.0020	181	219	254	285	312	333	350	363	372
0.0030	199	244	287	327	364	401	433	459	486
0.0040	211	261	309	355	398	439	480	517	552
0.0050	217	269	321	371	421	468	513	556	597
0.0060	220	274	328	381	433	484	534	582	630
0.0070	223	278	333	387	441	493	546	597	648
0.0080	226	282	337	392	446	501	554	607	660
0.0090	228	284	340	396	451	506	561	615	669
0.0100	230	287	343	399	455	511	567	622	676
0.0120	233	290	348	405	462	519	576	632	688
0.0140	235	294	352	410	468	526	583	640	697
0.0160	238	297	356	414	473	531	590	648	705
0.0180	240	299	359	418	477	536	595	654	712
0.0200	241	302	362	421	481	541	600	659	718
0.0240	245	306	366	427	488	548	609	669	729
0.0280	247	309	371	432	494	555	616	677	738
0.0320	250	312	375	437	499	561	623	684	746
0.0360	252	315	378	441	503	566	629	691	753
0.0400	254	318	381	444	508	571	634	697	760
0.0500	259	323	388	453	517	581	646	710	774
0.0600	263	328	394	459	525	590	656	721	786
0.0700	266	333	399	466	532	598	665	731	797
0.0800	269	337	404	471	538	605	672	739	806
0.0900	272	340	408	476	544	612	680	747	815
0.1000	275	343	412	481	549	618	686	755	823

Table A.6: Local buckling stresses for ferritic Grade 1.4462.

ε_{LB}	$\sigma_{0.2}$ (N/mm^2)								
	200	250	300	350	400	450	500	550	600
0.0005	92	96	99	100	100	100	100	100	100
0.0010	138	159	174	184	190	194	198	198	198
0.0020	177	214	248	277	302	324	340	355	366
0.0030	200	244	285	324	360	394	425	451	474
0.0040	212	262	311	357	400	441	478	514	546
0.0050	217	270	322	374	424	472	518	561	601
0.0060	220	274	328	381	434	486	537	586	635
0.0070	223	278	332	387	441	494	547	599	650
0.0080	225	280	336	391	446	500	554	607	660
0.0090	226	283	339	394	450	505	559	614	668
0.0100	228	285	341	397	453	509	564	619	674
0.0120	231	288	345	402	459	515	572	628	684
0.0140	233	291	348	406	464	521	578	635	692
0.0160	235	293	351	410	468	525	583	641	698
0.0180	236	295	354	413	471	530	588	646	704
0.0200	238	297	356	415	474	533	592	651	709
0.0240	240	300	360	420	480	540	599	658	718
0.0280	243	303	364	424	485	545	605	665	725
0.0320	245	306	367	428	489	550	611	671	732
0.0360	247	308	370	431	493	554	615	677	738
0.0400	248	311	373	434	496	558	620	682	743
0.0500	252	315	378	441	504	567	630	692	755
0.0600	255	319	383	447	511	574	638	701	765
0.0700	258	323	387	452	516	581	645	709	774
0.0800	261	326	391	456	521	586	651	716	781
0.0900	263	329	395	460	526	592	657	723	788
0.1000	265	332	398	464	530	597	663	729	795

APPENDIX - B

DESIGN TABLES FOR GENERALISED SHAPE FACTOR CONSTANTS

Generalised shape factor a_g is a parameter proposed in the present research to take appropriate account of the nonlinearity in bending stress distributions for stainless steel members. This parameter is function of geometric shape factor a_p, 0.2% elastic strain of the material ε_0 and the maximum stress at the outermost fibre of the cross-section, which is eventually governed by the deformation capacity ε_{LB}. For a specific value of ε_{LB}, generalised shape factor a_g may be obtained using Equation B.1, which was originally proposed in Chapter 6.

$$a_g = A_1 + A_2\, \varepsilon_0 + A_3\, a_p + A_4\, \varepsilon_0\, a_p \qquad (B.1)$$

The following tables give values for the constants A_1 to A_4 for different grades of stainless steel. The values were determined by the numerical integration of the nonlinear bending stress distributions, obtained using the proposed material model, over the depth of a cross-section.

Table B.1: Generalised shape factor constants for the press-braked sections of austenitic Grade 1.4301.

ε_{LB}	A_1	A_2	A_3	A_4
0.0005	0.534	-133.39	0.099	-40.32
0.0010	0.395	-4.95	0.488	-191.40
0.0015	0.268	89.06	0.699	-253.07
0.0020	0.225	115.28	0.789	-249.66
0.0025	0.218	113.50	0.834	-227.08
0.0030	0.222	104.78	0.863	-203.61
0.0035	0.203	106.16	0.906	-191.82
0.0040	0.135	127.69	0.979	-196.60
0.0045	0.095	139.38	1.022	-193.27
0.0050	0.075	141.59	1.045	-182.92
0.0060	0.107	89.04	1.032	-122.82
0.0070	0.121	63.95	1.034	-92.76
0.0080	0.129	50.20	1.040	-75.31
0.0090	0.134	41.43	1.048	-63.72
0.0100	0.138	35.31	1.056	-55.42
0.0120	0.134	31.61	1.079	-47.62
0.0140	0.155	17.76	1.079	-33.10
0.0160	0.159	18.03	1.093	-31.37
0.0180	0.164	15.49	1.103	-27.65
0.0200	0.170	13.05	1.112	-24.39
0.0240	0.179	11.88	1.130	-21.59
0.0280	0.188	9.13	1.144	-18.02
0.0320	0.196	8.46	1.157	-16.49
0.0360	0.204	7.23	1.170	-14.77
0.0400	0.213	5.94	1.180	-13.10
0.0500	0.229	5.28	1.206	-11.47
0.0600	0.244	4.54	1.227	-10.13
0.0700	0.257	3.95	1.246	-9.08
0.0800	0.272	3.34	1.263	-8.20
0.0900	0.280	4.17	1.282	-8.55
0.1000	0.293	3.32	1.295	-7.55
0.1500	0.341	2.66	1.358	-6.14
0.2000	0.380	2.00	1.408	-5.08

Table B.2: Generalised shape factor constants for the roll-formed sections of austenitic Grade 1.4301.

ε_{LB}	A_1	A_2	A_3	A_4
0.0005	0.462	-105.54	0.132	-53.23
0.0010	0.392	-10.74	0.437	-167.51
0.0015	0.323	53.85	0.610	-212.45
0.0020	0.299	77.29	0.701	-215.86
0.0025	0.296	82.52	0.757	-205.44
0.0030	0.302	80.99	0.796	-191.94
0.0035	0.290	85.03	0.842	-185.09
0.0040	0.212	116.02	0.933	-199.52
0.0045	0.154	138.59	0.998	-205.70
0.0050	0.116	152.17	1.040	-204.24
0.0060	0.134	107.09	1.043	-147.72
0.0070	0.149	76.92	1.048	-111.56
0.0080	0.157	59.74	1.057	-90.03
0.0090	0.160	49.82	1.069	-76.65
0.0100	0.165	42.15	1.078	-66.40
0.0120	0.157	38.26	1.108	-57.46
0.0140	0.182	21.19	1.108	-39.61
0.0160	0.184	21.30	1.126	-37.37
0.0180	0.188	19.35	1.140	-33.75
0.0200	0.192	17.38	1.152	-30.61
0.0240	0.202	14.21	1.172	-25.76
0.0280	0.213	10.79	1.188	-21.32
0.0320	0.219	10.39	1.206	-19.86
0.0360	0.228	9.31	1.220	-18.04
0.0400	0.237	7.19	1.231	-15.58
0.0500	0.249	8.39	1.265	-15.29
0.0600	0.267	6.26	1.287	-12.64
0.0700	0.282	4.75	1.309	-10.70
0.0800	0.291	5.35	1.331	-10.71
0.0900	0.305	4.13	1.348	-9.28
0.1000	0.315	4.39	1.365	-9.17
0.1500	0.364	2.27	1.434	-6.34
0.2000	0.396	5.18	1.496	-8.17

Table B.3: Generalised shape factor constants for austenitic Grades 1.4306 and 1.4318.

ε_{LB}	A_1	A_2	A_3	A_4
0.0005	0.472	-108.24	0.118	-46.54
0.0010	0.403	-16.69	0.429	-160.98
0.0015	0.324	52.33	0.611	-210.81
0.0020	0.297	77.41	0.705	-215.60
0.0025	0.289	84.63	0.764	-206.60
0.0030	0.295	82.32	0.802	-192.13
0.0035	0.271	90.58	0.857	-188.36
0.0040	0.135	142.46	0.990	-218.06
0.0045	0.055	172.41	1.063	-227.34
0.0050	0.011	188.28	1.102	-224.75
0.0060	0.060	109.34	1.065	-137.56
0.0070	0.081	71.51	1.057	-95.44
0.0080	0.088	53.58	1.060	-73.98
0.0090	0.092	42.98	1.064	-60.64
0.0100	0.094	35.86	1.070	-51.41
0.0120	0.088	30.30	1.088	-42.08
0.0140	0.104	17.25	1.086	-28.31
0.0160	0.104	16.68	1.097	-25.95
0.0180	0.107	13.90	1.104	-22.13
0.0200	0.109	11.79	1.111	-19.28
0.0240	0.111	10.17	1.124	-16.30
0.0280	0.115	8.51	1.135	-13.83
0.0320	0.120	6.58	1.143	-11.42
0.0360	0.125	5.18	1.150	-9.67
0.0400	0.126	5.54	1.159	-9.49
0.0500	0.132	5.10	1.177	-8.30
0.0600	0.142	2.80	1.188	-5.87
0.0700	0.146	3.22	1.202	-5.84
0.0800	0.153	2.44	1.212	-4.88
0.0900	0.158	2.22	1.222	-4.48
0.1000	0.162	1.88	1.231	-4.01
0.1500	0.182	1.41	1.270	-3.05
0.2000	0.199	1.26	1.299	-2.59

Table B.4: Generalised shape factor constants for ferritic Grade 1.4003.

ε_{LB}	A_1	A_2	A_3	A_4
0.0005	0.631	-170.62	0.034	-13.89
0.0010	0.423	-12.91	0.536	-210.46
0.0015	0.190	137.50	0.824	-311.63
0.0020	0.110	178.35	0.921	-306.23
0.0025	0.111	158.68	0.940	-258.99
0.0030	0.123	133.67	0.946	-216.73
0.0035	0.147	109.18	0.943	-181.42
0.0040	0.114	111.18	0.984	-171.18
0.0045	0.073	118.54	1.026	-166.20
0.0050	0.043	126.37	1.055	-162.07
0.0060	0.048	94.57	1.056	-118.97
0.0070	0.066	63.02	1.048	-83.32
0.0080	0.072	47.53	1.050	-64.63
0.0090	0.075	37.72	1.053	-52.47
0.0100	0.077	31.58	1.058	-44.45
0.0120	0.071	26.66	1.073	-36.24
0.0140	0.085	14.72	1.071	-23.80
0.0160	0.084	14.73	1.080	-22.15
0.0180	0.086	12.00	1.086	-18.61
0.0200	0.086	11.02	1.093	-16.82
0.0240	0.091	8.11	1.101	-13.01
0.0280	0.093	6.85	1.110	-11.03
0.0320	0.096	5.60	1.117	-9.33
0.0360	0.100	3.94	1.123	-7.44
0.0400	0.101	3.98	1.130	-7.09
0.0500	0.104	3.95	1.145	-6.38
0.0600	0.110	2.86	1.155	-5.04
0.0700	0.112	3.10	1.167	-4.94
0.0800	0.118	2.44	1.174	-4.13
0.0900	0.122	1.29	1.181	-3.02
0.1000	0.125	1.48	1.189	-3.02
0.1500	0.139	1.55	1.219	-2.62
0.2000	0.151	0.68	1.241	-1.68

Table B.5: Generalised shape factor constants for ferritic Grade 1.4016.

ε_{LB}	A_1	A_2	A_3	A_4
0.0005	0.595	-156.45	0.057	-22.99
0.0010	0.413	-10.59	0.515	-201.10
0.0015	0.223	116.34	0.772	-286.06
0.0020	0.159	150.70	0.867	-281.49
0.0025	0.153	140.17	0.898	-245.98
0.0030	0.161	123.14	0.914	-212.42
0.0035	0.180	103.50	0.920	-182.12
0.0040	0.137	111.69	0.972	-177.16
0.0045	0.089	123.52	1.021	-175.55
0.0050	0.054	134.13	1.056	-173.17
0.0060	0.060	100.35	1.058	-127.48
0.0070	0.078	67.44	1.051	-90.13
0.0080	0.085	51.00	1.054	-70.24
0.0090	0.088	41.08	1.059	-57.71
0.0100	0.090	34.16	1.064	-48.81
0.0120	0.084	29.06	1.082	-40.10
0.0140	0.099	16.39	1.080	-26.81
0.0160	0.098	16.27	1.091	-24.90
0.0180	0.100	13.95	1.099	-21.56
0.0200	0.103	11.92	1.105	-18.79
0.0240	0.107	8.69	1.115	-14.55
0.0280	0.110	7.40	1.126	-12.47
0.0320	0.113	6.66	1.135	-11.11
0.0360	0.116	5.95	1.143	-9.95
0.0400	0.120	4.03	1.149	-7.90
0.0500	0.124	4.64	1.167	-7.62
0.0600	0.131	2.99	1.179	-5.74
0.0700	0.137	2.20	1.190	-4.71
0.0800	0.141	2.71	1.201	-4.85
0.0900	0.147	1.58	1.209	-3.69
0.1000	0.149	2.40	1.220	-4.19
0.1500	0.167	1.35	1.255	-2.79
0.2000	0.182	1.09	1.282	-2.29

Table B.6: Generalised shape factor constants for duplex Grade 1.4462.

ε_{LB}	A_1	A_2	A_3	A_4
0.0005	0.515	-126.43	0.112	-45.72
0.0010	0.388	-3.24	0.480	-188.76
0.0015	0.284	79.74	0.674	-242.49
0.0020	0.244	105.55	0.766	-241.01
0.0025	0.239	105.01	0.814	-221.11
0.0030	0.245	98.03	0.843	-200.09
0.0035	0.234	97.32	0.882	-187.50
0.0040	0.117	140.37	0.997	-209.78
0.0045	0.045	166.33	1.063	-216.20
0.0050	0.004	179.79	1.098	-212.23
0.0060	0.049	103.07	1.064	-128.06
0.0070	0.067	67.09	1.056	-88.08
0.0080	0.073	50.24	1.058	-67.93
0.0090	0.076	40.08	1.062	-55.27
0.0100	0.077	33.29	1.067	-46.54
0.0120	0.070	28.35	1.083	-38.10
0.0140	0.086	14.70	1.080	-24.12
0.0160	0.084	15.58	1.090	-23.10
0.0180	0.084	13.22	1.097	-19.82
0.0200	0.087	10.87	1.102	-16.84
0.0240	0.088	9.11	1.113	-13.96
0.0280	0.093	6.57	1.119	-10.89
0.0320	0.095	5.90	1.127	-9.64
0.0360	0.099	4.02	1.133	-7.55
0.0400	0.100	4.04	1.140	-7.14
0.0500	0.106	2.78	1.152	-5.43
0.0600	0.110	2.25	1.164	-4.51
0.0700	0.112	2.26	1.175	-4.24
0.0800	0.117	1.77	1.182	-3.59
0.0900	0.120	1.75	1.191	-3.35
0.1000	0.122	2.23	1.199	-3.62
0.1500	0.137	0.77	1.227	-1.95
0.2000	0.147	0.79	1.251	-1.74

APPENDIX - C

CORRELATION BETWEEN STAINLESS STEEL DESIGNATIONS

There are a number of stainless steel designation systems. The system adopted in the present research is the 'steel number' given in the European material standard BS EN 10088-1 (1995). Correlations between BS EN 10088, UK, USA, French, Swedish, Japanese, Chinese and universal numbering systems are presented in Table C.1.

Table C.1: Correlation between stainless steel designations

Type	EN	Typical chemical composition, %						UK (BS)	USA (ASTM)	France (NF)	Sweden (SS)	Japan (JIS)	China (PR)	UNS
		C	N	Cr	Ni	Mo	Others							
Austenitic	1.4310	0.10	-	17	7	-	-	301S21	301	Z11 CN 18-08	2331	SUS 301	1Cr17Ni7	S30100
	1.4318	0.02	0.14	17.7	6.5	-	-	-	301LN	Z3 CN 18-07 Az	-	SUS 301L	-	-
	1.4372	0.05	0.15	17	5	-	Mn	-	201	Z12 CMN 17-07 Az	-	SUS 201	1Cr17Mn6Ni5N	S20100
	1.4301	0.04	-	18.1	8.3	-	-	304S31	304	Z7 CN 18-09	2333	SUS 304	0Cr18Ni9	S30400
	1.4307	0.02	0.15	18.1	8.3	-	-	304S11	304L	Z3 CN 18-10	2352	SUS 304L	00Cr19Ni10	S30403
	1.4311	0.02	-	18.5	10.5	-	-	304S61	304LN	Z3 CN 18-10 Az	2371	SUS 304LN	00Cr18Ni10N	S30453
	1.4541	0.04	0.04	17.3	9.1	-	Ti	321S31	321	Z6 CNT 18-10	2337	SUS 321	0Cr18Ni10Ti	S32100
	1.4550	0.05	-	17.5	9.5	-	Nb	347S31	347	Z6 CNNb 18-10	2338	SUS 347	0Cr18Ni11Nb	S34700
	1.4305	0.05	-	17.3	8.2	-	S	303S31	303	Z8 CNF 18-09	2346	SUS 303	Y1Cr18Ni9	S30300
	1.4303	0.04	-	17.7	12.5	-	-	305S19	305	Z1 CN 18-12	-	SUS 305J1	1Cr18Ni12	S30500
	1.4306	0.02	-	18.2	10.1	-	-	304S11	304L	Z3 CN 18-10	2352	SUS 304L	00Cr19Ni10	S30403
	1.4567	0.01	-	17.7	9.7	-	Cu	304S17	-	Z3 CNU 18-09 FF	-	SUS XM7	0Cr18Ni9Cu3	S30430
	1.4401	0.04	-	17.2	10.2	2.1	-	316S31	316	Z7 CND 17-11-02	2347	SUS 316	0Cr17Ni2Mo2	S31600
	1.4404	0.02	-	17.2	10.1	2.1	-	316S11	316L	Z3 CND 17-11-02	2348	SUS 316L	00Cr17Ni14Mo2	S31603
	1.4436	0.04	-	16.9	10.7	2.6	-	316S33	316	Z7 CND 18-12-03	2343	SUS 316	0Cr17Ni12Mo2	S31600
	1.4432	0.02	-	16.9	10.7	2.6	-	316S13	316L	Z3 CND 18-14-03	2353	SUS 316L	00Cr17Ni14Mo2	S31603
	1.4406	0.02	0.14	17.2	10.3	2.1	-	316S61	316LN	Z3 CND 17-11 Az	-	SUS 316LN	00Cr17Ni12Mo2N	S31653
	1.4429	0.02	0.14	17.3	12.5	2.6	-	316S63	-	Z3 CND 17-12 Az	2375	SUS 316LN	00Cr17Ni13Mo2N	S31653
	1.4571	0.04	-	16.8	10.9	2.1	Ti	320S31	316Ti	Z6 CNDT 17-12	2350	SUS 316Ti	0Cr18Ni12Mo2Ti	S31635
	1.4435	0.02	-	17.3	12.6	2.6	-	316S13	316L	Z3 CND 18-14-03	2353	SUS 316L	00Cr17Ni14Mo2	S31603
	1.4438	0.02	-	18.2	13.7	3.1	-	317S12	317L	Z3 CND 19-15-04	2367	SUS 317L	00Cr19Ni13Mo3	S31703
	1.4439	0.02	0.14	17.8	12.7	4.1	-	-	317LMN	Z3 CND 18-14-05 Az	-	-	-	S31726
	1.4539	0.01	-	20	25	4.3	Cu	904S13	904L	Z2 NCDU 25-20	2562	-	-	N08904
	1.4547	0.01	0.20	20	18	6.1	Cu	-	S31254	-	2378	-	-	S31254
	1.4565	0.02	0.45	24	17	4.5	Mn	-	S34565	-	-	-	-	S34565
	1.4948	0.05	-	18.1	8.3	-	-	304S51	304H	Z6 CN 18-09	2333	SUS 304	1Cr18Ni9	S30409
	1.4878	0.05	-	17.3	9.1	-	Ti	321S51	321	Z6 CNT 18-10	2337	SUS 321	1Cr18Ni9Ti	S32100
	1.4818	0.05	0.15	18.5	9.5	-	Si, Ce	-	-	-	2372	-	-	S40415
	1.4833	0.06	-	22.3	12.6	-	-	309S16	309S	Z15 CNS 20-12	-	SUS 309	0Cr23Ni13	S30908
	1.4828	0.04	-	20	12	-	Si	-	-	Z17 CNS 20-12	-	SUH 309	1Cr20Ni14Si2	-
	1.4835	0.09	0.17	21	11	-	Si, Ce	-	S30815	-	2368	-	-	S30815
	1.4845	0.05	-	25	20	-	-	310S16	310S	Z18 CN 25-20	2361	SUS 310S	0Cr25Ni20	S31008
	1.4854	0.05	0.17	25	35	-	Si, Ce	-	S35315	-	-	-	-	S35315
Ferritic	1.4016	0.04	-	16.5	-	-	-	430S17	430	Z8 C17	2320	SUS 430	1Cr17	S43000
	1.4003	0.03	0.03	11.5	0.65	-	Si, Mn, P, S	-	A240	-	-	-	3Cr12	S41003
Duplex	1.4162	0.03	0.22	21.5	1.5	0.3	Mn	-	S32101	-	-	-	-	S32101
	1.4362	0.02	0.10	23	4.8	0.3	-	-	S32304	Z3 CN 23-04 Az	2237	-	-	S32304
	1.4462	0.02	0.17	22	5.7	3.1	-	318S13	S32205	Z3 CND 22-05 Az	2377	SUS 329J3L	00Cr22Ni5Mo3N	S32205
	1.4410	0.02	0.27	25	7	4	-	-	S32750	Z3 CND 25-06 Az	2328	-	-	S32750
Martensitic	1.4006	0.15	0.04	12	-	-	-		410	Z10 C13	2302	SUS 410	1Cr12	S41000
	1.4005	0.10	0.04	13	-	-	S		416	Z11 CF13	2380	SUS 416	Y1Cr13	S41600
	1.4021	0.20	-	13	-	-	-		420	Z20 C13	2303	SUS 420J1	2Cr13	S42000
	1.4028	0.30	-	12.5	-	-	-		420	Z33 C13	2304	SUS 420J2	3Cr13	S42000
	1.4418	0.03	-	16	5	1	-		-	Z6 CND 16-05-01	2387	-	-	-